nature chemical biology

SUPPLEMENTARY INFORMATION

https://doi.org/10.1038/s41589-020-0602-1

In the format provided by the authors and unedited.

A bioluminescent probe for longitudinal monitoring of mitochondrial membrane potential

Arkadiy A. Bazhin[1], Riccardo Sinisi[1], Umberto De Marchi[2], Aurélie Hermant[2], Nicolas Sambiagio[1], Tamara Maric[1], Ghyslain Budin[1] and Elena A. Goun[1]✉

[1]Institute of Chemical Sciences and Engineering, School of Basic Sciences, Swiss Federal Institute of Technology Lausanne (EPFL), Lausanne, Switzerland. [2]Nestlé Research, Lausanne, Switzerland. ✉e-mail: elena.goun@epfl.ch

Supplementary Table 1.

Chemical structures, abbreviations, and reaction rate constants of various MAL probes. Each probe consists of two compounds — an organic azide (azido-TPP) and a triphenylphosphine derivative (TPP-CL) that react with each other via a “click” reaction (Staudinger ligation).

Probe	TPP-Azide	TPP-Caged luciferin (TPP-CL)	Reaction rate, $M^{-1}s^{-1}$
MAL1	Azido-TPP1 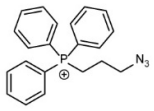	TPP-CL1 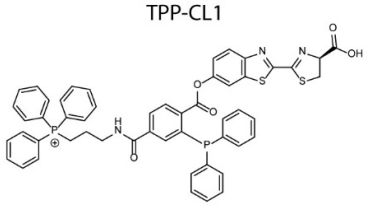	0.135±0.023
MAL2	Azido-TPP2 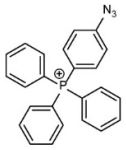	TPP-CL1 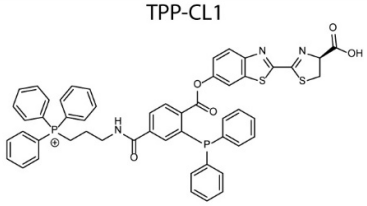	29.87 ± 0.84
MAL3	Azido-TPP1 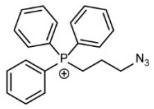	TPP-CL2 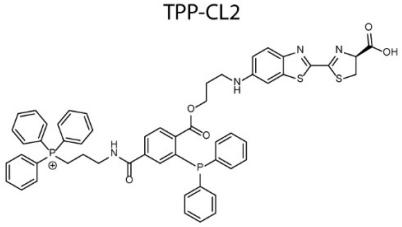	$1.07 \pm 0.2 \cdot 10^{-3}$
MAL4	Azido-TPP2 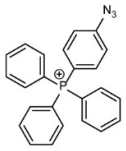	TPP-CL2 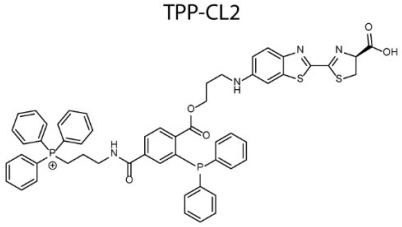	Not applicable

Supplementary Table 2.

Primers for mitochondrial and nuclear DNA.

	mtco-1	atp-5
Forward	TACTATTCGGAGCCTGAGCG	GCTTCAGTACTTGGCTCCCTACTC
Reverse	GATTTCCGGCTAGAGGTGGG	TCCTTTGACCTGCTTGGATAGATC

Supplementary Table 3.

Formulation of low and high K^+ medium

"Low K^+" medium	
Component	Concentration
$CaCl_2$	1.261 mM
$MgCl_2$	0.492 mM
$MgSO_4$	0.406 mM
KCl	5.333 mM
KH_2PO_4	0.441 mM
$NaHCO_3$	4.166 mM
NaCl	137.931 mM
Na_2HPO_4	0.338 mM
Glucose	5.555 mM
FBS	10%

"High K^+" medium	
Component	Concentration
$CaCl_2$	1.261 mM
$MgCl_2$	0.492 mM
$MgSO_4$	0.406 mM
KCl	125.33 mM
KH_2PO_4	0.441 mM
$NaHCO_3$	4.166 mM
NaCl	17.931 mM
Na_2HPO_4	0.338 mM
Glucose	5.555 mM
FBS	10%

Supplementary Figures

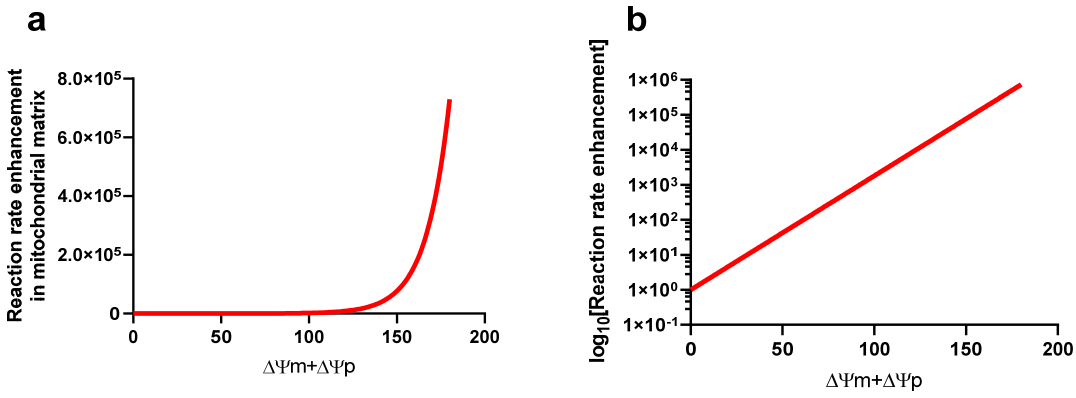

Supplementary Figure 1. Calculated dependence of the reaction rate enhancement in mitochondrial matrix compared to extracellular media on ΔΨm+ ΔΨp. **a**. linear scale of Y-axis, **b**. logarithmic scale of Y-axis.

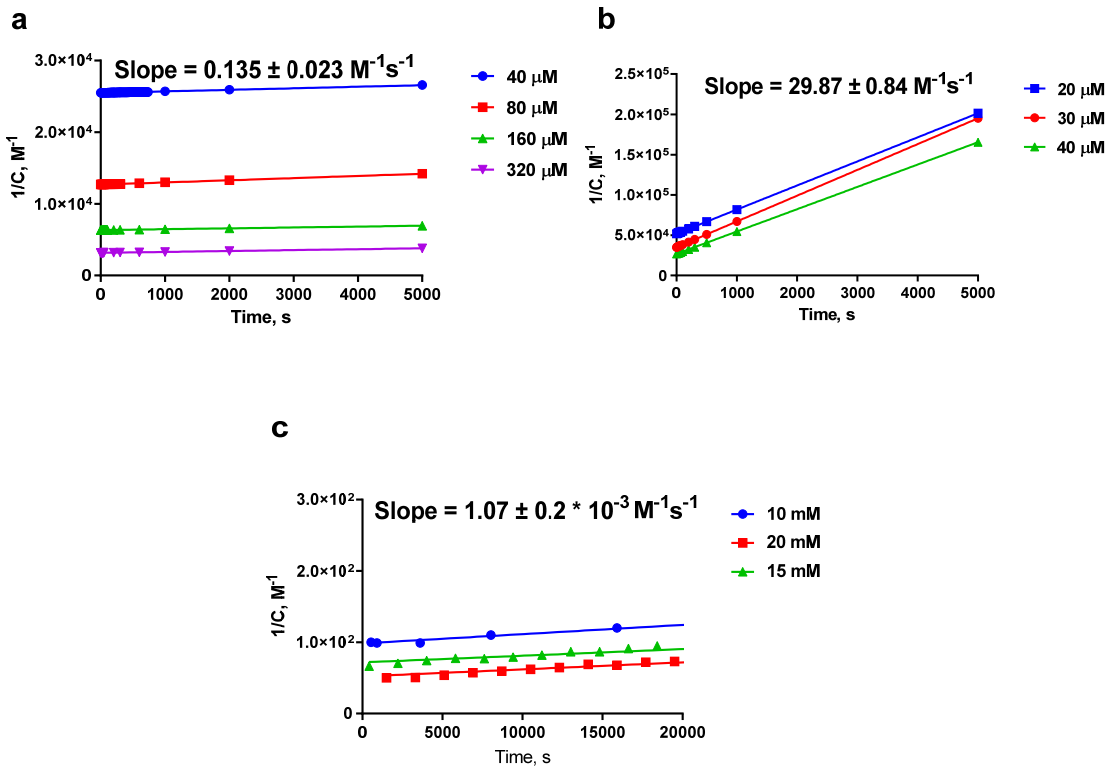

Supplementary Figure 2. Kinetic analysis of luciferin uncaging in reaction of phosphines (**13** and **21**) with either azido-TPP1 or azido-TPP2. **a**. Plot of 1/[**13**] versus time to determine the second order rate of uncaging reaction between phosphine **13** and azido-TPP1 under stochiometric conditions in DMA with 50% (v/v) PBS. n = 3 for each point, n = 4 for slope calculation (independent replicates) **b**. Plot of 1/[**13**] versus time to determine the second order rate of uncaging reaction between phosphine **13** and azido-TPP2 under stochiometric conditions in DMA with 50% (v/v) PBS. n = 3 for each point, n = 3 for slope calculation (independent replicates) **c**. Plot of 1/[**21**] versus time to determine the second order rate of uncaging reaction between phosphine **21** and azido-TPP1 under stochiometric conditions in DMF-*d7* with 2% (v/v) water. n = 3 for each point, n = 3 for slope calculation (independent replicates)The second-order rate constant is equal to the slope of the linear fits according to the kinetic model of second-order reaction. The measured slopes were 0.135 ± 0.023 for **a**, 29.87± 0.84 for **b**, and 1.1 ± 0.2*10^{-3} M^{-1}s^{-1} for **c** (mean ± CI 95%). All presented experiments were repeated independently twice.

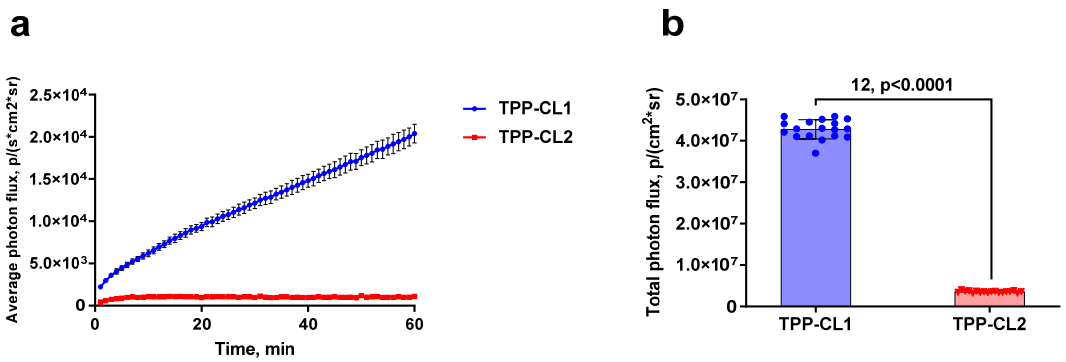

Supplementary Figure 3. Investigation of *in vitro* hydrolytic stability of TPP-CL probes. **a**. HT-1080 cells were incubated with 5 µM solution of either TPP-CL1 or TPP-CL2 probes in EMEM growth media and the resulting light output was quantified for 1 h using IVIS spectrum camera. Each point represents mean value, error bars – SD. n = 18, independent biological replicates. **b**. Total photon flux calculated by integrating the area under the curves in panel **a**. TPP-CL2 reagent demonstrated 12-fold lower background signal than TPP-CL1 compound. Data are presented as mean ± SD. n =18, independent biological replicates. p value was calculated by two tailed t test. The presented experiment was repeated independently twice.

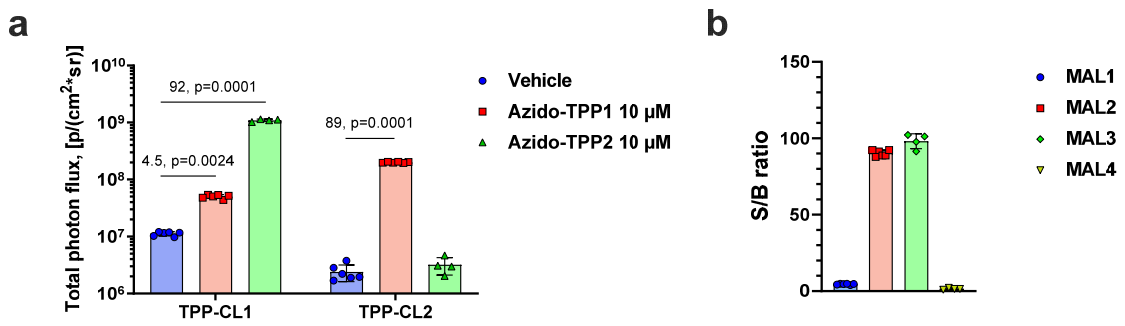

Supplementary Figure 4. a. The total photon flux obtained after the pretreatment of HT-1080-luc cells with either TPP-CL1 or TPP-CL2, followed by 1x PBS washing, and the subsequent addition of media containing azido-TPP1 or azido-TPP2 as described above (or just media for the background (*blue bars*)). Total photon flux resulting from cells was integrated over 1 h. The numbers above the bars represent the fold increase of the signal compared to corresponding background. The data are presented as mean ± SD, n = 6 (vehicle, azido-TPP1), n = 4 (azido-TPP2). p values were calculated using one-way ANOVA with Dunnett's multiple comparisons test. **b.** Signal to background (S/B) ratio for each of the 4 MAL probes in HT-1080-luc cells. The data are presented as mean ± SD, n = 6 (vehicle, azido-TPP1), n = 4 (azido-TPP2). n values represent number of independent biological replicates. The presented experiment was repeated independently three times.

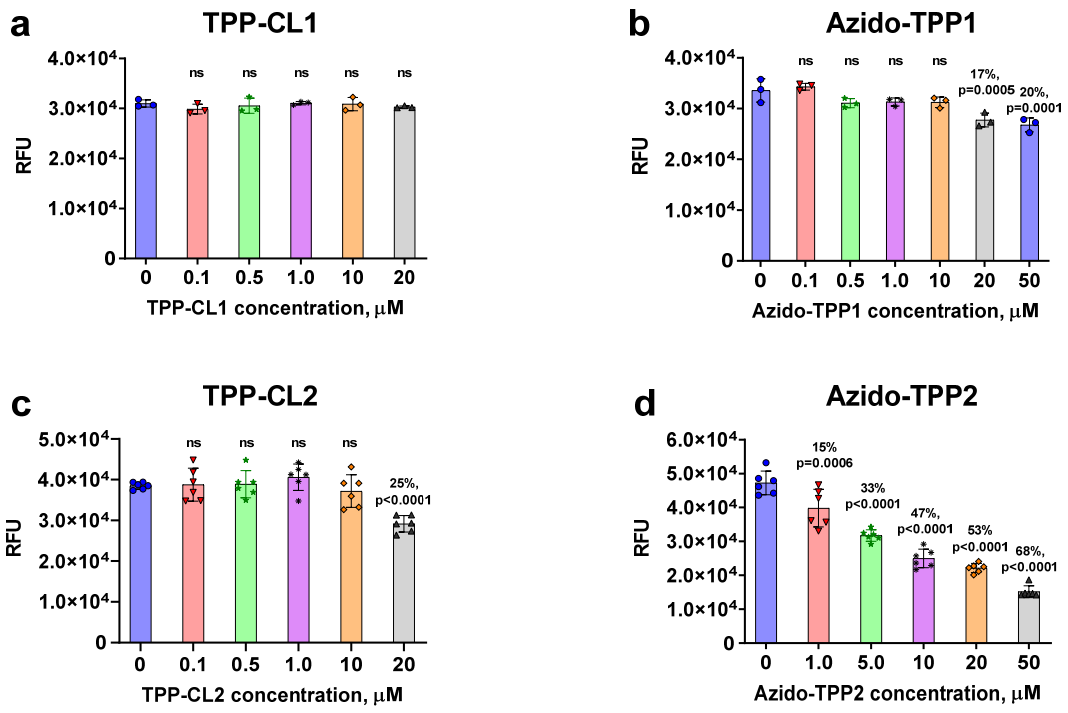

Supplementary Figure 5. Investigation of the influence of MAL reagents on ΔΨm level in live cells measured by TMRM assay **a**. The effect of TPP-CL1 on the ΔΨm levels measured by TMRM assay[1, 2]. No detectable effects on ΔΨm levels was observed in all the tested concentrations. n =3. **b**. The effect of azido-TPP1 on the ΔΨm levels measured by TMRM assay[1, 2]. The data indicate that azido-TPP1 results in only mild depolarization of mitochondria starting from a concentration of 20 μM, that are much higher than used in the MAL assay. n = 3. **c**. The effect of TPP-CL2 on the ΔΨm level measured by TMRM assay. No detectable effects on ΔΨm levels was observed in all the tested concentrations. n = 6. **d**. The effect of azido-TPP2 on the ΔΨm levels measured by TMRM assay. n = 6. Percentage over bars represent a decrease of fluorescent signal relative to control. Data in **a-d** are presented as mean ± SD. p values were calculated by one-way ANOVA with Dunnett's multiple comparisons test, ns – p>0.05. n values represent number of independent biological replicates. All presented experiments were repeated independently twice.

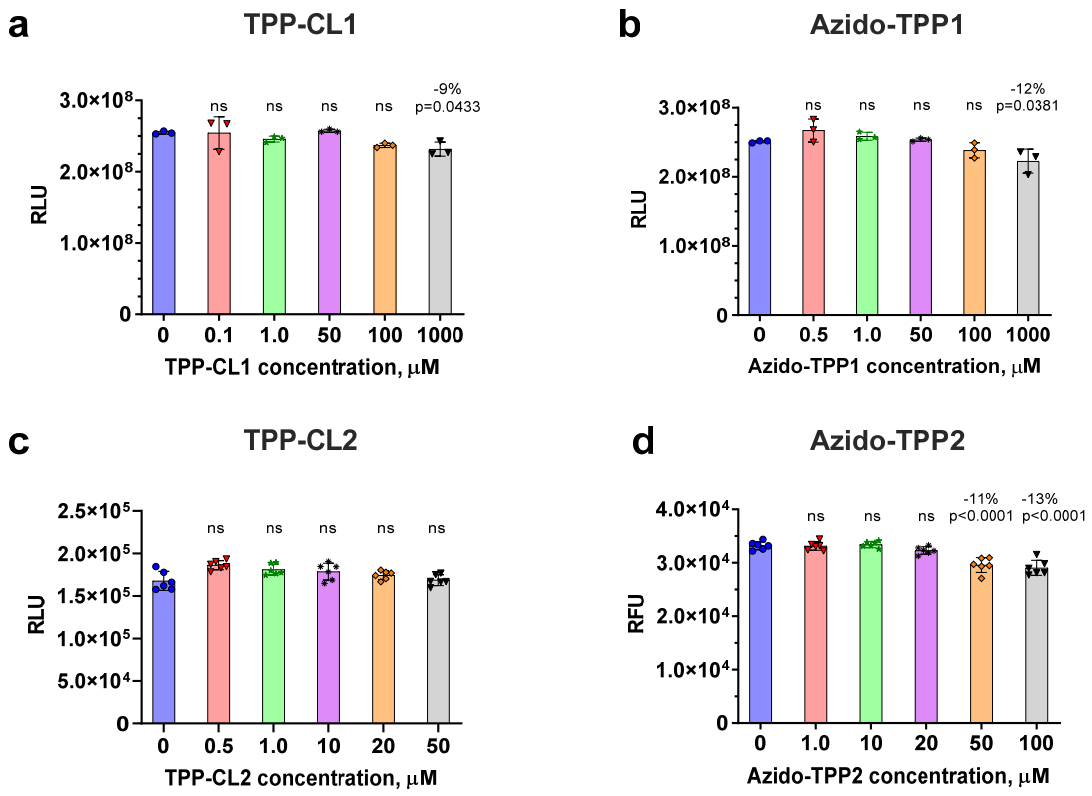

Supplementary Figure 6. Influence of MAL reagents on viability of HT-1080-luc cells. **a**. The effect of TPP-CL1 on cell viability. Only mild effect was observed at concentration as high as 1000 μM. n = 3. **b**. The effect of azido-TPP1 on cell viability. n = 3. **c**. The effect of TPP-CL2 on cell viability measured. n = 6. **d**. The effect of azido-TPP2 on cell viability. n = 6.

Results in **a-c** were obtained using CellTiter Glo assay (Promega), results in **d** were generated using Alamar Blue assay. Percentage over bars represent a decrease of fluorescent signal relative to control. Data presented as mean ± SD. p values were calculated by one-way ANOVA with Dunnett's multiple comparisons test, ns – $p>0.05$. n values represent number of independent biological replicates. All presented experiments were repeated independently twice.

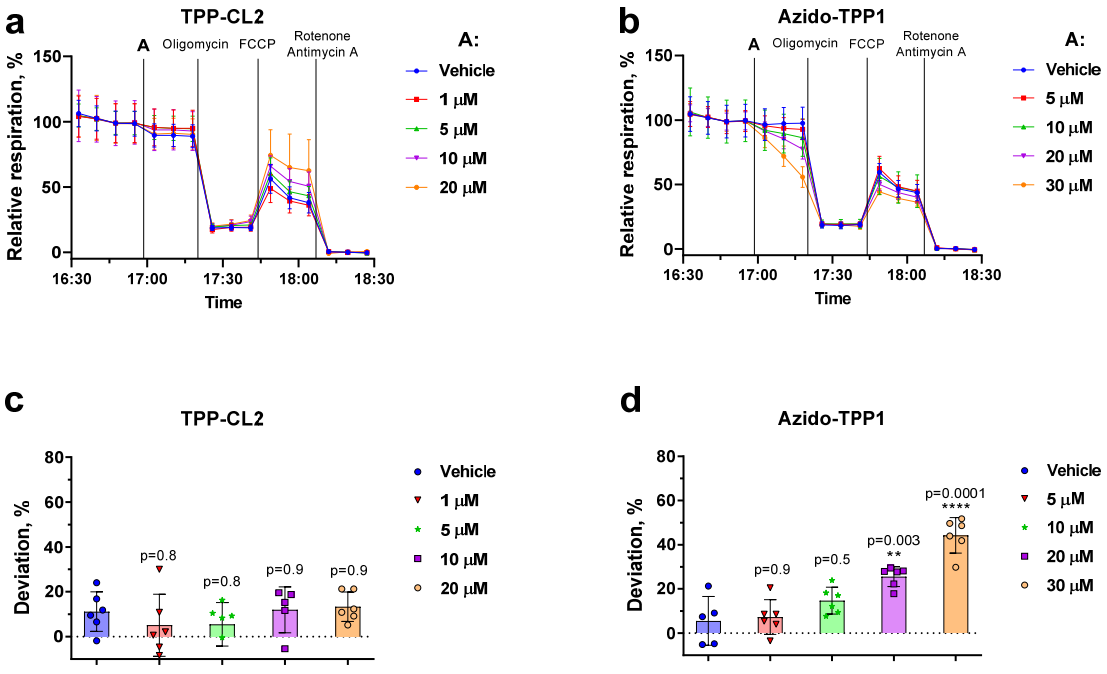

Supplementary Figure 7. Dose dependent effect of MAL3 components on basal respiration of HT-1080-luc cells. **a**. Effect of TPP-CL2 at various concentrations on respiration rate. n = 6. **b**. Effect of azido-TPP1 at various concentrations on respiration rate. Relative respiration is plotted over time. Lines mark addition of a corresponding compound which name is indicated above the line. n = 6. **c**. Deviation of relative OCR 21 min after addition of TPP-CL2 or vehicle (0.5% DMA in KRBH) from average basal level. n = 6. **d**. Deviation of relative OCR 21 min after addition of azido-TPP1 or vehicle (KRBH) from average basal level. n = 6. Data are presented as mean ± SD, n values represent number of independent biological replicates. P values were calculated by one-way ANOVA with Dunnett's multiple comparisons test. All presented experiments were repeated independently twice.

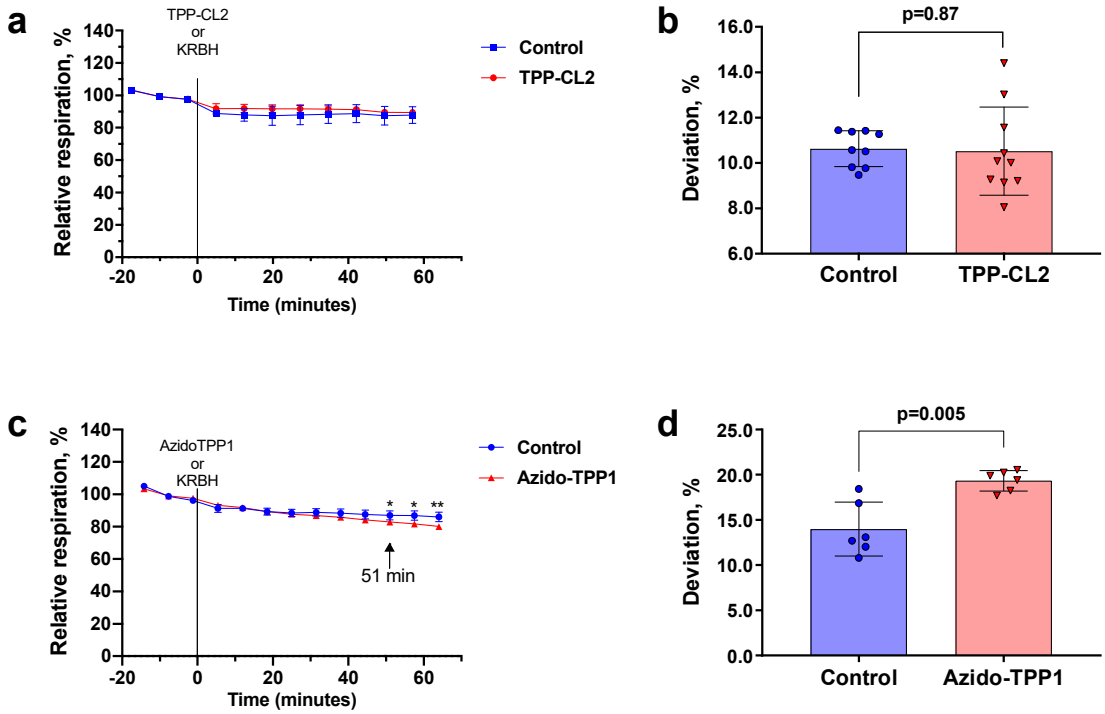

Supplementary Figure 8. Effect of MAL3 probe components on basal respiration of HT-1080-luc cells monitored for 1 hour. **a**. Relative respiration over time of the cells incubated with 5 µM TPP-CL2 for 1 hour. n = 9. **b**. Deviation of relative respiration 1 h after addition of TPP-CL2 or vehicle (KRBH) from average basal level. Data are presented as mean ± SD, n = 9. p value was calculated by two tailed t-test. **c.** Relative respiration over time of the cells incubated with 10 µM azido-TPP1 for 65 min. n = 6. * - $p<0.05$, ** - $p<0.01$; p = 0.0314 for 51 min, p = 0.0149 for min 58, p = 0.0078 for 65 min by two-way ANOVA with Dunnett's multiple comparisons test. **d**. Deviation of relative respiration 65 min after addition of azido-TPP1 or vehicle (KRBH) from average basal level. n = 6. p value was calculated by two tailed t-test. Data for panels **a**-**d** are presented as mean ± SD. n values represent number of independent biological replicates. All presented experiments were repeated independently twice.

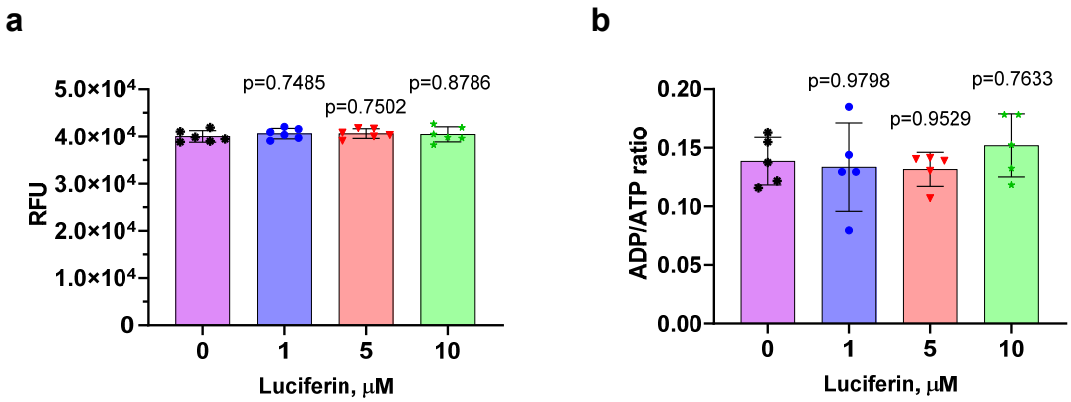

Supplementary Figure 9. Investigation of potential influence of luciferin (1-10 μM) on ΔΨm and ADP/ATP ratio in HT-1080 cells **a.** Influence of various concentrations of luciferin on ΔΨm measured by TMRM. HT-1080-luc cells were incubated in media supplemented with luciferin and 50 nM TMRM for 45 min followed by signal acquisition. **b**. Influence of various concentrations of luciferin on ADP/ATP ratio in HT-1080 cells measured by commercial kit (Abcam, ab65313). p values were calculated by one-way ANOVA with Dunnett's multiple comparisons test. Data are presented as mean ± SD, n=6 in **a**, n=5 in **b**. n values represent number of independent biological replicates in single experiment. All presented experiments were repeated independently twice.

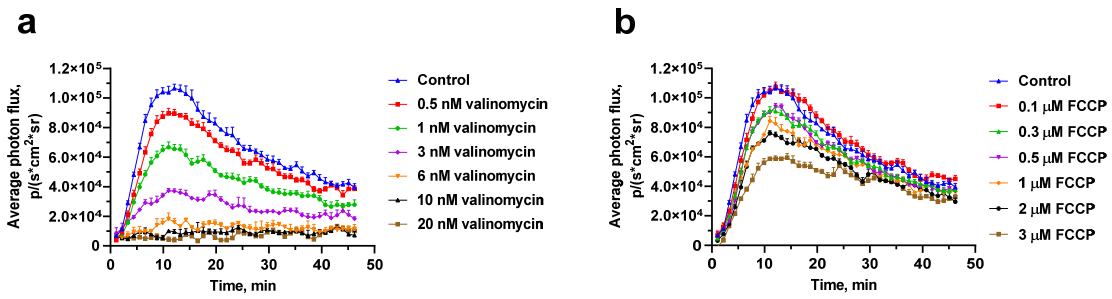

Supplementary Figure 10. Effect of valinomycin or FCCP on signal of MAL3 probe from HT-1080-luc cells. **a.** bioluminescent signal plotted over time from the cells treated with various concentrations of valinomycin (0.5 nM – 20 nM). **b.** bioluminescent signal plotted over time from the cells treated with various concentrations of FCCP (0.1 μM – 3 μM). Data for each time point are presented as mean ± SD. n=6 (independent biological replicates). Total photon flux data obtained by integrating the kinetic curves in **a** and **b** is shown in **Fig. 2 b, d**. All presented experiments were repeated independently three times.

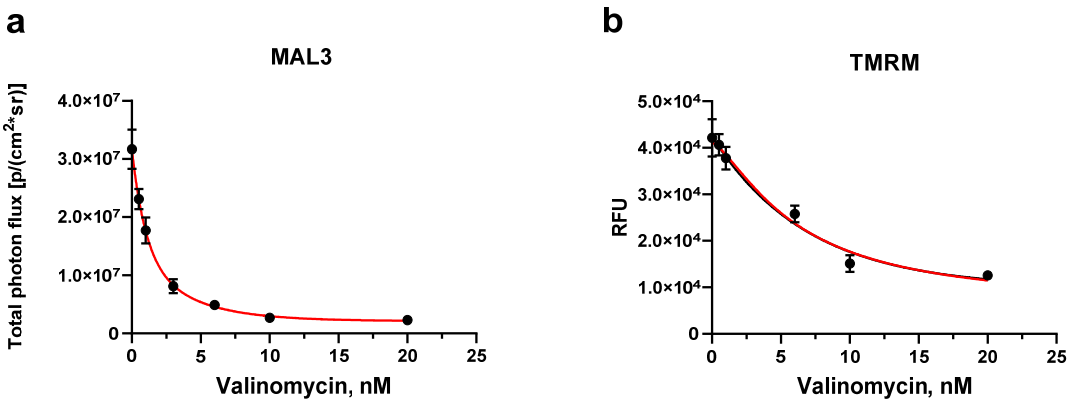

Supplementary Figure 11. Dose dependent effect of depolarizers on signal from MAL3 or TMRM resulted from HT-1080-luc cells. **a**. Effect of various concentrations of valinomycin on MAL3 signal. **b.** Effect of various concentrations of valinomycin on TMRM fluorescent signal. These data are the same as in Figure 2 b, c and presented in a different way; double exponential decay curve was fit in (red line, $R^2 = 0.97$). Data presented as mean ±SD, n= 3 for **a** and **b** (independent biological samples). All presented experiments were repeated independently twice.

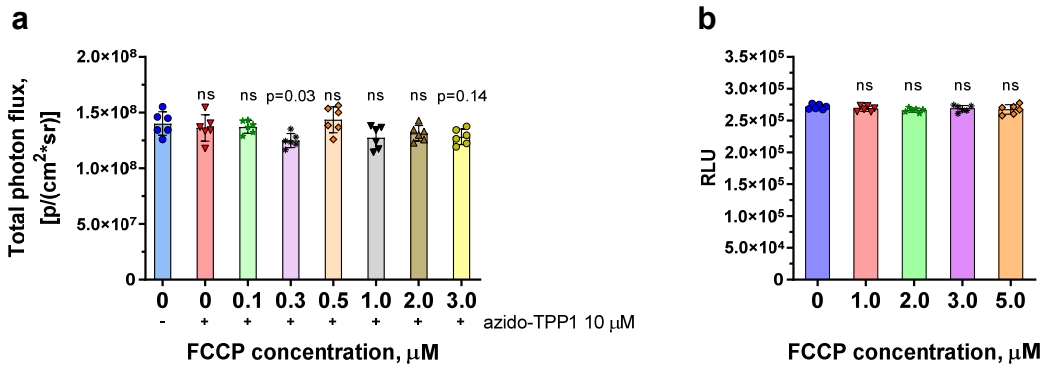

Supplementary Figure 12. Influence of FCCP treatment on luciferase activity and viability of HT-1080-luc cells. **a.** Total photon flux from HT-1080-luc cells after preincubation of cells with FCCP (various concentrations) for 1 hour, washing and addition of medium supplemented with 5 µM luciferin ± 10 µM azido-TPP1 ± FCCP (various concentrations). Data are presented as mean ± SD, n = 6. **b.** The influence of FCCP (1h incubation) on cell viability was determined using the CellTiter-Glo assay (Promega) according to manufacturer's instruction. Data are presented as mean ± SD, n = 6.

n values represent independent biological replicates. p values were calculated by one-way ANOVA with Dunnett's multiple comparisons test, ns – $p>0.05$. All presented experiments were repeated independently twice.

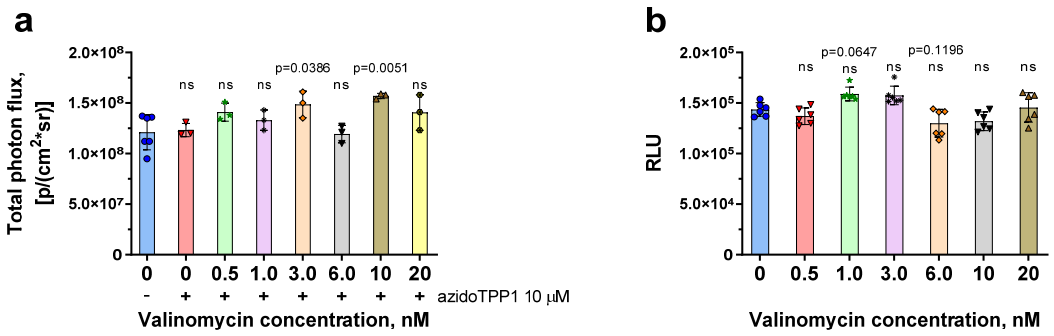

Supplementary Figure 13. Influence of valinomycin on luciferase activity and viability of HT-1080-luc cells. **a**. Total photon flux from HT-1080-luc cells after preincubation of cells with various concentrations of valinomycin for 1 hour, washing and addition of medium containing 5 µM luciferin ± 10 µM azido-TPP1 ± valinomycin (various concentrations). Data are presented as mean ± SD, n = 6 for luciferin only and n = 3 for all other conditions. **b.** The influence of valinomycin (1 h incubation) on cell viability was determined using the CellTiter-Glo assay (Promega) according to manufacturer's instruction. Data are presented as mean ± SD, n = 6.

p values were calculated by one-way ANOVA with Dunnett's multiple comparisons test, ns – p>0.05. n values represent independent biological replicates. All presented experiments were repeated independently twice.

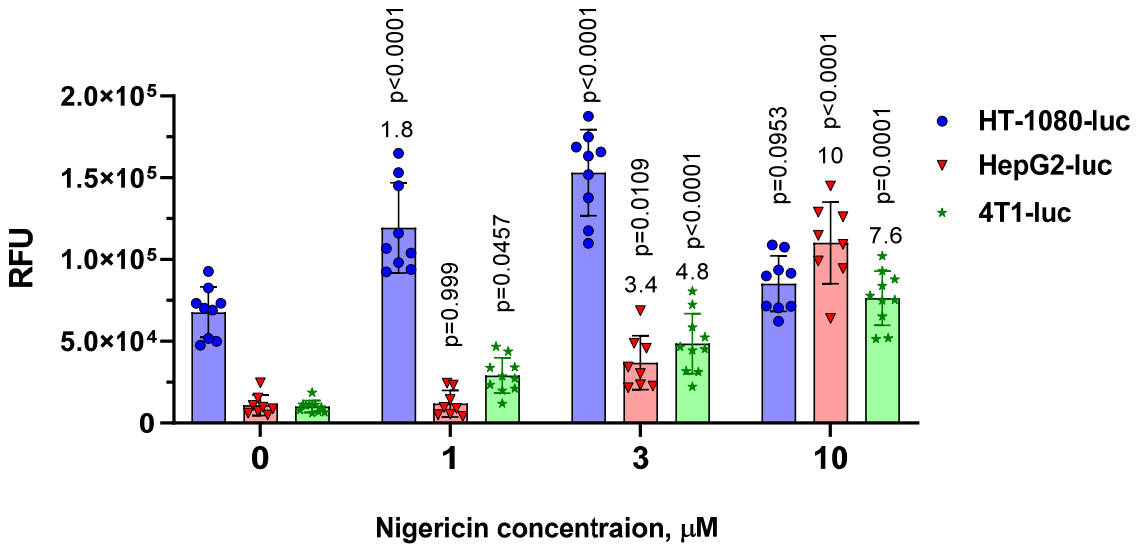

Supplementary Figure 14. The effect of nigericin on different cell lines was measured using TMRM. Cells were incubated in HBSS supplemented with 30 nM TMRM ± nigericin (1-10 μM) for 1 hour at 37 °C, then washed with HBSS that was followed by fluorescence signal measurement on Tecan M1000 plate reader. The values represent the mean ± SD (n = 3). Numbers above bars represent fold difference of signal induced by nigericin. *p* values were calculated by two-way ANOVA with Dunnett's multiple comparisons test. n values represent independent biological replicates. The presented experiment was repeated independently twice.

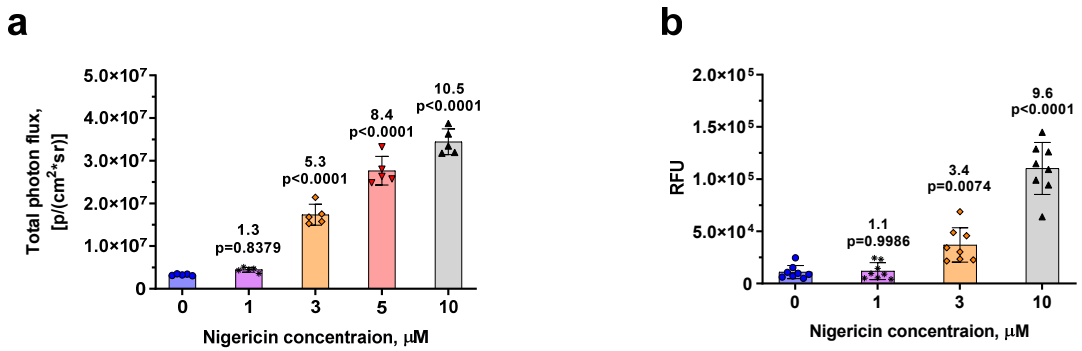

Supplementary Figure 15. Imaging and quantification of nigericin-induced hyperpolarization of mitochondria by MAL3 and TMRM assays in HepG2-luc cells. **a**. Monitoring of ΔΨm levels with MAL3 based assay. The total photon flux values were obtained by integrating the kinetic curves over 50 min. The Z' factor = 0.69, n=5. **b**. Measurement of ΔΨm levels by TMRM based assay[1, 2]. The Z' factor = 0.29, n=10. The values represent the mean ± SD and the experiments were performed on two separate occasions. The numbers above the bars represent the fold increase of signal as compared to the control group. P values were calculated by one-way ANOVA with Dunnett's multiple comparisons test. n values represent independent biological replicates in single experiment. All presented experiments were repeated independently twice.

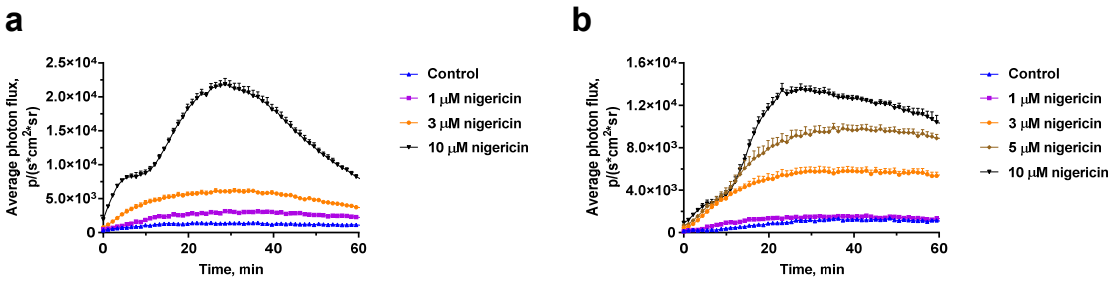

Supplementary Figure 16. Dose-dependent effect of nigericin on signal of MAL3 probe from 4T1-luc or HepG2-luc cells. **a.** Bioluminescent signal plotted over time from 4T1-luc cells incubated with 1-10 µM of nigericin. **b.** Bioluminescent signal plotted over time from HepG2-luc cells incubated with 1-10 µM of nigericin. Data for each time point are presented as mean ± SD, n=5 (independent biological replicates). All presented experiments were repeated independently twice.

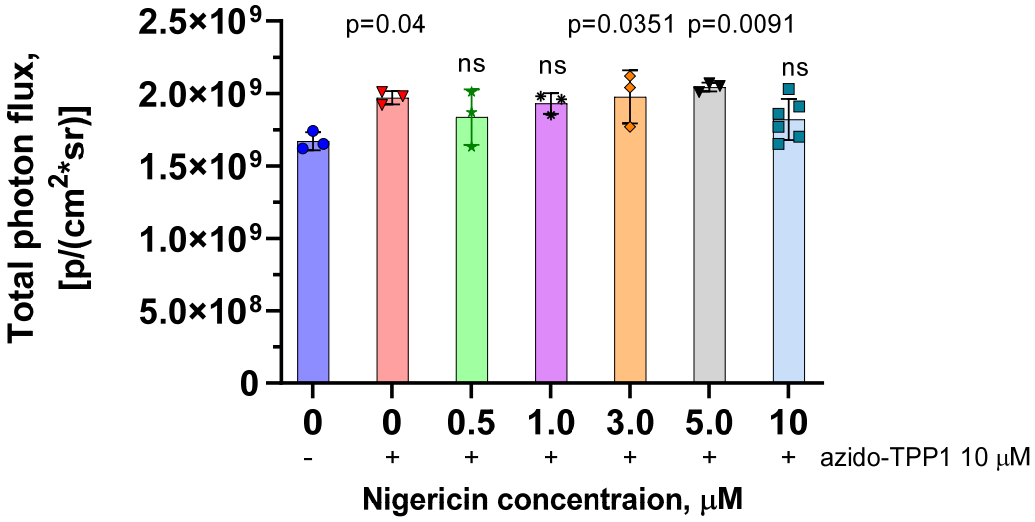

Supplementary Figure 17. Investigation of nigericin effect on luciferase activity in 4T1-luc cells. Total photon flux from 4T1-luc cells after preincubation with various concentrations of nigericin for 1 h, followed by washing with PBS (1x), and addition of medium containing 5 μM luciferin ± 10 μM azido-TPP1 ± nigericin (0.5-10 μM). Data are presented as mean ± SD, n = 3. ns - $p > 0.05$ by one-way ANOVA with Dunnett's multiple comparisons test. n values represent independent biological replicates in single experiment. The presented experiment was repeated independently twice.

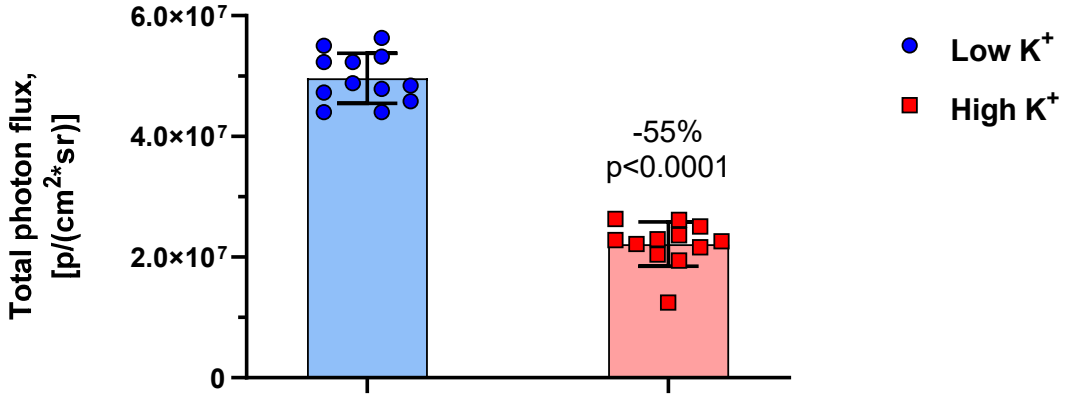

Supplementary Figure 18. Total photon flux over 1 h resulting from HT-1080-luc cells incubated with MAL3 probe in low K^+ and high K^+ medium. Data are presented as mean ± SD, n=12. Total photon flux from the cells in high K^+ medium was 55% lower. P value was calculated by two tailed t test. n values represent independent biological replicates in single experiment. The presented experiment was repeated independently twice.

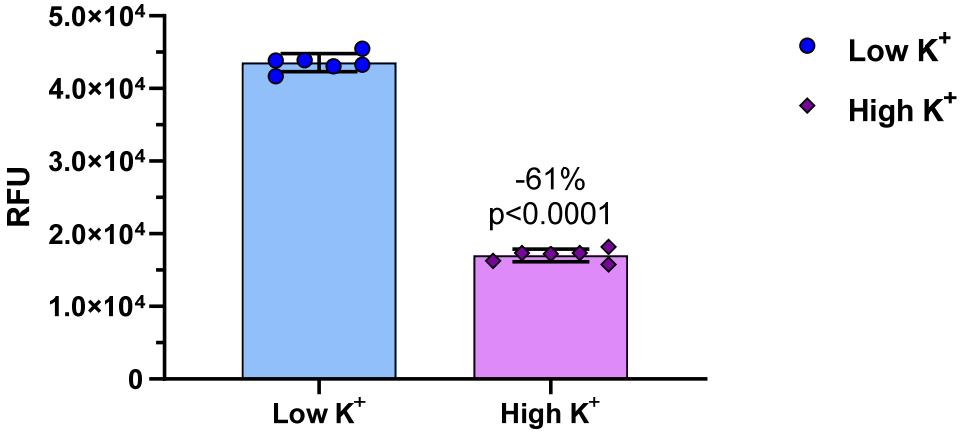

Supplementary Figure 19. Fluorescence signal from HT-1080-luc cells in incubated with 50 nM TMRM in either low or high K^+ medium. Data are presented as mean ± SD, n=6. RFU from the cells in high K^+ medium was 61% lower. P value was calculated by two tailed t-test. n values represent independent biological replicates in single experiment. The presented experiment was repeated independently twice.

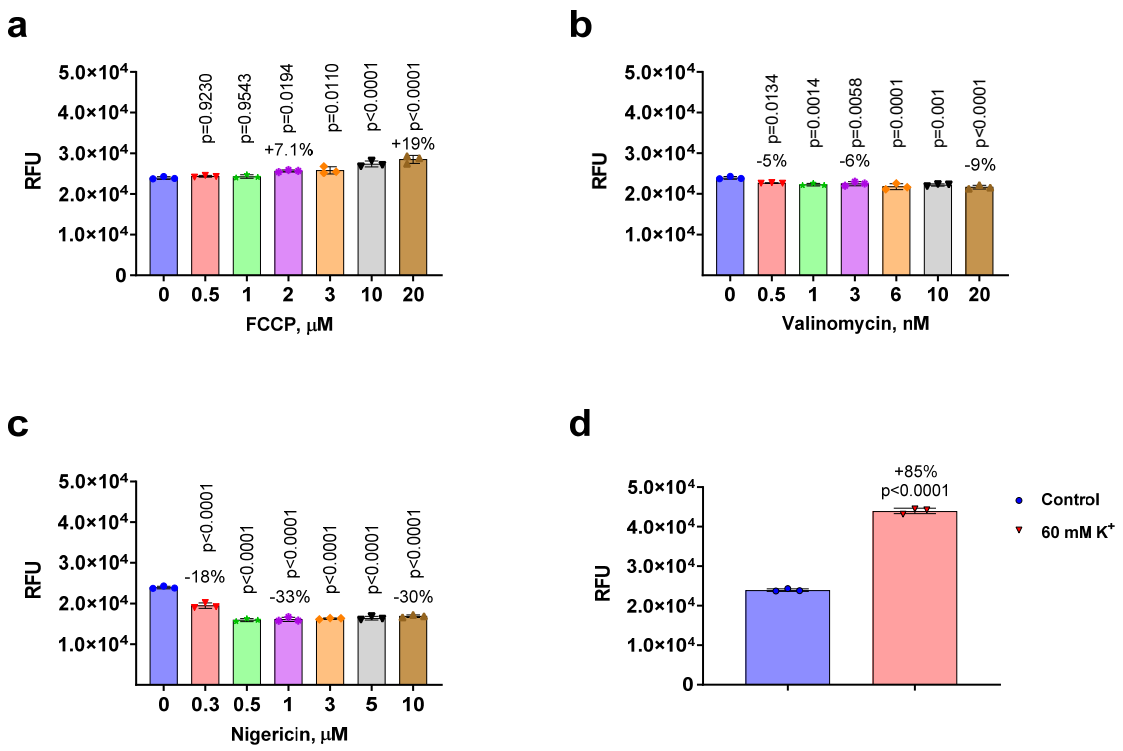

Supplementary Figure 20. Dose-dependent effect of FCCP (**a**), valinomycin (**b**) and nigericin (**c**) on ΔΨp of HT-1080-luc cells. Medium supplemented with 60 mM K^+ concentration was used as positive control (**d**). The resulting fluorescent signal was measured after 50 min of incubation of the cells with various concentrations of abovementioned compounds. Changes in ΔΨp were monitored using membrane potential evaluation assay kit (Molecular Devices, USA) according to the manufacturer instructions (Ex.: 488, Em.: 540-590 nm). Data are presented as mean ± SD. n = 3 (**a-d**). p values were calculated by one-way ANOVA with Dunnett's multiple comparisons test (**a-c**) or two-tailed t test (**d**). n values represent number of independent biological replicates. All presented experiments were repeated independently twice.

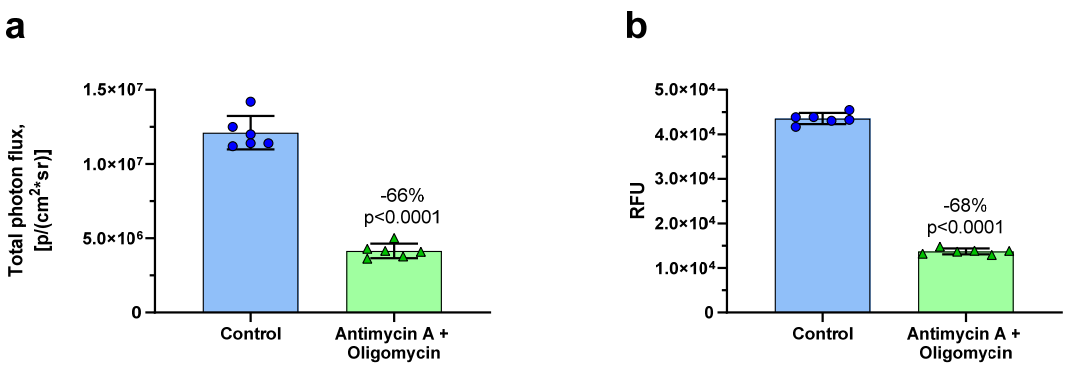

Supplementary Figure 21. Effect of ETC inhibition by mixture of 7 µM oligomycin with 10 µM antimycin on the signal from either MAL3 probe (**a**) or TMRM (**b**) in HT-1080-luc cells. Data are presented as mean ± SD, n = 6 (**a, b**). p values were calculated by two-tailed t test. n values represent independent biological replicates in single experiment. All presented experiments were repeated independently twice.

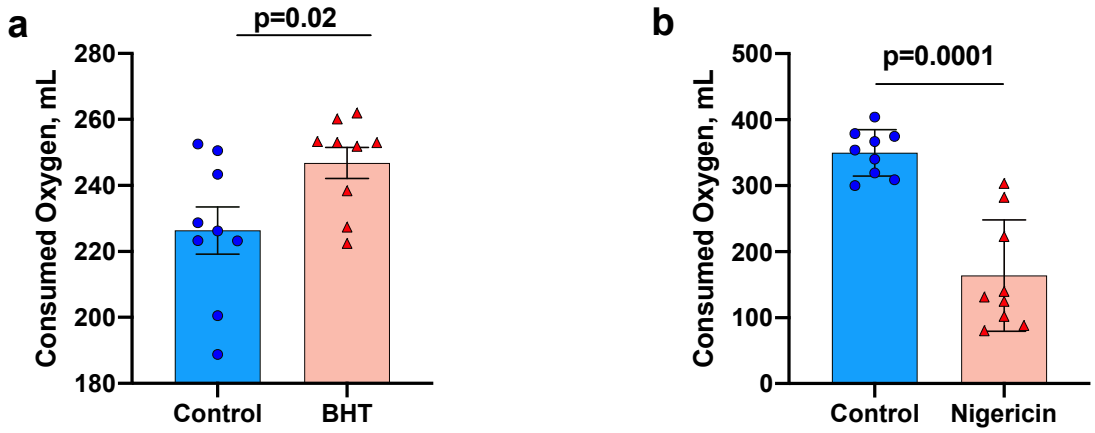

Supplementary Figure 22. Total oxygen consumption upon treatment of FVB-luc+ mice with BHT or nigericin. **a.** Effect of 60 mg/kg BHT vs vehicle (oral gavage of corn oil, 100 µL) on total amount of oxygen consumption by FVB-luc+ mice over 3 h. n = 9. **b.** Effect of 3.2 mg/kg of nigericin vs vehicle (i.p. injection of 0.1% BSA in PBS, 100 µL) on total amount of oxygen consumption by FVB-luc+ mice over 3 h. n = 9. Data in **a** and **b** are presented as mean ± SEM. n – number of biologically independent samples in single experiment. p values were calculated using two sided Mann-Whitney test. All presented experiments were performed once.

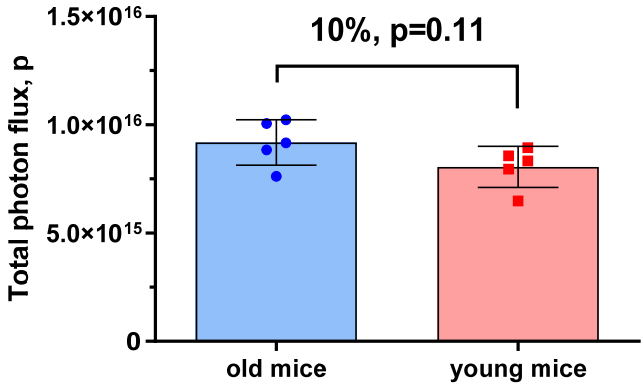

Supplementary Figure 23. Total phonon flux (AUC over 1 h) after injection of luciferin (high dose) from young and old FVB-luc+ mice used in the experiments described in "Imaging and quantification of age-related mitochondria depolarization" Results section of the manuscript. All mice received an i.p. injection of 200 µL of 100 mM luciferin potassium salt solution in PBS, followed by 1 h of signal quantification using IVIS Spectrum. n = 5, independent biological replicates. Data are presented as mean ± SD. p value was calculated by two-tailed t-test. The presented experiment was repeated independently twice.

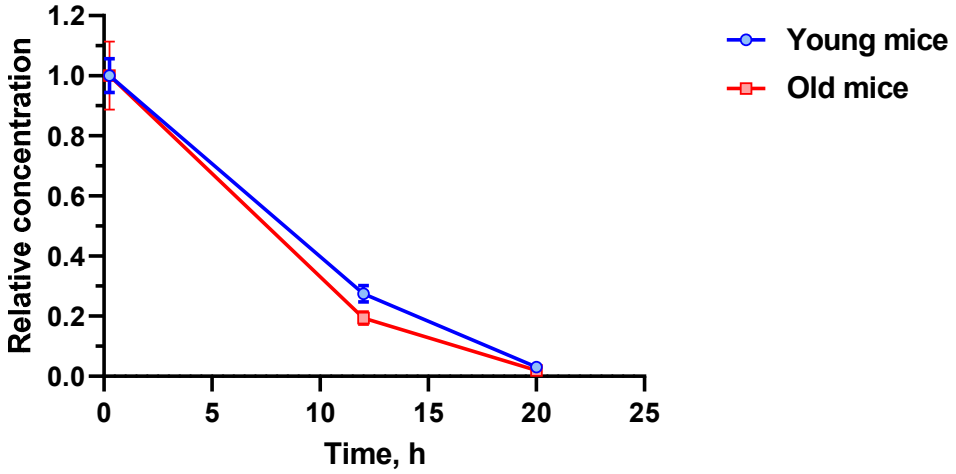

Supplementary Figure 24. Clearance of TPP-CL2 from plasma of old (>80 weeks, n=3) and young FVB-luc+ mice (<30 weeks, n=3). Data are presented as mean ± SD. n values represent number of independent biological replicates. The presented experiment was repeated independently twice.

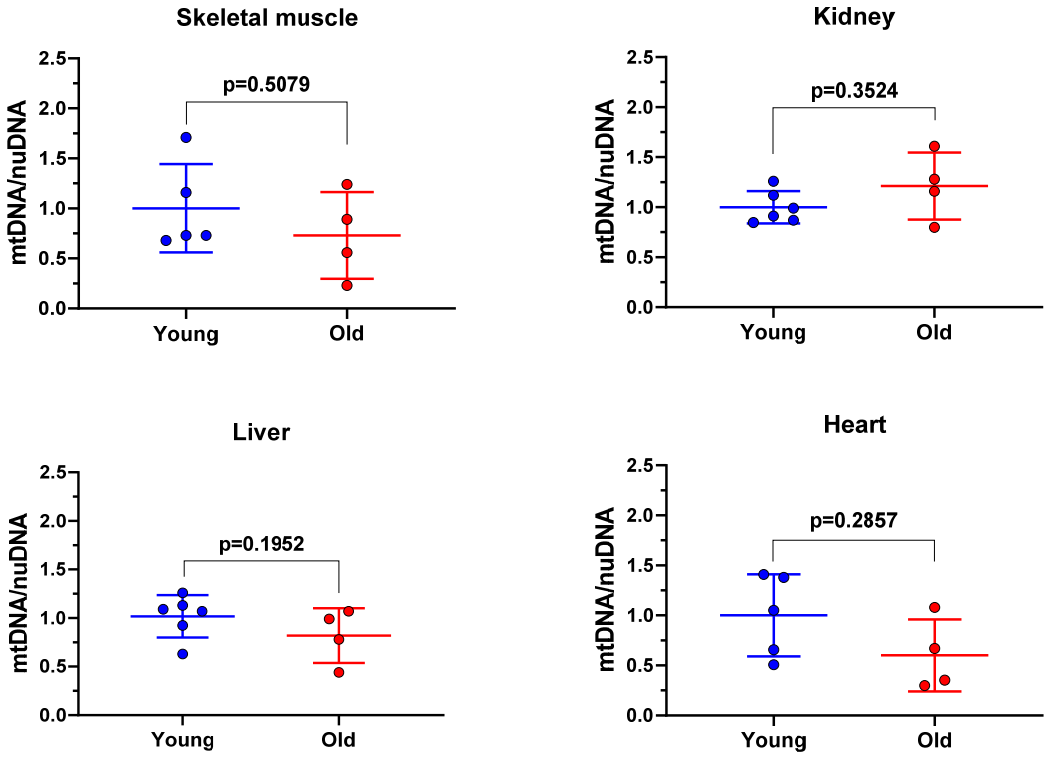

Supplementary Figure 25. Comparison of mtDNA/nuDNA ratio in various organs of young (13 weeks) and old (>90 weeks) FVB-luc+ mice. n=6 (young mice), n=4 (old mice). Data are presented as mean ± SD. n values represent independent biological replicates in single experiment. p values were calculated by two sided Mann-Whitney test. The presented experiment was repeated independently twice.

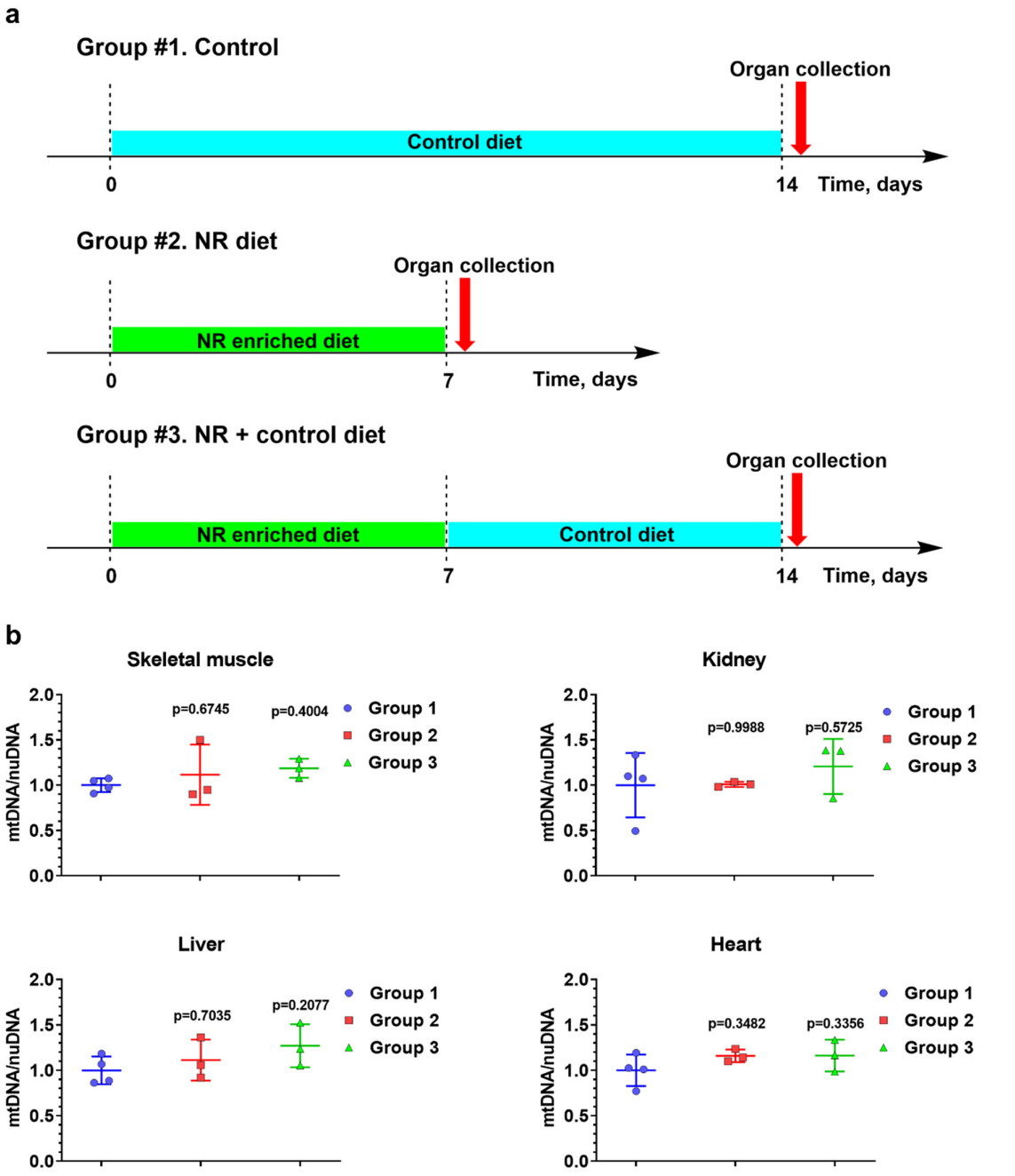

Supplementary Figure 26. a. The experimental outline for the measurements of ΔΨm levels in the study of NR-enriched diet induced mitobiogenesis. **b**. Ratios between mtDNA (mtco-1) and nuDNA (atp-5) in various organs for the three tested groups of FVB-luc+ mice described above. No significant difference between groups was detected by one-way ANOVA. n=4 (group1), n=3 (groups 2 and 3). n values represent independent biological replicates. Data are presented as mean ± SD. p values were calculated by one-way ANOVA with Dunnett's multiple comparisons test. The presented experiment was repeated independently twice.

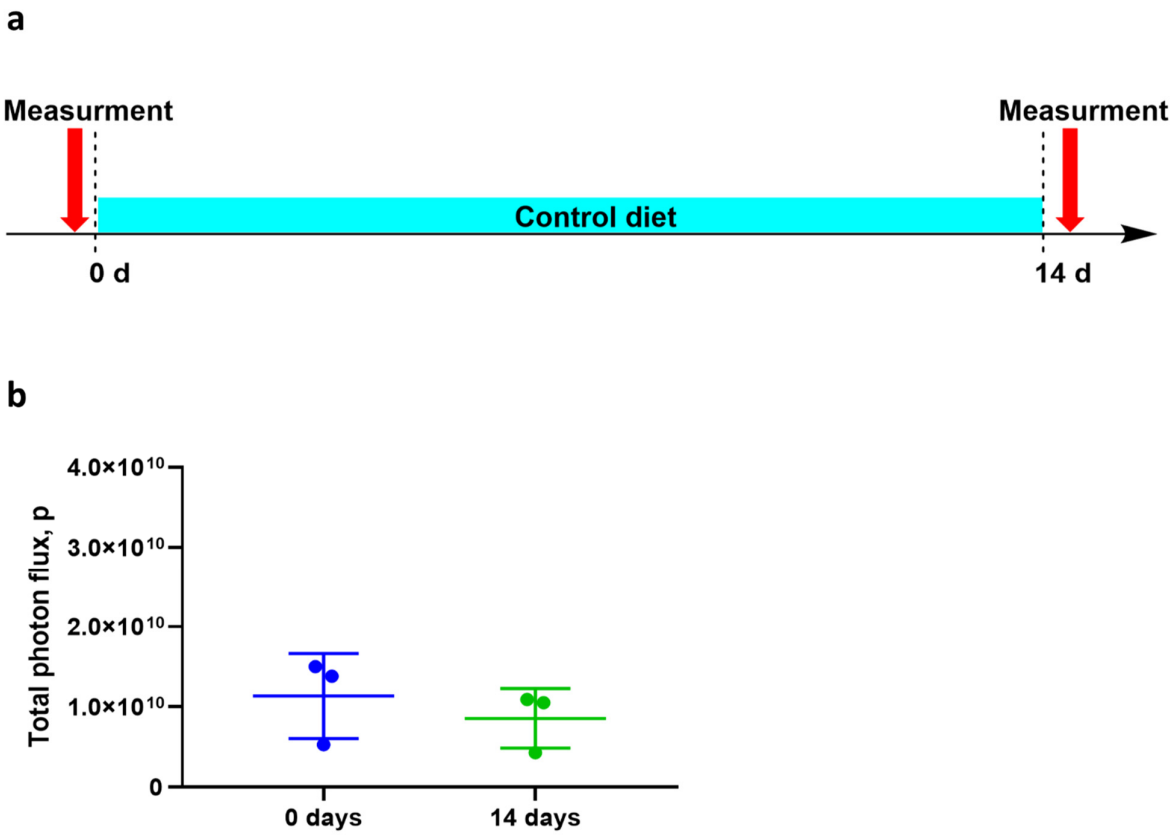

Supplementary Figure 27. a. The experimental outline for the measurements of ΔΨm levels in aged FVB-luc+ mice (90 weeks) using MAL3 probe fed by regular chow diet (control group). **b**. Total photon flux resulting from the aged mice administered MAL3 probe on Day 0 and Day 14 of the experiment, n = 3. Each point represents whole body light output from a mouse resulted from administration of MAL3 probe. n values represent independent biological replicates. Data are presented as mean ± SD. p>0.05 by two-tailed t test. The presented experiment was repeated independently twice.

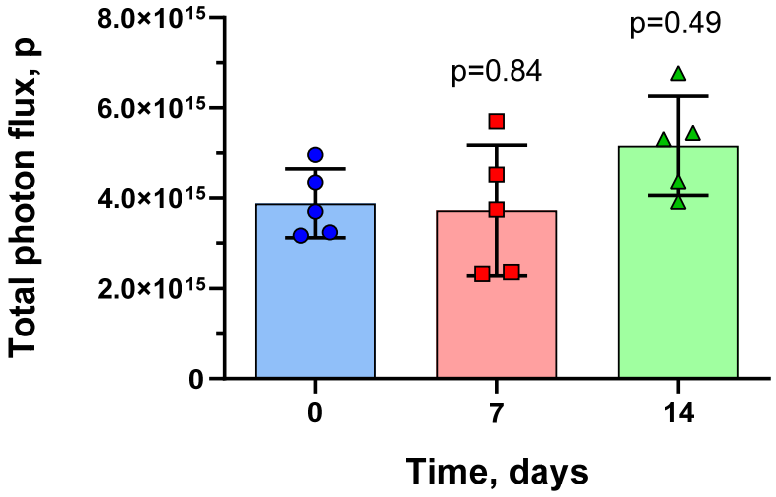

Supplementary Figure 28. Average total photon flux resulting from the group of 5 aged FVB+luc mice after injection of high dose of luciferin compound. The measurements were performed before the beginning of NR-enriched diet (0 days), right after the end of NR-enriched diet (7 days), and a week after the diet was changed back to control non-NR diet (14 days). Data are presented as mean ± SD (n = 5). p values were calculated using one-way ANOVA with Dunnett's multiple comparisons test. n values represent independent biological replicates in single experiment. The presented experiment was repeated independently twice.

References

1. Erlich-Hadad, T. et al. TAT-MTS-MCM fusion proteins reduce MMA levels and improve mitochondrial activity and liver function in MCM-deficient cells. *J Cell Mol Med* **22**, 1601-1613 (2018).
2. Zha, L. et al. The Histone Demethylase UTX Promotes Brown Adipocyte Thermogenic Program Via Coordinated Regulation of H3K27 Demethylation and Acetylation. *J Biol Chem* **290**, 25151-25163 (2015).

Supplementary Note 1. Equations

Equation 1. Ratio of concentrations of TPP cations or an azido-TPP or a TPP-CL in mitochondrion and cytosol (R_1). The Equation was derived from Nernst equation taking in account that T = 310 K

$$R_1 = \frac{[TPP_{mt}]}{[TPP_{cyto}]} \approx \frac{[AzidoTPP_{mt}]}{[AzidoTPP_{cyto}]} = \frac{[TPPCL_{mt}]}{[TPPCL_{cyto}]} = 10^{\frac{-\Delta\Psi\mathrm{m}}{61.4}},$$

$\Delta\Psi$m – mitochondrial membrane potential, mV

R_1 – ratio of concentrations of TPP ion (azido-TPP or TPP-CL) in mitochondrion and cytosol

$[TPP_{mt}]$ – concentration of TPP ion in mitochondrion, M

$[TPP_{cyto}]$ – concentration of TPP ion in cytosol, M

Equation 2. Ratio of concentrations of TPP cations in cytosol and extracellular medium (R_2).

$$R_2 = \frac{[TPP_{cyto}]}{[TPP_0]} = 10^{\frac{-\Delta\Psi p}{61.4}}$$

$[TPP_0]$ – concentration of TPP ion in extracellular medium, M

$\Delta\Psi p$ – plasma membrane potential, mV

Equation 3. Ratio of concentrations of TPP cations in mitochondrion and extracellular medium (R_3).

$$R_3 = \frac{[TPP_{mt}]}{[TPP_0]} = \frac{R_2[TPP_{mt}]}{[TPP_{cyto}]} = R_1R_2 = 10^{\frac{-\Delta\Psi m-\Delta\Psi p}{61.4}}$$

Equation 4. Reaction rate enhancement in mitochondrial matrix compared to extracellular medium.

$$\frac{\upsilon_{mt}}{\upsilon_0} = \frac{k[AzidoTPP_{mt}][TPPCL_{mt}]}{k[AzidoTPP_0][TPPCL_0]} = \frac{R_3^2[AzidoTPP_0][TPPCL_0]}{[AzidoTPP_0][TPPCL_0]} = R_3^2 = 10^{\frac{2(-\Delta\Psi\mathrm{m}-\Delta\Psi\mathrm{p})}{61.4}} = 10^{\frac{-\Delta\Psi\mathrm{m}-\Delta\Psi\mathrm{p}}{30.7}},$$

υ_{mt} – rate of luciferin release in mitochondrion matrix, M*s^{-1}

υ_0 – rate of luciferin release in cytosol, M*s^{-1}

k – reaction rate constant, M^{-1}*s^{-1}

R_3 – ratio of concentrations of a TPP ion (azido-TPP or TPP-CL) in mitochondrion matrix and extracellular medium

According to the **Eq. 4** the reaction rate increases 10-fold per each 30.7 mV of -$\Delta\Psi$m-$\Delta\Psi$p. Since the normal range of $\Delta\Psi$m is -120 – -180 mV and $\Delta\Psi$p is -30 – -70 mV, the reaction rate will increase in mitochondrion 10^5 – 10^8 fold.

Reaction rate enhancement is independent from mitochondrial volume and cellular volume. However, contribution of mitochondria in total amount of produced luciferin must depend on mitochondrial volume density, i.e. volume of cytoplasm occupied by mitochondria. **Eq. 5** below shows ratio of luciferin produced in mitochondria and in cytosol

Equation 5.

$$\frac{n_{mt}}{n_{cyto}} = \frac{\upsilon_{mt} V_{mt}}{\upsilon_{cell} V_{cyto}} = \frac{\upsilon_{mt}}{\upsilon_{cyto}} 10^{x} \quad = R_1^2\, 10^{x} = 10^{\frac{-\Delta\Psi m + 30.7x}{30.7}}$$

Where

$x = \log_{10}(\frac{V_{mt}}{V_{cyto}}), x < 0$

$\frac{n_{mt}}{n_{cell}}$ – ratio of luciferin amount formed in mitochondria to luciferin amount formed in cytosol

If $\Delta\Psi m$ is -100 mV, the minimal ratio between mitochondrial and cytosolic volumes required to get equal contribution of mitochondria and cytosol is 0.055%. Unfortunately, it is hard to measure the ratio of mitochondria volume to cytosol volume because it requires to measure volume of all existing organelles in a cell. However, it is way easier to quantify volume of cytoplasm occupied by mitochondria, i.e. mitochondrial volume density. It depends greatly on a cell type and species[1,2], for example it reaches 35% cardiomyocytes [3], 5% in astrocytes[4], 8% in perineuronal satellite cells[5], 18% in hepatocytes[6]. Due to obvious reasons the mitochondrial volume density must be lower than the ratio between mitochondrial and cytosolic volumes. Therefore, to get equal contribution of mitochondria and cytosol in formation of luciferin mitochondrial volume density must be even lower than 0.055% if $\Delta\Psi m$ is -100 mV.

Likewise, total photon flux from a well containing cells depends on volume of the cells and extracellular media volume.

Equation 6

$$\frac{n_{cells}}{n_0} = \frac{\upsilon_{cells} V_{cells}}{\upsilon_0 V_0} = \frac{N(\upsilon_{cell} V_{cell})}{\upsilon_0 V_0} = \frac{\upsilon_{cell}}{\upsilon_0} N \frac{V_{cell}}{V_0}$$

Where N – number of cells per well, V_{cell} – volume of one cell, υ_{cell} – rate of the reaction in one cell, n_0 – amount of luciferin formed in extracellular media, V_0 – volume of extracellular media, υ_0 – rate of the reaction in extracellular media.

If we estimate the volume of an average mammalian cell around 1 pL[7-9], number of cells from 1 *10^4 to 5*10^4 and volume of extracellular media as 100 µL, which is typical for a 96-well plate, **Eq.7** can be transformed in following way.

Equation 7

$$\frac{n_{cells}}{n_0} = \frac{v_{cell}}{v_0}\frac{y \times 10^4 \times 10^{-12}}{10^{-4}} = y \times 10^{-4}\frac{v_{cell}}{v_0}.$$

$$y \in [1; 5]$$

Since $v_{cell} \approx v_{mt} + v_{cyto}$,

$$\frac{n_{cells}}{n_0} = y \times 10^{-4}\frac{v_{mt} + v_{cyto}}{v_0} = y \times 10^{-4}(R_3^2 + R_2^2) = y \times 10^{-4}\left(10^{\frac{-\Delta\Psi\mathrm{m}-\Delta\Psi\mathrm{p}}{30.7}} + 10^{\frac{-\Delta\Psi p}{30.7}}\right)$$
$$= y\left(10^{\frac{-\Delta\Psi\mathrm{m}-\Delta\Psi\mathrm{p}}{30.7}-4} + 10^{\frac{-\Delta\Psi p}{30.7}-4}\right)$$

According to **Eq. 7** then luciferin production in cells of a well is 7-fold higher than in extracellular medium If $\Delta\Psi m$ is -120 mV, $\Delta\Psi p$ is -30 mV, y=1.

References

1 Massaro, G. D., Gail, D. B. & Massaro, D. Lung oxygen consumption and mitochondria of alveolar epithelial and endothelial cells. *J Appl Physiol* **38**, 588-592, doi:10.1152/jappl.1975.38.4.588 (1975).

2 Else, P. L. & Hulbert, A. J. An allometric comparison of the mitochondria of mammalian and reptilian tissues: The implications for the evolution of endothermy. *Journal of Comparative Physiology B* **156**, 3-11, doi:10.1007/BF00692920 (1985).

3 Urschel, M. R. & Brien, K. M. High mitochondrial densities in the hearts of Antarctic icefishes are maintained by an increase in mitochondrial size rather than mitochondrial biogenesis. *Journal of Experimental Biology* **211**, 2638, doi:10.1242/jeb.018598 (2008).

4 Ju, W.-K. *et al.* Increased mitochondrial fission and volume density by blocking glutamate excitotoxicity protect glaucomatous optic nerve head astrocytes. *Glia* **63**, 736-753, doi:10.1002/glia.22781 (2015).

5 Martinelli, C., Sartori, P., Ledda, M. & Pannese, E. Age-related quantitative changes in mitochondria of satellite cell sheaths enveloping spinal ganglion neurons in the rabbit. *Brain Research Bulletin* **61**, 147-151, doi:https://doi.org/10.1016/S0361-9230(03)00101-1 (2003).

6 Krähenbühl, S., Krähenbühl-Glauser, S., Stucki, J., Gehr, P. & Reichen, J. Stereological and functional analysis of liver mitochondria from rats with secondary biliary cirrhosis: impaired mitochondrial metabolism and increased mitochondrial content per hepatocyte. *Hepatology* **15**, 1167-1172 (1992).

7 Puck, T. T., Marcus, P. I. & Cieciura, S. J. Clonal growth of mammalian cells in vitro; growth characteristics of colonies from single HeLa cells with and without a feeder layer. *J Exp Med* **103**, 273-283, doi:10.1084/jem.103.2.273 (1956).

8 Krombach, F. *et al.* Cell size of alveolar macrophages: an interspecies comparison. *Environ Health Perspect* **105 Suppl 5**, 1261-1263, doi:10.1289/ehp.97105s51261 (1997).

9 Frisch, T. & Thoumine, O. Predicting the kinetics of cell spreading. *J Biomech* **35**, 1137-1141, doi:10.1016/s0021-9290(02)00075-1 (2002).

Supplementary Note 2. Chemical Synthesis and Characterization of MAL Probes

Materials and methods

General materials and methods

HPLC analysis was performed on an Agilent Infinity 1260 HPLC system with a Waters SunFire C18 3.5 µm, 2.1 x 20 mm column. The products of the reactions were initially analyzed using an Agilent 6120 Quadrupole LC−MS spectrometer from Agilent, which was directly connected to the HPLC. Synthetic products were purified using an Agilent Infinity 1260 semipreparative HPLC system with either a YMC Pro C-4 column (5 µm, 120 Å, 250 × 20 mm) or a Waters Sunfire C-18 column (5 µm, 50 × 30 mm).

HRMS measurements were conducted at the EPFL ISIC Mass Spectrometry Service using a Micro Mass QTOF Ultima from Waters Corp.

NMR spectra were recorded on a Bruker AVANCE III-400 machine (9.4 T, 52 mm probe, BBFOz) or a Bruker AVANCE III HD-600 (14.1 T, 52 mm probe, BBFOz) using Brucker TopSpin 4.1 software. The spectra were analyzed using MestReNova 12.0.0-20080 software.

X-ray diffraction and crystal structure determination was performed at the EPFL ISIC XRD facility using a SuperNova, Dual, Cu at zero, Atlas S2 diffractometer (CuKα radiation) or Bruker P4 diffractometer (MoKα radiation). Data was collected and processed using CrysAlisPro (Rigaku, V1.171.38.43, 2015). The structure was solved with the **ShelXT** [1] structure solution program using the dual solution method and by using **Olex2** [2] as the graphical interface. The model was refined with version 2018/3 of ShelXL [3] using full matrix least squares on $|\boldsymbol{F}|^2$ minimisation. All non-hydrogen atoms were refined anisotropically. Hydrogen atom positions were calculated geometrically and refined using the riding model.

Measurement of second-order rate constant of reaction between phosphine 13 and azido-TPP molecules

Equimolar amounts of compounds **13** and **3** were mixed in the 1:1 mixture of dimethylacetamide (DMA) and PBS reaction progress was monitored by the monitoring fluorescence intensity of free luciferin that was released during the reaction (Ex.: 380 nm, Em.: 500 nm). The calculation of the luciferin concentration was done using a calibration curve that had been previously generated. To evaluate the constant, we calculated the average slope of curves for the three starting concentrations of the reactants (**Supplementary Fig. 2**).

Measurement of second-order rate constant of reaction between phosphine 21 and azido-TPP1

Phosphine **21** was used as a simplified of TPP-CL2 probe for the reaction rates kinetics studies due to the similarity of the reactive parts of the molecule and simplicity of the synthesis. To determine the reaction rate constant we utilized previously reported method by Lin et al[4]. Briefly, stock solutions of the phosphine **21**, azido-TPP1, and the standard (triphenylphosphine sulfide) were prepared in deuterated DMF

(DMF-*d6*) at the concentration of 100 mM. All solutions were kept under argon at -80 ^{0}C. In a typical experiment 120 µL of the phosphine solution, 12 µL of water, 60 µL of the solution of the standard, 288 µL of DMF-*d6*, and 120 µL of azido-TPP1 solution were mixed in a 5 mm NMR tube to give a final volume of 600 µL. Immediately after the mixing the tube with the mixture was flushed with argon, sealed, and placed in NMR spectrometer and ^{31}P spectrum was acquired to monitor the reaction rate.

The rate constant of the reaction between phosphine **21** and azidoTPP1 was 1.1 ± 0.2 x 10^{-3} $M^{-1}s^{-1}$ (mean ± CI 95%), which is quite typical for a Staudinger ligation[4].

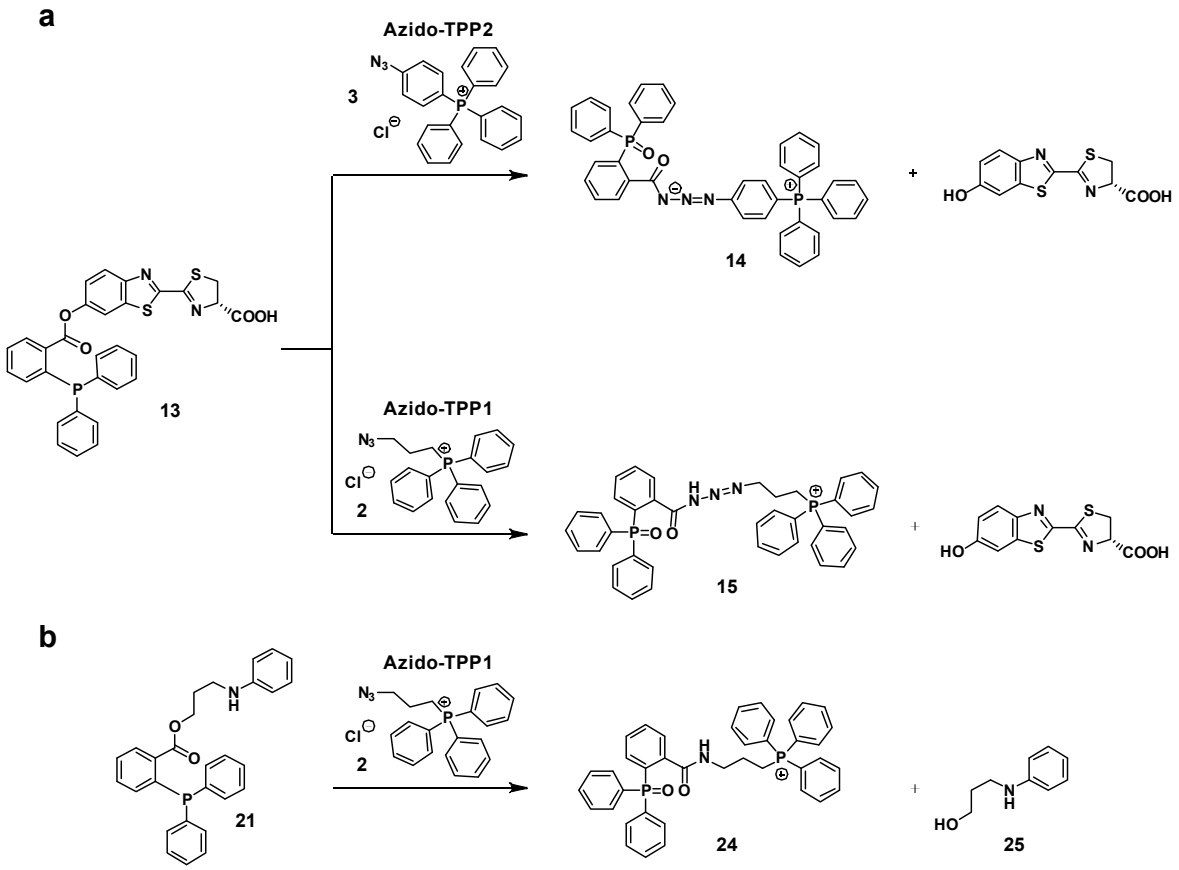

Scheme S1. a) Mechanism of reaction between caged luciferin **13** (simplified version of TPP-CL1) with either azido-TPP1 (**2**) or azido-TPP2 (**3**). **b**) Mechanism of reaction between triphenyl phosphine **21** (simplified version of TPP-CL2) and azido-TPP1.

1.1 Synthesis of TPP-CL1

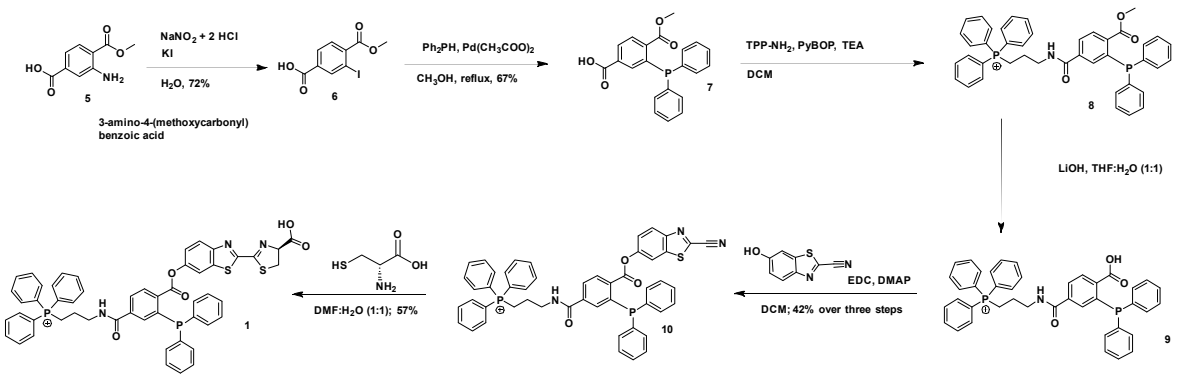

Scheme S2. Synthetic route to TPP-CL1 (**1**).

1.1.1 Synthesis of 3-iodo-4-(methoxycarbonyl)benzoic acid (6)

To a solution of 3-amino-4-(methoxycarbonyl)benzoic acid (12.24 g, 62.71 mmol) in hydrochloric acid (4 M, 80 mL) cooled in an ice-salt bath, an aqueous solution (25 mL) of sodium nitrite (4.8 g, 69.6 mmol) was slowly added over a period of 0.5 h. The mixture was stirred at this temperature for another 0.5 h. An aqueous solution (100 mL) of potassium iodide (30.00 g, 180.70 mmol) was cooled to -15°C and then added into the reaction mixture. The mixture was stirred at room temperature for 4 h. After the addition of a saturated sodium sulphite aqueous solution (50 mL), the precipitation was collected by filtration and washed with a large amount of water. Recrystallization of this crude product from a methanol/water solution gave us **2** as a brownish powder (13.82 g, 72%).

^{1}H NMR (400 MHz, Chloroform-*d*): δ 3.97 (s, 3H), 7.84 (d, J = 8.0 Hz, 1H), 8.12 (dd, J = 1.4 and 8.0 Hz, 1H), 8.69 (d, J = 1.4 Hz, 1H), which matched the literature [5].

1.1.2 Synthesis of 1-Methyl-2-(diphenylphosphino) terephthalate (7)

To a dry methanol (15 mL) solution of **6** (1.50 g, 4.901 mmol) were added anhydrous triethylamine (TEA) (2.05 mL, 14.703 mmol) and $Pd(OAc)_2$ (110 mg, 0.490 mmol) under a nitrogen atmosphere. Diphenylphosphine (1.0233 mL, 5.881 mmol) was slowly added at room temperature via a syringe with stirring. The resultant solution turned deep red immediately and was heated at reflux for 16 hours. The reaction mixture was filtered, and the resulting filtrate was evaporated under reduced pressure. The residue was dissolved in CH_2Cl_2 (70 ml). the solution was washed with HCl (1 M, 20 mL) three times. The organic layer was collected and evaporated under reduced pressure. The remaining solid was washed with cold methanol on the glass filter to get rid of red impurity. Finally, **7** was obtained as a yellow powder (1.198 g, 3.289 mmol, 67.1%).

^{1}H NMR (400 MHz, Chloroform-*d*) δ 8.10 (dd, *J* = 3.3, 2.1 Hz, 2H), 7.77–7.65 (m, 1H), 7.42–7.26 (m, 10H), 3.78 (s, 3H).

^{31}P NMR (162 MHz, Chloroform-*d*) δ -4.35.

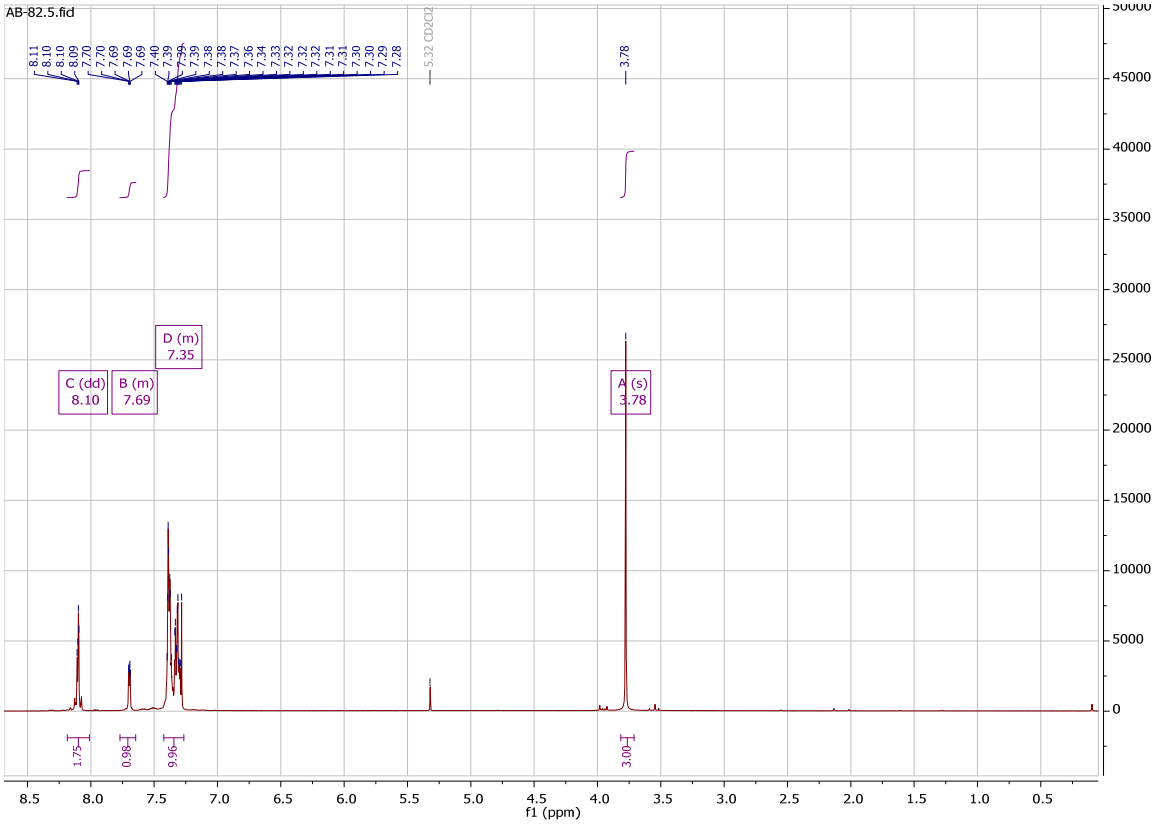

^{1}H spectrum of compound **7**

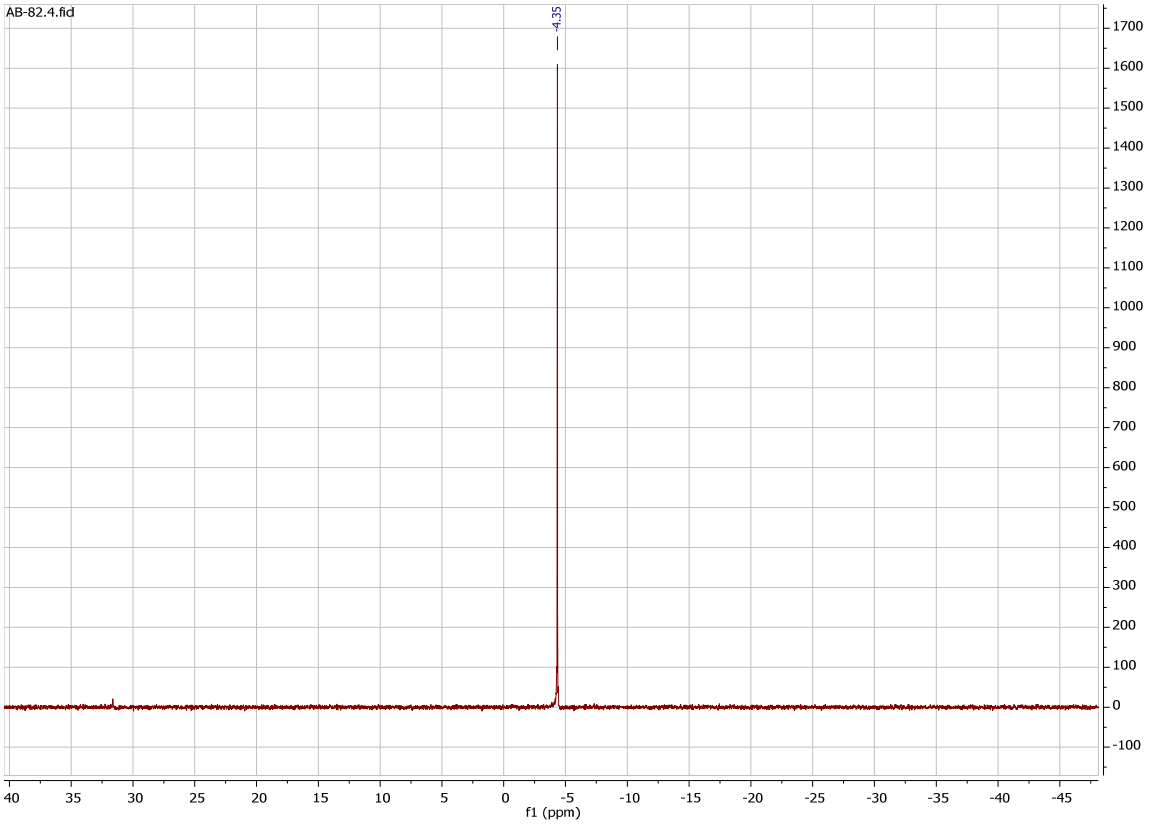

^{31}P spectrum of compound **7**

1.1.3 Synthesis of (3-(3-(diphenylphosphanyl)-4-(methoxycarbonyl)benzamido) propyl)triphenylphosphonium bromide (8).

To a dry 25 ml double neck flask, **7** (78 mg, 0.21 mmol) and PyBOP (117 mg, 0.22 mmol) were added. The apparatus was flushed with nitrogen. Dichloromethane (8 ml) was added to the flask, and the mixture was stirred before DIPEA (100 µL) was added. After stirring for 30 min under a nitrogen atmosphere, 3-aminopropyltriphenylphosphonium bromide (72 mg, 0.22 mmol) was added to the solution. The reaction was left stirring at room temperature under a nitrogen atmosphere until disappearance of **7** by LCMS. The reaction mixture was evaporated under reduced pressure to afford crude material used for the following step.

1.1.4 Synthesis of (3- (4-carboxy-3- (diphenylphosphanyl) benzamido) propyl) triphenylphosphonium chloride (9)

Lithium hydroxide (87 mg, 3.63 mmol) and TCEP (91 mg, 0.32 mmol) were dissolved in degassed bi-distilled water (5 ml) under an argon atmosphere. The solution was added to a solution of crude material (**8**) in 5 ml of degassed MeOH under an argon atmosphere. The reaction was left stirring at room temperature and monitored with LCMS. After 7 hours, the reaction was stopped by the addition of 1 M HCl to pH = 2–3. The cloudy solution was washed twice with 20 ml DCM. The organic layer was collected and evaporated to afford the crude material **9** used for the following step**.**

1.1.5 Synthesis of (3-(4-(((2-cyanobenzo[d]thiazol-5-yl)oxy)carbonyl)-3-(diphenylphosphanyl) benzamido)propyl)triphenylphosphonium (10).

DMAP (41.2 mg, 0.34 mmol) was dissolved in 5 ml DCM and added to 25 ml double neck flask with crude material (**9**) from the previous step under a nitrogen atmosphere. The mixture was stirred for 5 min at room temperature. EDC (71 mg, 0.37 mmol) and DMAP (41.2 mg, 0.34 mmol) were dissolved in 2 ml of DCM and added to the double neck flask with the solution of **9** under a nitrogen atmosphere. The mixture was stirred for 10 min, then 6-hydroxybenzo[d]thiazole-2-carbonitrile (62.4 mg, 0.35 mmol) was added to the mixture. The disappearance of the starting material was monitored by LCMS. The solvent was evaporated and the remaining solid was dissolved in 4 ml of MeCN and purified by preparative HPLC (YMC Pro C-4 column, MeCN + 0.1% FA solution in water, 20 ml/min, 0–3 min 15–35% MeCN, 3–30 min 35–40% MeCN, 30–50 min 40–70% MeCN, 50–53 min 70–95% MeCN, 53–54 min 95–100%; retention time 41 min). Fractions containing the product were frozen in liquid nitrogen and lyophilized. Finally, 73.2 mg (73.6 µmole, 42% yield over three steps) of **10** were obtained as a yellowish powder.

^{1}H NMR (600 MHz, Methylene Chloride-d_2) δ 8.69 (s, 0H), 8.66 (t, J = 5.4 Hz, 1H), 8.35 (dd, J = 8.0, 3.6 Hz, 1H), 8.19 (d, J = 9.0 Hz, 1H), 8.16 (d, J = 8.3 Hz, 1H), 7.85 (dtd, J = 7.0, 4.0, 1.9 Hz, 3H), 7.73–7.66 (m, 12H), 7.64 (d, J = 2.3 Hz, 1H), 7.62 (dd, J = 4.0, 1.3 Hz, 1H), 7.40–7.32 (m, 10H), 7.29 (dd, J = 9.0, 2.3 Hz, 1H), 3.59 (q, J = 5.8 Hz, 2H), 3.38 (td, J = 12.7, 7.3 Hz, 2H), 1.99 (q, J = 7.6, 6.7 Hz, 2H).

^{13}C NMR (151 MHz, Methylene Chloride-d_2) δ 167.68, 166.43, 164.48 (d, J = 2.4 Hz), 150.30 (d, J = 76.8 Hz), 142.01 (d, J = 29.6 Hz), 137.89, 137.17 (d, J = 10.9 Hz), 136.90, 136.16, 135.27 (d, J = 3.2 Hz), 134.79 (d, J = 18.4 Hz), 134.07 (d, J = 21.1 Hz), 133.93, 133.40 (d, J = 9.9 Hz), 131.50, 130.50 (d, J = 12.7 Hz), 129.04, 128.69 (d, J = 7.4 Hz), 126.89, 125.62, 125.22, 122.80, 120.07, 118.12, 117.55, 114.73, 112.90, 109.41, 39.84 (d, J = 17.8 Hz), 22.36 (d, J = 3.8 Hz), 20.20 (d, J = 53.5 Hz).

^{13}C NMR (151 MHz, Methylene Chloride-d_2) δ 166.76, 164.80 (d, J = 2.5 Hz), 150.63 (d, J = 76.7 Hz), 142.34 (d, J = 29.6 Hz), 138.21, 137.49 (d, J = 10.9 Hz), 137.22, 136.48, 135.59 (d, J = 3.1 Hz), 135.11 (d, J = 18.3 Hz), 134.40 (d, J = 21.1 Hz), 134.25, 133.72 (d, J = 10.0 Hz), 131.83, 130.82 (d, J = 12.5 Hz), 129.36, 129.01 (d, J = 7.5 Hz), 127.21, 125.94, 123.12, 118.44, 117.87, 115.05, 113.22, 109.73, 40.15 (d, J = 17.8 Hz), 22.67 (d, J = 3.9 Hz), 20.51 (d, J = 53.4 Hz).

^{31}P NMR (162 MHz, Chloroform-d) δ +23.94, -3.43.

ESI-TOF-MS: $C_{49}H_{38}N_3O_3P_2S^+$, calculated m/z = 810.2109, found 810.2117.

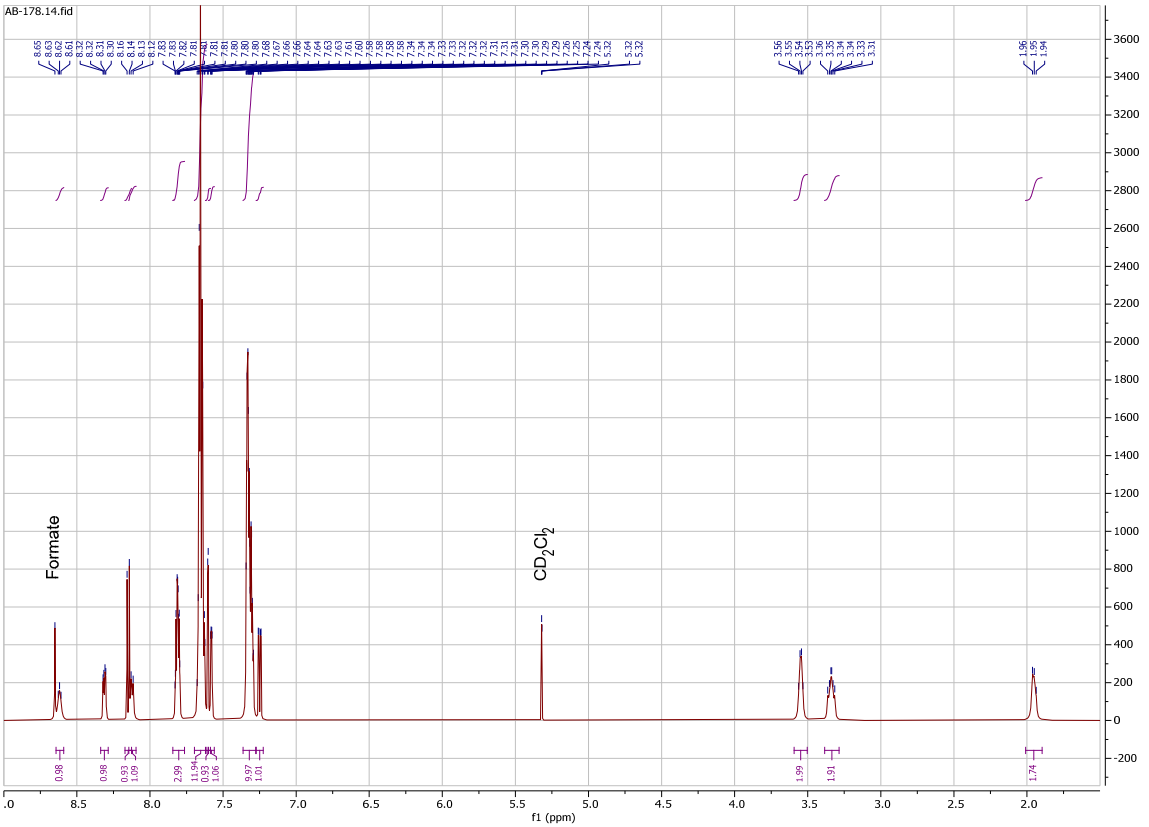

^{1}H spectrum of compound **10**

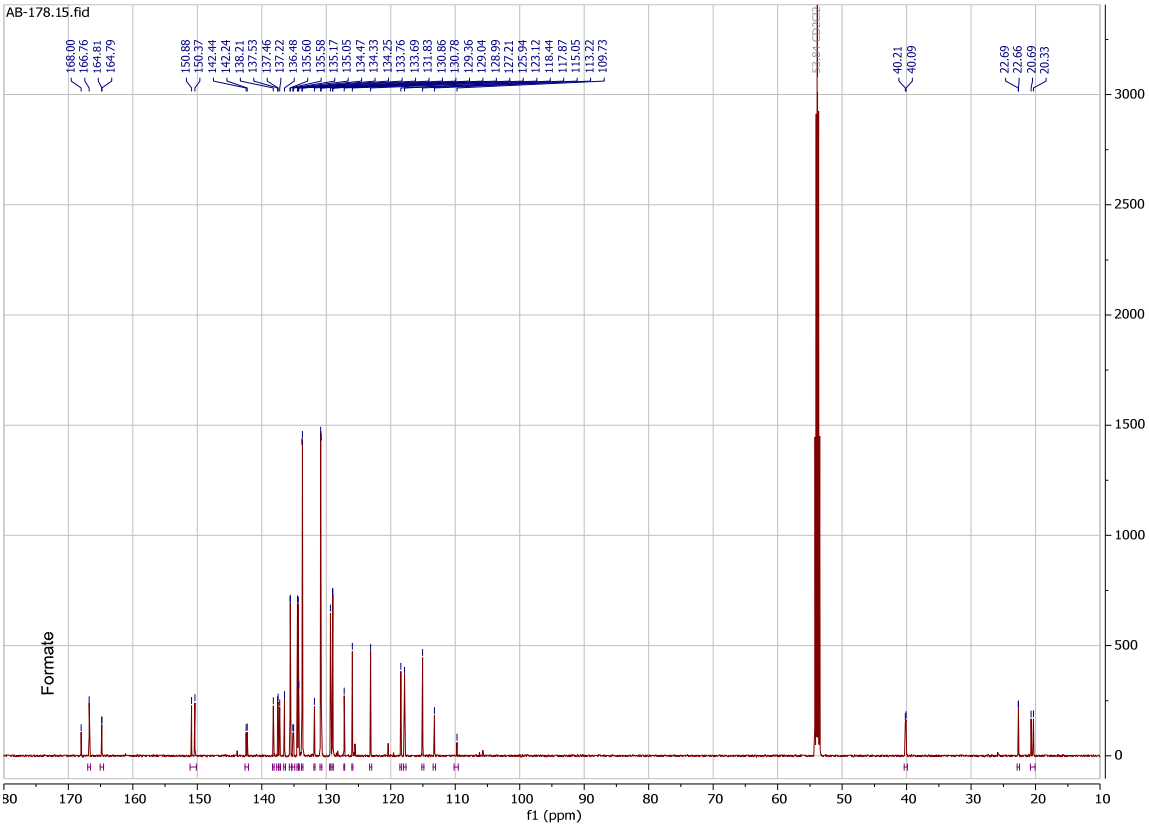

^{13}C spectrum of compound **10**

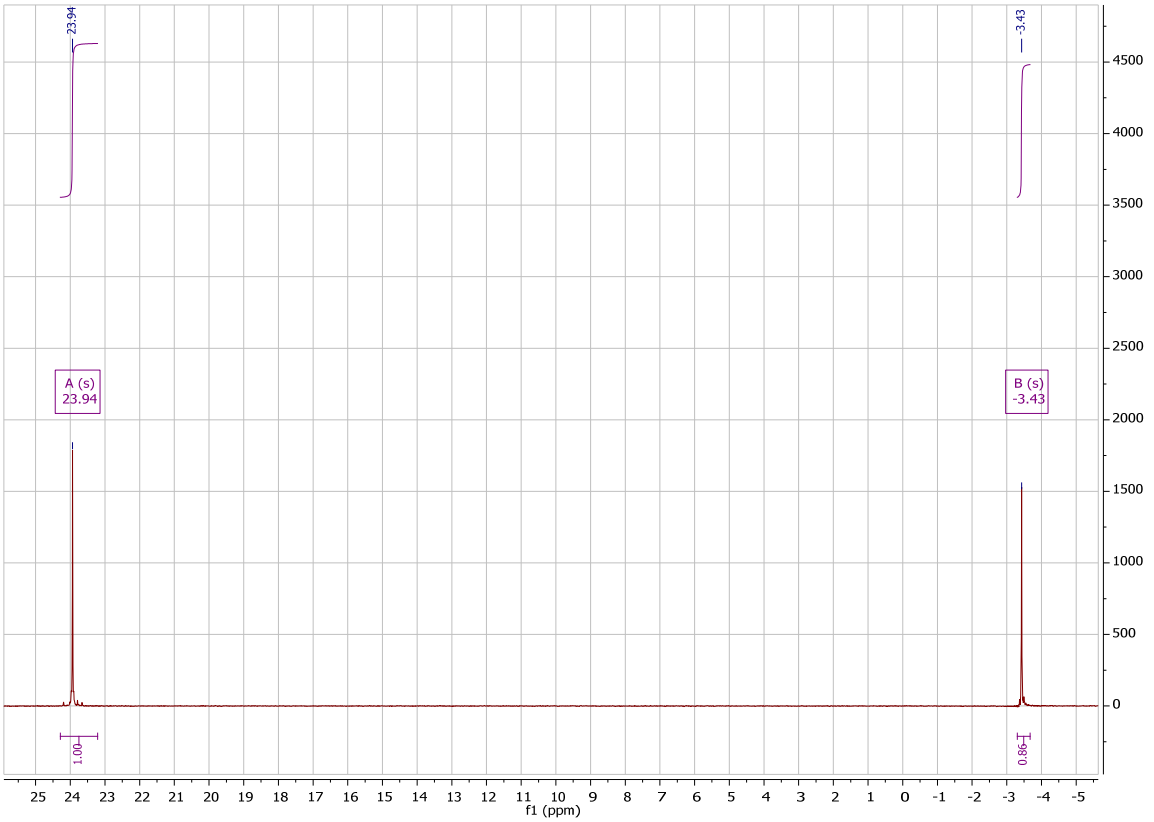

^{31}P spectrum of compound **10**

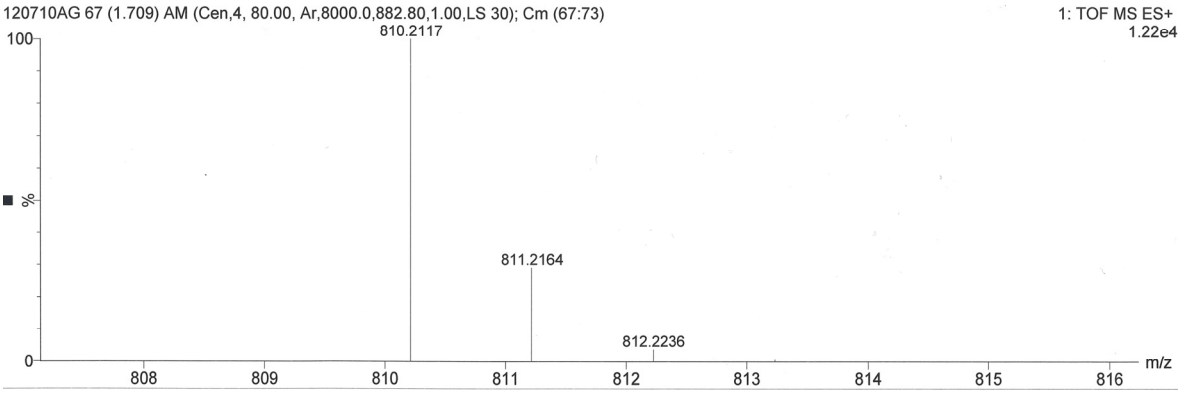

HRMS of compound **10**

1.1.6 **Synthesis of TPP-CL1 (1)**

10 (60 mg, 64.9 µmol) was dissolved in 4.5 ml of degassed MeCN in a 10-ml flask under a nitrogen atmosphere. A D-cysteine (78.6 mg, 649 µmol) solution in 3 ml of degassed PBS (pH 7.2, 1x) was added drop wise to a solution of 6 while stirring under a nitrogen atmosphere. The reaction mixture was stirred at room temperature for 1.5 h then injected into a preparative HPLC and purified using a Waters Atlantis C-18 column (MeCN + 0.1% FA solution in water, 20 ml/min, 0–1 min 5% MeCN, 1–20 min 5–70% MeCN, 20–21 min 70–100% MeCN, 21–25 min 100% MeCN retention time 13 min). Fractions containing the product were frozen in liquid nitrogen and lyophilized. Finally, 38 mg (37 µmol, 57% yield) of **1** was obtained as a yellowish powder. The compound was recrystallized from methanol at -20 ^{0}C.

^{1}H NMR (400 MHz, Chloroform-*d*) δ 8.76 (t, *J* = 5.7 Hz, 1H), 8.17 (dd, *J* = 8.1, 3.6 Hz, 1H), 8.05 (d, *J* = 8.2 Hz, 1H), 7.89 (d, *J* = 8.9 Hz, 1H), 7.73–7.63 (m, 3H), 7.61–7.49 (m, 13H), 7.23 (m, 11H), 6.93 (dd, *J*

= 8.9, 2.3 Hz, 1H), 5.25 (t, J = 9.8, 1.5 Hz, 1H), 3.64 (d, J = 11.1, 8.6 Hz, 2H), 3.56 (dd, J = 6.4 Hz, 2H), 3.42–3.33 (m, 2H), 1.94–1.81 (m, 2H).

^{13}C NMR (151 MHz, $CDCl_3$) δ 166.97, 166.56, 164.54, 160.48, 150.83, 149.31, 137.41, 137.06, 136.98, 136.35, 135.18, 134.22, 134.17, 134.08, 133.37, 133.30, 131.51, 130.53, 130.44, 129.00, 128.65, 128.63, 126.90, 125.00, 121.33, 118.31, 117.73, 114.71, 78.40, 39.65, 35.28, 29.68, 27.31, 22.33.

^{31}P NMR (162 MHz, Chloroform-d) δ +24.22, -3.60.

ESI-QTOF-MS analysis calculated for m/z = 914.2041 found m/z = 914.2045.

Crystal Data. $C_{52}H_{41}N_3O_5P_2S_2$, M_r = 913.94, monoclinic, $I2/a$ (No. 15), a = 27.7068(5) Å, b = 16.7035(2) Å, c = 26.8015(6) Å, β = 102.3414(19)°, α = γ = 90°, V = 12117.1(4) Å^3, T = 100.00(10) K, Z = 8, Z' = 1, μ(CuKα) = 1.614, 42956 reflections measured, 12322 unique (R_{int} = 0.0339) which were used in all calculations. The final wR_2 was 0.1277 (all data) and R_1 was 0.0427 (I > 2(I)).

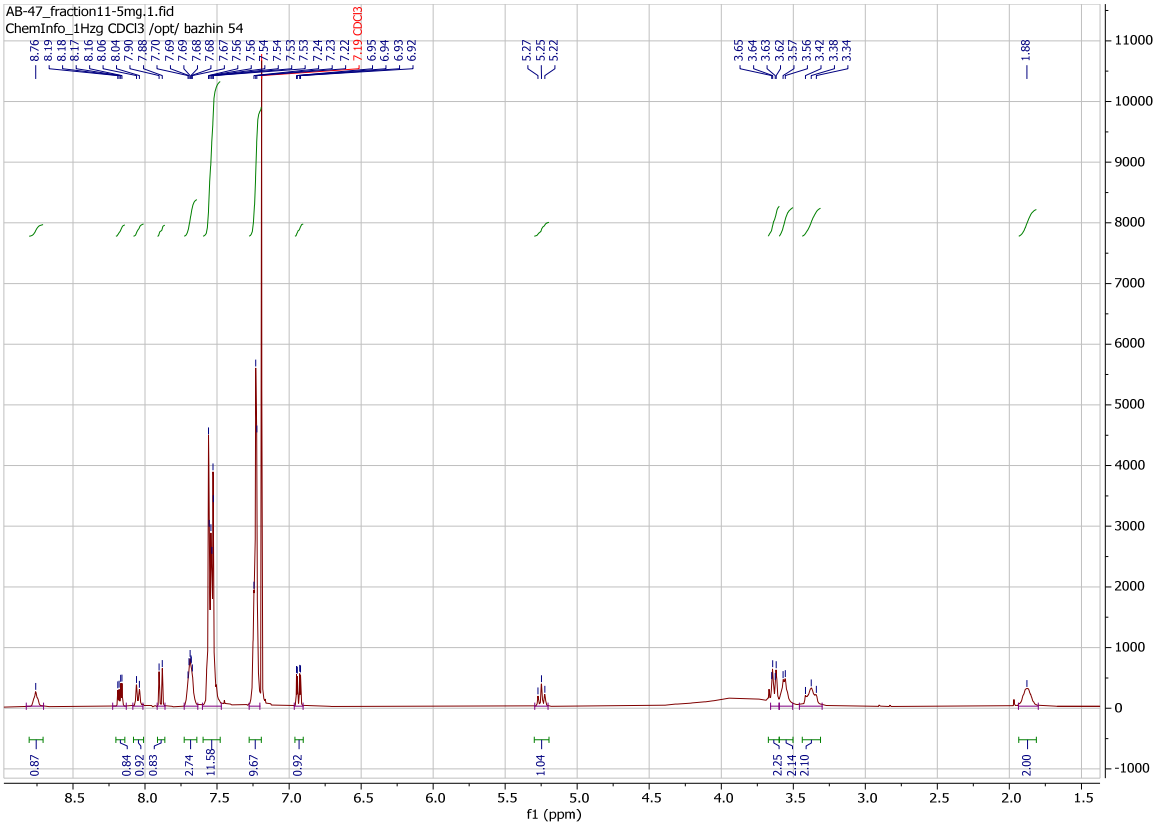

^{1}H spectrum of compound **1**

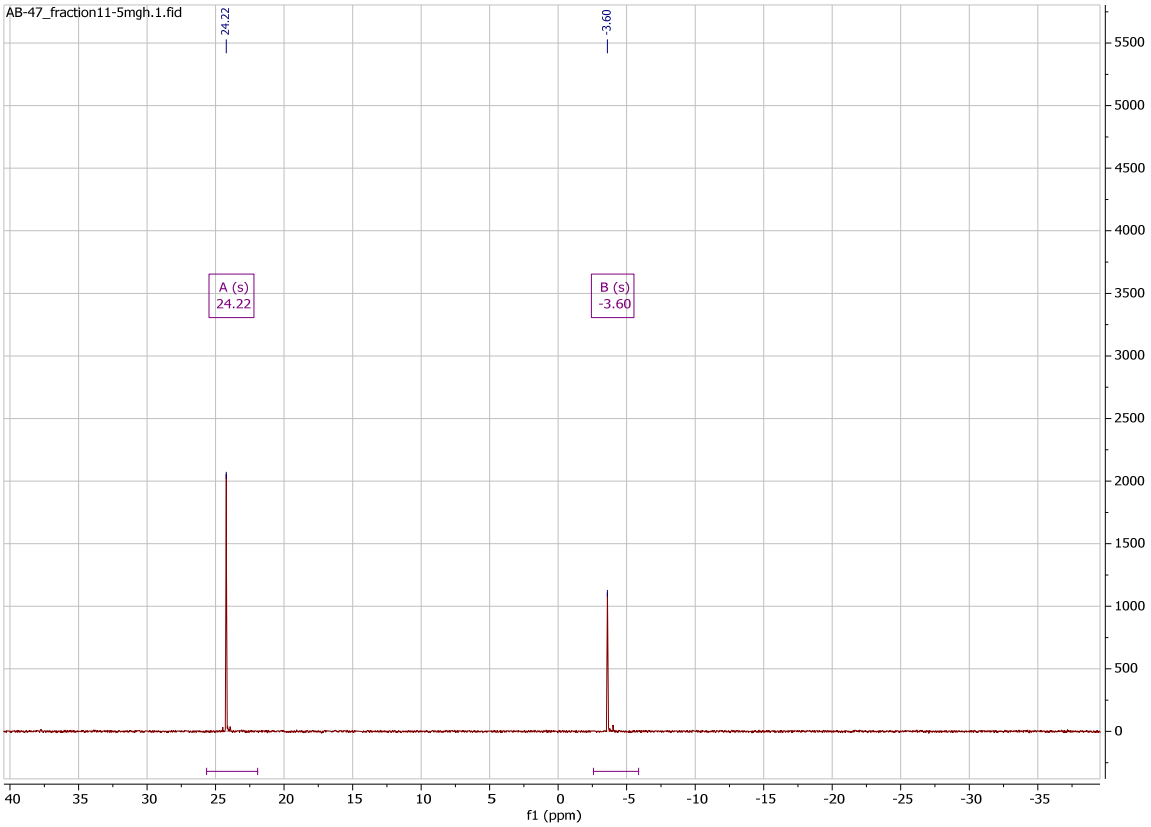

^{31}P spectrum of compound **1**

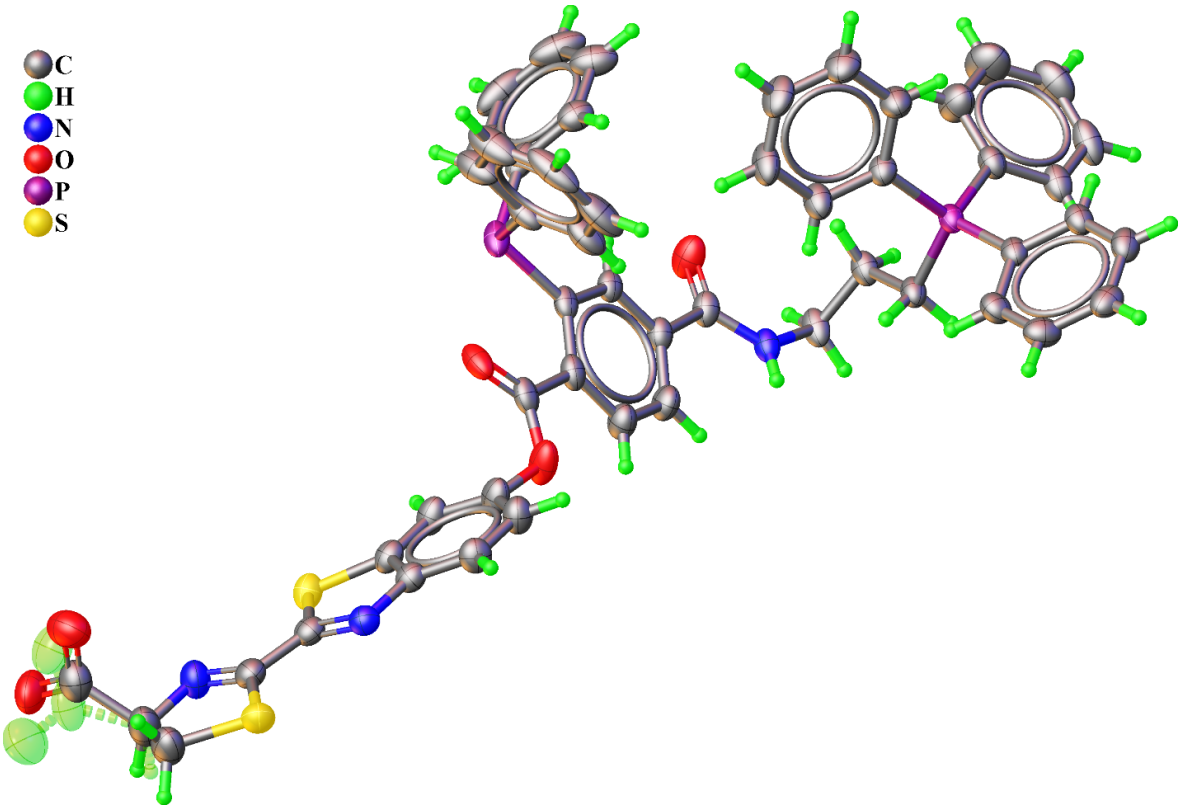

Single-crystal X-ray structure of compound **1**

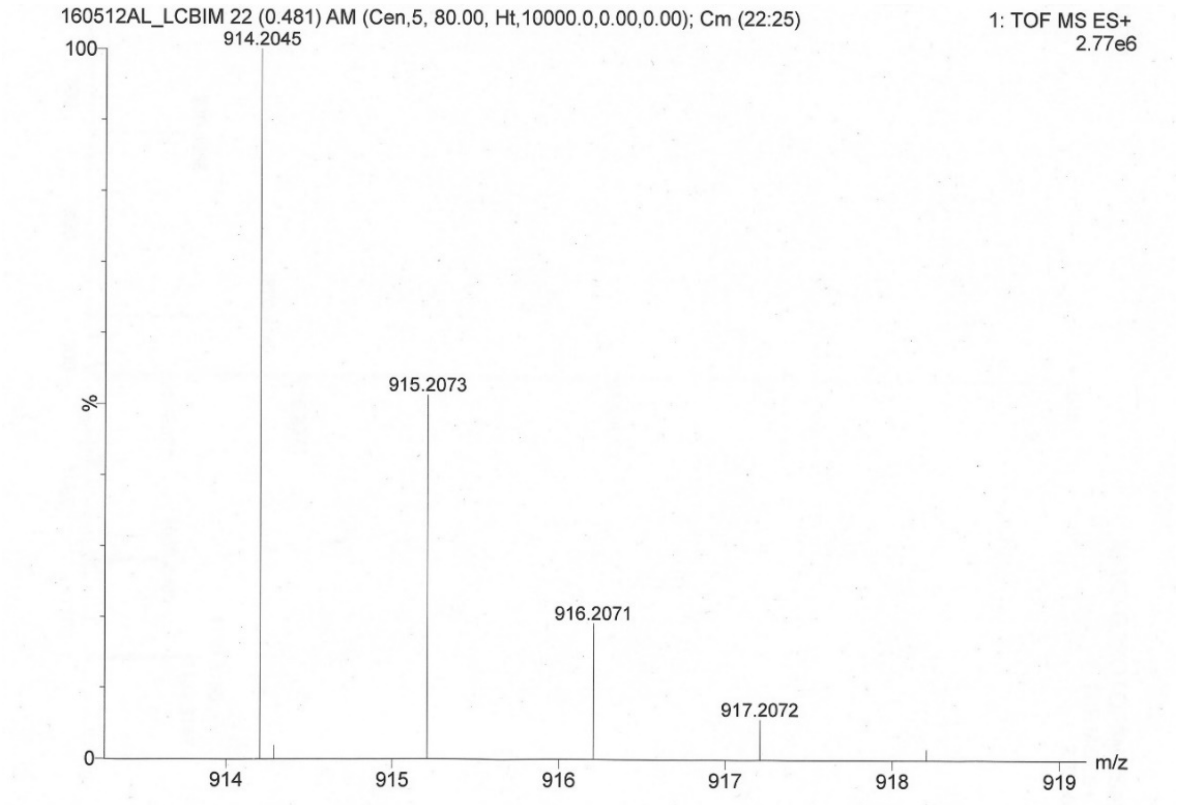

HRMS spectrum of compound **1**

1.2 Synthesis of Azido-TPP1 (9)

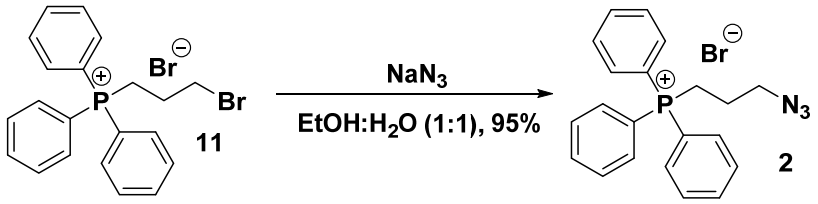

Scheme S3. Synthetic route to azido-TPP1 (**2**)

3-bromopropyltriphenylphosphonium bromide (2g, 4.29 mmol) was dissolved in 50 ml of a mixture of ethanol and water (1:1, v:v) in a 100-ml flask. A sodium azide (279 mg, 4.29 mmol) solution in 5 ml of water was added to the flask. The reaction mixture was heated at reflux for 12 hours. Then, the solvent was evaporated under reduced pressure. The remaining solid was purified using preparative HPLC. Fractions that contained the product were lyophilized to a white powder (1.737g, 94.6% yield). The pure product was recrystallized from water.

^{1}H NMR (400 MHz, Deuterium Oxide) δ 7.85 (tt, *J* = 7.2, 1.6 Hz, 3H), 7.80–7.64 (m, 12H), 3.50 (td, *J* = 6.3, 1.2 Hz, 2H), 3.43–3.32 (m, 2H), 2.00–1.87 (m, 2H).

^{13}C NMR (101 MHz, Deuterium Oxide) δ 135.06 (d, *J* = 3.1 Hz), 133.50 (d, *J* = 10.0 Hz), 130.06 (d, *J* = 12.7 Hz), 117.71 (d, *J* = 87.3 Hz), 50.82 (d, *J* = 17.9 Hz), 21.63 (d, *J* = 3.2 Hz), 19.22 (d, *J* = 54.3 Hz).

^{31}P NMR (162 MHz, D_2O) δ +23.36.

ESI-QTOF-MS analysis calculated for $C_{21}H_{21}N_3P^+$ *m/z* = 346.1468, found *m/z* = 346.1465.

Crystal Data. $C_{21}H_{23}BrN_3OP$, M_r = 444.30, triclinic, $P\bar{1}$ (No. 2), a = 9.4450(3) Å, b = 10.0767(3) Å, c = 11.7449(4) Å, α = 91.245(3)°, β = 109.554(3)°, γ = 100.928(3)°, V = 1029.85(7) Å^3, T = 100.01(10) K, Z = 2, Z' = 1, μ(CuKα) = 3.574, 7019 reflections measured, 4119 unique (R_{int} = 0.0189) which were used in all calculations. The final wR_2 was 0.0617 (all data) and R_1 was 0.0231 (I > 2(I)).

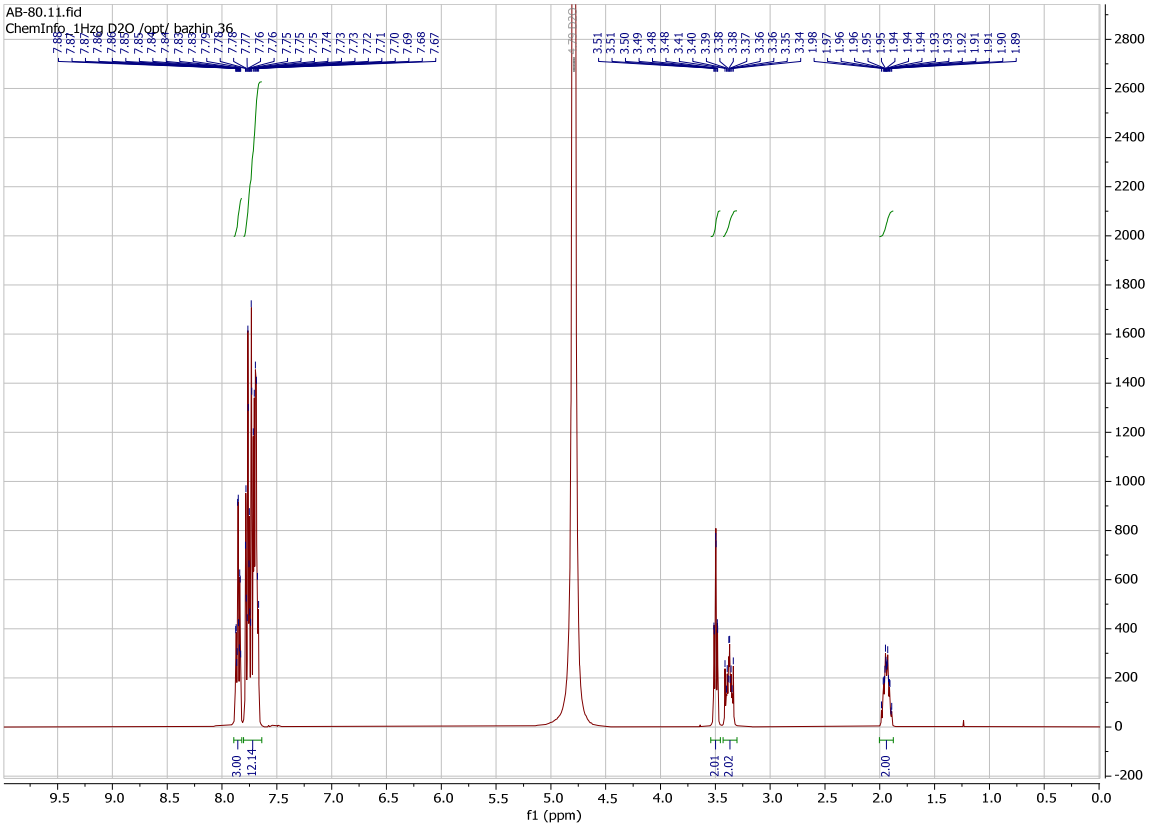

^{1}H spectrum of compound **2**

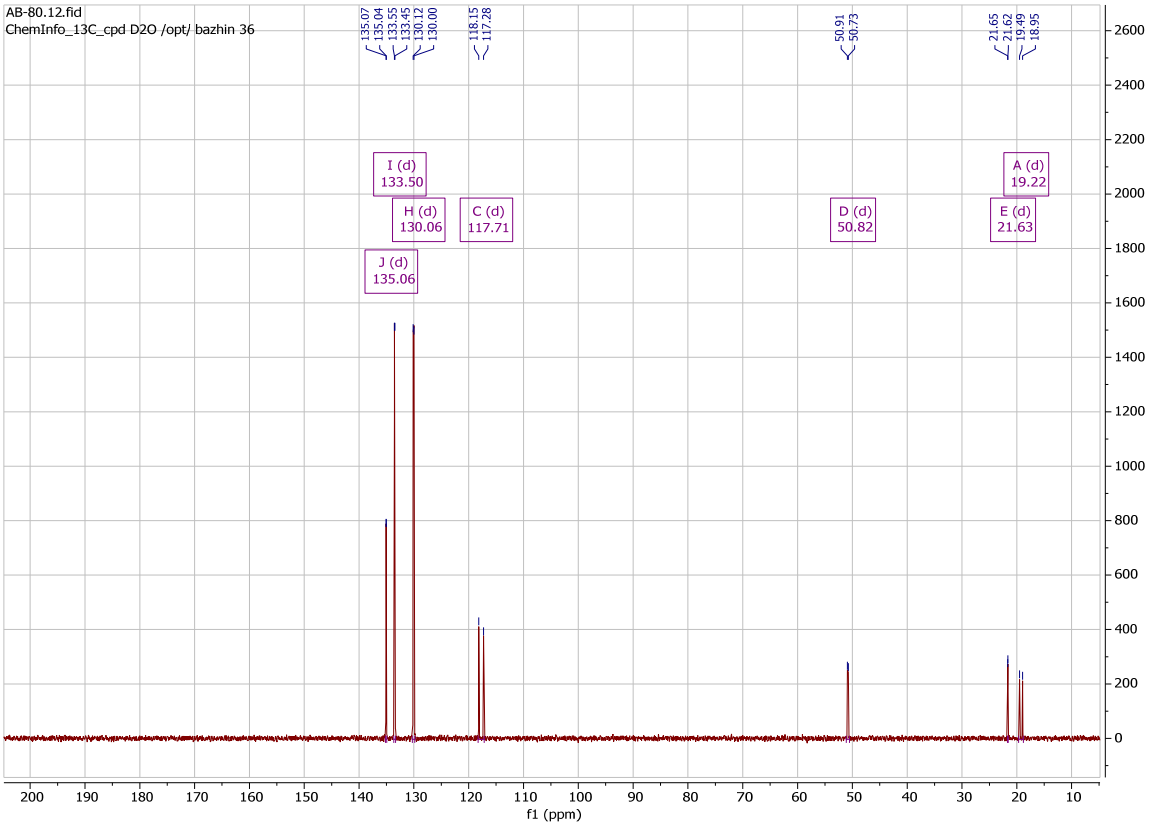

^{13}C spectrum of compound **2**

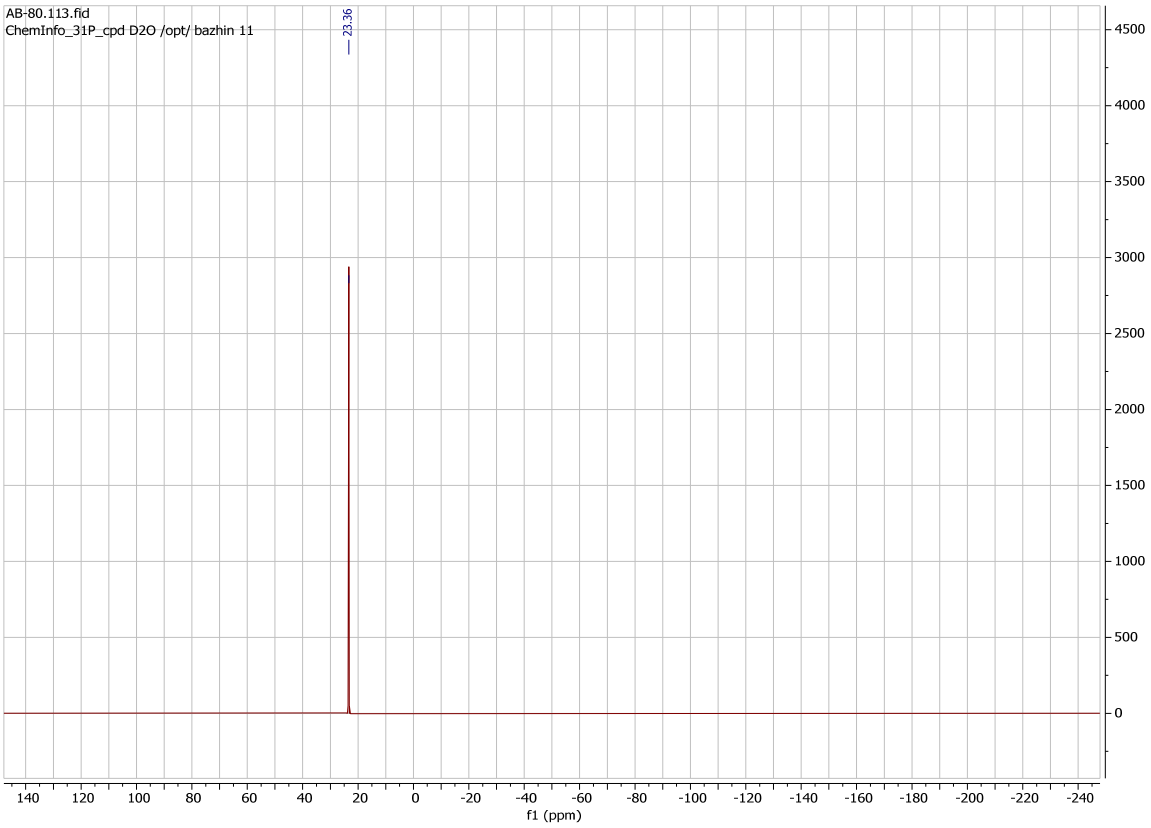

^{31}P spectrum of compound **2**

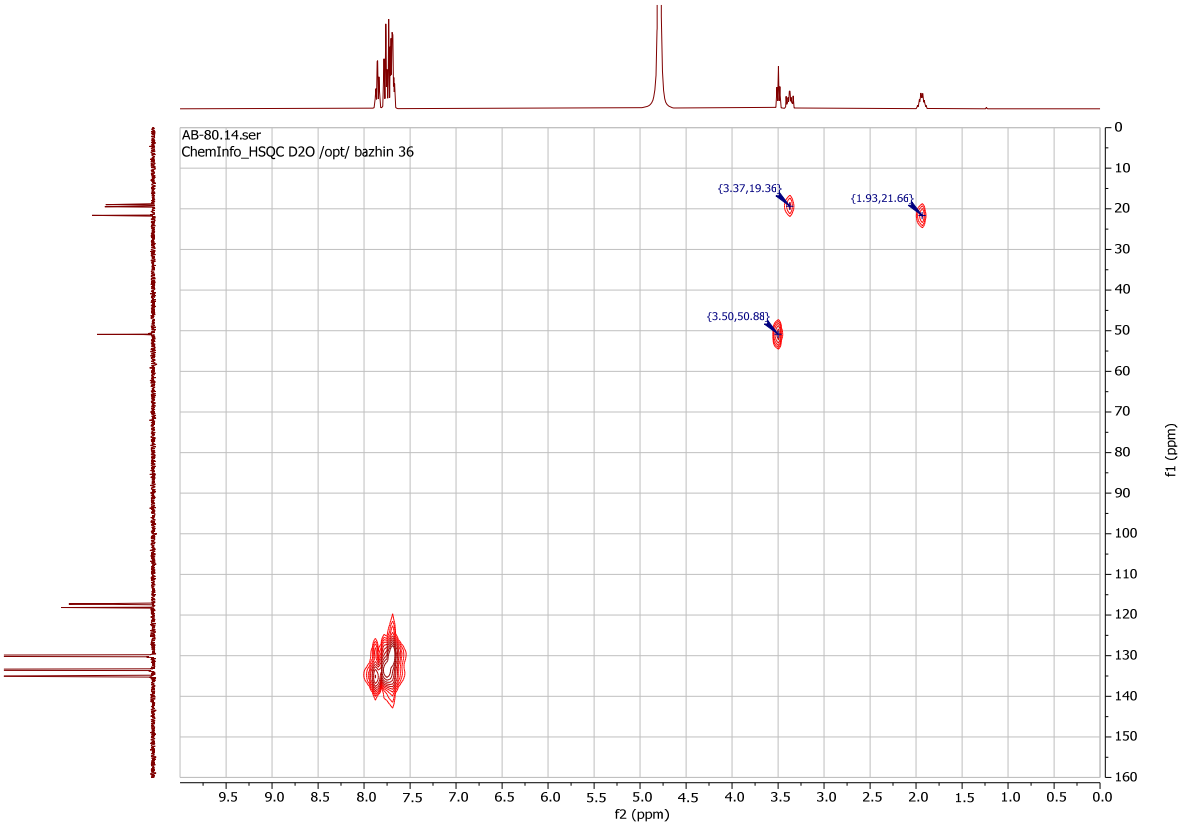

^{1}H-^{13}C HSQC spectrum of compound **2**

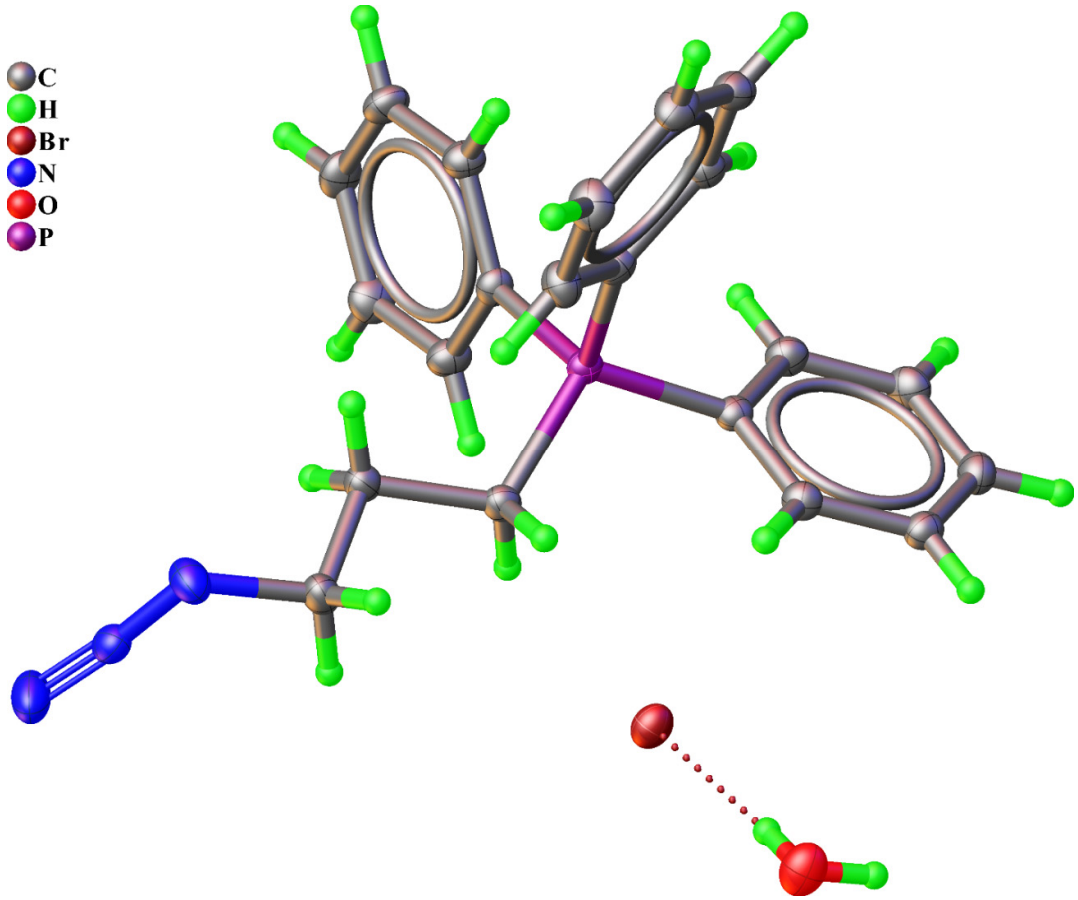

Single-crystal X-ray structure of the compound **2**

For synthesizing the labeled version of **2**, the same procedure was used as for non-labeled compound with one exception — Sodium azide enriched with ^{15}N on the terminal position was used. The product was characterized by NMR and HRMS.

^{1}H NMR (400 MHz, Deuterium Oxide) δ 7.99–7.89 (m, 3H), 7.89–7.64 (m, 12H), 3.57 (t, J = 6.4 Hz, 2H), 3.44 (t, J = 14.9 Hz, 2H), 1.99 (d, J = 14.2 Hz, 2H).

^{13}C NMR (101 MHz, Deuterium Oxide) δ 134.20 (d, J = 3.2 Hz), 132.29 (d, J = 10.1 Hz), 129.27 (d, J = 12.7 Hz), 116.53 (d, J = 86.8 Hz), 49.62 (dd, J = 18.0, 3.2 Hz), 20.70, 18.08 (d, J = 54.0 Hz).

^{31}P NMR (162 MHz, D_2O_salt) δ 23.45.

^{15}N NMR (41 MHz, Deuterium Oxide) δ 211.77, 70.61.

ESI-QTOF-MS analysis calculated for $C_{21}H_{21}N_2{}^{15}NP^+$ m/z = 347.1443, found m/z = 347.1444.

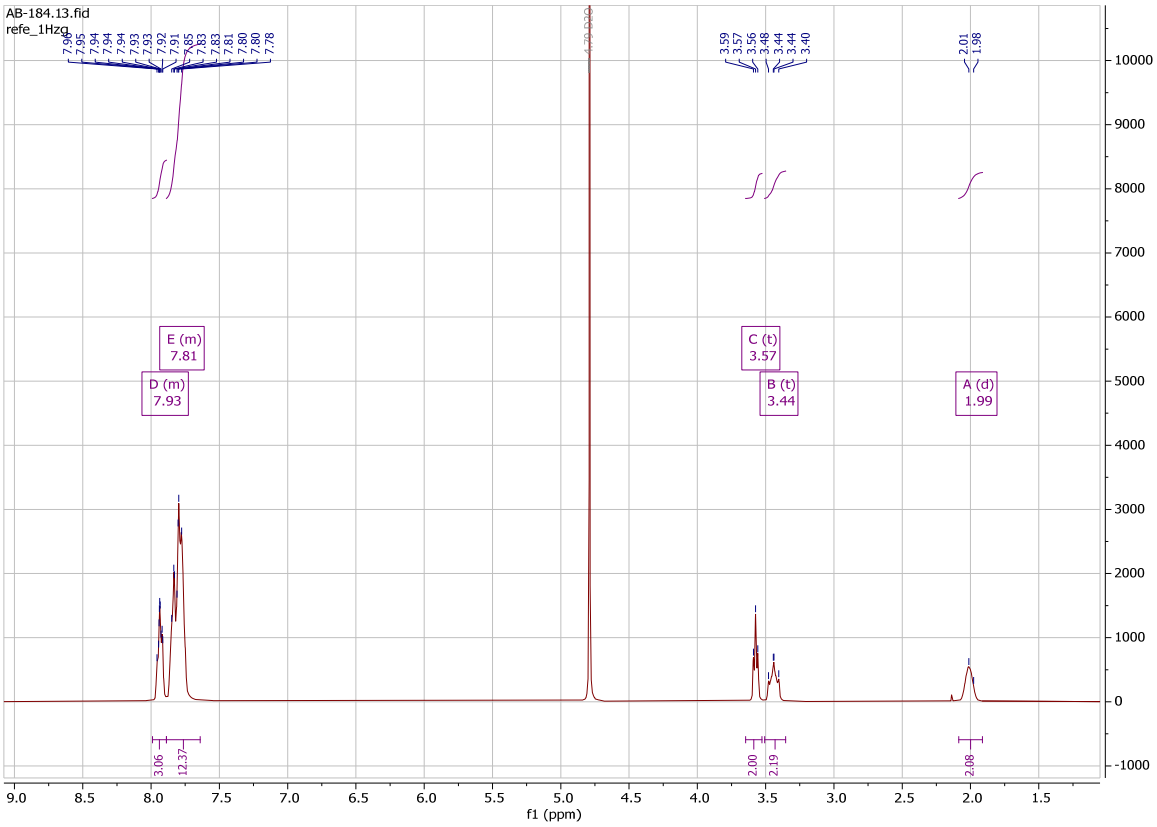

^{1}H spectrum of ^{15}N-labelled compound **2**

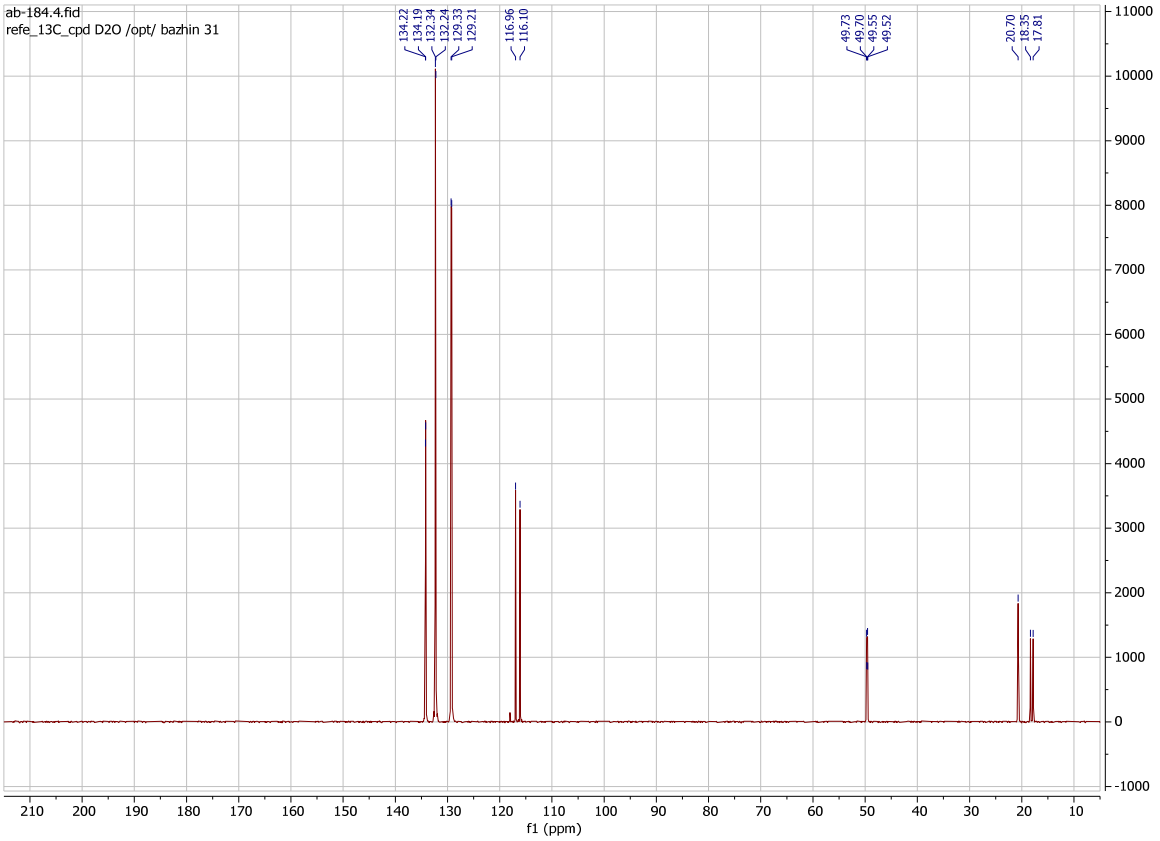

^{13}C spectrum of ^{15}N-labelled compound **2**

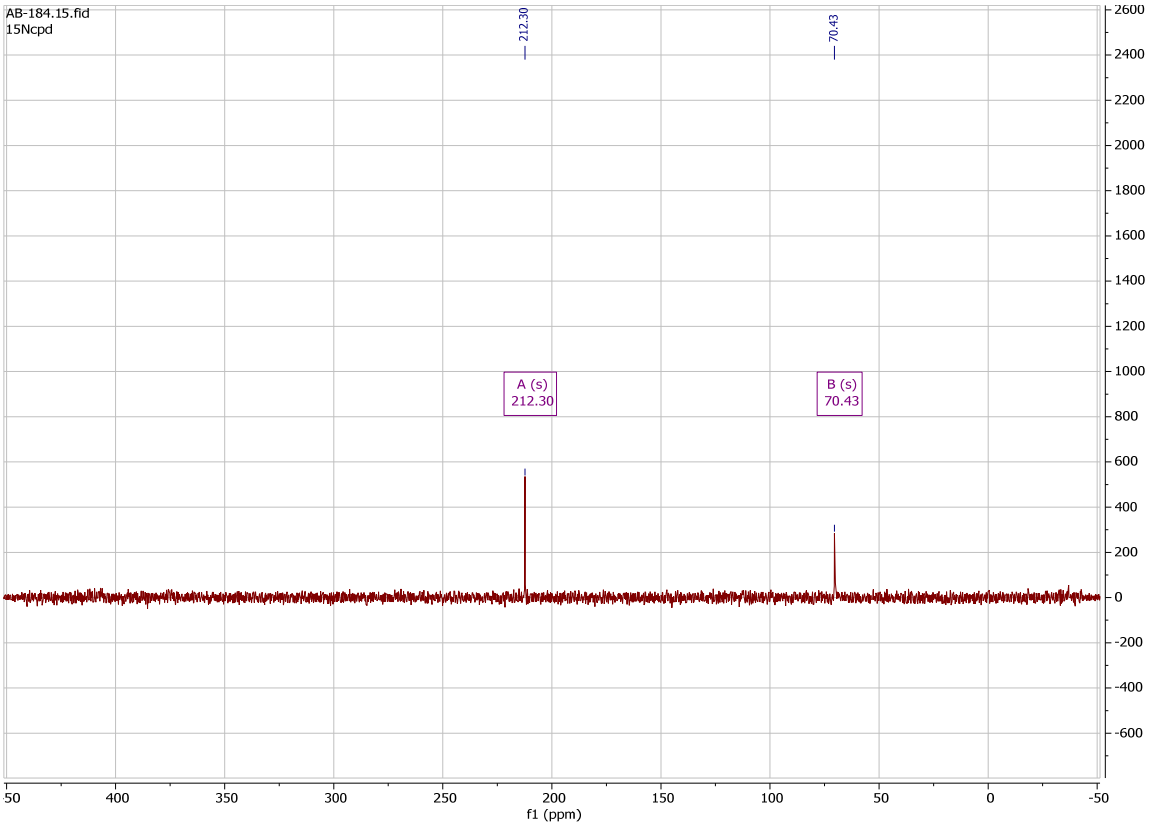

^{15}N spectrum of ^{15}N-labelled compound **2**

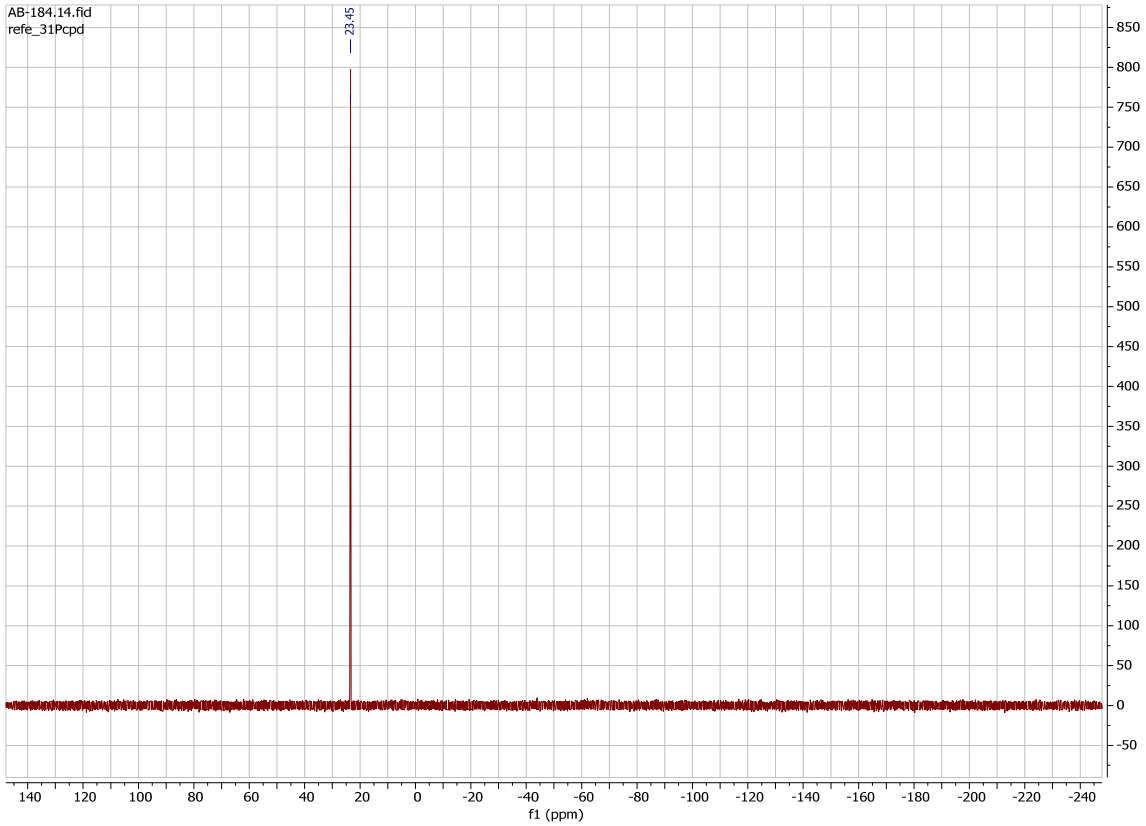

^{31}P spectrum of ^{15}N-labelled compound **2**

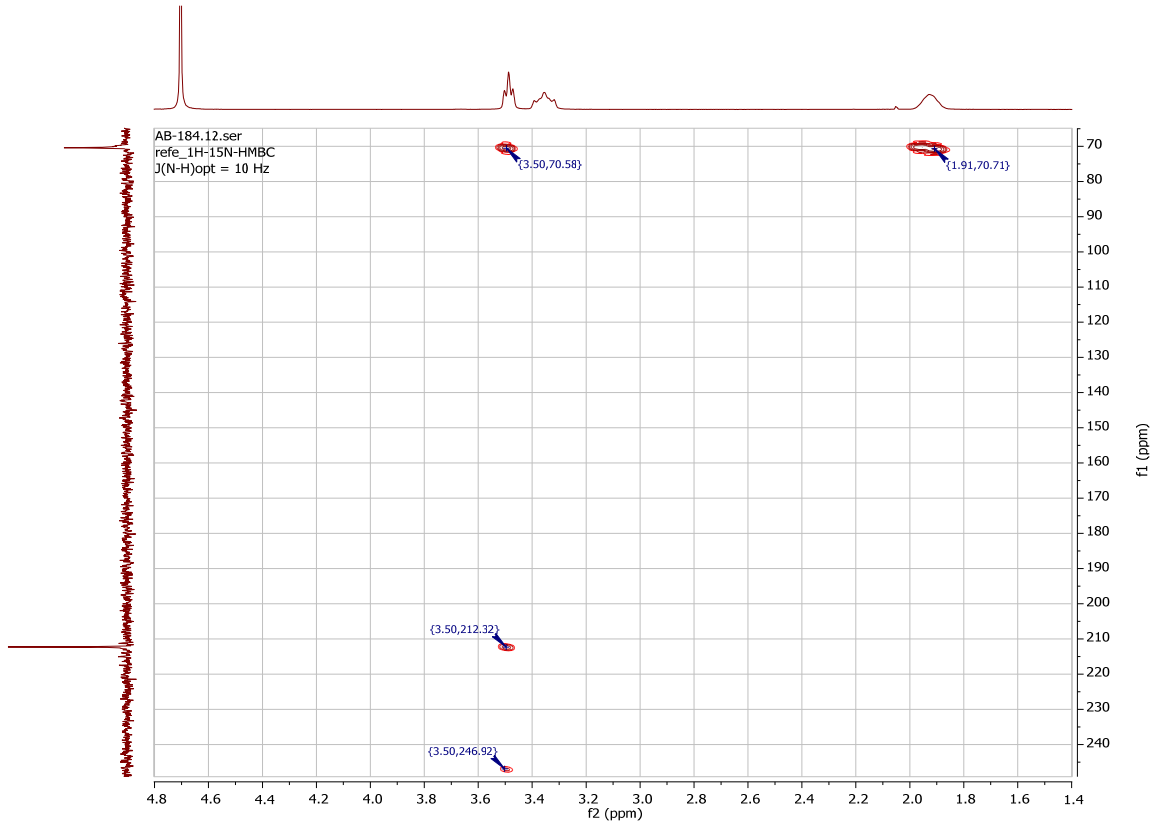

^{1}H-^{15}N HMBC spectrum of ^{15}N-labelled compound **2**

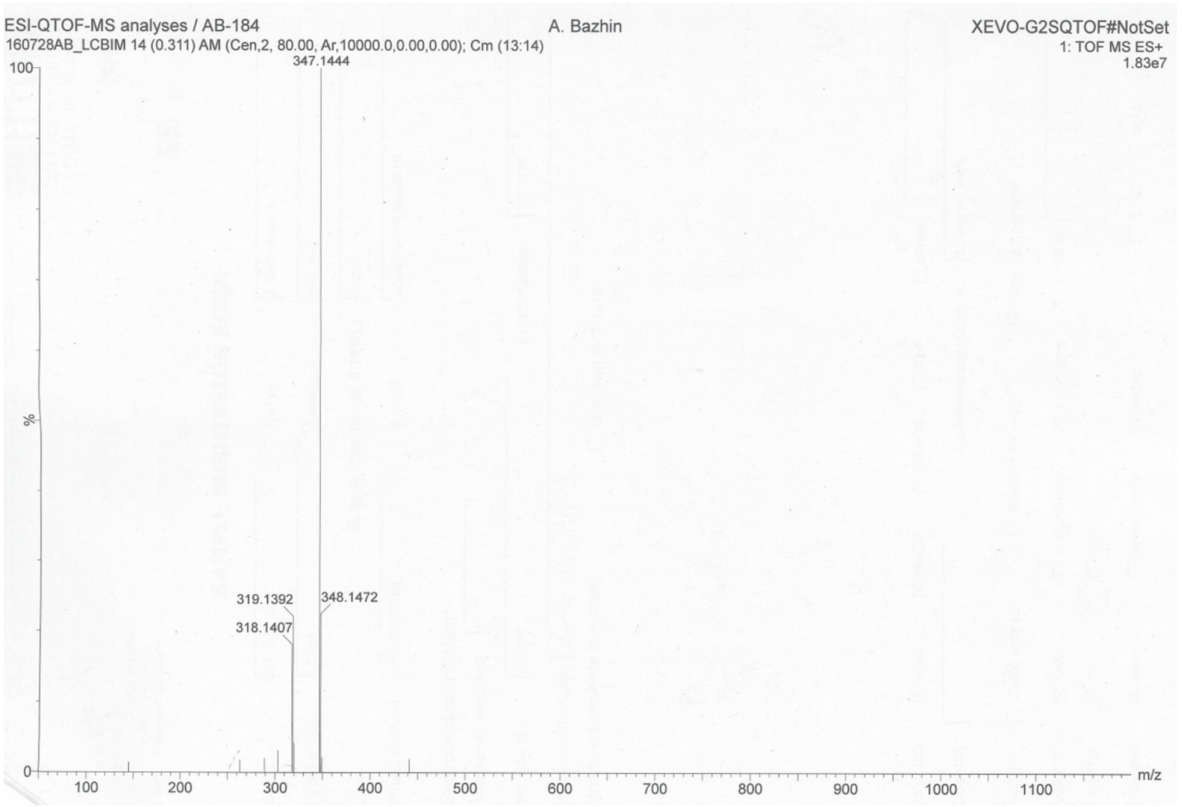

HRMS spectrum of ^{15}N-labeled azido-TPP1 (**2**). The azide is partially fragmented in an ionization chamber to corresponding nitrene and nitrogen gas. Two nitrenes can be observed on the spectrum since the analyzed compound is a mixture of two isotopomers. One nitrene ion contains ^{15}N (319.1392, Δ = 4.9 ppm) and the other contains ^{14}N (318.1407, Δ = 4 ppm). The ratio of abundancies of these two peaks corresponds to molar ratio of the isotopomers in the analyzed solution.

1.3 Synthesis of Azido-TPP2 (3)

1.3.1 Synthesis of (4-((tert-butoxycarbonyl)amino)phenyl)triphenylphosphonium formate (12)

Tert-butyl (4-iodophenyl)carbamate (500 mg, 1.567 mmol) and triphenylphosphine (493 mg, 1.88 mmol) were dissolved in a mixture comprising 10 ml of ethanol (not dry) and 2 ml of dry DMF in a 100-ml flask. Palladium acetate (35 mg, 0.156 mmol) and triethylamine 330 µL were added to the flask. The reaction mixture was stirred at 90°C for 18 h. Then, the solvent was evaporated under reduced pressure. The remaining solid was purified using preparative reverse phase LC (column biotage HP C-18 30 g; Eluent A – water plus 0.1% formic acid, eluent B – acetonitrile + 0.1% formic acid; 0–3 CV – 5% B, 3–9 CV – 55% B, 9–12 CV – 55% B, 12–13 CV – 55–60% B, 13–15 CV – 60% B, 15–16 CV – 60–95% B, 16–18 CV – 95% B). Fractions that contained the product were lyophilized to a white powder (440 mg, 56.3% yield).

^{1}H NMR (400 MHz, Methylene Chloride-d_2) δ 8.15–8.09 (m, 2H), 7.95–7.88 (m, 3H), 7.80–7.72 (m, 6H), 7.69–7.60 (m, 6H), 7.52–7.44 (m, 2H), 1.54 (s, 9H).

^{13}C NMR (101 MHz, CD_2Cl2) δ 152.94, 147.33, 147.30, 135.39, 135.36, 135.26, 134.37, 134.27, 130.49, 130.37, 119.65, 119.52, 118.92, 118.03, 107.24, 106.28, 80.83, 49.69, 27.96.

^{31}P NMR (162 MHz, CD_2Cl2) δ 22.36.

ESI-QTOF-MS analysis calculated for $C_{29}H_{29}NO_2P^+$ *m/z* = 454.1936 found *m/z* = 454.1939.

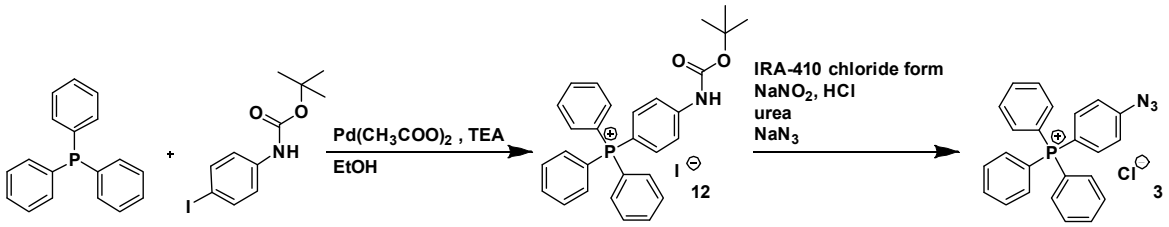

Scheme S4. Synthetic route to azido-TPP2 (**3**)

1.3.2 **Synthesis of (4-azidophenyl)triphenylphosphonium chloride (3, azido-TPP2)**

390 mg (0.781 mmol, 1 eq) of **12** were dissolved in methanol, and 6 ml of wet IRA-410 resin were added. The mixture was stirred for 2 h and filtered to remove resin particles. The filtrate was evaporated under reduced pressure. The resulting solid material was dissolved in 10 ml of 15% HCl. The reaction mixture was stirred at room temperature until complete deprotection of the amine occurred (reaction was monitored by HPLC-MS). Then the mixture was cooled to 0°C in ice bath. During all of the following operations, the temperature of the reaction mixture was maintained at 0°C by the ice bath. 250 mg (3.62 mmol, 3 eq) of sodium nitrite was dissolved in 5 ml of water, which was added dropwise to the stirring reaction mixture. 20 min afterwards, 3 ml of aqueous solution of 170 mg urea (2.84 mmol, 3.4 eq) was added to the reaction mixture with stirring. After another 20 min, 101.5 mg of sodium azide solution in 10 ml of water was added dropwise to the reaction mixture. 1 h later, the reaction mixture was evaporated at a reduced pressure to obtain the crude material. The crude was purified using preparative reverse phase LC (column biotage HP C-18 30 g; Eluent A – water plus 0.1% HCl, eluent B – acetonitrile; 0–3 CV – 5% B, 3–9 CV – 55% B, 9–12 CV – 55% B, 12–13 CV – 55–60% B, 13–15 CV – 60% B, 15–16 CV – 60–95% B, 16–18 CV – 95% B). Fractions that contained the product were lyophilized to a yellowish powder (266 mg, 80% yield).

^{13}C NMR (101 MHz, Deuterium Oxide) δ 147.37 (d, *J* = 3.3 Hz), 136.27 (d, *J* = 11.6 Hz), 135.28 (d, *J* = 3.2 Hz), 134.43 (d, *J* = 10.4 Hz), 130.06 (d, *J* = 13.0 Hz), 120.43 (d, *J* = 13.9 Hz), 118.16, 117.27 .

^{1}H NMR (400 MHz, Deuterium Oxide) δ 7.76 (td, *J* = 7.0, 2.1 Hz, 3H), 7.62–7.46 (m, 14H), 7.18 (dd, *J* = 8.6, 2.7 Hz, 2H).

^{31}P NMR (162 MHz, D_2O) δ +22.09.

HRMS (ESI QTOF ES+) calc. [M^+] 380.1317, found [M^+] 380.1314.

To shed some light on the mechanism of the reaction between **1** and **3**, we decided to synthesize the ^{15}N-labeled compound. Sodium azide with an ^{15}N atom on the terminal position (98% enrichment) was used for the synthesis instead of the usual sodium azide. As a result, we got a mixture of unlabeled and labeled azido-TPP2. The labelled azido-TPP2 contained of two isotopomers, where ^{15}N was either terminal or middle (**Scheme S5**).

^{1}H NMR (400 MHz, Deuterium Oxide) δ 7.71 (q, *J* = 11.3, 7.5 Hz, 3H), 7.62–7.36 (m, 13H), 7.09 (dd, *J* = 8.6, 2.7 Hz, 2H).

^{31}P NMR (162 MHz, Deuterium Oxide) δ +21.87.

^{15}N NMR (41 MHz, Deuterium Oxide) δ 238.95, 237.92.

^{13}C NMR (101 MHz, Deuterium Oxide) δ 147.33 (d, *J* = 3.4 Hz), 136.17 (d, *J* = 11.8 Hz), 135.40 (d, *J* = 3.1 Hz), 134.28 (d, *J* = 10.2 Hz), 130.19 (d, *J* = 13.0 Hz), 120.50 (d, *J* = 13.8 Hz), 117.56 (d, *J* = 90.2 Hz), 112.73 (d, *J* = 94.3 Hz).

HRMS (ESI QTOF ES+) calc. [M^+] 381.1287, found [M^+] 381.1306.

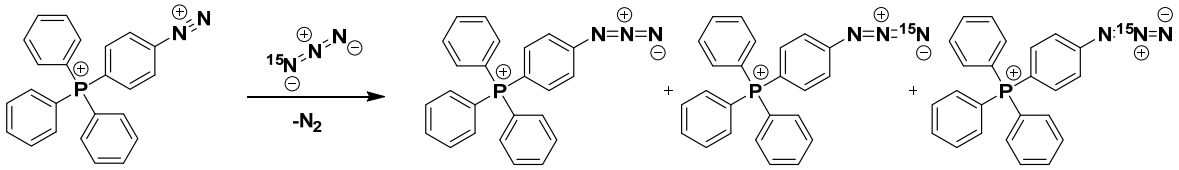

Scheme S5. Reaction between diazonium salt and terminally ^{15}N-labelled sodium azide.

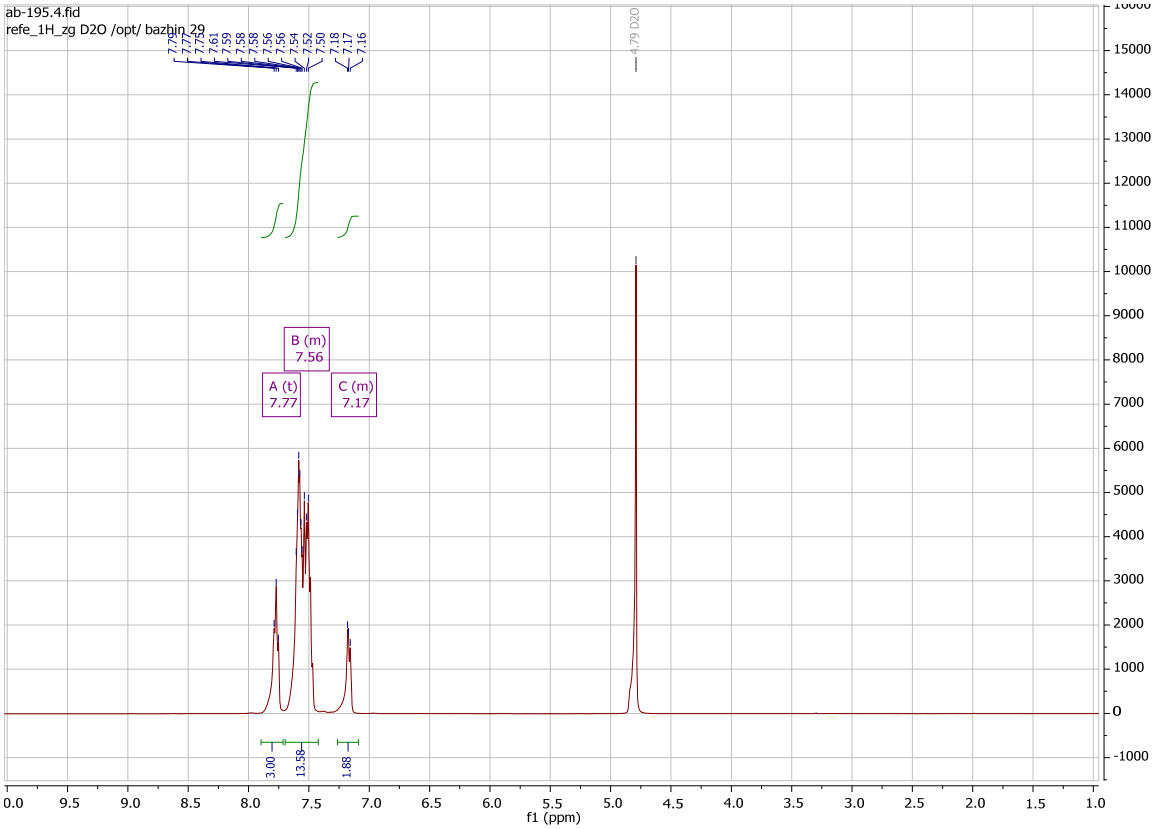

^{1}H spectrum of compound **3**

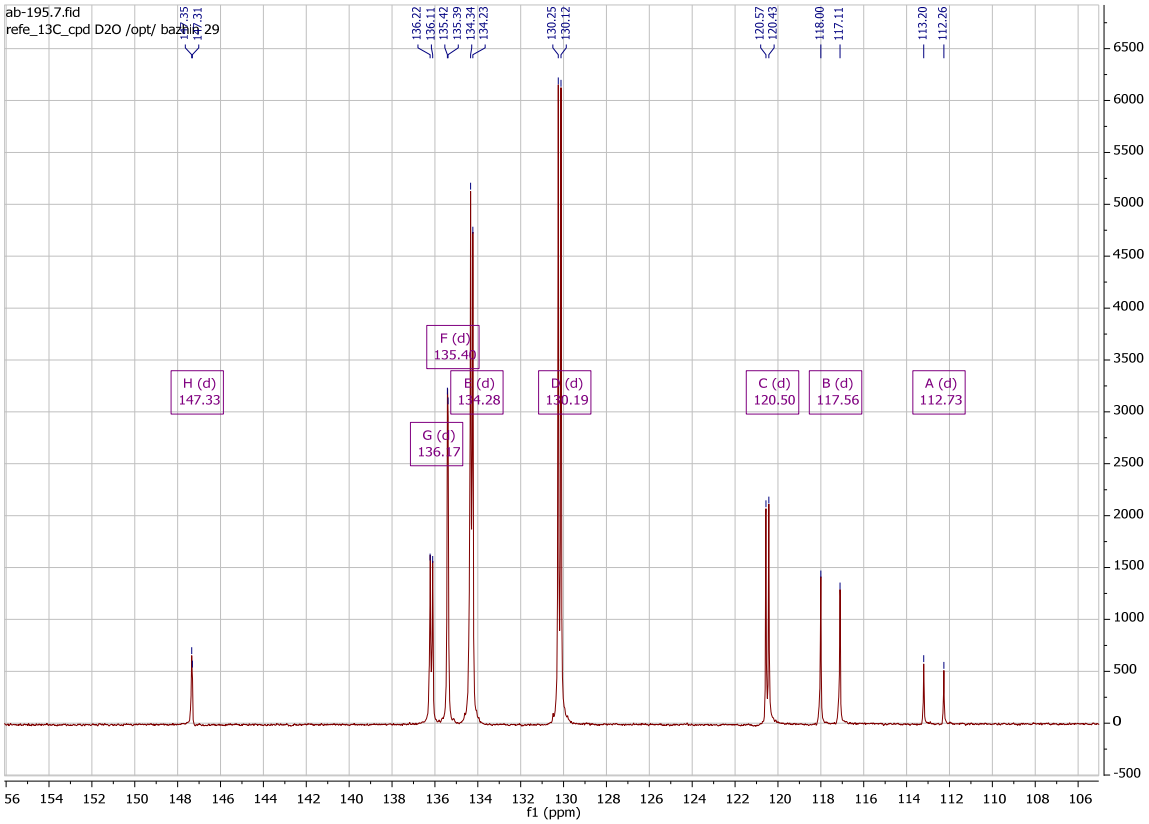

^{13}C spectrum of compound **3**

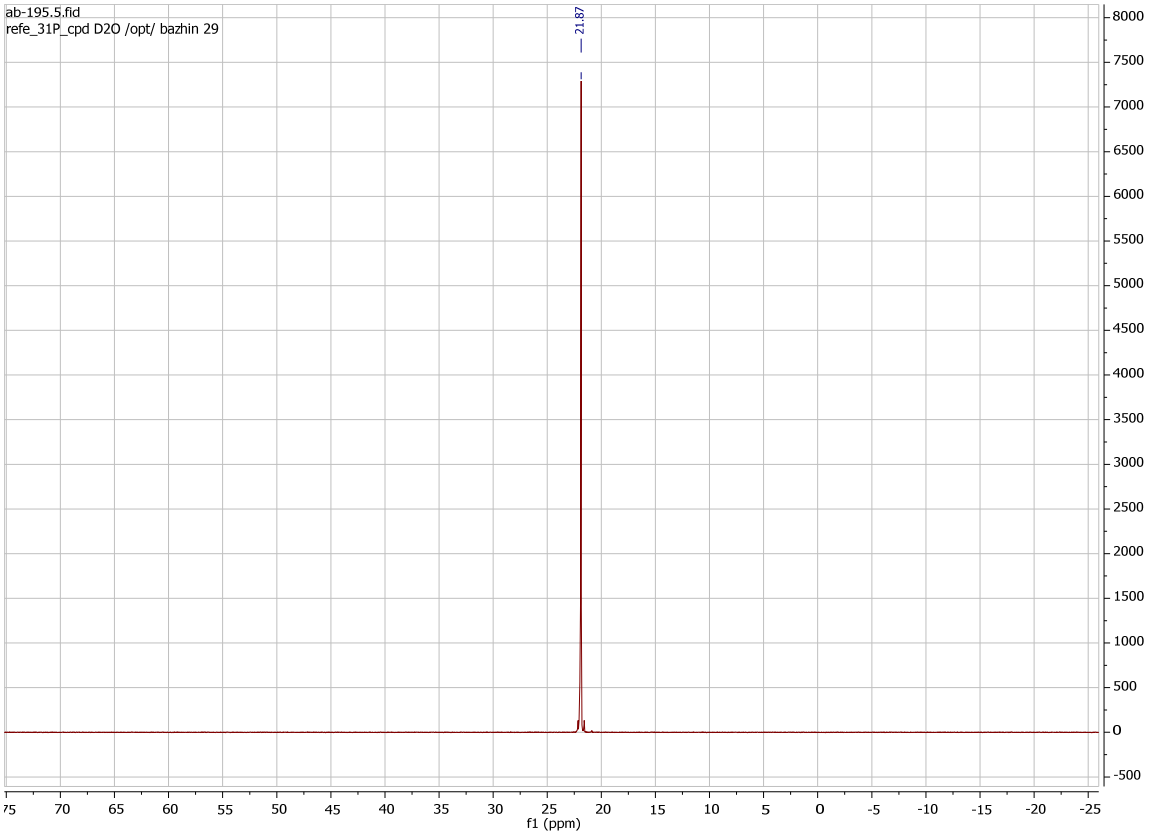

^{31}P spectrum of ^{15}N-labelled compound **3**

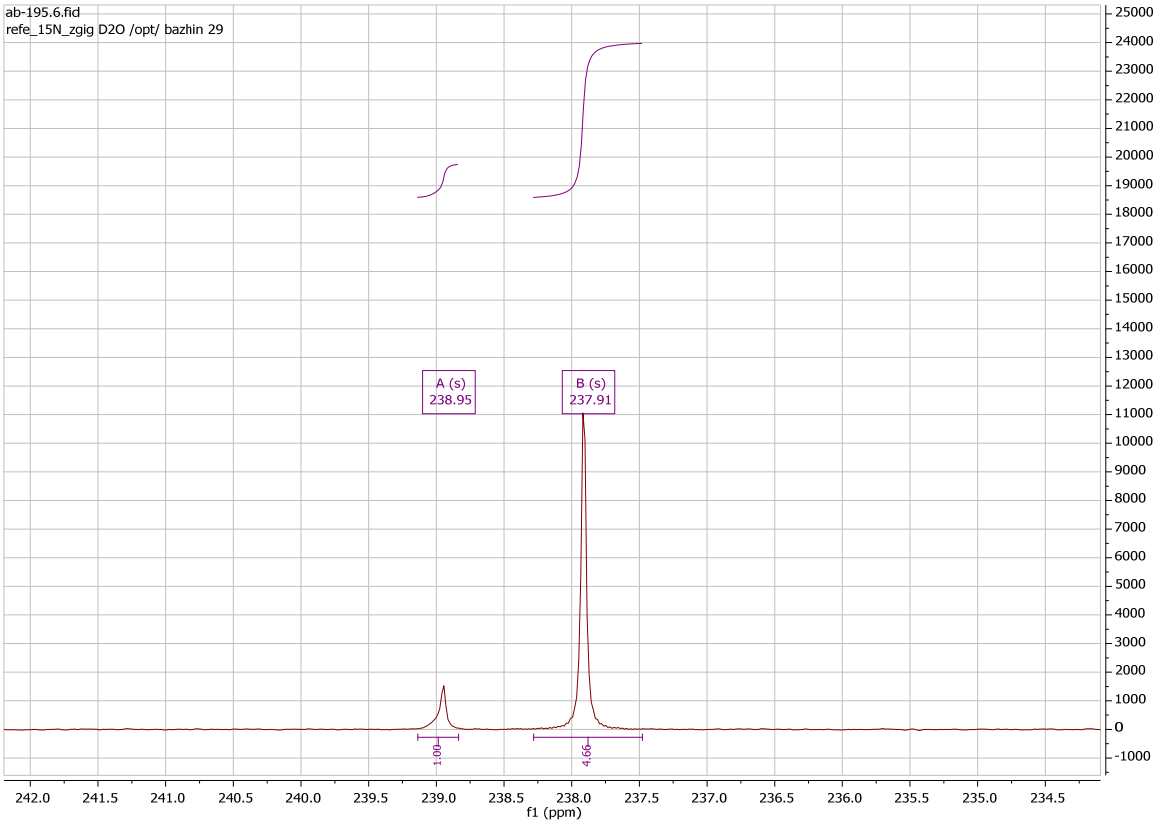

^{15}N spectrum of ^{15}N-labelled compound **3**

The reaction mechanism is rather complex and was described by Ugi in 1957. The reaction proceeds via the formation of phenylpentazene that can later cyclize to phenylpentazole derivative[6-11]. Interestingly, that the product (azide) is formed from both pentazene and pentazole intermediates by elimination of N_2 gas.

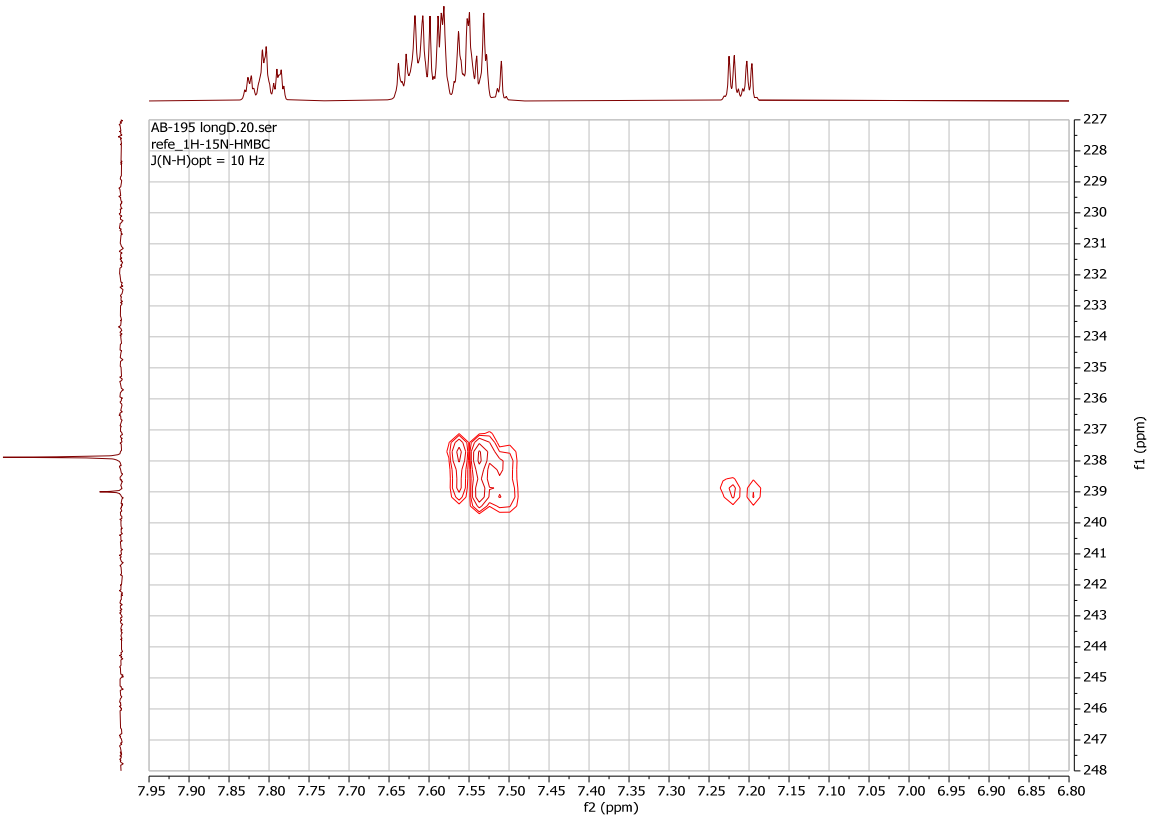

^{1}H-^{15}N HMBC spectrum of ^{15}N-labelled compound **3**. F1 axis enlarged in range 227-248 ppm

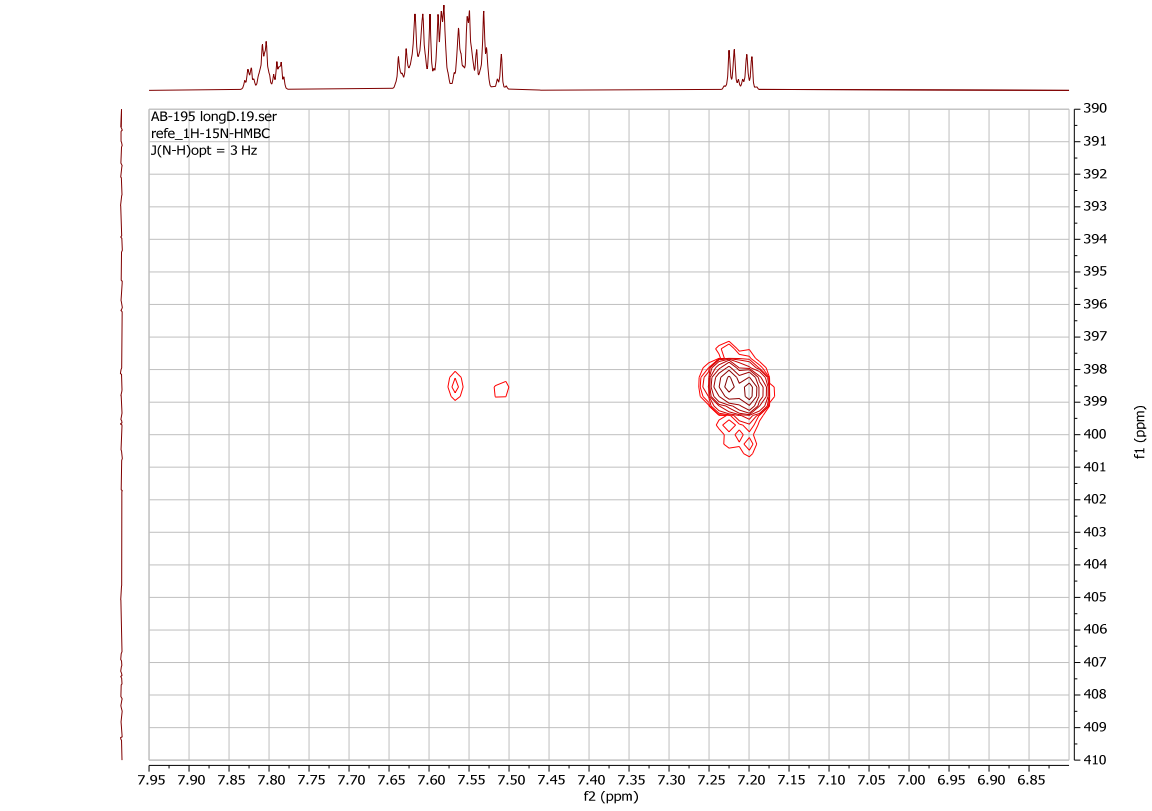

^{1}H-^{15}N HMBC spectrum of ^{15}N-labelled compound **3**. F1 axis enlarged in range 390-410 ppm

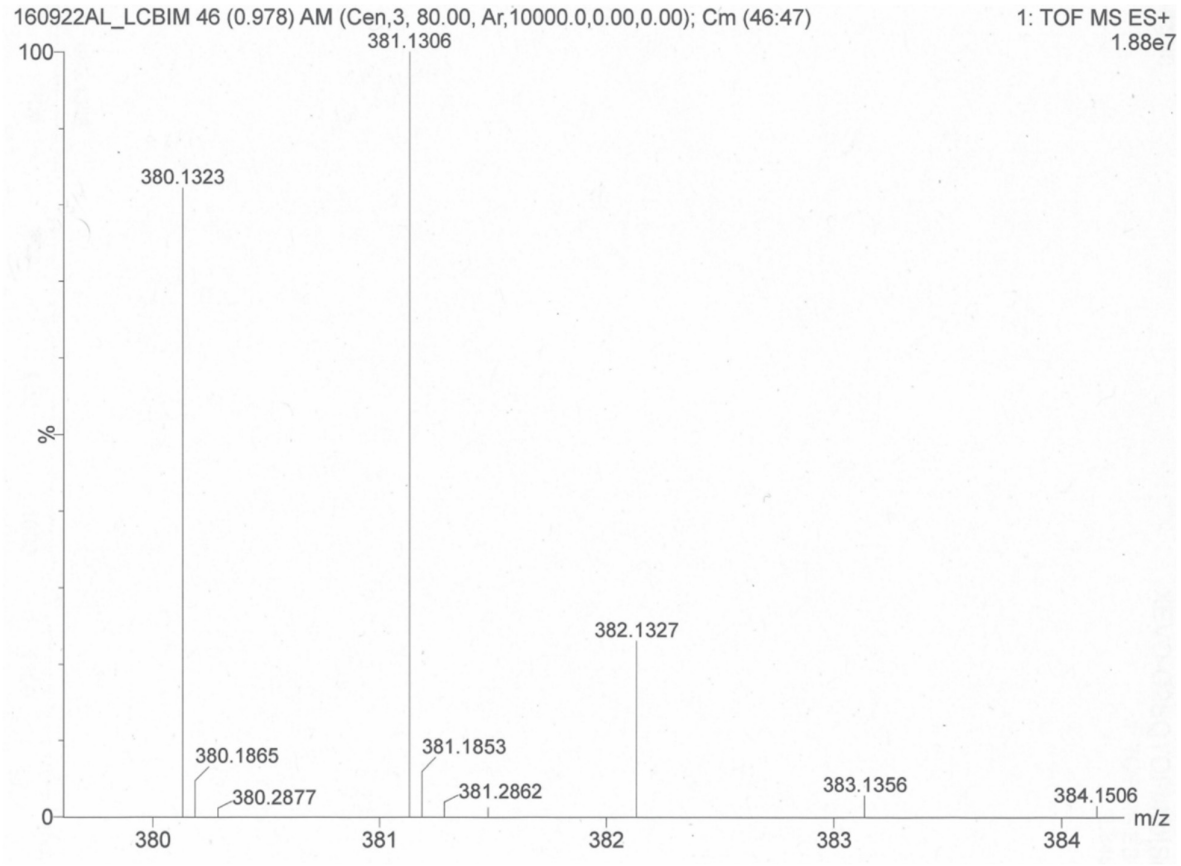

HRMS spectrum of the ^{15}N-labeled compound **3**, molecular ion region

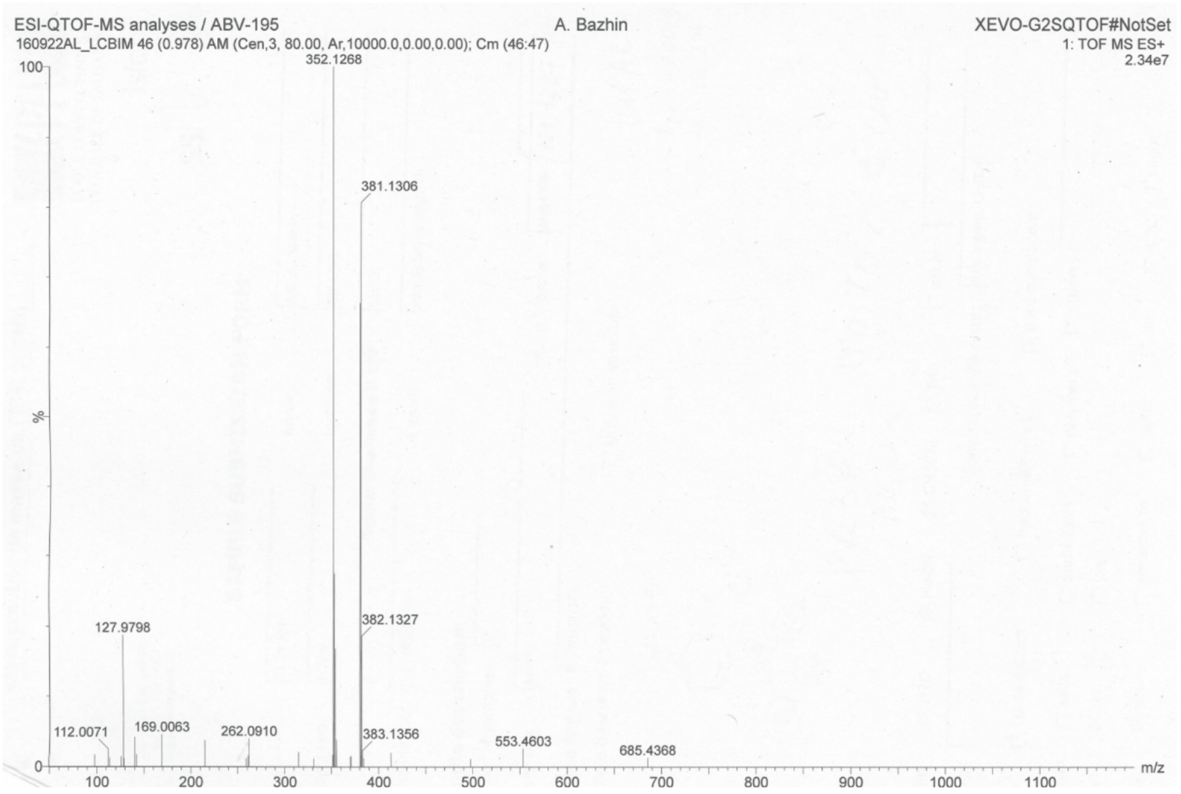

HRMS spectrum of the ^{15}N-labeled compound **3**, full view. Only one nitrene ion (352.1268, unlabeled) was detected

To assign observed ^{15}N peaks we synthesized compound **3** where only middle nitrogen was labeled. For this, we used ^{15}N labeled sodium nitrite and unlabeled sodium azide and the same procedure as before (**Scheme S6**). Characterization of the resulting compound showed one peak at 239 ppm on the ^{15}N NMR spectrum and correlation with the ortho- and meta-protons of the phenyl ring on ^{1}H-^{15}N HMBC.

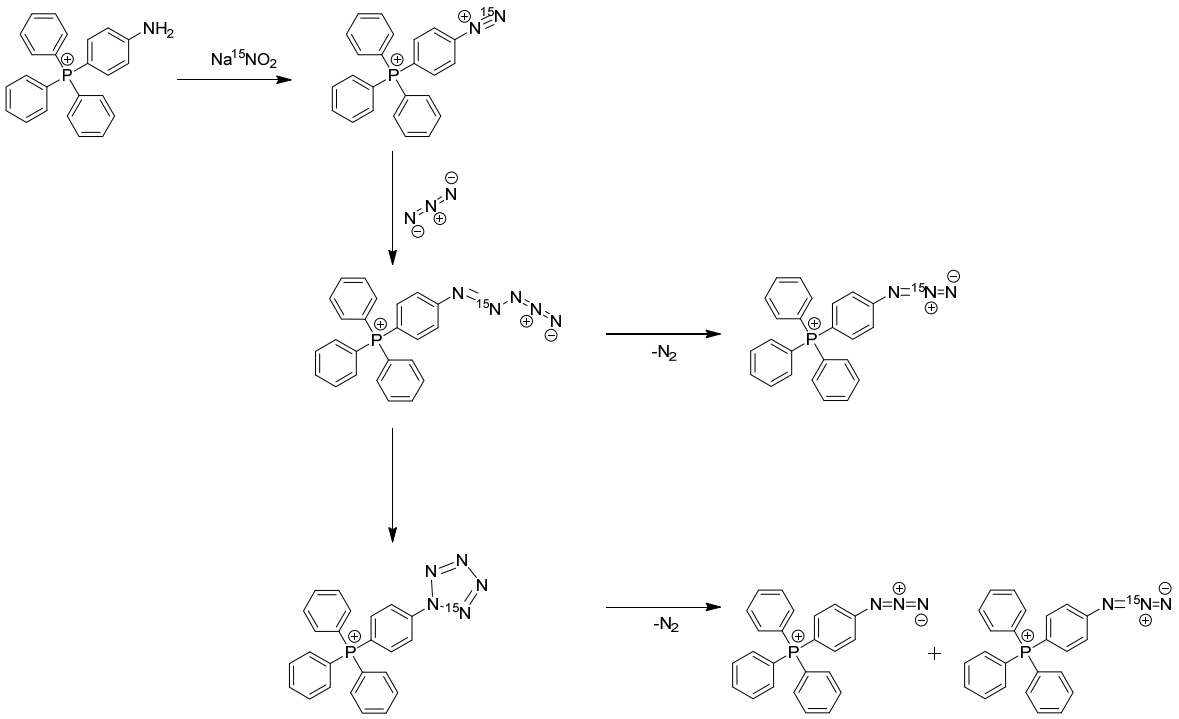

Scheme S6. Synthetic route for compound **3** with labeled middle nitrogen in the azide group.

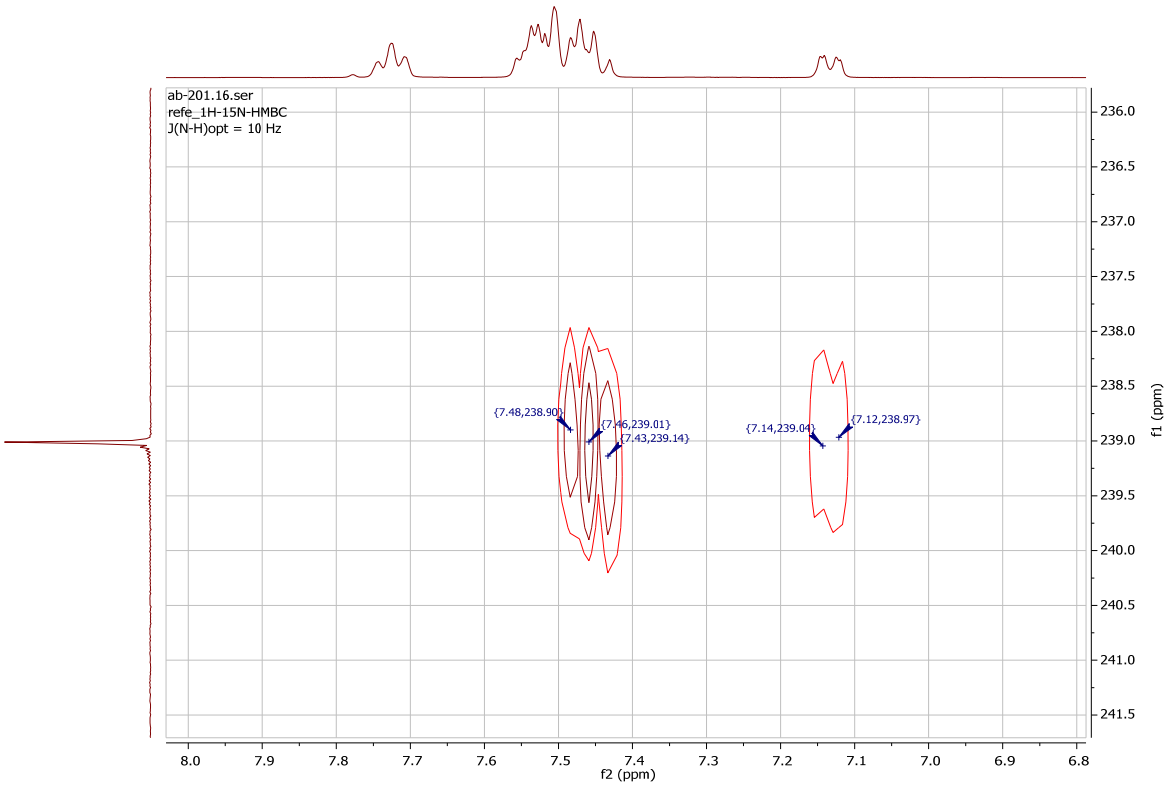

H-^{15}N HMBC spectrum of compound **3** with labeled middle nitrogen.

Assignment of ^{15}N NMR signals of compound **3**

Chemical shift, ppm	Nitrogen	Formula
398.5	Internal	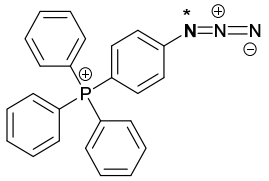
239	Internal (middle)	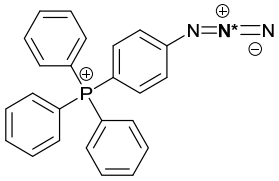
238	Terminal	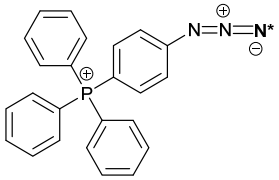

1.4 Reaction of TPP-CL1 with organic azides leads to the formation of acyltriazenes

1.4.1 Characterization of the ligation product in the reaction of compound 13 with azido-TPP2

Synthesis and purification of 2-(6-((2-(diphenylphosphanyl)benzoyl)oxy)benzo[d]thiazol-2-yl)-4,5-dihydrothiazole-4-carboxylic acid (**12**) was performed according to a published procedure[12]. The NMR spectra of **12** match the published ones.

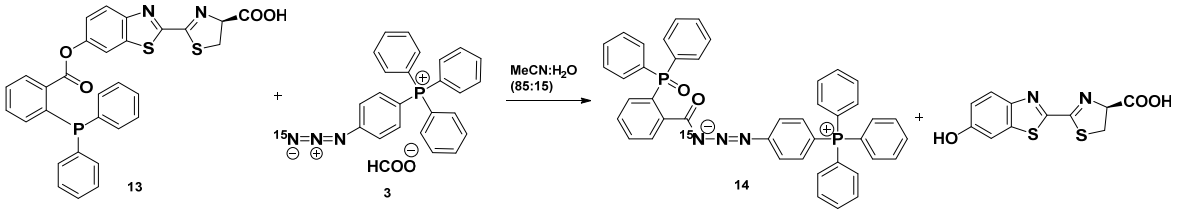

Scheme S7. Formation of acyltriazene derivative **13**.

10.7 mg of compound **13** was dissolved 3 ml of acetonitrile, then 530 µL of an aqueous solution of 13 mg of compound **3** was added. The reaction mixture was stirred at room temperature for 2 h. The product **14** was purified by semi-preparative HPLC (**Scheme S7**).

The same reaction was performed also using the ^{15}N labeled azide. The product was characterized by NMR and HRMS. The ^{15}N spectrum clearly shows the presence of two peaks (464 and 220 ppm) that are only possible if the N_2 release did not take place. The peak at 464.5 ppm is much less intense than the other one, which can be explained by the ratio of isotopomers in starting azide, meaning that the signal comes from the middle nitrogen in the product.

The product was crystallized from a mixture EtOH:EtOEt. The resulting crystals were used for X-Ray analysis. Based on the measurement of bond lengths, it seems that there is a charge separation in the molecule rather than the quinoid structure. Phosphorus of the phosphonium is positively charged and the negative charge can be delocalized within three N atoms.

^{1}H NMR (400 MHz, Methanol-d_4) δ 7.95 (td, J = 7.2, 1.8 Hz, 3H), 7.87–7.53 (m, 24H), 7.53–7.38 (m, 6H).

^{13}C NMR (101 MHz, Methanol-d_4) δ 170.25, 156.40, 136.88 (d, J = 11.2 Hz), 136.66 (d, J = 3.0 Hz), 135.84 (d, J = 10.4 Hz), 135.22 (d, J = 10.2 Hz), 133.78, 133.47, 133.23 (d, J = 7.6 Hz), 132.70, 131.62 (d, J = 13.0 Hz), 130.93 (d, J = 12.0 Hz), 130.47 (d, J = 10.1 Hz), 129.52 (d, J = 12.5 Hz), 124.60 (d, J = 13.6 Hz), 119.98, 119.09.

^{15}N NMR (41 MHz, CD_3CN) δ 490.25, 264.41.

^{31}P NMR (162 MHz, CD_3CN) δ 29.32, 22.45.

HRMS (ESI TOF ES+) calc. [M+1] 686.2126, found [M+1] 686.2127.

Crystal Data. $C_{45}H_{39}N_3O_3P_2$, M_r = 731.73, monoclinic, $P2_1/n$ (No. 14), a = 12.1755(2) Å, b = 9.8681(2) Å, c = 31.6381(5) Å, β = 99.658(2)°, α = γ = 90°, V = 3747.41(12) Å^3, T = 140.00(10) K, Z = 4, Z' = 1, μ(CuKα) = 1.416, 25938 reflections measured, 7668 unique (R_{int} = 0.0264) which were used in all calculations. The final wR_2 was 0.0971 (all data) and R_1 was 0.0371 (I > 2(I)).

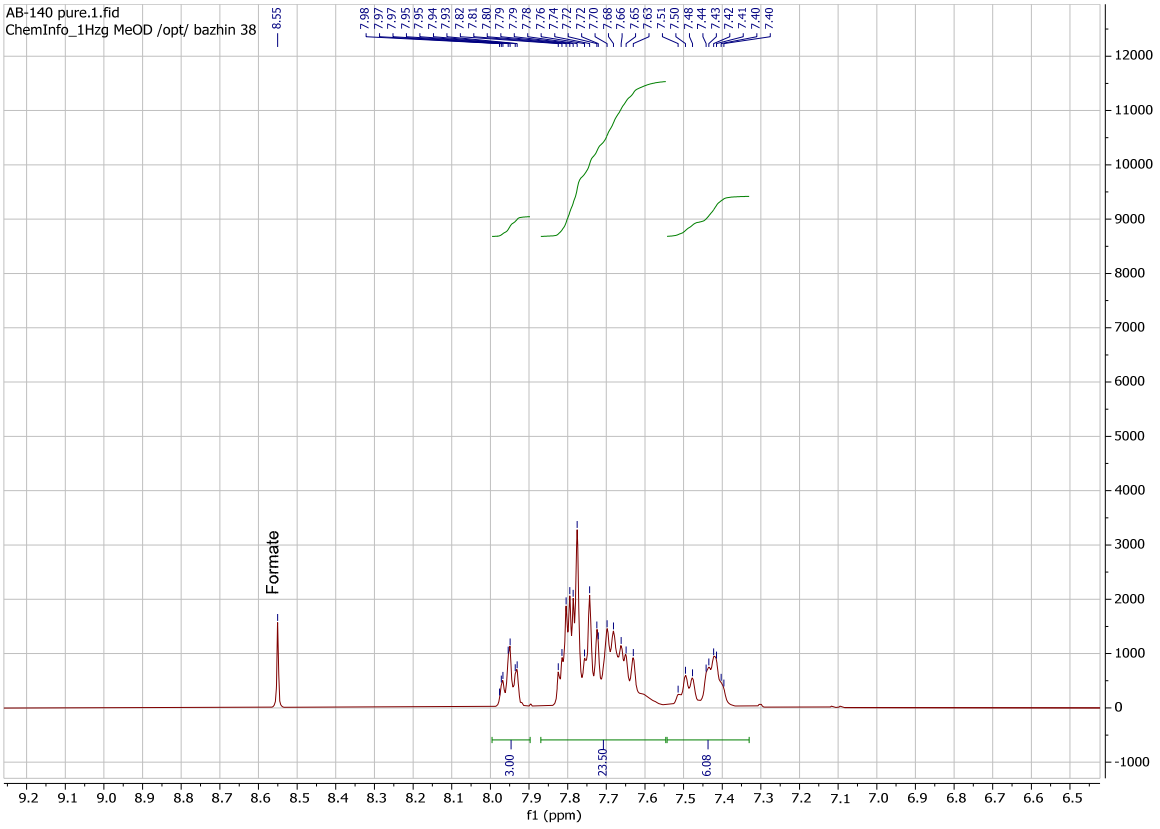

^{1}H spectrum of compound **14**

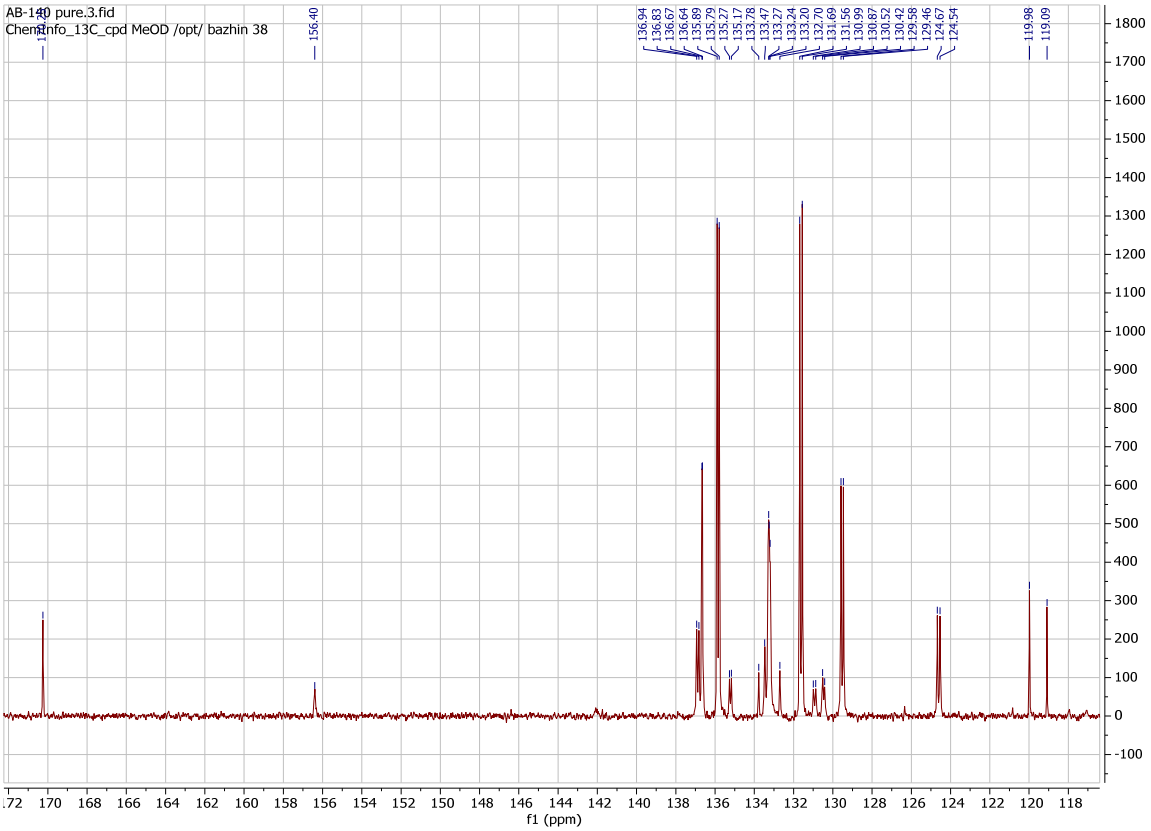

^{13}C spectrum of compound **14**

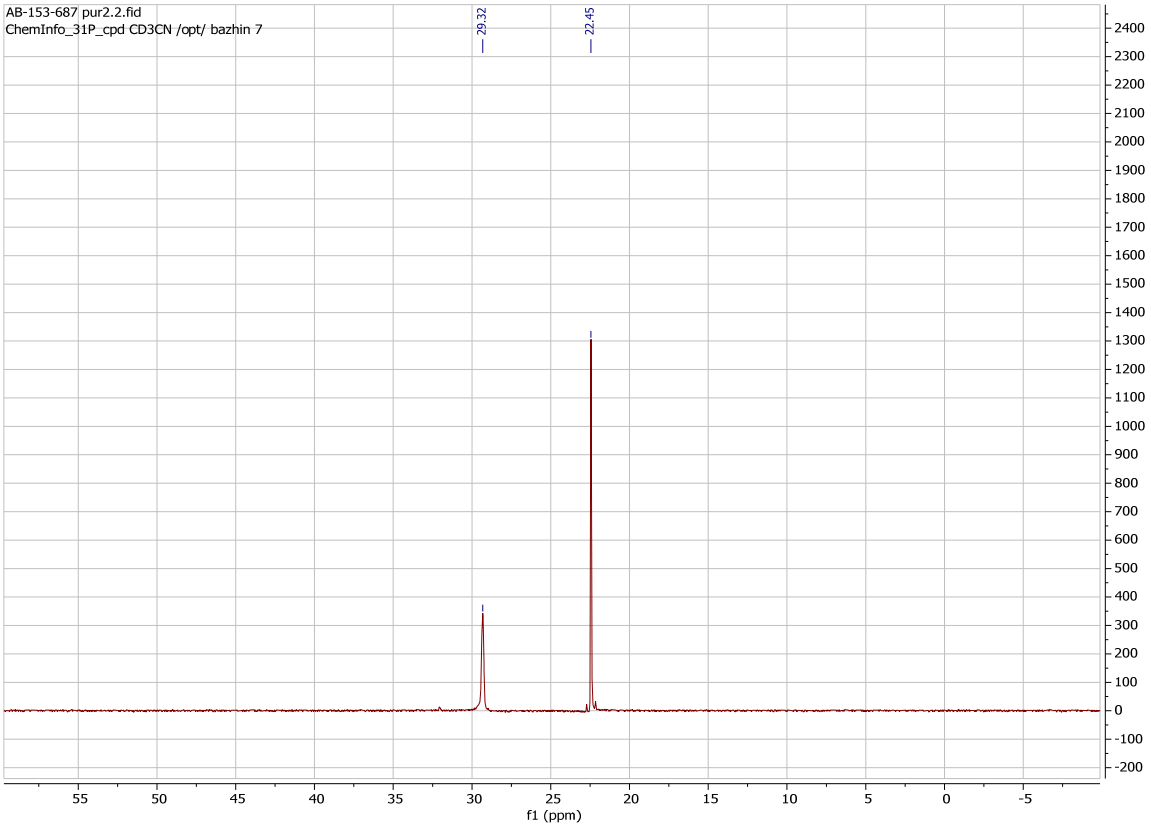

^{31}P spectrum of compound **14**

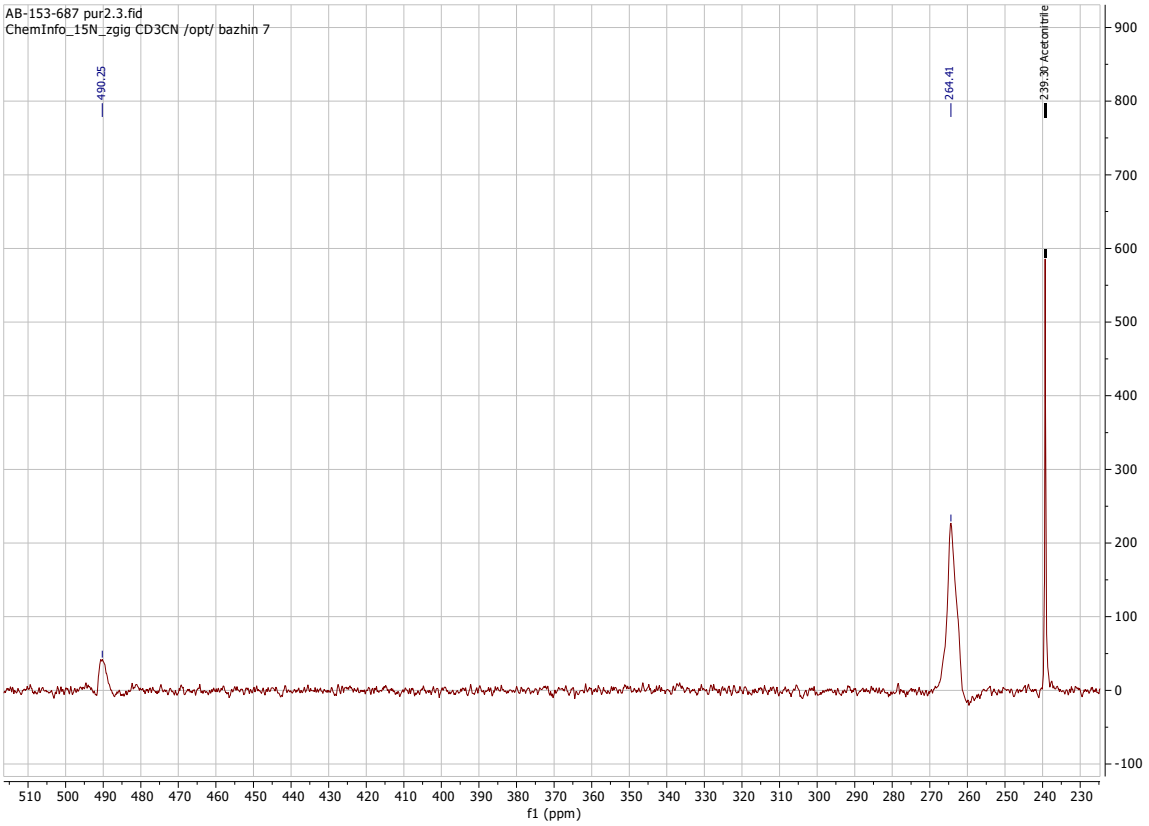

^{15}N spectrum of compound **14**

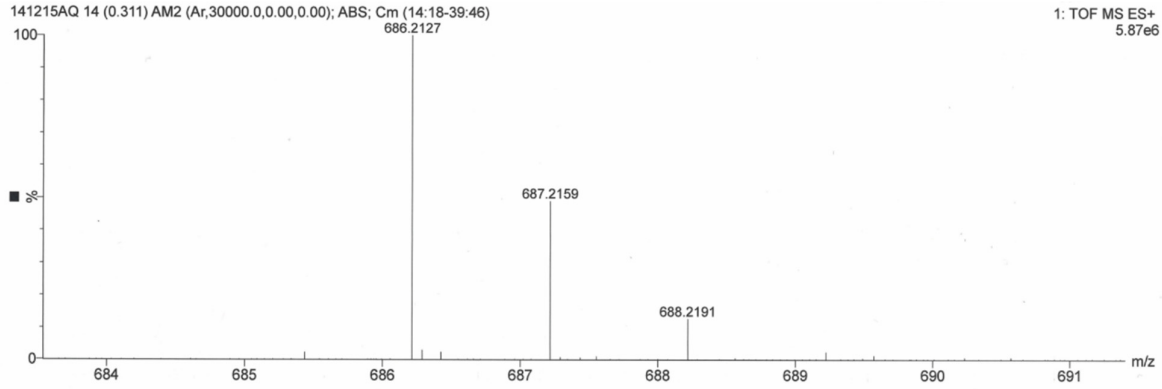

HRMS spectrum of compound **14**

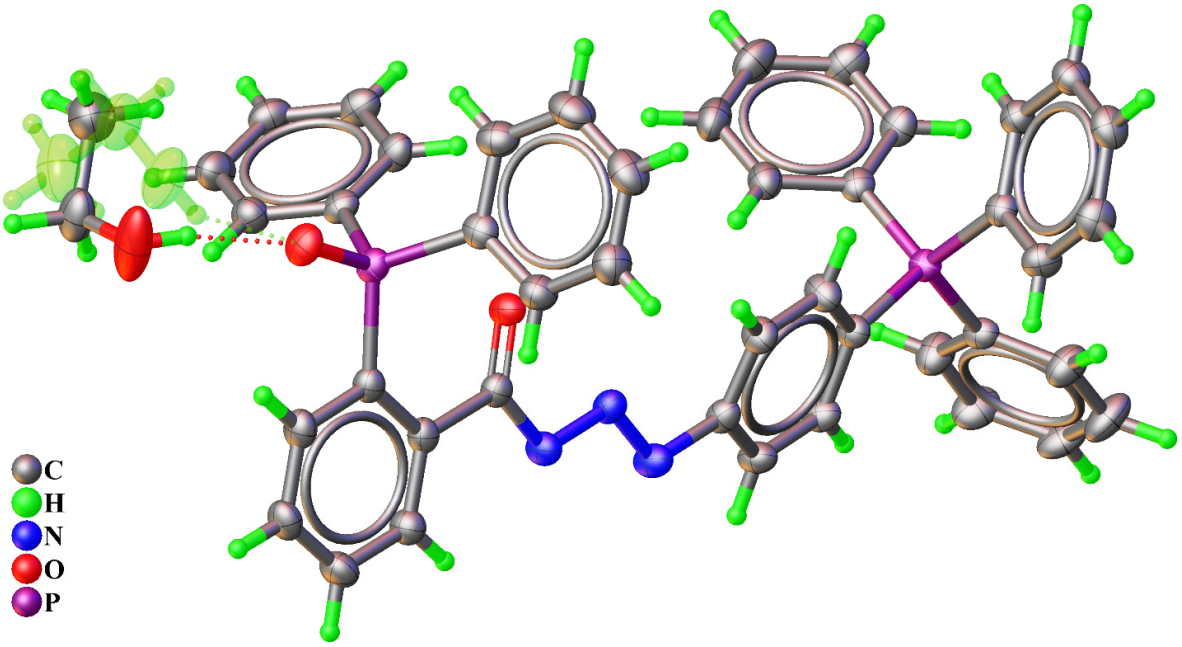

Single-crystal X-ray structure of compound **14**.

We propose that the reaction goes through a known mechanism that involves the formation of acyl triazenophosphonium salt, which is then hydrolyzed to acyltriazene[13] (**Scheme S8**).

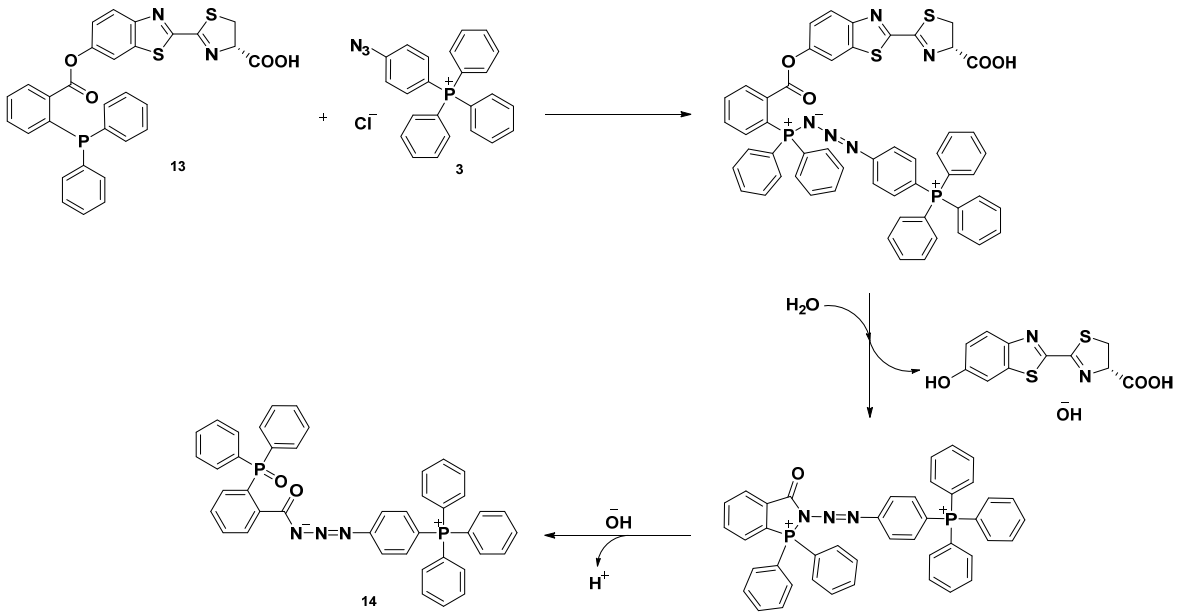

Scheme S8. Mechanism of the acyltriazene **14** formation.

1.4.2 Formation of acyltriazene 14 in the reaction between compound 12 and labeled azido-TPP1

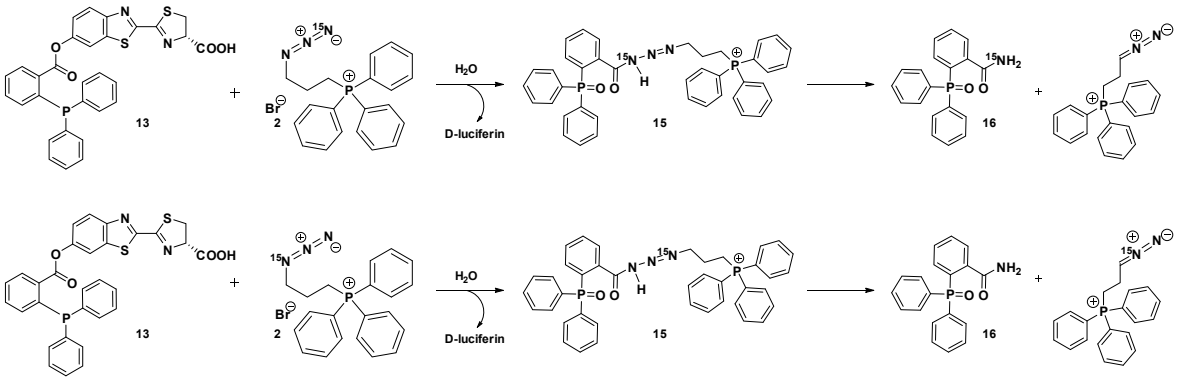

Scheme S9. Reaction of ^{15}N labelled azido-TPP1 with an analogue of TPP-CL1 results in the formation of acyltriazene derivative **15**

50 mg of compound 12 were dissolved in 0.7 mL of DCM, and to the resulting solution, 52 mg of ^{15}N-labeled azido-TPP1 were added. The reaction was monitored by ^{31}P, ^{15}N NMR, and HPLC-MS. The reaction was completed in 8 h. The reaction mixture was evaporated and purified by semi-preparative HPLC.

During the reaction, in ^{15}N spectrum four signals (437.9, 428.9, 213.3, 209.8 ppm) appeared that do not correspond to azido-TPP1. It can be explained only by formation of phosphazide that subsequently converts to the corresponding acyltriazene (**15**, **Scheme S9**). On the HRMS spectrum of the reaction mixture, we can clearly observe a peak with m/z equal to 653.2260 that corresponds to compound **15** with a theoretical m/z of 653.2253 (1 ppm difference).

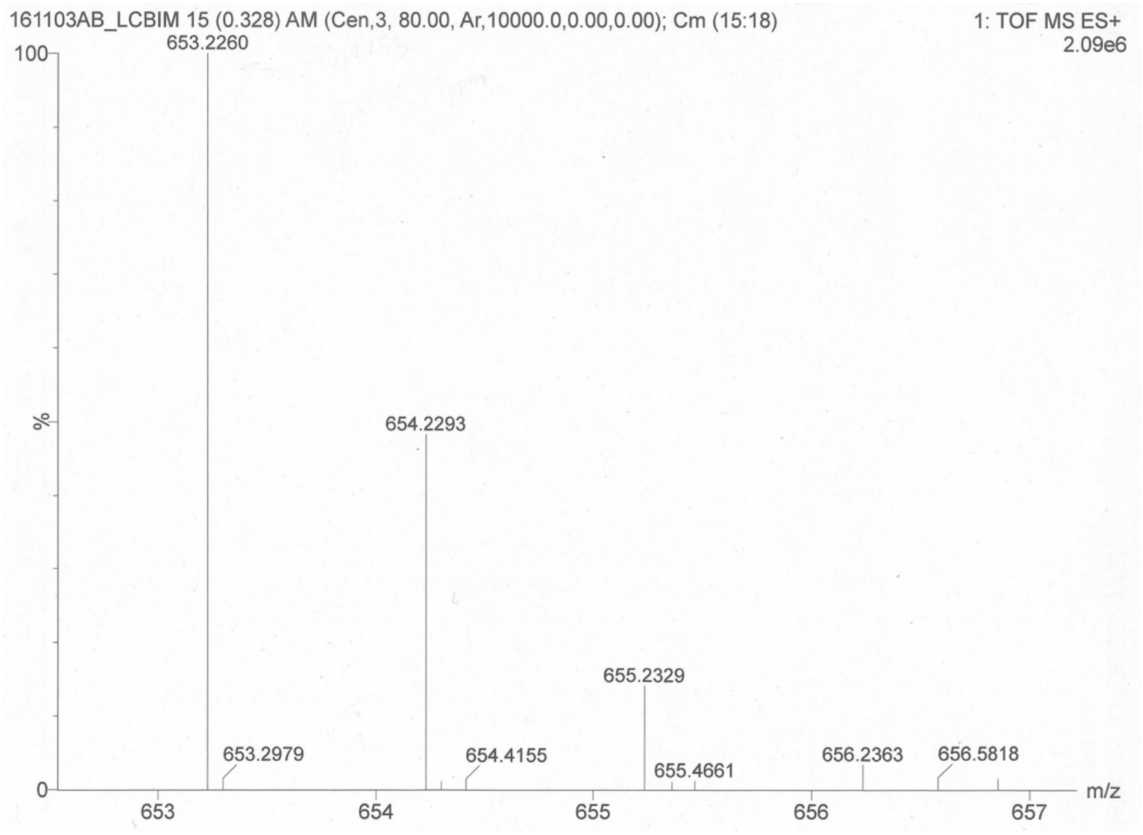

HRMS spectrum of the reaction mixture (**13, 2, 15**).

During the work-up and HPLC purification, product **15** decomposed to 2-(diphenylphosphoryl)benzamide (**16**, mixture of unlabeled and ^{15}N-labeled, **Scheme S9**) that was purified by ion-exchange chromatography (Dowex 50WX8 resin). The decomposition was anticipated because alkyl substituted acyltriazenes are known to be unstable and degrade to primary amides and the corresponding alkyldiazo derivative[13]. Identification of the decomposition product was done by HRMS and NMR.

Signals from two protons of the primary amide group have very different chemical shifts (8.69 and 5.67 ppm) that can be explained by magnetic field anisotropy and the formation of a hydrogen bond with an oxygen of the phosphoryl moiety. The signals are observed as pseudo-triplets because the doublet of the ^{15}N-labeled isotopomer (^{1}H-^{15}N ^{1}J = 90 Hz) is overlapping with a singlet of the unlabeled analogue. From the ^{15}N and ^{31}P spectra, it is clear that the compound contains only one nitrogen atom and one phosphorus, which have typical chemical shifts for a primary amide and phosphine oxide, respectively. The fact that the decomposition product is a primary amide of aromatic carbonic acid is further supported by ^{1}H-^{15}N HSQC, ^{1}H-^{13}C HMBC spectra, and HRMS.

^{1}H NMR (400 MHz, Methylene Chloride-d_2) δ 8.69 (d, J = 90.0 Hz, 0.5H), 8.69 (s, 0.5H), 7.95 (ddd, J = 7.7, 4.1, 1.3 Hz, 1H), 7.68–7.54 (m, 8H), 7.48 (tdd, J = 8.3, 3.1, 1.6 Hz, 4H), 7.40 (tdd, J = 7.6, 2.1, 1.3 Hz, 1H), 7.10 (ddd, J = 14.5, 7.7, 1.3 Hz, 1H), 5.78 (d, J = 2.1 Hz, 0H), 5.67 (d, J = 86.8 Hz, 0.5H), 5.67 (s, 0.5H).

^{13}C NMR (101 MHz, Methylene Chloride-d_2) δ 169.58–169.31 (m), 140.69 (dt, J = 8.5, 4.5 Hz), 133.84 (d, J = 11.9 Hz), 132.85 (d, J = 2.6 Hz), 132.65 (d, J = 2.9 Hz), 132.37, 132.26 (d, J = 9.9 Hz), 131.94 (d, J = 9.4 Hz), 131.31, 130.54, 130.34 (d, J = 12.1 Hz), 129.56, 129.02 (d, J = 12.3 Hz).

^{31}P NMR (162 MHz, Methylene Chloride-d_2) δ 34.39.

^{15}N NMR (41 MHz, Methylene Chloride-d_2) δ 110.49.

HRMS (ESI TOF ES+) calculated for $C_{19}H_{16}NO_2P$ [M+Na$^+$] 344.0816, found [M+Na$^+$] 344.0811; calculated for $C_{19}H_{16}{}^{15}NO_2P$ [M+Na$^+$] 345.0787, found [M+Na$^+$] 345.0792.

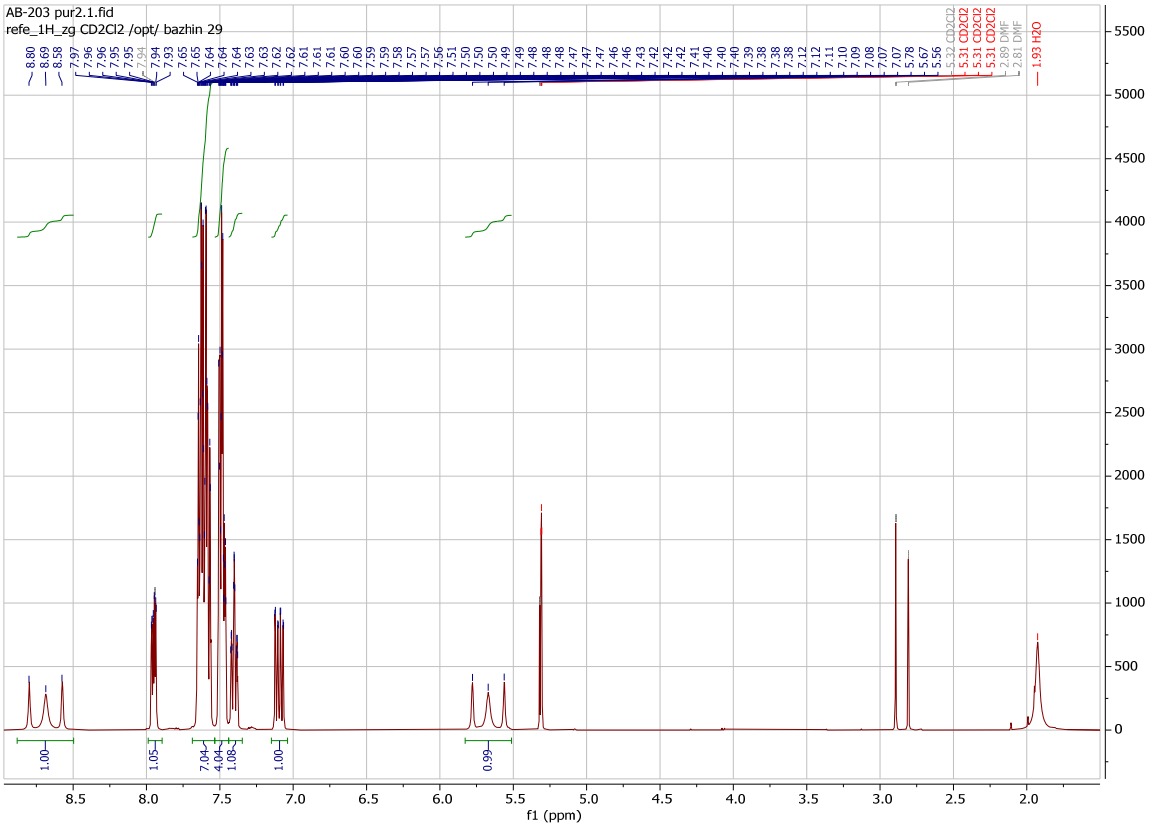

^{1}H spectrum of the decomposition product **16**

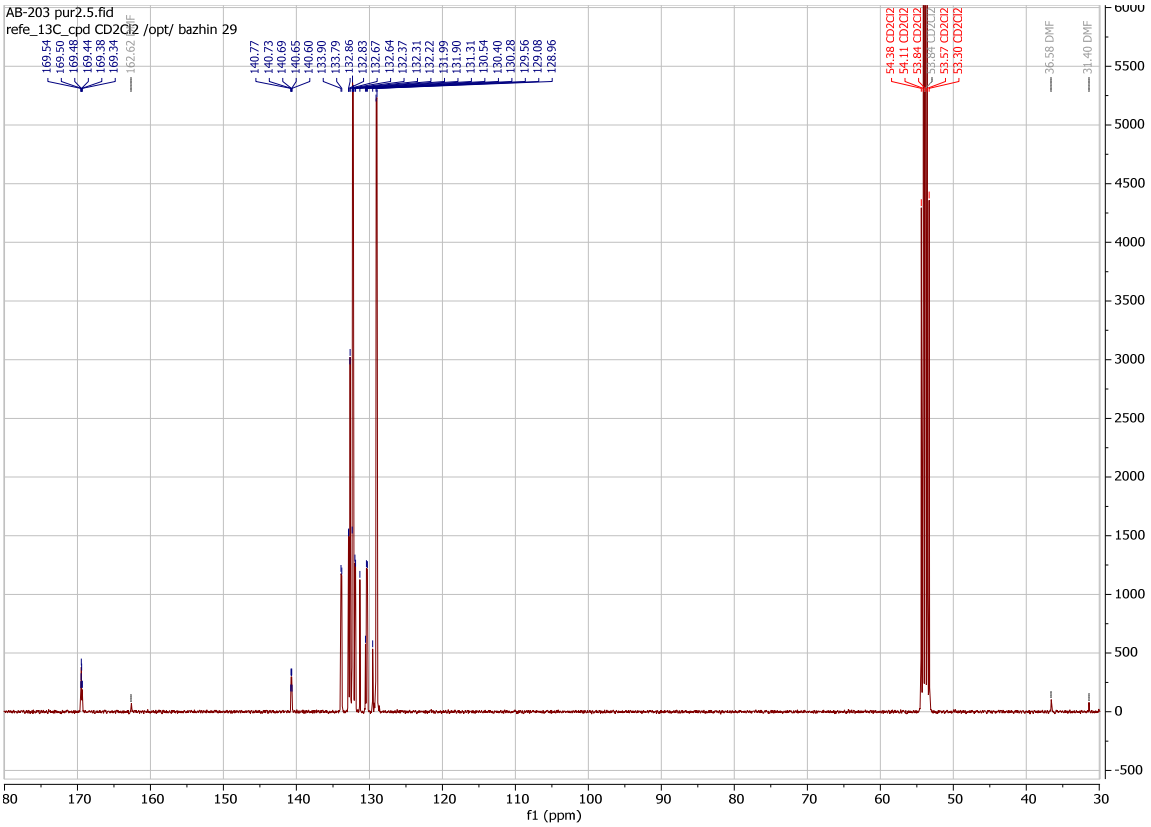

^{13}C spectrum of the decomposition product **16**

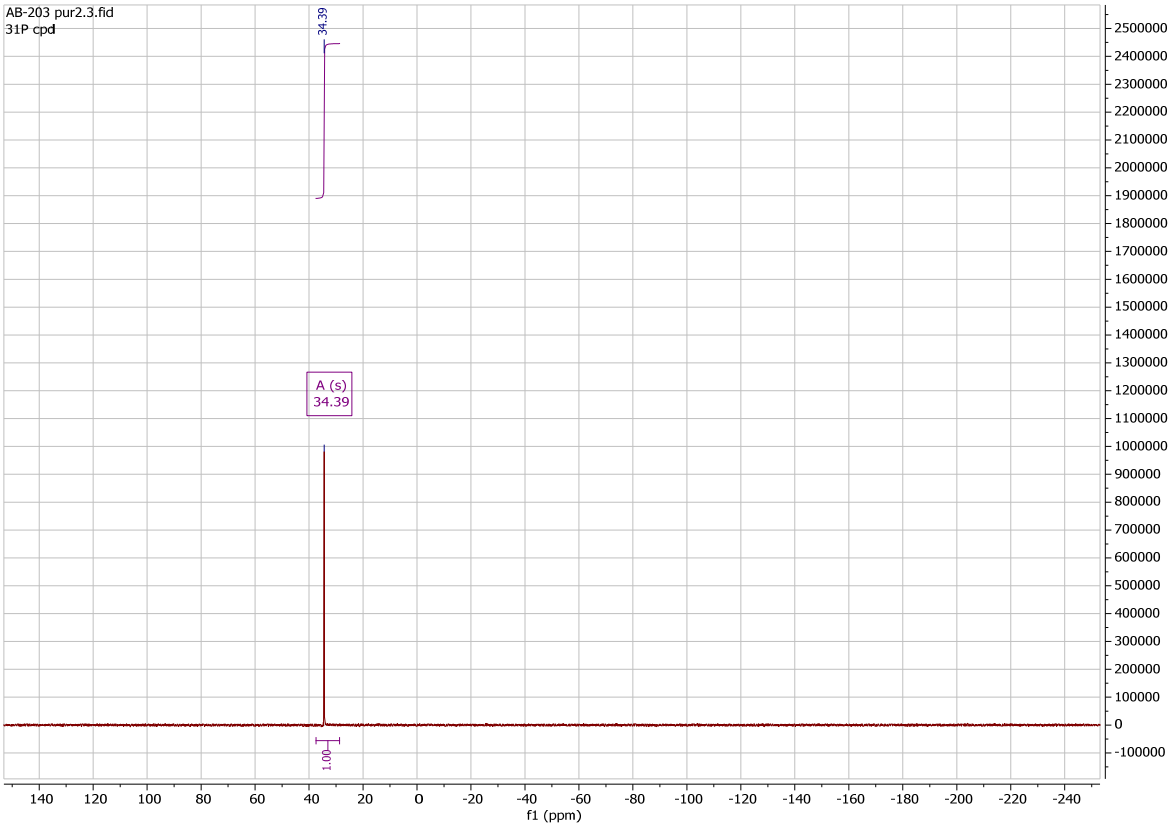

^{31}P spectrum of the decomposition product **16**

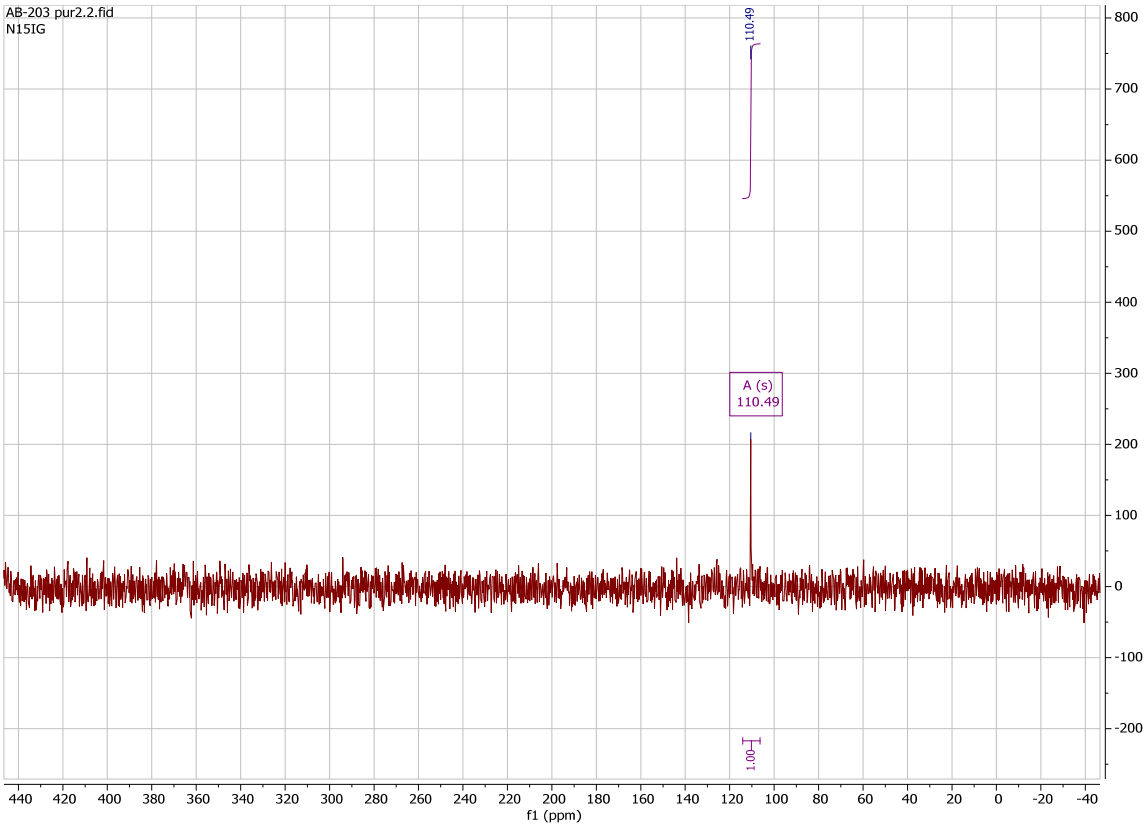

^{15}N spectrum of the decomposition product **16**

^{1}H-^{13}C HMBC spectrum the decomposition product **16**

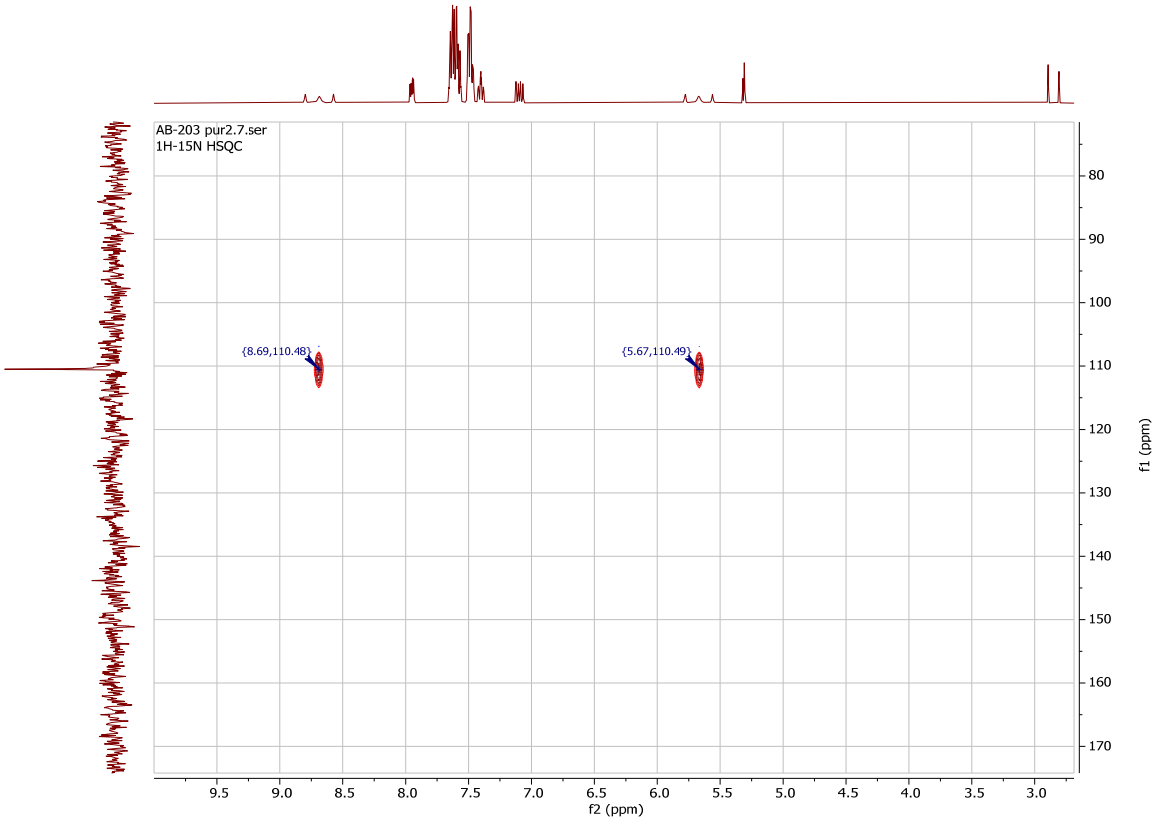

^{1}H-^{15}N HSQC spectrum of the decomposition product **16**

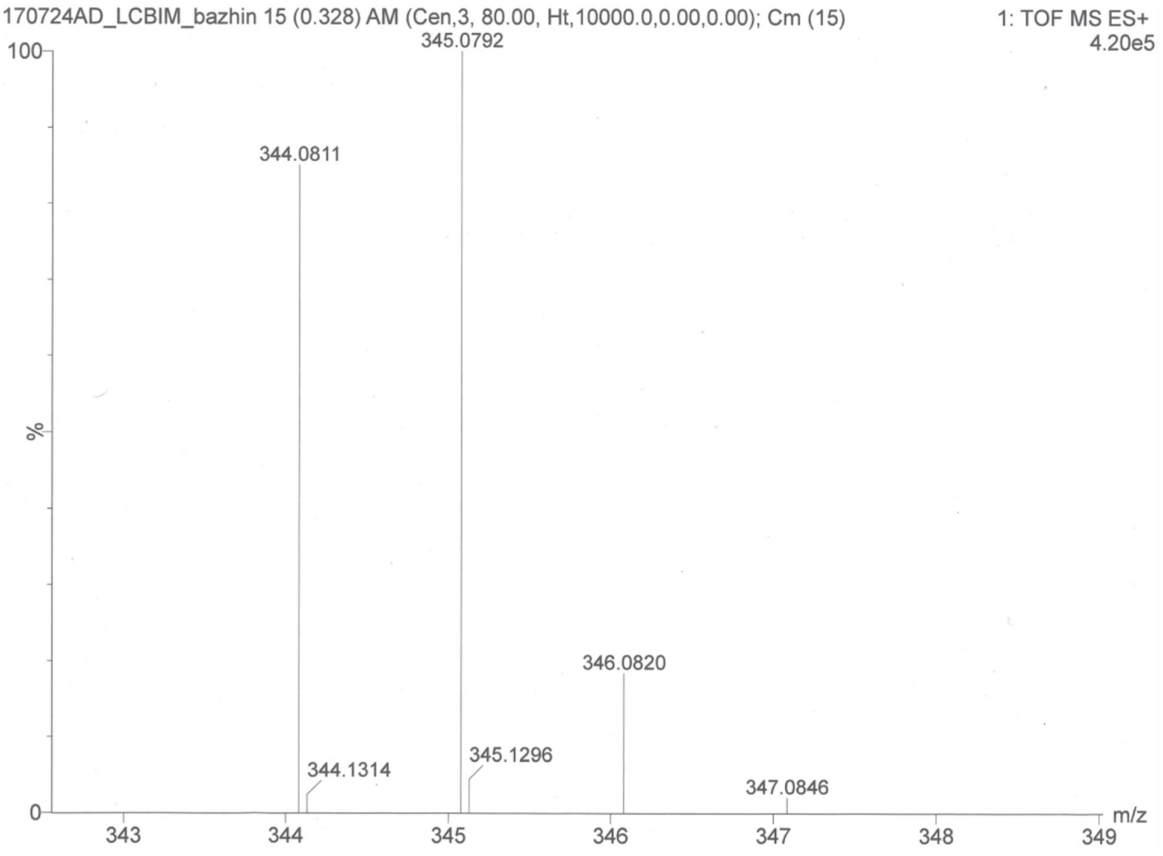

HRMS spectrum of the decomposition product **16**. [M+Na$^+$] adducts are observed.

1.5 Synthesis of TPP-CL2

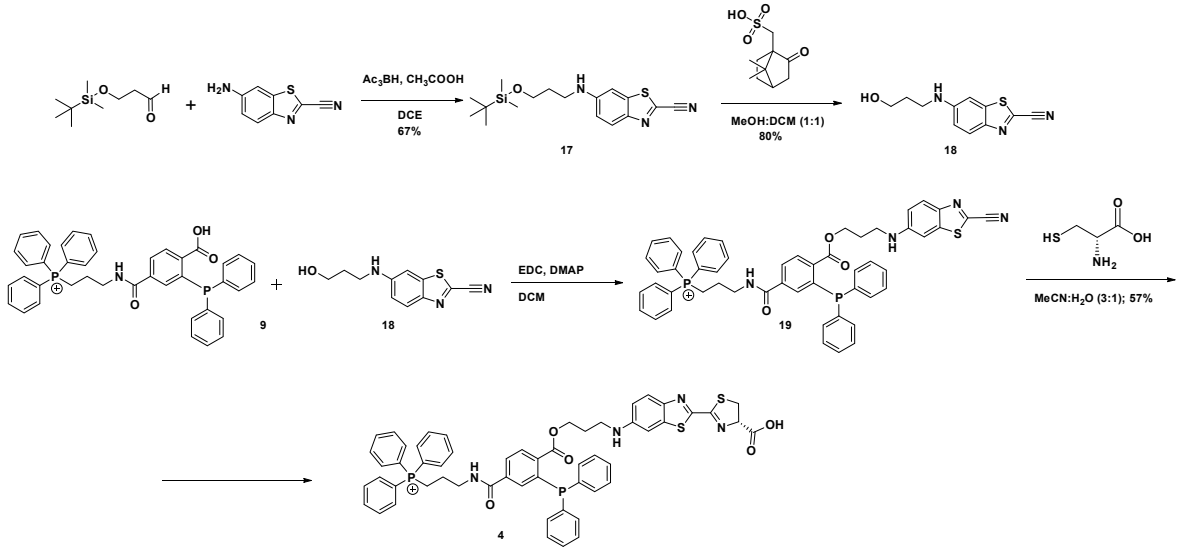

Scheme S10. Synthetic route to TPP-CL2.

1.5.1 Synthesis of 6-((3-((tert-butyldimethylsilyl)oxy)propyl)amino)benzo[d]thiazole-2-carbonitrile (17).

6-aminobenzothiazole-2-carbonitrile (100 mg, 0.571 mmol, 1 eq.) was mixed with TBDMS-protected 3-hydroxypropanale (151 mg, 0.8 mmol, 1.4 eq.) in 6 mL of THF at room temperature. A few drops of glacial acetic acid were added to the mixture. The reaction mixture was stirred at room temperature for 12 h. Then, 600 mg of triacetoxyborohydride were added to the mixture to reduce the azomethine. After the reduction

was complete, the reaction mixture was evaporated under reduced pressure. Crude material was dissolved in 30 mL DCM and washed three times with 10 mL of water. The organic layer was separated, dried over sodium sulfate, and then evaporated to a yellow solid material that was later purified by HPLC. The weight of the pure product was 115 mg (yield 58%). The pure product was recrystallized from methanol. The resulting crystals were used for X-ray analysis.

^{1}H NMR (400 MHz, Methanol-d_4) δ 7.74 (d, J = 8.9 Hz, 1H), 7.00–6.84 (m, 2H), 3.75 (t, J = 5.9 Hz, 2H), 3.22 (t, J = 6.8 Hz, 2H), 1.83 (p, J = 6.4 Hz, 2H), 0.90 (s, 9H), 0.05 (s, 6H).

^{13}C NMR (101 MHz, Methanol-d_4) δ 151.60, 144.96, 140.23, 129.49, 125.79, 118.30, 114.86, 99.80, 61.91, 41.25, 32.88, 26.44, 19.11.

HRMS (ESI TOF ES+) calc. for [$C_{17}H_{25}N_3OSSi$ + H^+] 348.1566, found 348.1566.

Crystal Data. $C_{17}H_{25}N_3OSSi$, M_r = 347.55, monoclinic, $P2_1/c$ (No. 14), a = 12.0200(10) Å, b = 6.7762(14) Å, c = 46.566(7) Å, β = 96.539(9)°, α = γ = 90°, V = 3768.1(10) Å^3, T = 120(2) K, Z = 8, Z' = 2, μ(MoKα) = 0.243, 28983 reflections measured, 5943 unique (R_{int} = 0.0431) which were used in all calculations. The final wR_2 was 0.1122 (all data) and R_1 was 0.0498 (I > 2(I)).

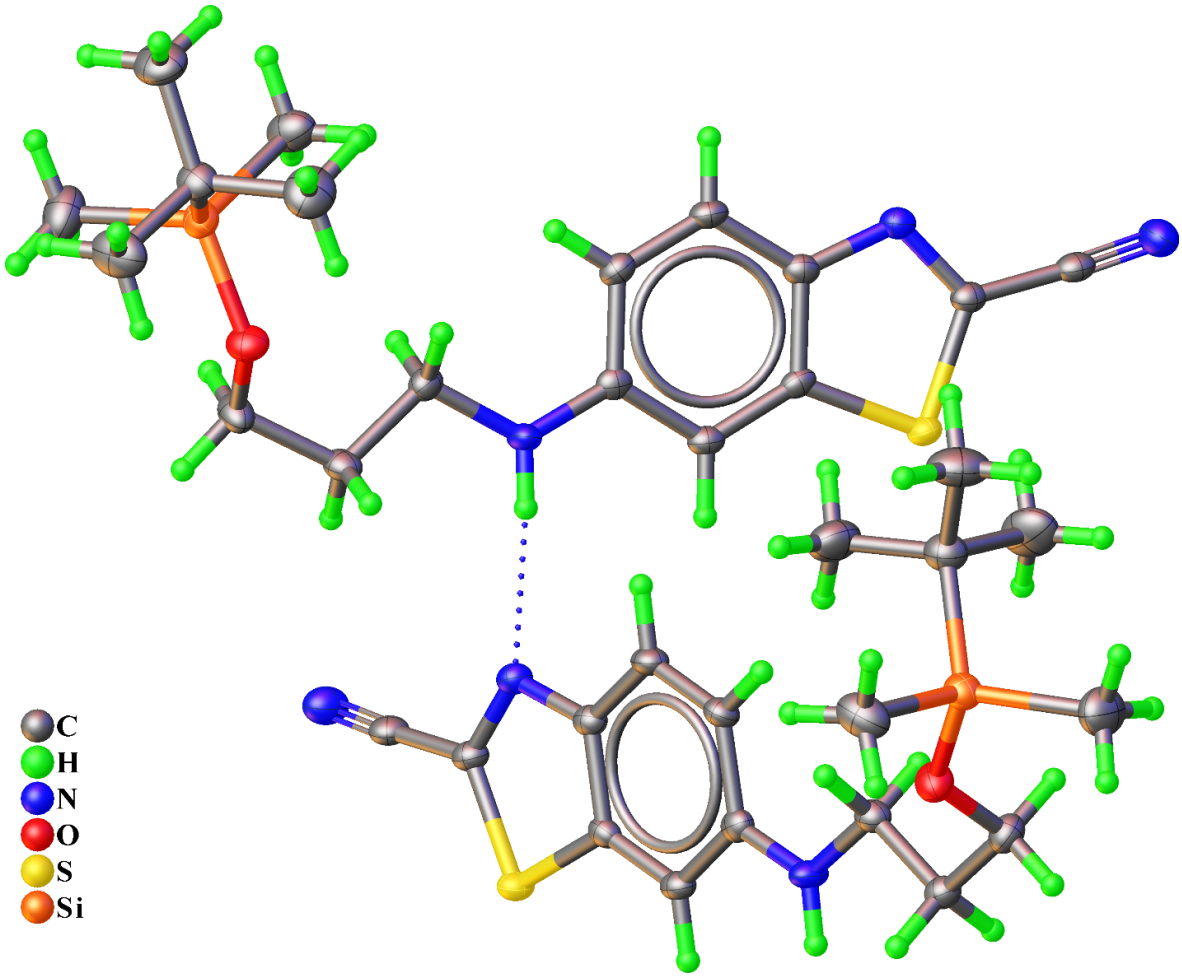

Single-crystal X-ray structure of compound **17**.

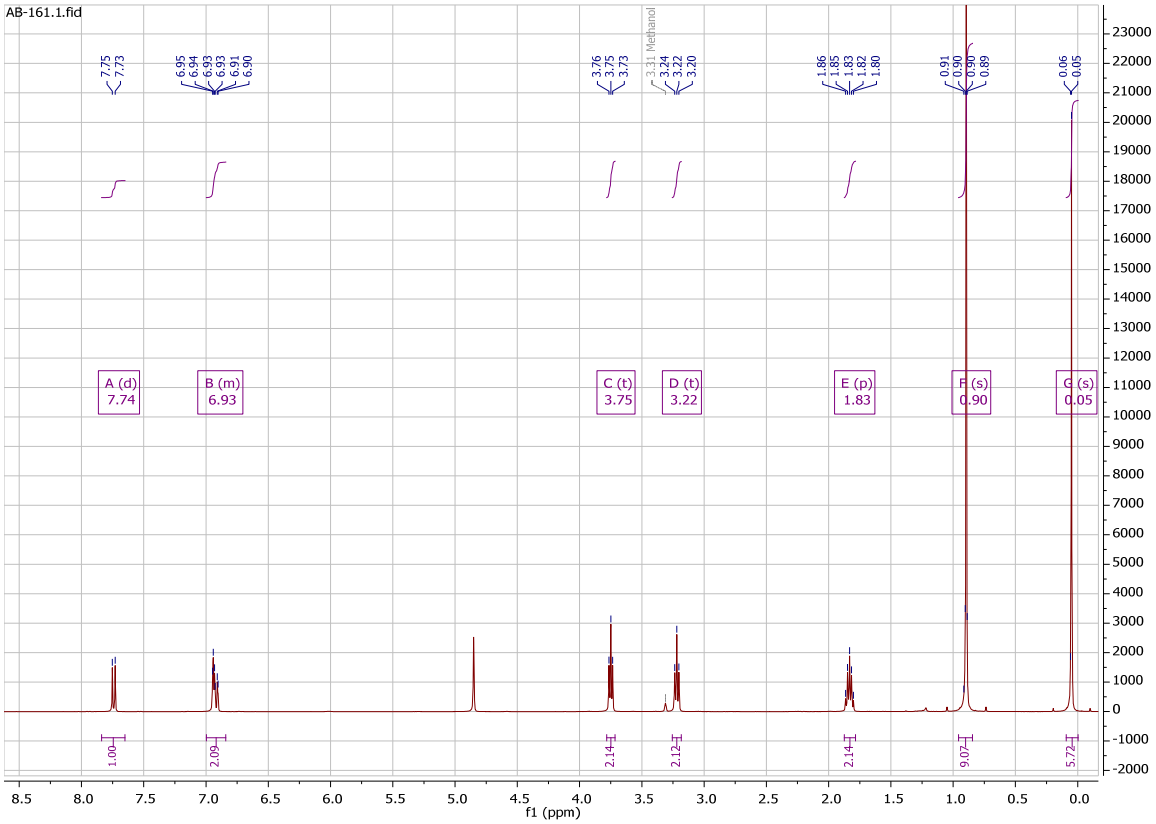

^{1}H spectrum of compound **17**

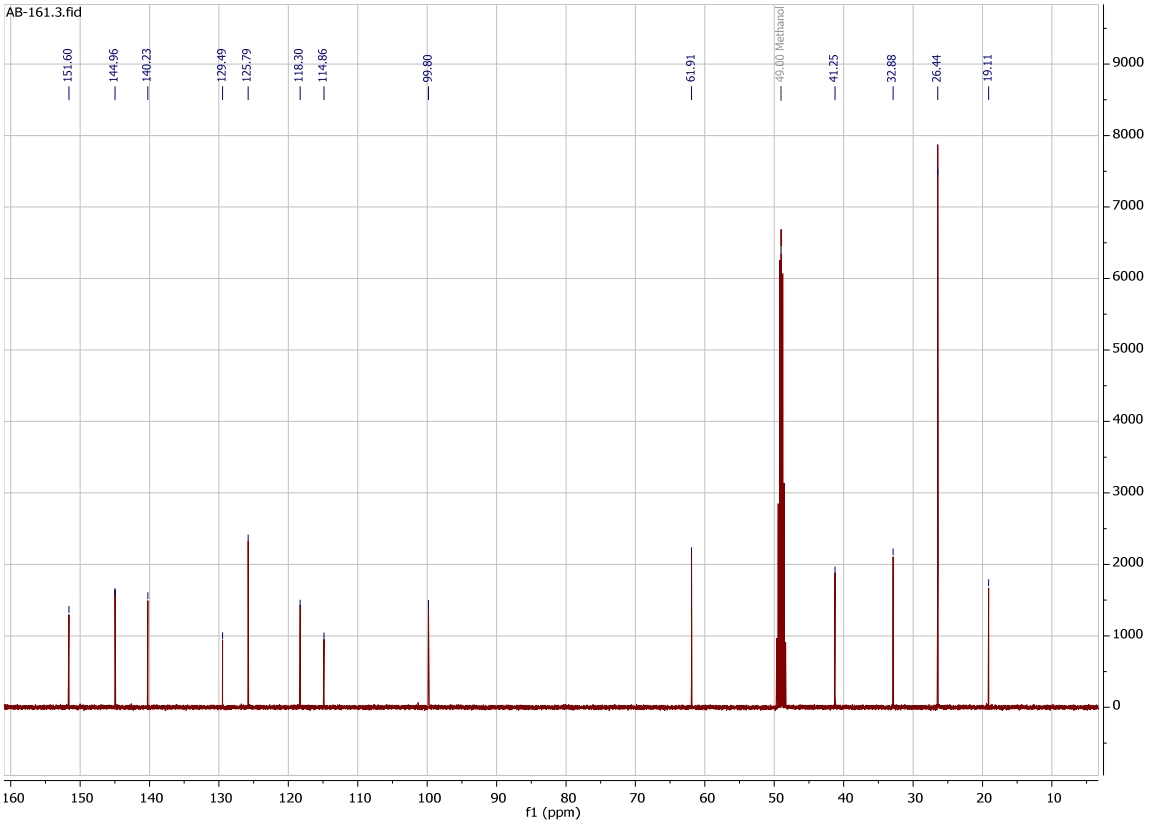

^{13}C spectrum of compound **17**

1.5.2 **Synthesis of 6-((3-hydroxypropyl)amino)benzo[d]thiazole-2-carbonitrile (18)**

100 mg of **17** were dissolved in 20 mL of methanol. Triethylsilane (1 eq, 33 mg, 46 µL) and camphorsulfonic acid (0.4 eq, 25.8 mg) were added to the solution. The reaction mixture was stirred at room temperature and monitored by UPLC-MS. After completion, the mixture was evaporated under reduced pressure to get the crude material that was then purified by preparative HPLC. Pure product was characterized by NMR and HRMS.

^{1}H NMR (400 MHz, Methanol-d_4) δ 7.72 (d, J = 8.9 Hz, 1H), 6.96–6.89 (m, 2H), 3.70 (t, J = 6.2 Hz, 2H), 3.23 (t, J = 7.0 Hz, 2H), 1.91–1.82 (m, 2H).

^{13}C NMR (101 MHz, Methanol-d_4) δ 150.22, 143.64, 138.90, 128.27, 124.41, 116.98, 113.54, 98.61, 59.32, 39.92, 31.32.

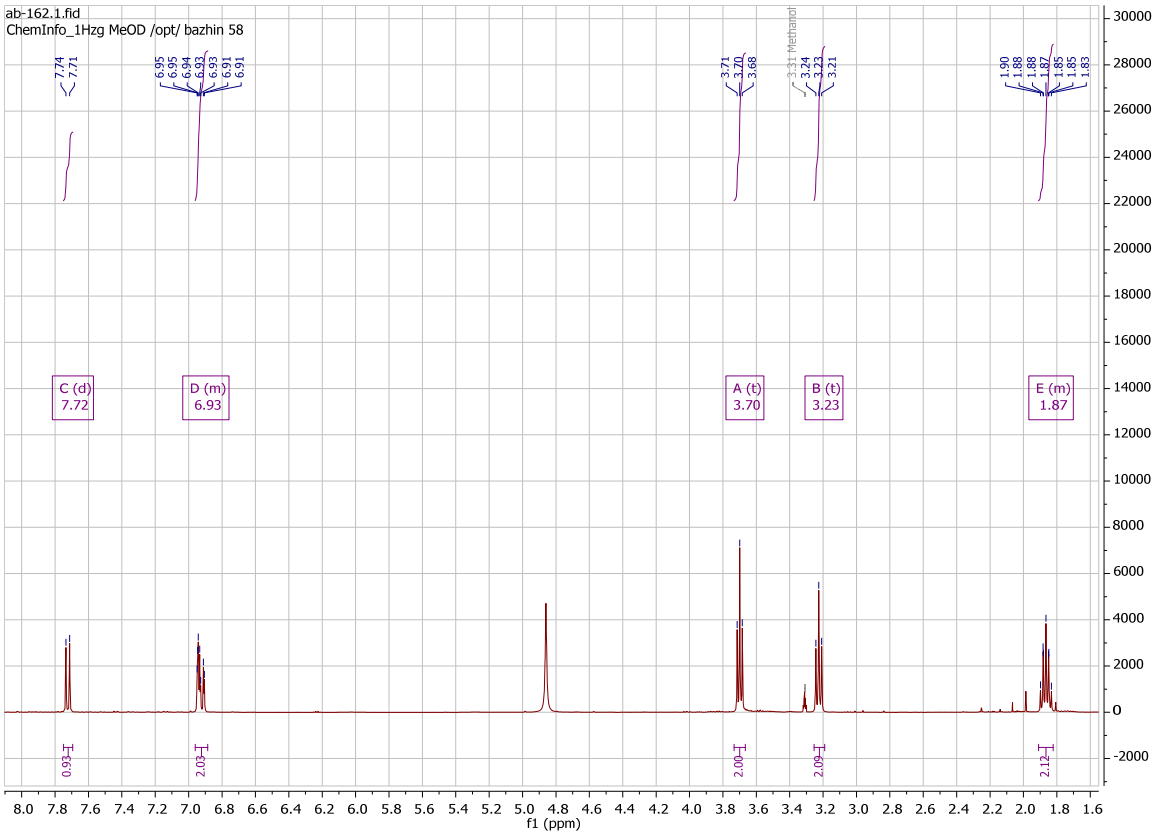

^{1}H spectrum of compound **18**

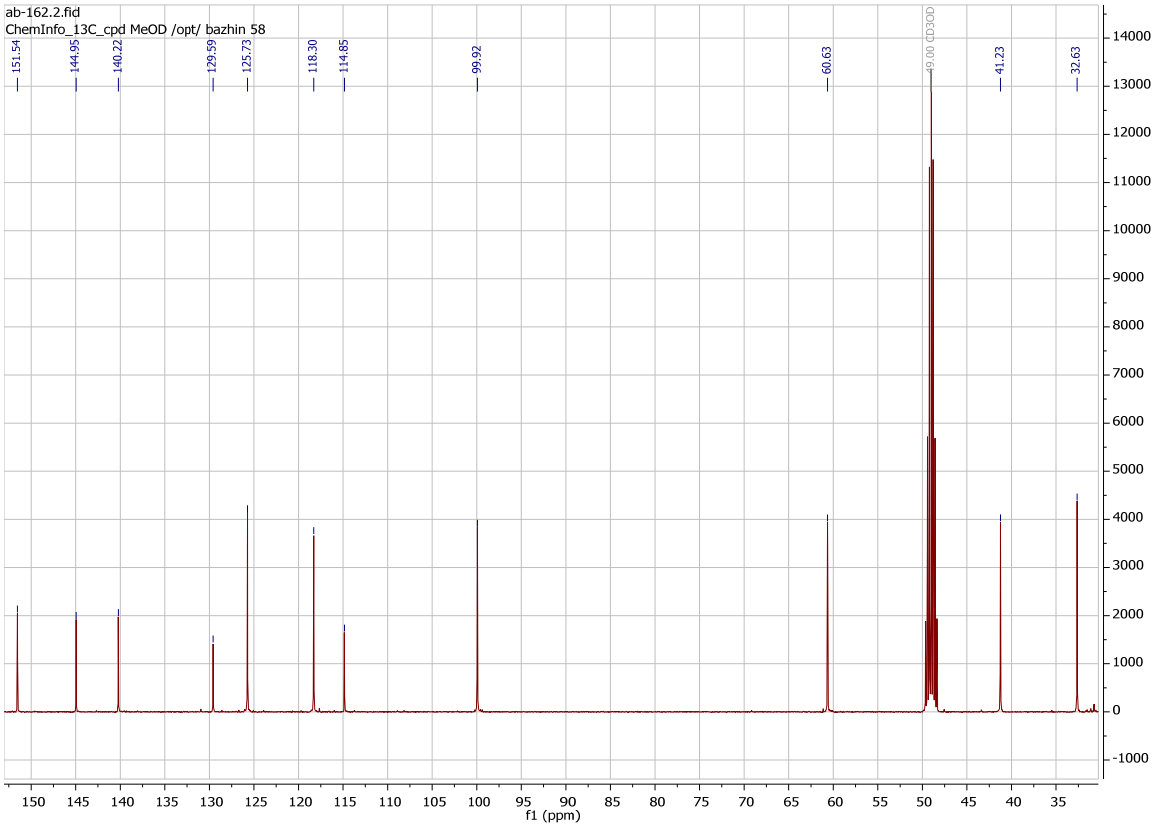

^{13}C spectrum of compound **18**

1.5.3 Synthesis of (3-(4-((3-((2-cyanobenzo[d]thiazol-6-yl)amino)propoxy)carbonyl)-3-(diphenylphosphanyl)benzamido)propyl)triphenylphosphonium (19).

The acid **9** (150 mg, 0.218 mmol, 1 eq) was dissolved in 10 mL of dry DCM under a nitrogen atmosphere. DMAP (2.5 eq, 67 mg) and EDCI (3 eq, 125 mg) were added to the solution to activate the acid. 56 mg of **18** dissolved in 5 mL of DCM were added dropwise to the stirred mixture under a nitrogen atmosphere. After completion, the reaction mixture was evaporated under reduced pressure to get the crude material. After purification with HPLC, 56 mg of the product were obtained with a 30% yield.

^{1}H NMR (400 MHz, Acetonitrile-d_3) δ 8.48 (dd, J = 8.0, 3.6 Hz, 1H), 8.36–8.24 (m, 4H), 8.22–8.02 (m, 15H), 8.02–7.86 (m, 1H), 7.84 (dd, J = 3.9, 1.7 Hz, 1H), 7.79–7.72 (m, 6H), 7.71–7.56 (m, 5H), 7.48 (d, J = 2.3 Hz, 1H), 7.39 (dd, J = 9.0, 2.4 Hz, 1H), 4.66 (t, J = 6.1 Hz, 2H), 3.85 (q, J = 6.4 Hz, 2H), 3.70–3.50 (m, 4H), 2.51–2.08 (m, 7H).

^{13}C NMR (151 MHz, Acetonitrile-d_3) δ 167.38, 167.19, 150.72, 145.12, 141.21 (d, J = 27.8 Hz), 139.93, 138.48 (d, J = 11.3 Hz), 138.38, 138.24, 138.14, 136.20 (d, J = 2.9 Hz), 134.79, 134.61 (d, J = 10.2 Hz), 134.20, 131.44 (d, J = 2.8 Hz), 131.28 (d, J = 12.5 Hz), 131.12, 130.00, 129.67 (d, J = 7.4 Hz), 127.54, 126.02, 119.29, 118.72, 118.10, 115.01, 100.58, 64.17, 40.90, 40.46 (d, J = 18.6 Hz), 28.39 (d, J = 6.7 Hz), 23.16, 20.63 (d, J = 53.5 Hz).

^{31}P NMR (162 MHz, Acetonitrile-d_3) δ 23.93, -4.88.

HRMS (ESI TOF ES+) calc. for [$C_{52}H_{45}N_4O_3P_2S^+$] 867.2687, found 867.2694.

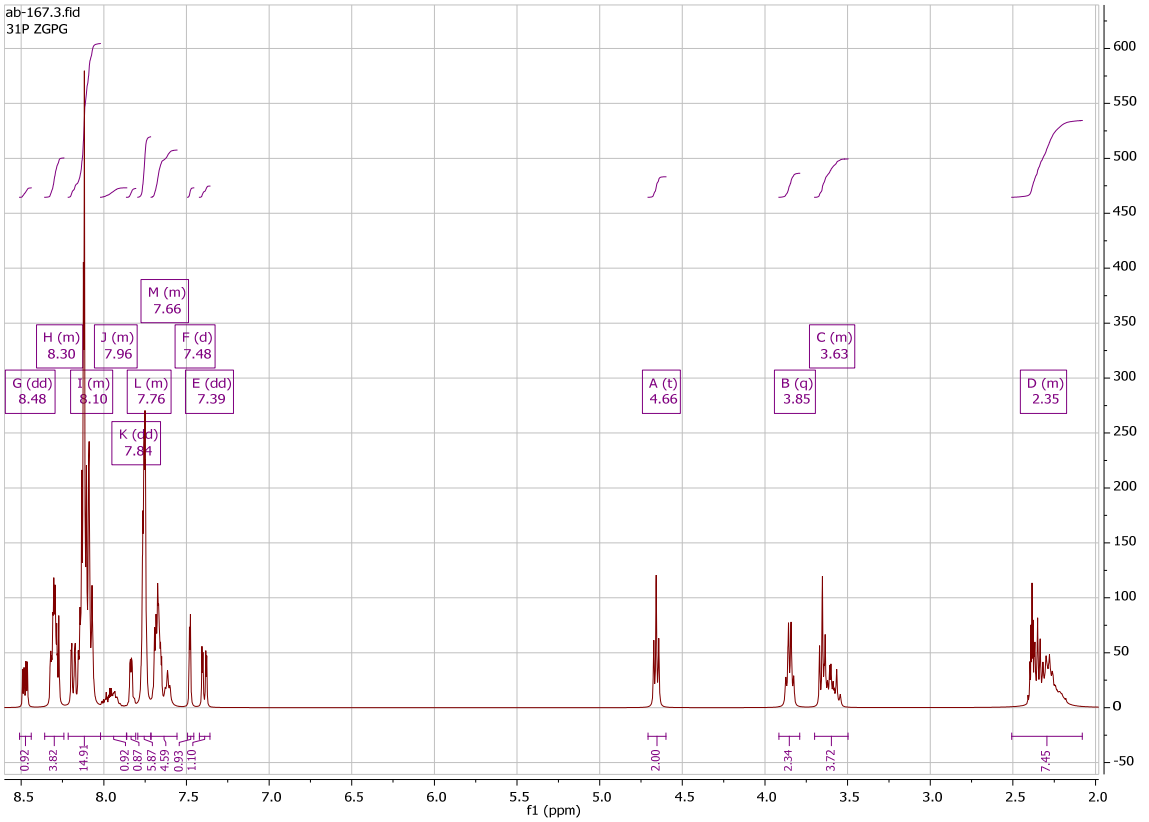

^{1}H spectrum of compound **19**

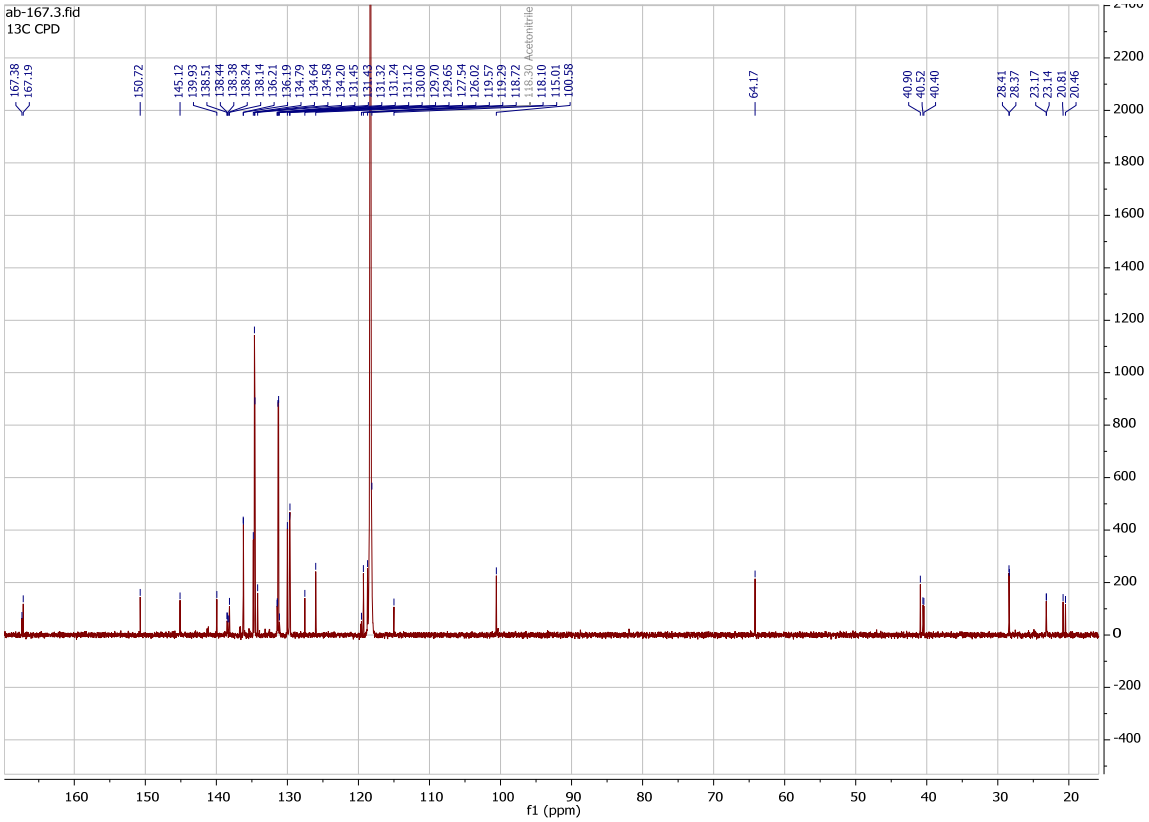

^{13}C spectrum. of compound **19**

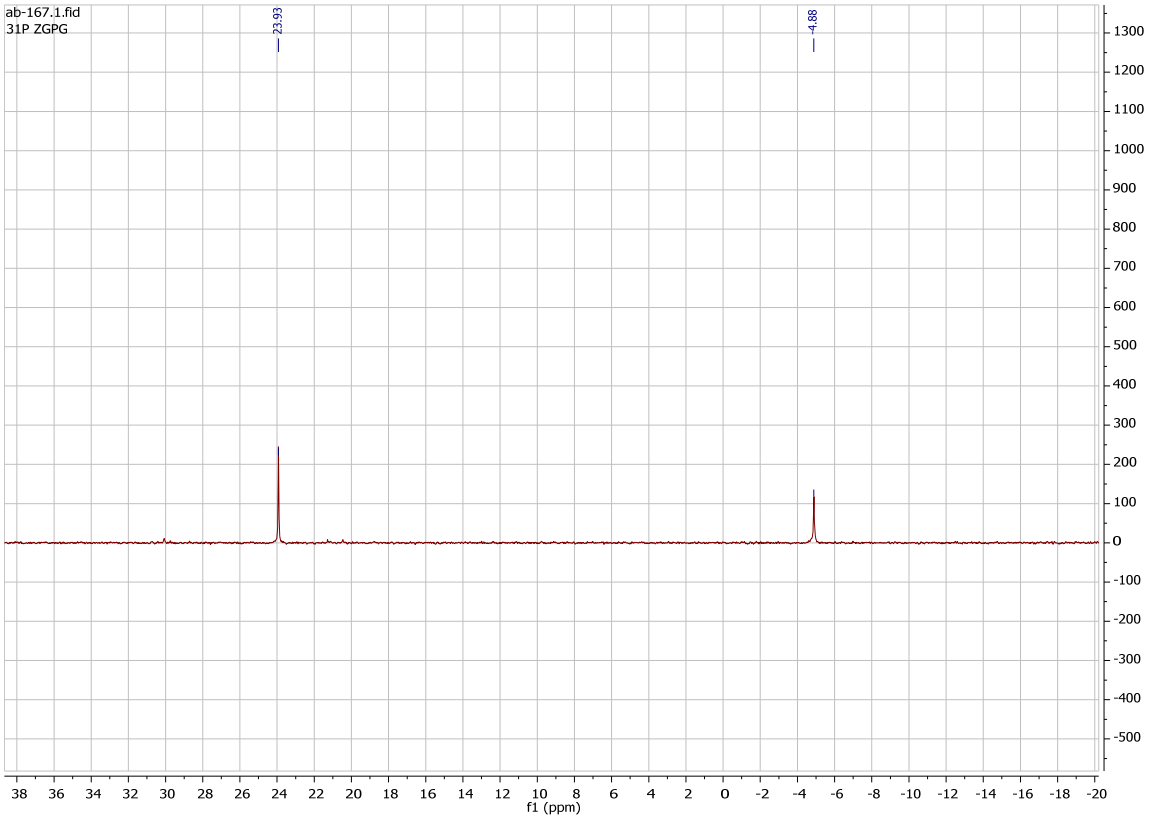

^{31}P spectrum of compound **19**

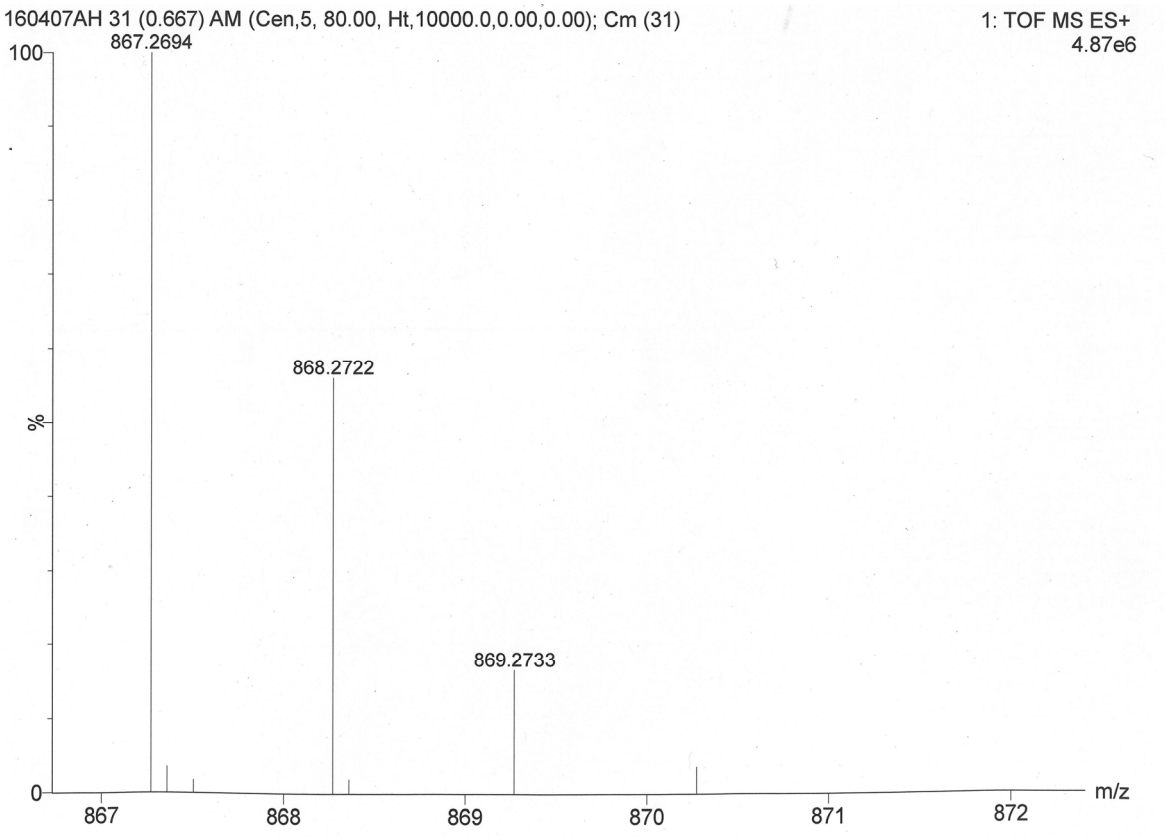

HRMS spectrum of compound **19**

1.5.4 Synthesis of (3-(4-((3-((2-(4-carboxy-4,5-dihydrothiazol-2-yl)benzo[d]thiazol-6-yl)amino)propoxy)carbonyl)-3-(diphenylphosphanyl)benzamido)propyl) triphenylphosphonium (4) or TPP-CL2

The synthetic procedure is identical to the one described previously for the synthesis of **1**. The pure product was characterized by NMR and HRMS.

^{1}H NMR (600 MHz, Methanol-d_4) δ 8.00 (dd, J = 8.1, 3.6 Hz, 1H), 7.88 (tq, J = 7.2, 1.7 Hz, 4H), 7.85–7.81 (m, 1H), 7.80–7.67 (m, 16H), 7.67–7.55 (m, 3H), 7.53–7.46 (m, 2H), 7.33–7.27 (m, 5H), 7.27–7.20 (m, 4H), 6.90 (d, J = 2.3 Hz, 1H), 6.84 (dd, J = 8.9, 2.3 Hz, 1H), 5.15 (td, J = 9.2, 3.6 Hz, 1H), 4.24 (td, J = 5.9, 2.9 Hz, 2H), 3.69 (qdd, J = 10.3, 9.2, 1.3 Hz, 2H), 3.58–3.36 (m, 4H), 3.17 (t, J = 6.8 Hz, 2H), 3.06 (t, J = 6.6 Hz, 1H), 2.02–1.83 (m, 3H), 1.73 (h, J = 6.5 Hz, 1H), 1.31 (s, 1H).

^{13}C NMR (151 MHz, Methanol-d_4) δ 175.19, 167.90, 166.60, 165.98, 164.37, 154.67, 148.85, 144.58, 140.51 (d, J = 28.0 Hz), 138.54, 137.40 (d, J = 20.1 Hz), 137.16 (d, J = 10.6 Hz), 136.89, 135.39 (d, J = 11.5 Hz), 134.96 (d, J = 3.4 Hz), 134.21 (d, J = 10.6 Hz), 133.75, 133.66, 133.61, 133.52, 133.38 (d, J = 10.1 Hz), 130.16 (d, J = 12.7 Hz), 128.70 (d, J = 4.0 Hz), 128.34 (d), 126.43, 123.82, 118.23 (d, J = 86.7 Hz), 115.60, 99.76, 80.83, 63.00, 39.70 (d, J = 12.1 Hz), 35.57, 27.41 (d, J = 93.4 Hz), 22.14, 19.28 (d, J = 53.0 Hz).

^{31}P NMR (162 MHz, Methanol-d4) δ 24.01, -4.53.

HRMS (ESI TOF ES+) calc. for [$C_{55}H_{49}N_4O_5P_2S_2^+$] 971.2614, found 971.2647.

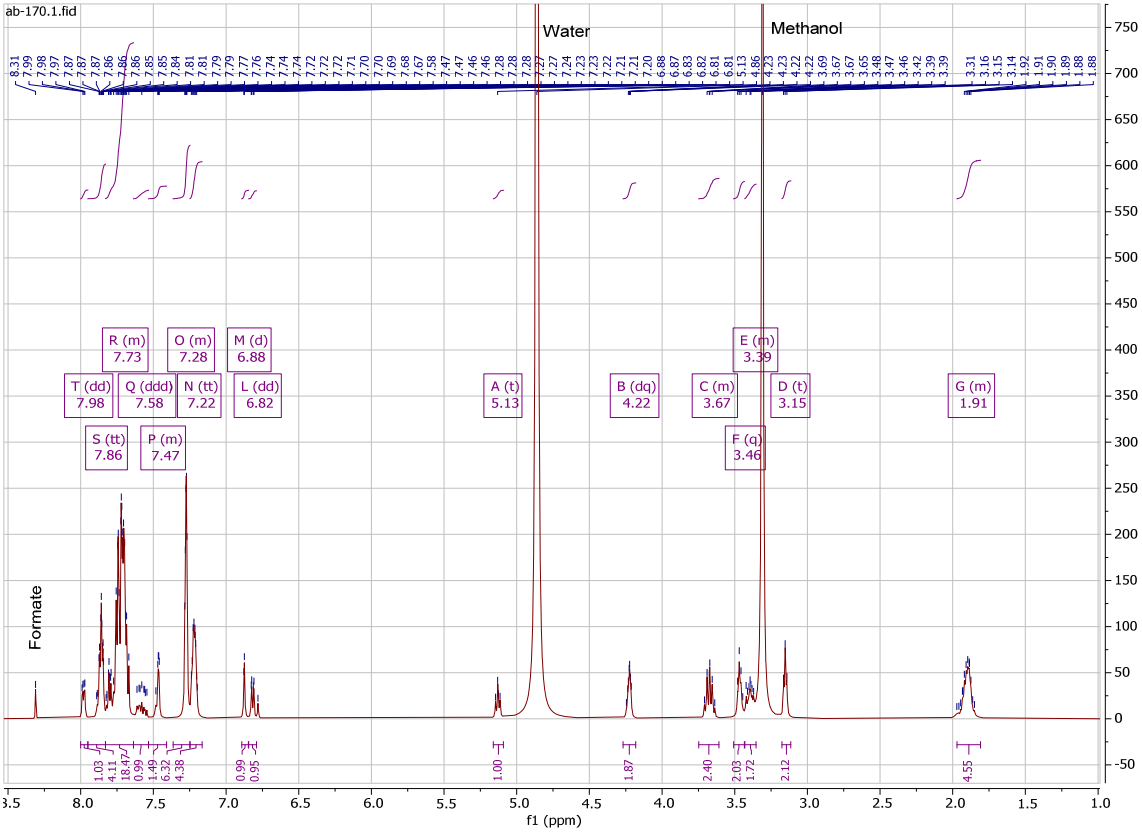

^{1}H spectrum of compound **4**

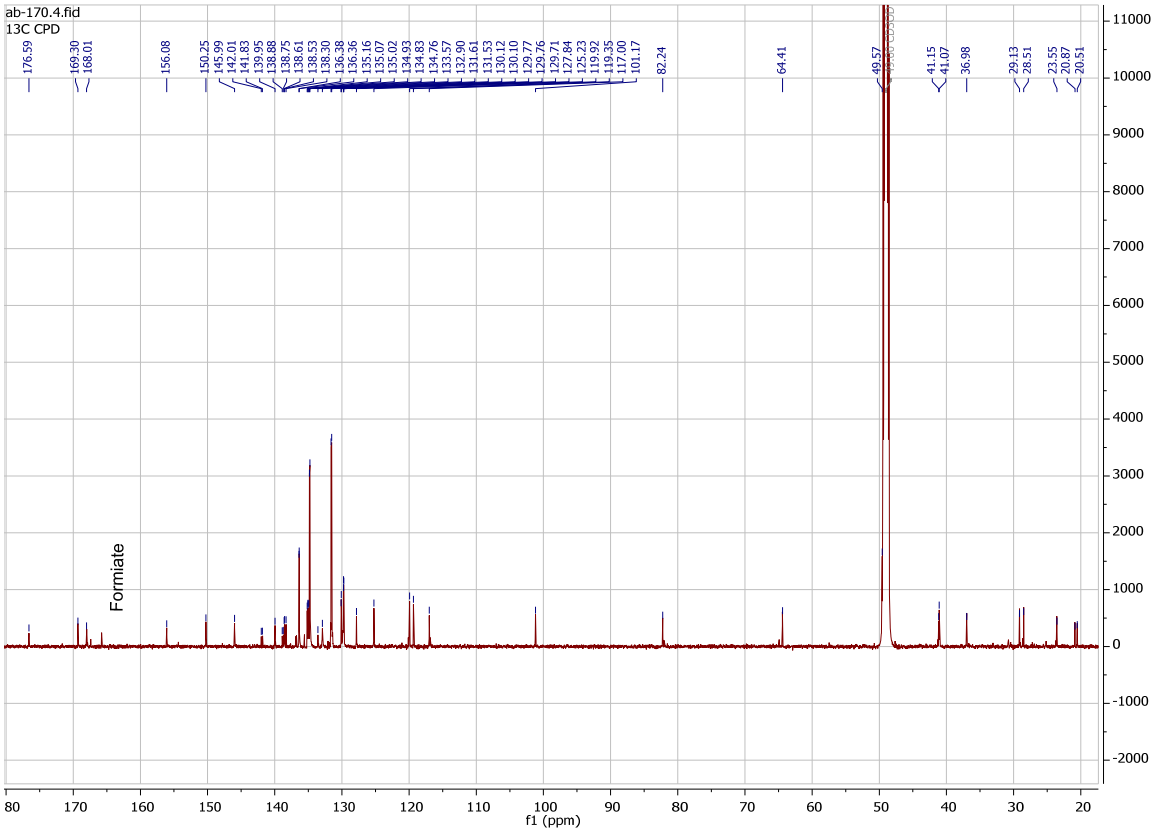

^{13}C spectrum compound **4**

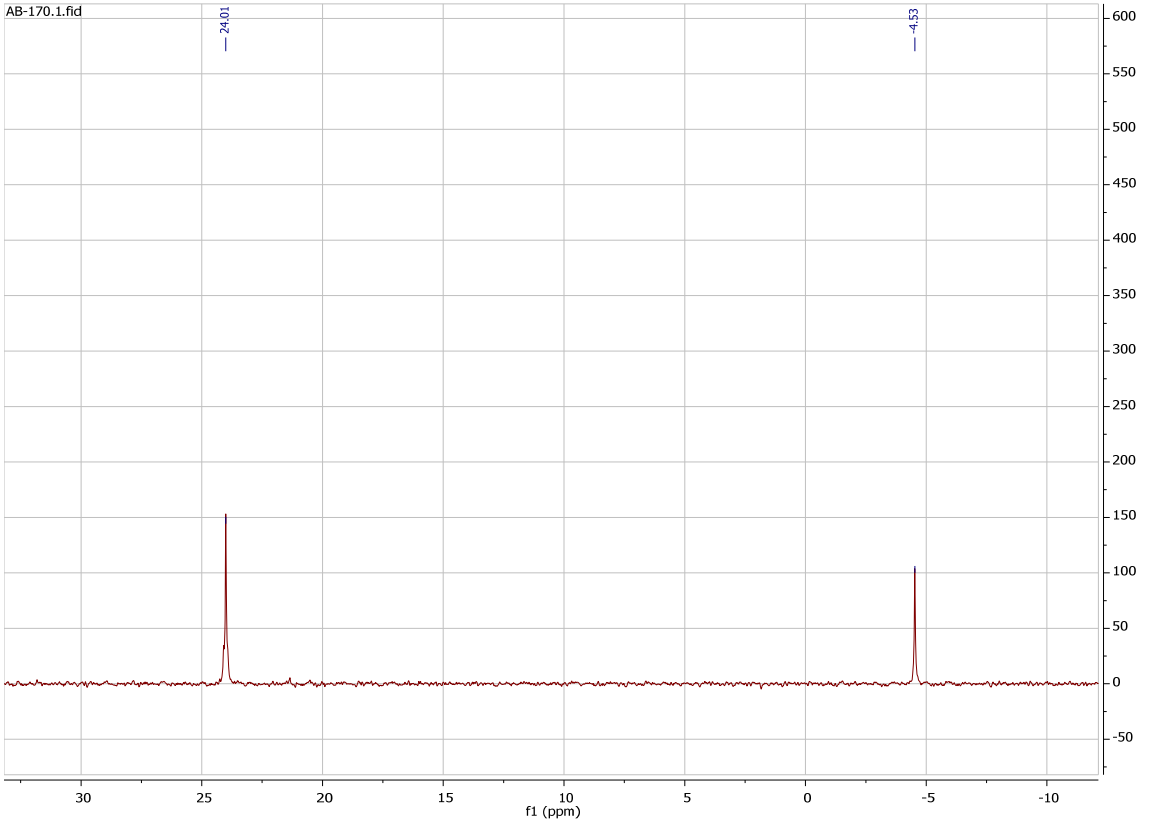

^{31}P spectrum of compound **4**

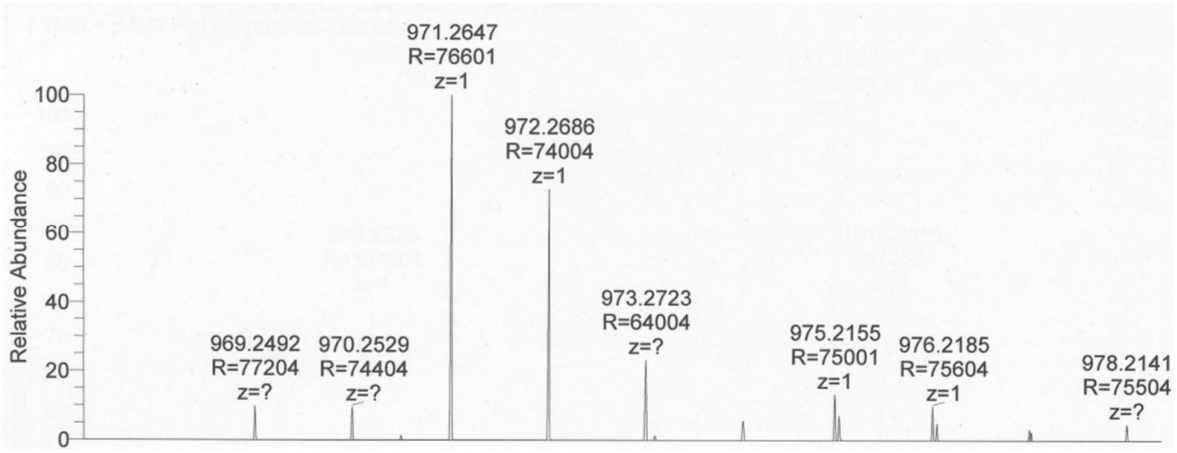

HRMS spectrum of compound **4**

1.6 TPP-CL2 reacts with organic azides via the Staudinger ligation mechanism

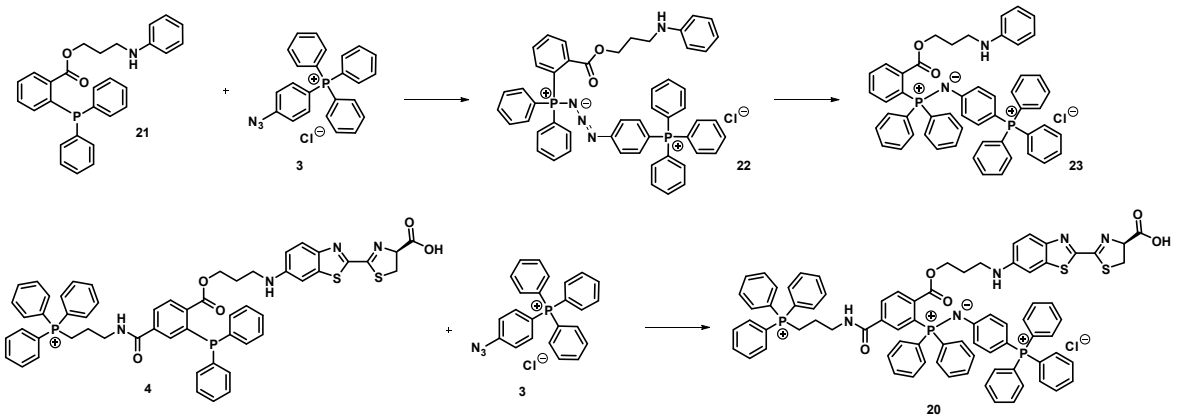

Scheme S11. Formation of stable aza-ylide during the reaction of alkyl-esters of diphenylphosphinobenzoic acid and azido-TPP2.

1.6.1 Azido-TPP2 reaction with 3-(phenylamino)propyl 2-(diphenylphosphanyl)benzoate (21)

First, 50 mg of **21** and 49 mg of ^{15}N-labeled azido-TPP2 were dissolved separately in 0.3 ml of deuterated DCM. The resultant solutions were then mixed in an NMR tube, and the mixture turned a deep yellow color and gas was released (likely N_2). Immediately following mixing, the ^{15}N NMR spectrum was recorded (400 MHz, NH_3 standard) and showed only one peak at 310.13 ppm that belongs to nitrogen gas. The product was then purified by normal phase LC and characterized by NMR and HRMS.

^{1}H NMR (600 MHz, Methylene Chloride-d2) δ 8.00–7.95 (m, 1H), 7.90–7.85 (m, 3H), 7.78 (td, J = 7.5, 3.7 Hz, 1H), 7.75– .69 (m, 10H), 7.68–7.56 (m, 10H), 7.53 (td, J = 7.8, 3.3 Hz, 4H), 7.13–7.05 (m, 4H), 6.88–6.84 (m, 2H), 6.61 (tq, J = 7.3, 1.0 Hz, 1H), 6.55–6.50 (m, 2H), 4.00 (t, J = 6.2 Hz, 2H), 2.94 (t, J = 6.8 Hz, 2H), 1.70 (p, J = 6.5 Hz, 2H).

^{13}C NMR (151 MHz, Methylene Chloride-d2) δ 167.15, 148.28, 135.18, 135.10, 134.97 (d, J = 3.0 Hz), 134.44 (d, J = 10.4 Hz), 134.21 (d, J = 10.2 Hz), 132.83, 132.41, 132.08 (d, J = 10.1 Hz), 131.49 (d, J =

12.6 Hz), 130.95 (d, J = 8.3 Hz), 130.70 (d, J = 12.9 Hz), 130.19 (d, J = 12.7 Hz), 129.04, 128.93 (d, J = 12.6 Hz), 124.20–123.09 (m), 119.81, 119.21, 116.78, 112.58, 63.72, 40.29, 27.77.

^{31}P NMR (162 MHz, Methylene Chloride-d2) δ 21.96, 9.47.

HRMS (ESI TOF ES+) calc.791.2957, found 791.2960.

A peak at 9.47 ppm in ^{31}P spectrum is typical for aza-ilydes (-P=N-). The absence of signals from ^{15}N atoms is directly connected to the fact that only the terminal and middle nitrogens of the azide **3** are labeled (discussed above), which are lost during nitrogen release. HRMS of the purified product shows that the most abundant ion has an m/z = 791.2960, which perfectly matches with the calculated m/z for the aza-ylide **23**. On the ^{1}H-^{13}C HMBC spectrum of compound **23**, the presence of the cross peak between the carbonyl (167.2 ppm) and methylene protons of the propyl moiety (4.0 ppm) unambiguously shows that the ester group is intact.

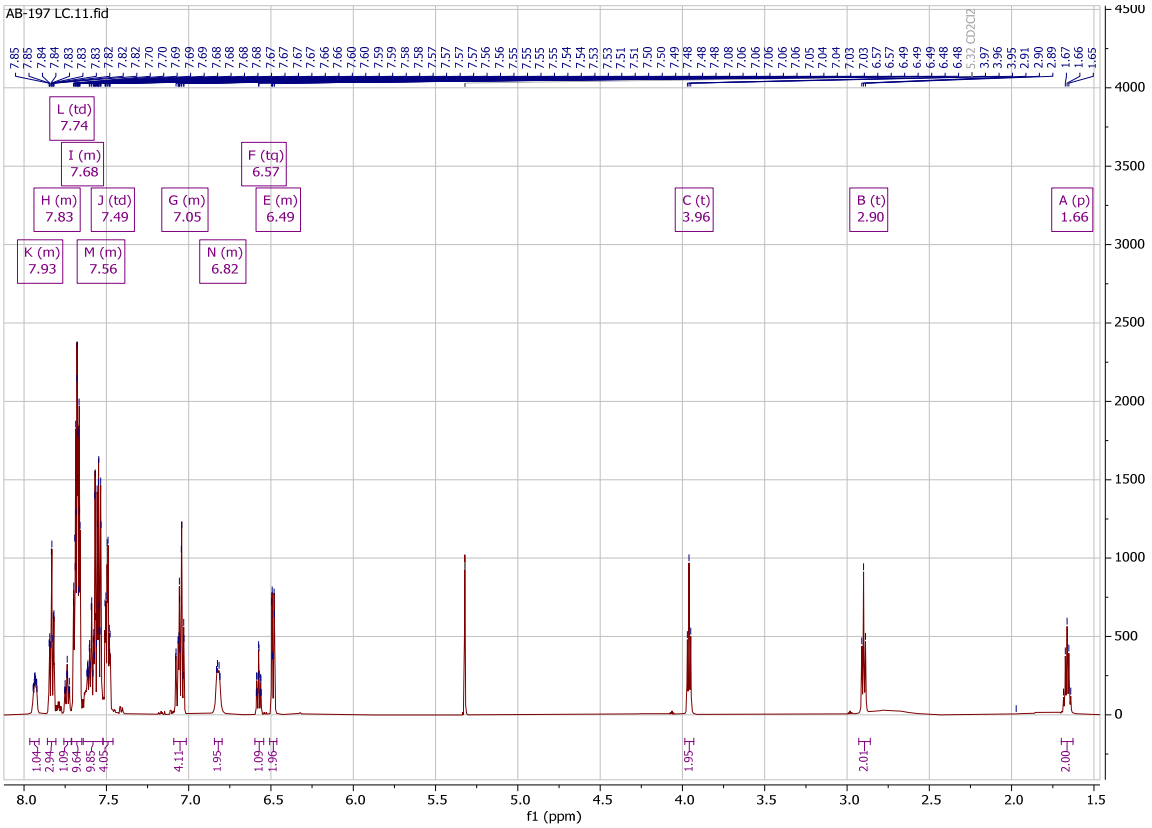

^{1}H spectrum of compound **23**

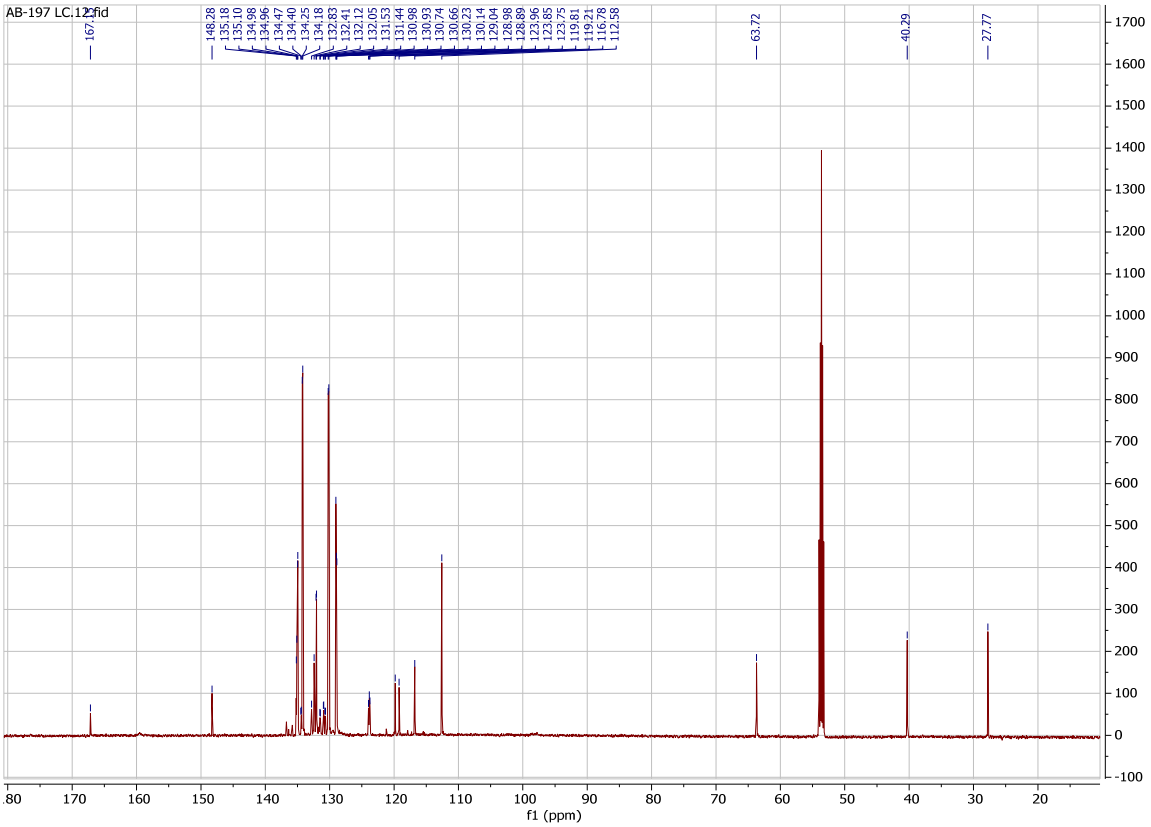

^{13}C spectrum of compound **23**

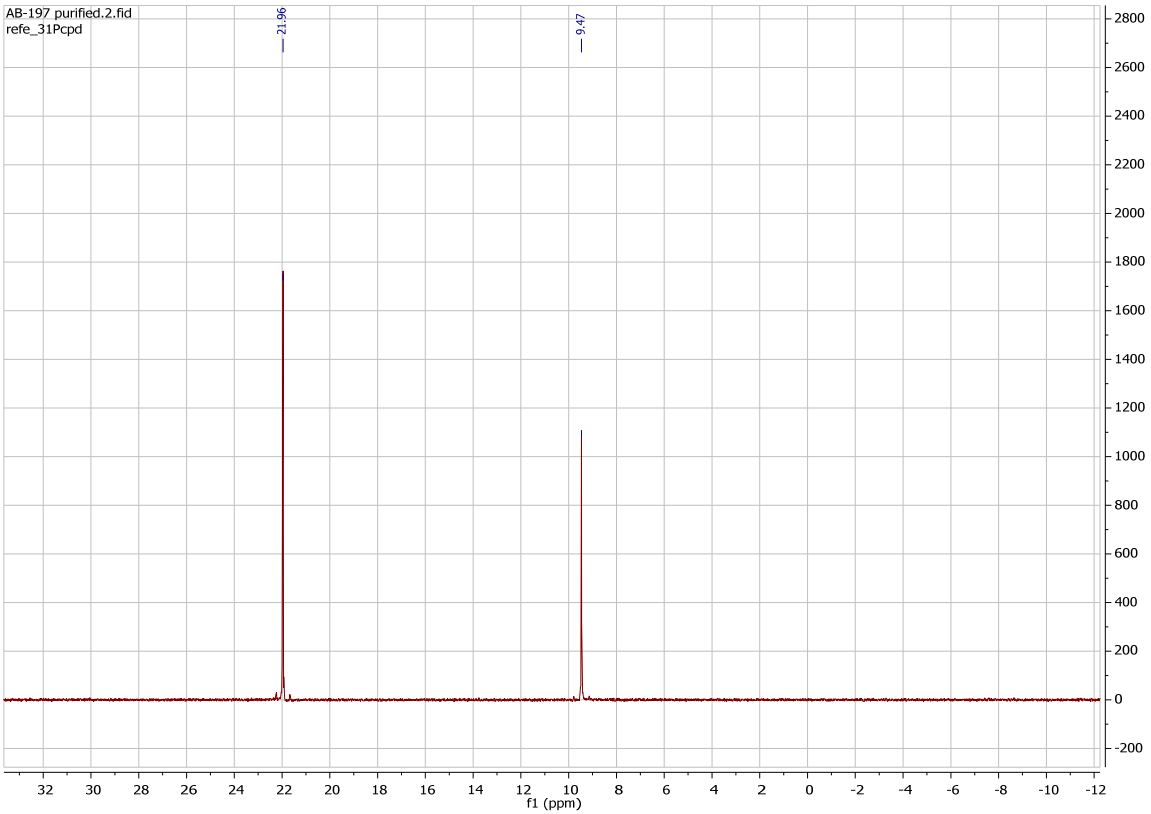

^{31}P spectrum of the compound **23**

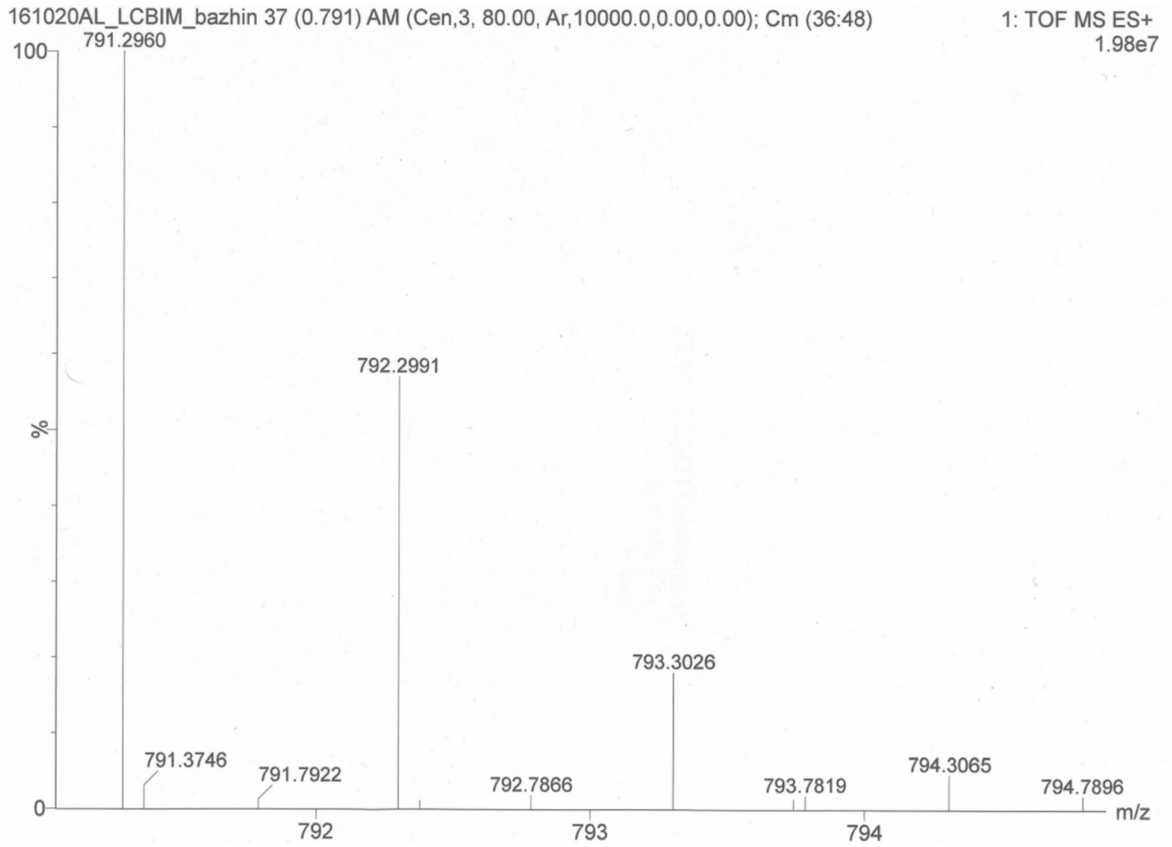

HRMS spectrum of compound **23**. The observed signal corresponds to the unlabeled compound.

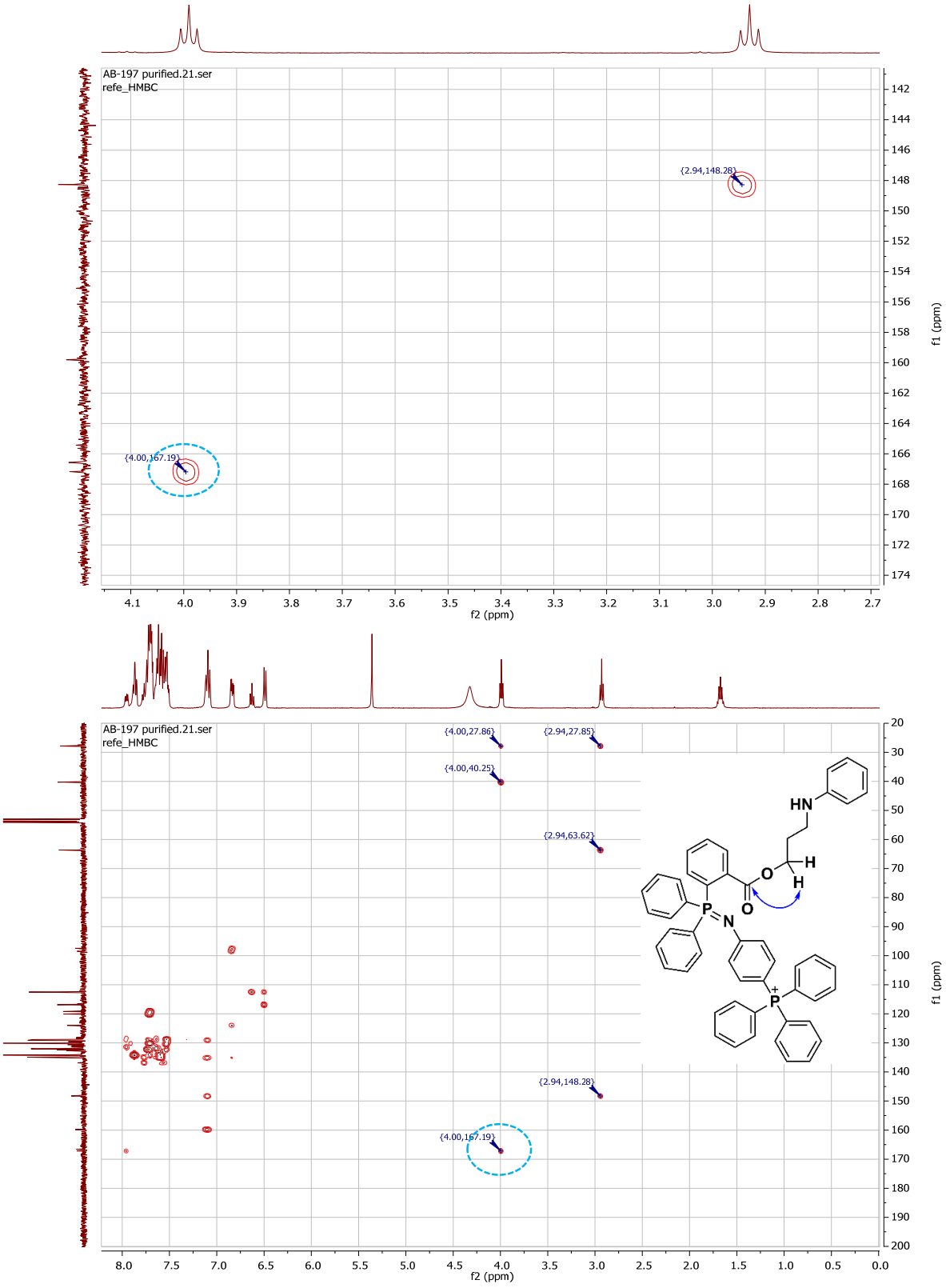

^{1}H-^{13}C HMBC spectrum of compound **23.** A correlation between the ^{13}C in the carbonyl (167.2 ppm) and the methylene protons of the propyl moiety (4.0 ppm) is present. On top – the enlarged region where the correlation is observed.

The ^{1}H-^{15}N HMBC spectrum showed a correlation between the hydrogens in alkyl group and a nitrogen at 65 ppm, which should be an aniline nitrogen. Additionally, there is another nitrogen at 103 ppm that has

correlations only with the aromatic protons at 6.83 ppm, and it should be the nitrogen of the P=N group. To confirm that compound **23** is an aza-ylide, we used an ^{1}H-^{31}P HMBC experiment with a pulse sequence optimized for ^{4}J (H-P) coupling constant. The spectrum showed a correlation between the protons at 7.1 ppm (meta-position to phosphorus of phosphonium cation) and the phosphorus at 9.5 ppm, which belongs to aza-ylide moiety. All of this evidence showed unequivocally that a stable aza-ylide is formed in the reaction between azide **11** and phosphine **21.** Therefore, our initial hypothesis was correct, and luciferin release does not take place due to high stability of an aza-ilyde intermediate (**Scheme S12**, compound **20**).

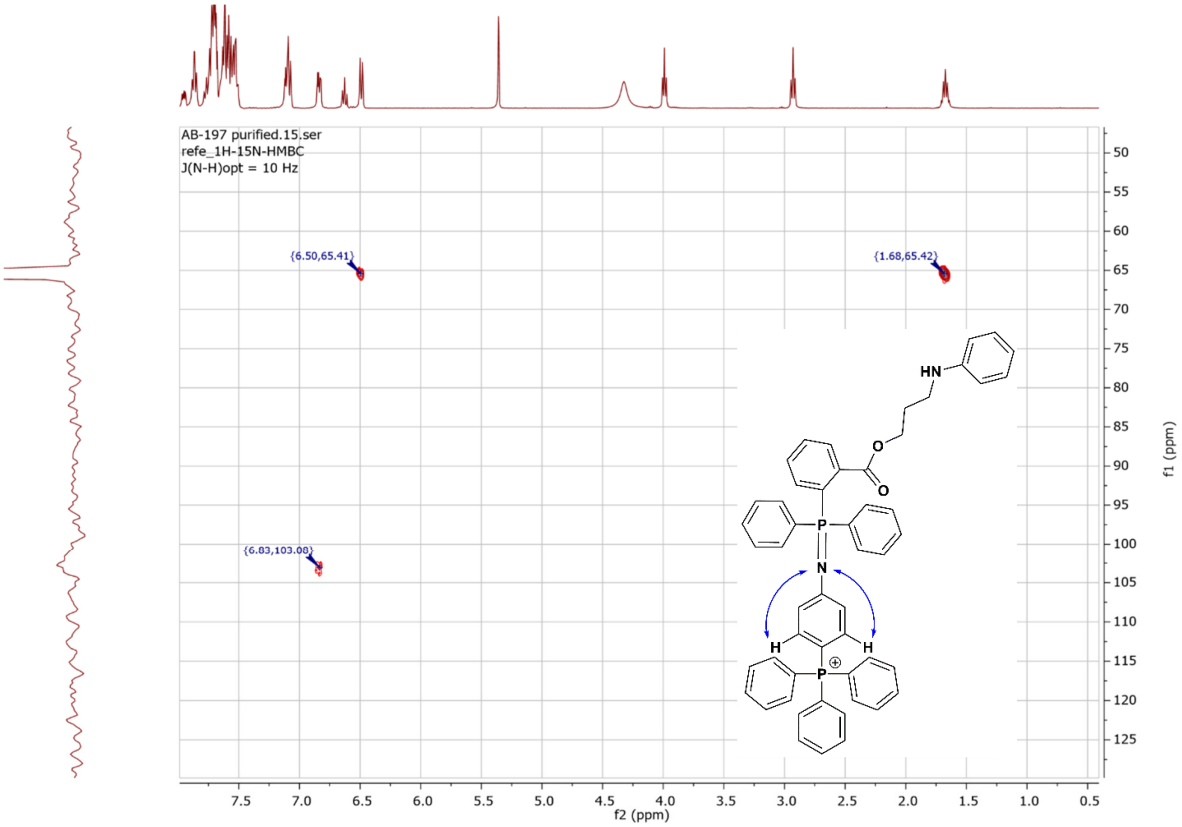

^{1}H-^{15}N HMBC spectrum of the compound **23**.

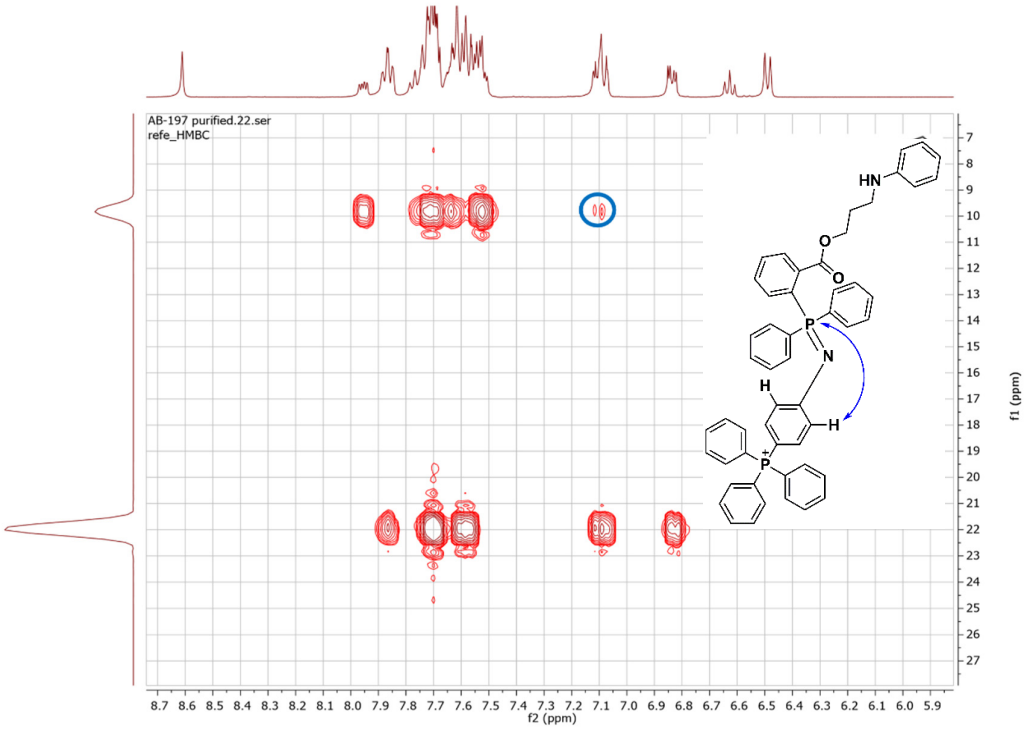

^{1}H-^{31}P HMBC spectrum of compound **23**.

1.6.2 Reaction of Azido-TPP1 with 3-(phenylamino)propyl 2-(diphenylphosphanyl)benzoate (21)

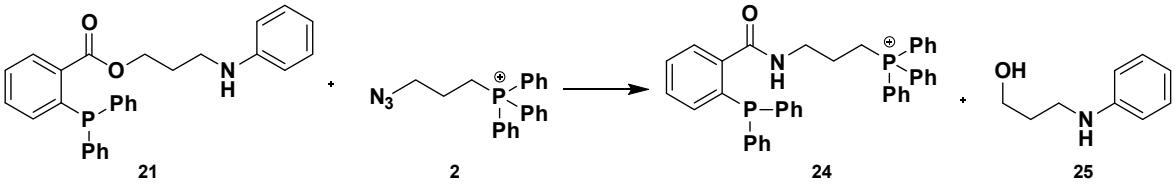

Scheme S12. Reaction between phosphine **21**, a model of TPP-CL2, with azido-TPP1.

43 mg of compound **21** was mixed with 44 mg of ^{15}N-labelled azido-TPP1 in 0.7 mL of deuterated dichloromethane in an NMR tube (**Scheme S13**). The reaction was monitored by ^{31}P and ^{15}N NMR at room temperature. A few minutes after the onset of the reaction, a release of gas started. Most probably, this was nitrogen formation, which is a sign of the Staudinger ligation.

The ^{15}N NMR spectrum recorded 15 min after the reaction onset showed peaks at 310 (s), 170.18 (d, J = 38.9 Hz). The singlet at 310 ppm belongs to ^{15}N-labeled nitrogen gas[14], and the doublet at 170.18 belongs to a nitrogen of the pentacoordinate phosphorane intermediate because of following reasons:

1. The coupling constant is very similar to published data for ^{31}P-^{15}N coupling (34 Hz)[15].
2. On a ^{31}P spectrum recorded at the same time, a doublet at -57ppm with the same coupling constant (J = 38.9 Hz) is observed, and it lies in the characteristic range for sp^{3}d-hybridized phosphorus[16].

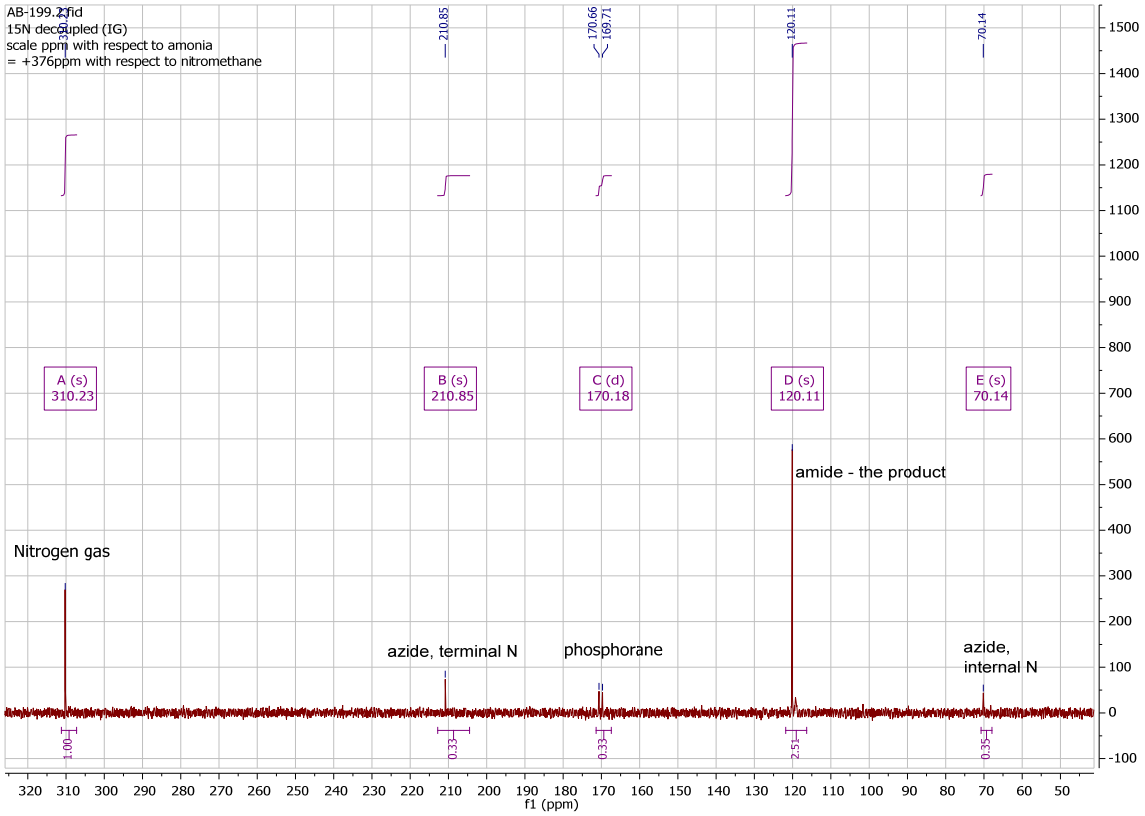

^{15}N NMR spectrum of the reaction mixture (**21** + **2**) 15 min after onset.

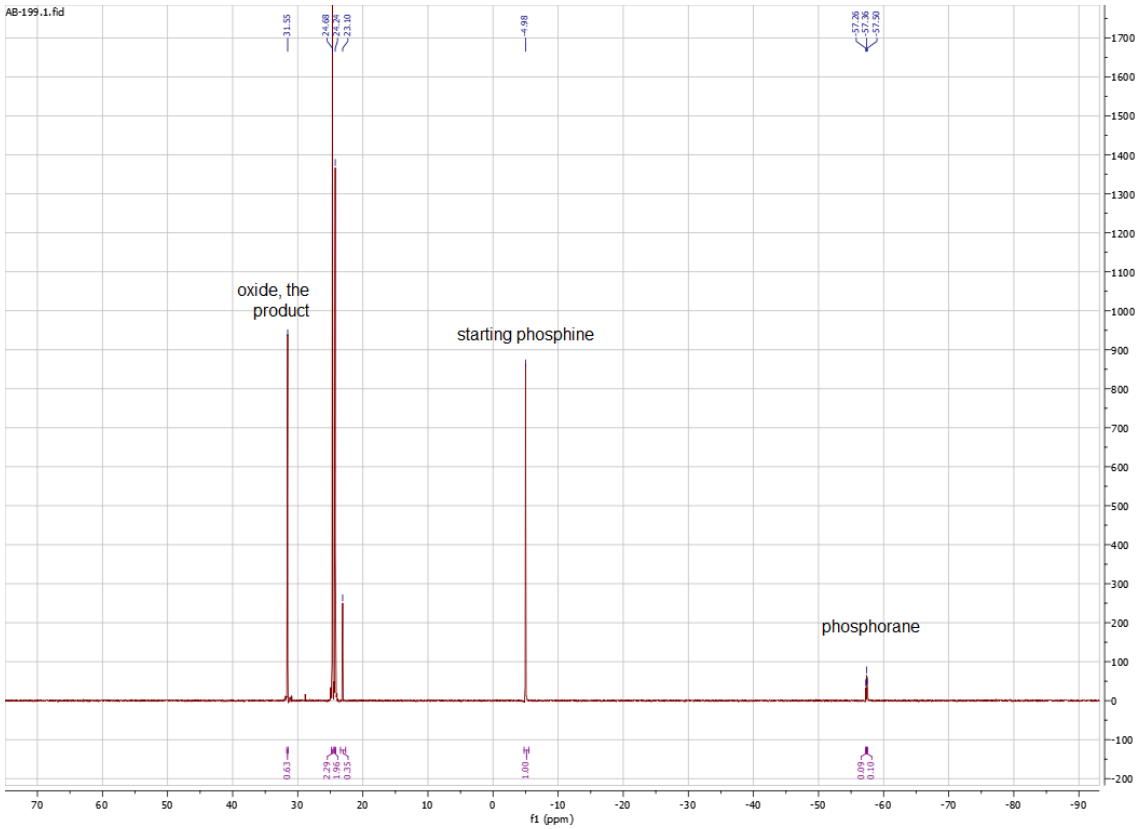

^{31}P NMR spectrum of the reaction mixture (**21** + **2**) 15 min after onset.

On the ^{31}P spectrum, additional peaks appeared at 31.55 (s, P=O of the product), 24.7 (s), 23.1 (s), -57.36 (s), -57.38 (d, J = 38.9 Hz). Since the starting azido-TPP1 is a mixture of two isotopomers with different

^{15}N positions within azide moiety (terminal or internal), the last two signals should belong to the same phosphorus of the phosphorane derivative bound to either the ^{14}N or ^{15}N atom, respectively.

After incubation of the reaction mixture overnight at room temperature, the reaction was completed. The product was purified by semi-preparative HPLC with a yield of 55 mg (90%). The pure product was characterized by NMR and HRMS. Interestingly, the triplet of triplets observed on the ^{1}H NMR at 9.58 ppm is a combination of a doublet of triplets from the ^{15}N-labeled product (splitting on nitrogen and vicinal protons) and a triplet from the non-labeled product (splitting on vicinal protons only).

^{1}H NMR (400 MHz, Methylene Chloride-d_2) δ 9.58 (tt, J = 46.0, 5.9 Hz, 1H), 8.49 (s, 1H), 8.02–7.80 (m, 9H), 7.77 (ddd, J = 7.7, 3.6, 1.3 Hz, 1H), 7.70 (td, J = 7.9, 3.5 Hz, 6H), 7.65–7.52 (m, 7H), 7.45 (tt, J = 6.8, 3.1 Hz, 4H), 7.38 (tdd, J = 7.6, 2.6, 1.3 Hz, 1H), 7.21 (ddd, J = 13.6, 7.7, 1.3 Hz, 1H), 3.97–3.75 (m, 2H), 3.43 (q, J = 5.9 Hz, 2H), 1.93 (q, J = 7.6, 7.1 Hz, 2H).

^{13}C NMR (101 MHz, Methylene Chloride-d_2) δ 169.97 (td, J = 9.3, 7.9, 3.5 Hz), 167.63, 142.44 (q, J = 4.8 Hz), 135.28 (d, J = 3.1 Hz), 134.57, 134.26 (d, J = 10.0 Hz), 133.52, 132.47 (d, J = 2.7 Hz), 132.31 (d, J = 9.8 Hz), 132.10 (d, J = 2.7 Hz), 130.85, 130.69 (d, J = 12.5 Hz), 129.85, 129.71 (d, J = 9.3 Hz), 129.33 (d, J = 12.4 Hz), 128.76 (d, J = 12.2 Hz), 119.17 (d, J = 86.0 Hz), 39.85 (d, J = 17.7 Hz), 23.09 (d, J = 3.9 Hz), 20.28 (d, J = 51.7 Hz).

^{15}N NMR (41 MHz, Methylene Chloride-d2) δ 119.09.

^{31}P NMR (162 MHz, Methylene Chloride-d2) δ 31.48, 24.85.

HRMS (ESI TOF ES+) calc.624.2221 for $C_{40}H_{36}NO_2P_2^+$, found 624.2223; calc. 625.2192 for $C_{40}H_{36}{}^{15}NO_2P_2^+$, found 625.2216.

The fact that compound **24** is a secondary amide was confirmed by the ^{1}H-^{15}N HSQC and ^{1}H-^{13}C HMBC spectra, which showed that the proton at 9.58 ppm is directly bound to the ^{15}N atom originating from azide **2** and coupled to ^{13}C of the carbonyl group at 169.5 ppm. Besides, the chemical shift of the ^{15}N is typical for amides.

Taking into consideration all of the evidence, we can conclude that the reaction followed the classical mechanism of a Staudinger ligation as reported by Bertozzi et al.[4] In general, the phosphine reacts with aromatic and aliphatic azides via the Staudinger ligation mechanism. Since compound **23** is a complete analog of TPP-CL2 in terms of reactivity, we can conclude that TPP-CL2 reacts with azides in exactly the same way.

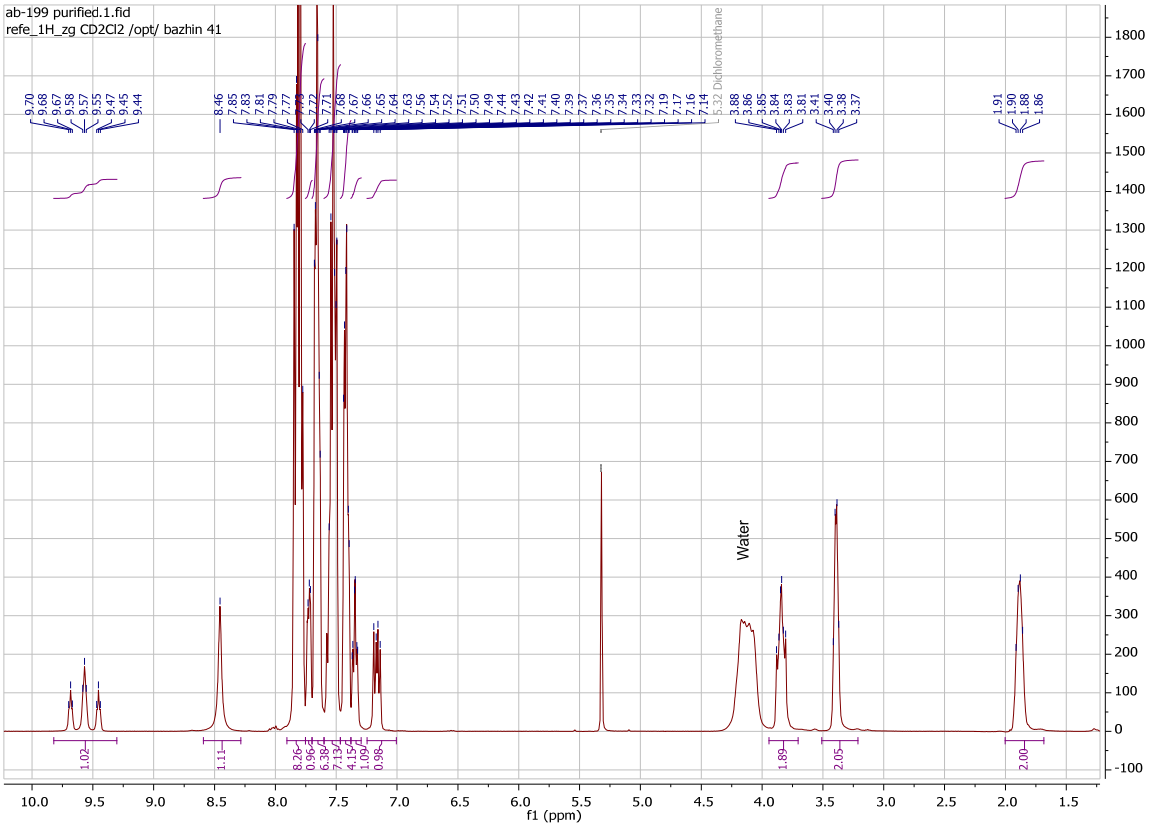

^{1}H spectrum of compound **24**

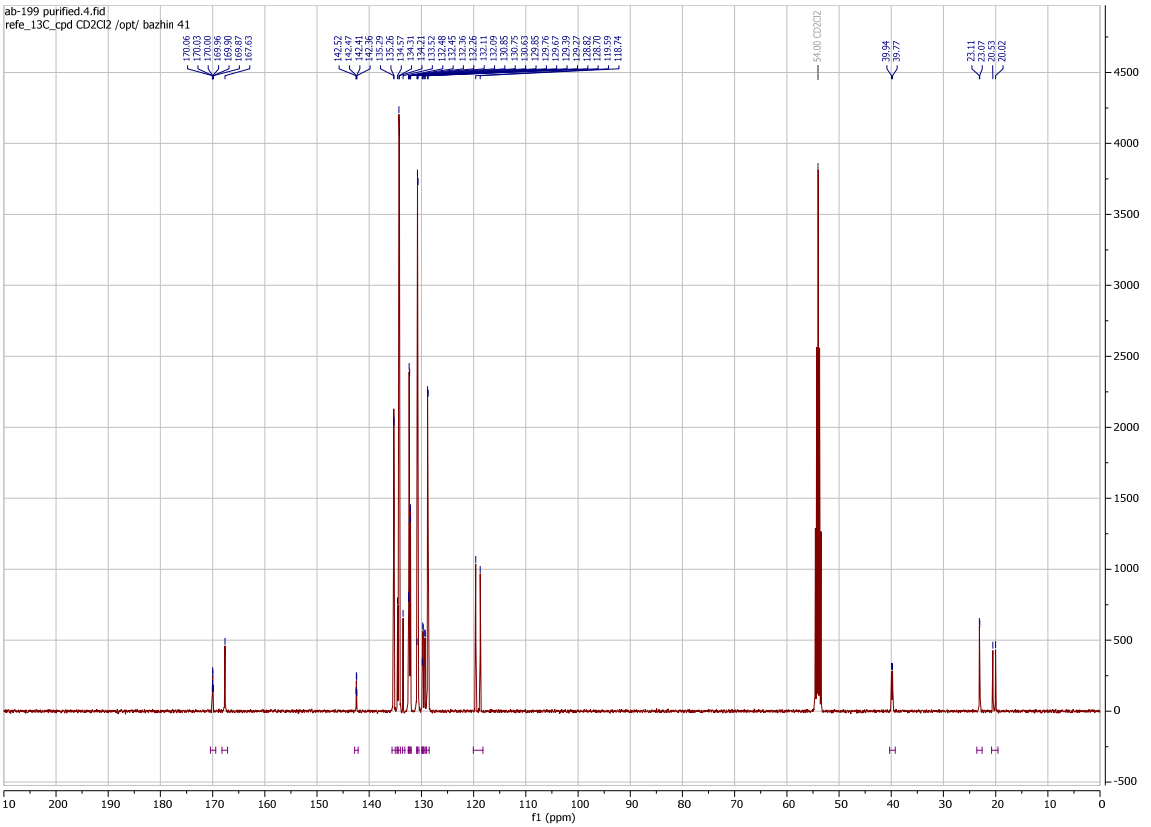

^{13}C spectrum of compound **24**

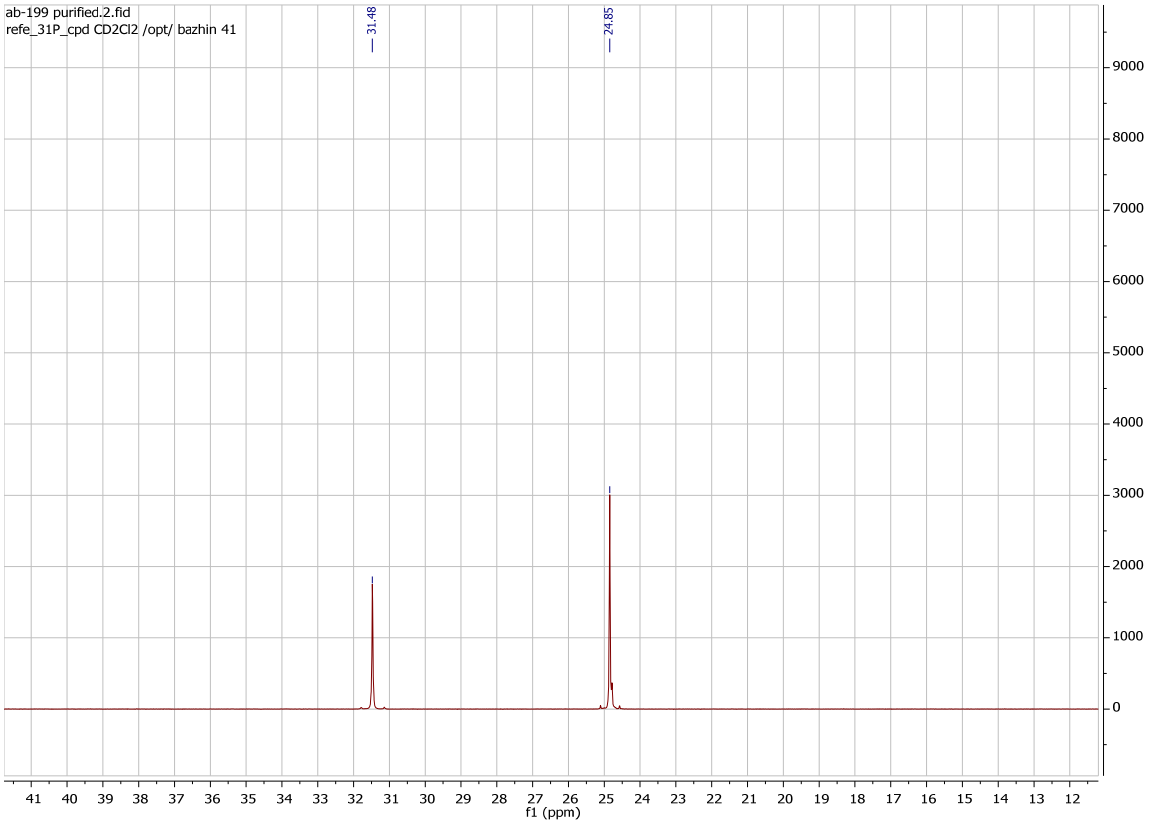

^{31}P spectrum of compound **24**

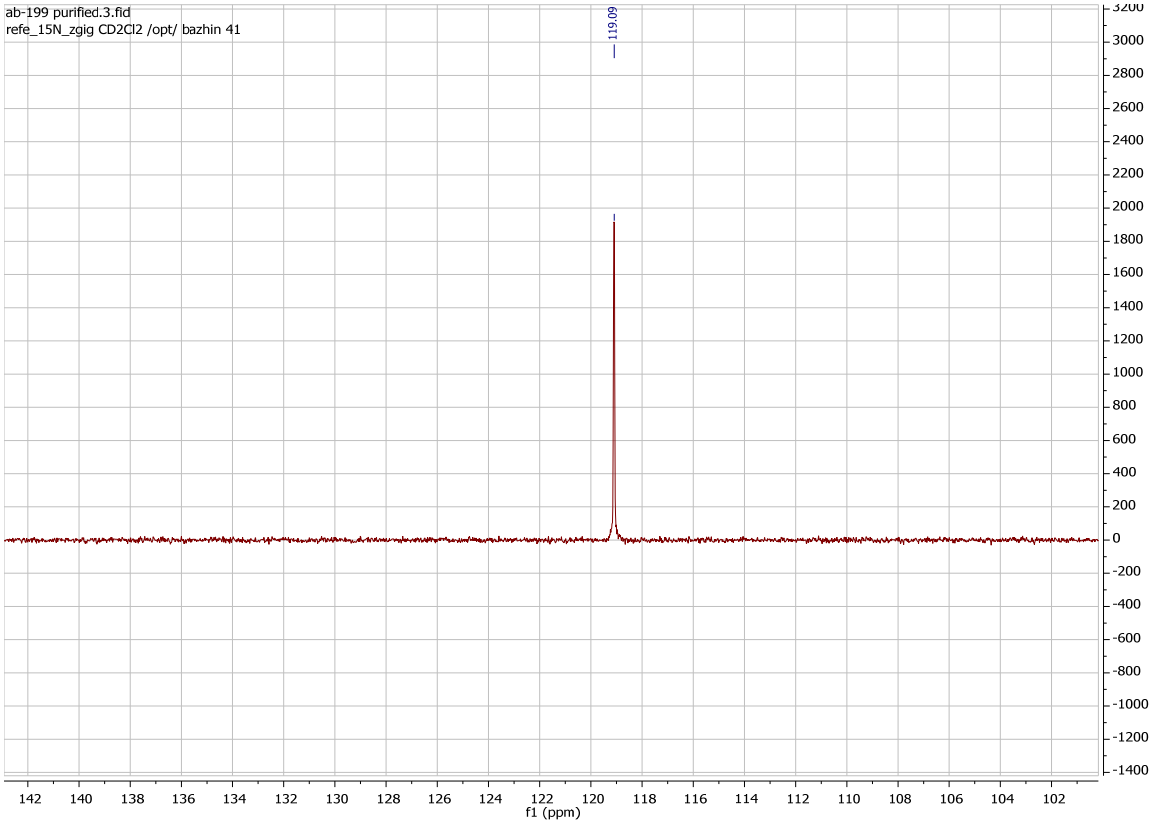

^{15}N spectrum of compound **24**.

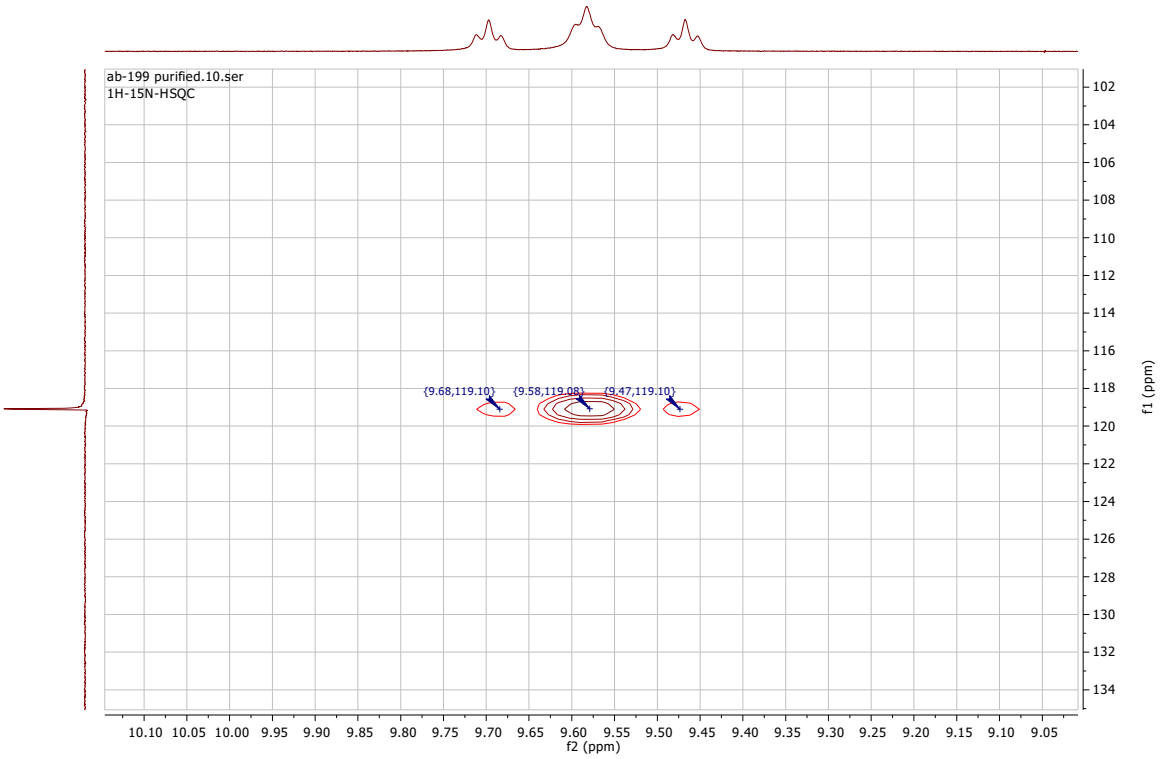

^{1}H-^{15}N HSQC spectrum of compound **24**. The proton at 9.58 ppm is directly connected to the only one ^{15}N atom in the product

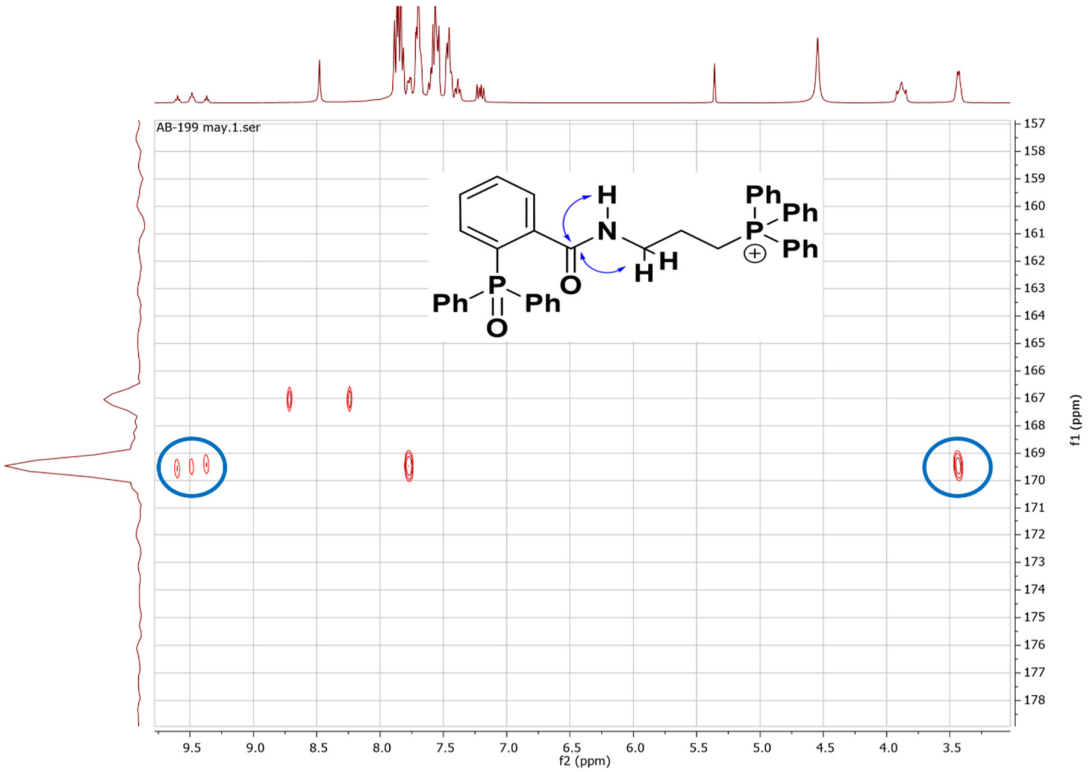

^{1}H-^{13}C HMBC spectrum of compound **24.**

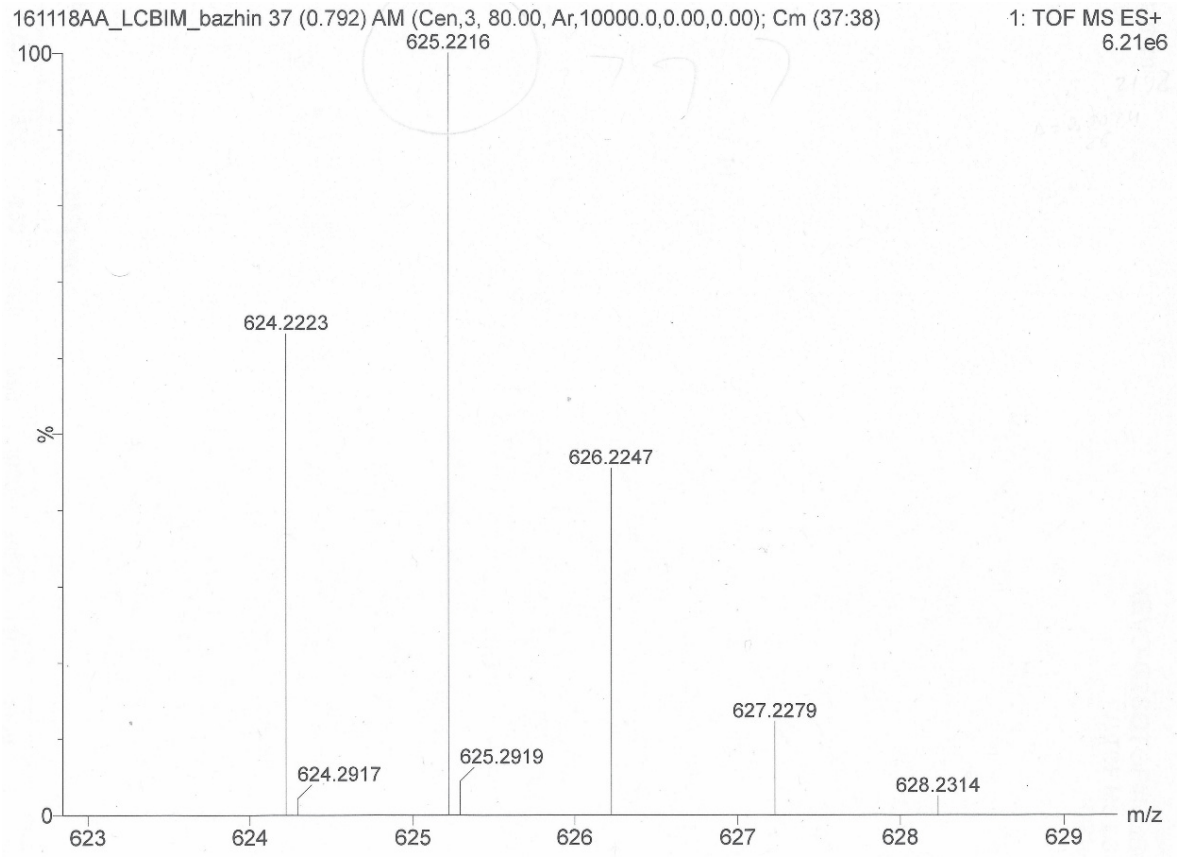

HRMS spectrum of compound **24**. Peaks of labeled and unlabeled product are observed.

1.6.3 Synthesis of 3-(phenylamino)propyl 2-(diphenylphosphanyl)benzoate (21)

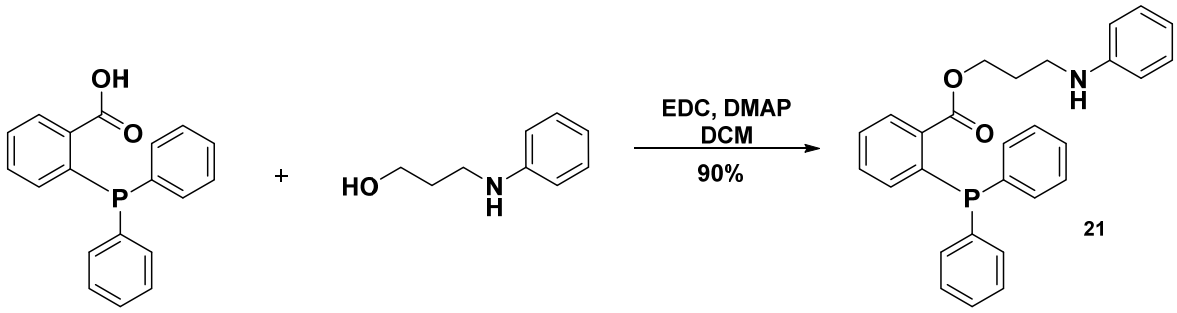

Scheme S13. Synthesis of compound **21**, an analogue of TPP-CL2.

200 mg of diphenylphosphinobenzoic acid (1eq, 0.652 mmol) were dissolved in dry DCM. To the resulting solution, 375 mg of EDC (3 eq.) and 160 mg of DMAP (2 eq.) were added. The solution was stirred for 10 min under a nitrogen atmosphere at room temperature. Then, 103 mg of 3-(phenylamino) propanol were added to the reaction mixture, which was then stirred for 2 h (room temperature, N_2 atmosphere). The product was purified by reversed phase liquid chromatography (yield 90%) and characterized (**Scheme S12**).

^{1}H NMR (400 MHz, Methylene Chloride-d_2) δ 8.19 (ddd, J = 7.6, 3.7, 1.6 Hz, 1H), 7.66–7.34 (m, 12H), 7.30–7.20 (m, 2H), 7.09 (ddd, J = 7.7, 3.9, 1.5 Hz, 1H), 6.77 (t, J = 7.3 Hz, 1H), 6.71–6.64 (m, 2H), 4.37 (t, J = 6.1 Hz, 2H), 3.90 (s, 1H), 3.23 (t, J = 6.8 Hz, 2H), 2.04–1.90 (m, 2H).

^{31}P NMR (162 MHz, Methylene Chloride-d_2) δ -4.72.

^{13}C NMR (101 MHz, Methylene Chloride-d_2) δ 167.16 (d, J = 2.1 Hz), 148.58, 140.44 (d, J = 26.8 Hz), 138.50 (d, J = 11.4 Hz), 135.00 (d, J = 19.7 Hz), 134.71, 134.21 (d, J = 20.8 Hz), 132.29, 130.91 (d, J = 2.9 Hz), 129.49, 129.01, 128.86 (d, J = 7.2 Hz), 128.67, 117.35, 112.96, 63.43, 40.85, 28.65.

HRMS (ESI TOF ES+) calc.440.1779, found 440.1785.

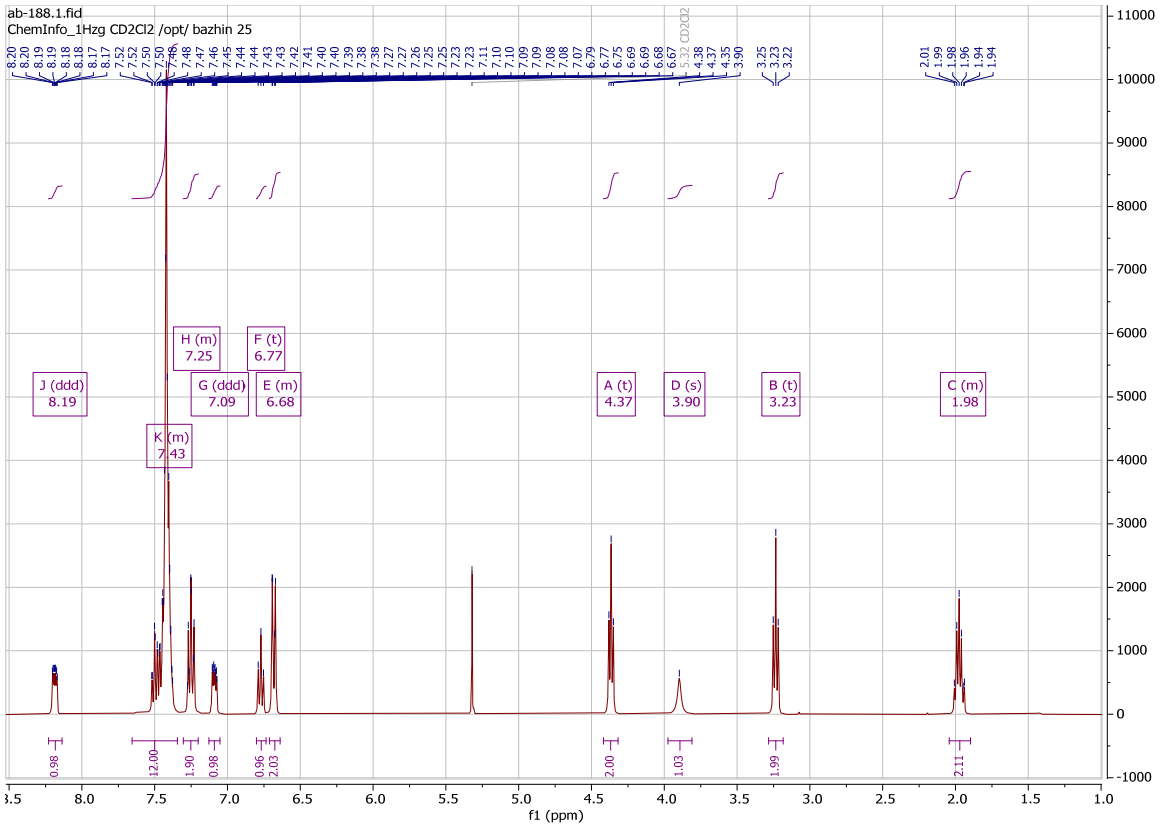

^{1}H spectrum of compound **21**

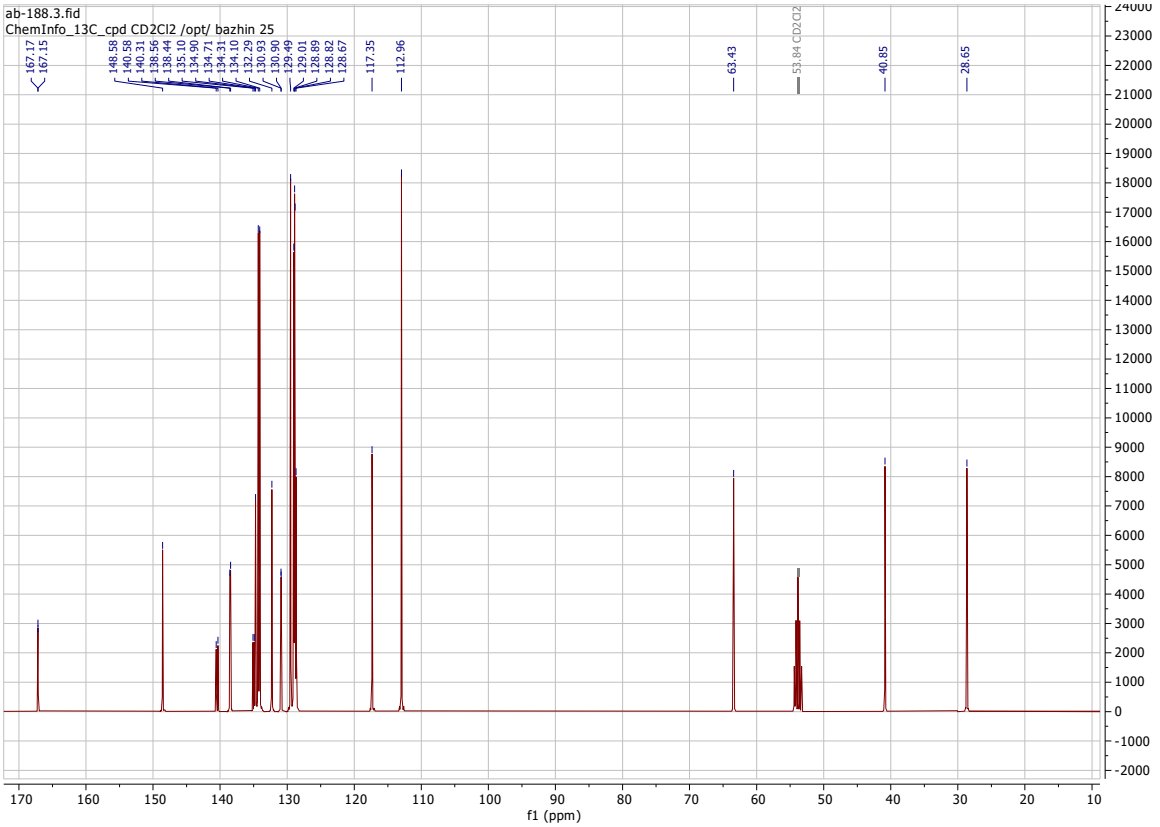

^{13}C spectrum of compound **21**

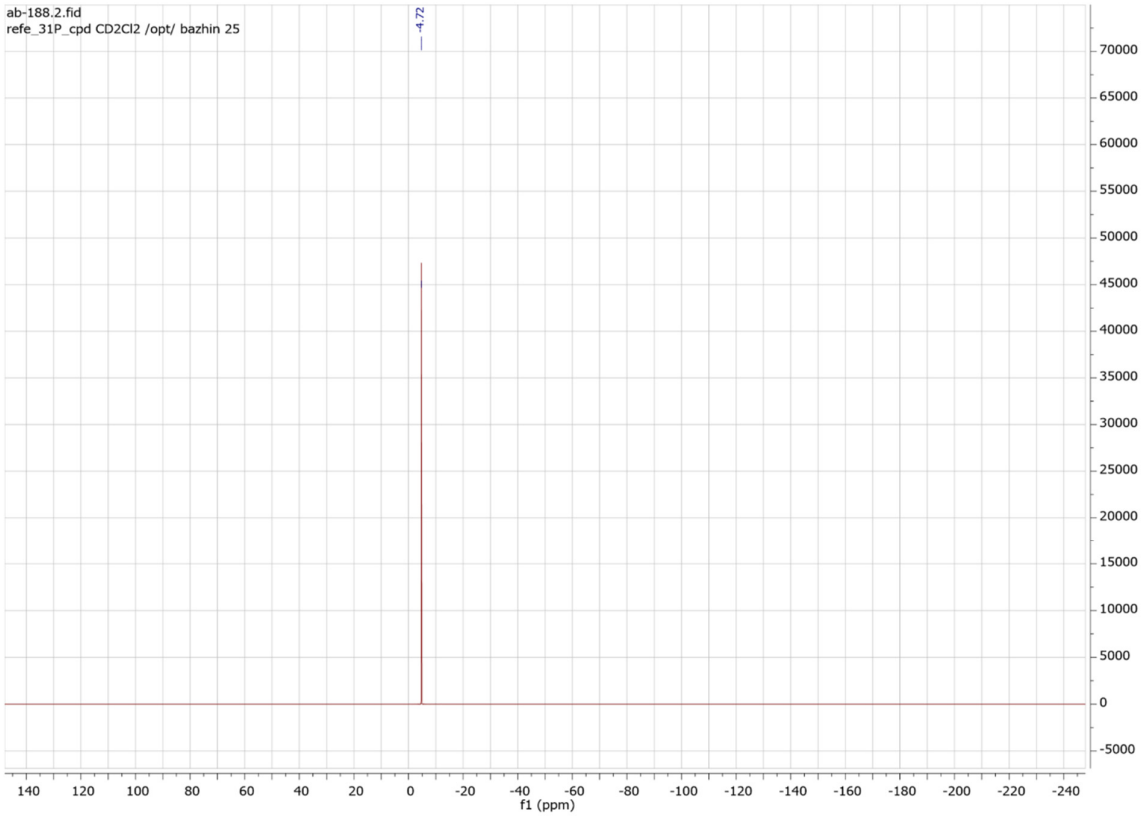

^{31}P spectrum of compound **21**

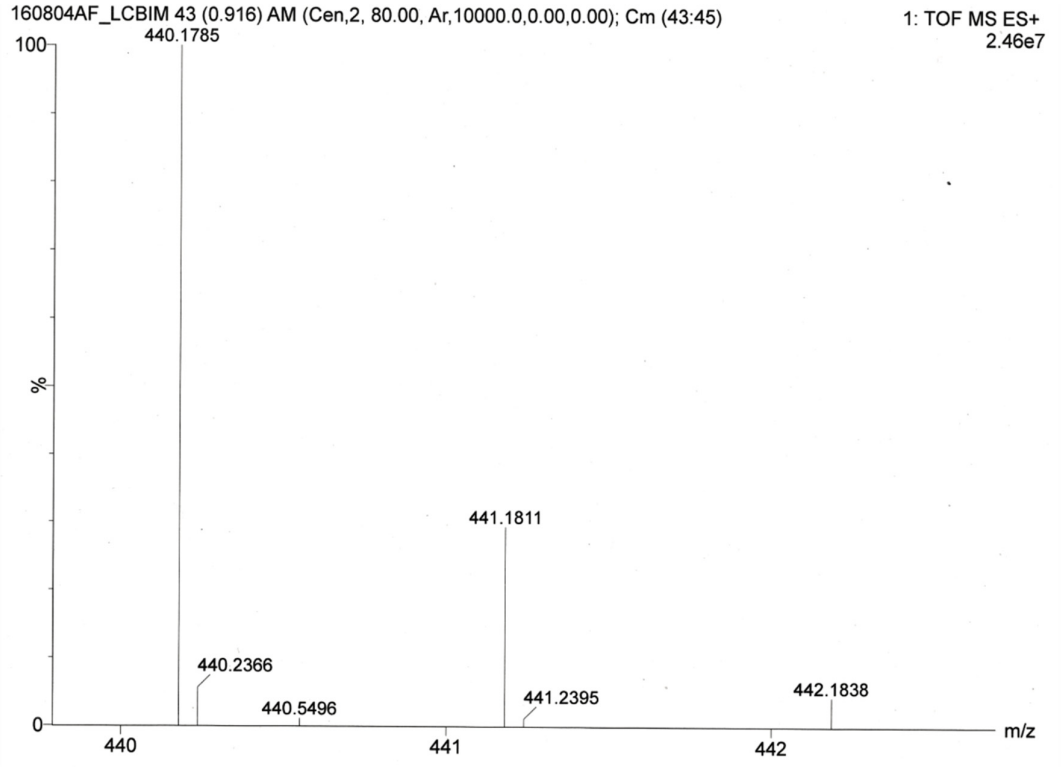

HRMS spectrum of compound **21**

References

1 Sheldrick, G. M. SHELXT - Integrated space-group and crystal-structure determination. *Acta Crystallogr A* **71**, 3-8, doi:10.1107/S2053273314026370 (2015).

2 Dolomanov, O. V., Bourhis, L. J., Gildea, R. J., Howard, J. A. K. & Puschmann, H. OLEX2: a complete structure solution, refinement and analysis program. *J Appl Crystallogr* **42**, 339-341, doi:10.1107/S0021889808042726 (2009).

3 Sheldrick, G. M. Crystal structure refinement with SHELXL. *Acta Crystallogr C* **71**, 3-8, doi:10.1107/S2053229614024218 (2015).

4 Lin, F. L., Hoyt, H. M., van Halbeek, H., Bergman, R. G. & Bertozzi, C. R. Mechanistic investigation of the Staudinger ligation. *J Am Chem Soc* **127**, 2686-2695, doi:10.1021/ja044461m (2005).

5 Kiick, K. L., Saxon, E., Tirrell, D. A. & Bertozzi, C. R. Incorporation of azides into recombinant proteins for chemoselective modification by the Staudinger ligation. *Proc Natl Acad Sci U S A* **99**, 19-24, doi:10.1073/pnas.012583299 (2002).

6 Wallis, J. D. & Dunitz, J. D. An all-nitrogen aromatic ring system: structural study of 4-dimethyl-aminophenylpentazole. *Journal of the Chemical Society, Chemical Communications*, 910-911, doi:10.1039/C39830000910 (1983).

7 Bazanov, B. & Haas, Y. Solution photochemistry of [p-(dimethylamino)phenyl]pentazole (DMAPP) at 193 and 300 nm. *J Phys Chem A* **119**, 2661-2671, doi:10.1021/jp509815y (2015).

8 Huisgen, R. & Ugi, I. Pentazole, I. Die Lösung Eines Klassischen Problems der Organischen Stickstoffchemie. *Chemische Berichte* **90**, 2914-2927, doi:10.1002/cber.19570901230 (1957).

9 Ugi, I. & Huisgen, R. Pentazole, II. Die Zerfallsgeschwindigkeit der Aryl-pentazole. *Chemische Berichte* **91**, 531-537, doi:10.1002/cber.19580910310 (1958).

10 Ugi, I., Perlinger, H. & Behringer, L. Pentazole, III. Kristallisierte Aryl-pentazole. *Chemische Berichte* **91**, 2324-2329, doi:10.1002/cber.19580911110 (1958).

11 Ugi, I., Perlinger, H. & Behringer, L. Pentazole, IV. Der Konstitutionsbeweis für kristallisiertes [p-Äthoxy-phenyl]-pentazol. *Chemische Berichte* **92**, 1864-1866, doi:10.1002/cber.19590920819 (1959).

12 Cohen, A. S., Dubikovskaya, E. A., Rush, J. S. & Bertozzi, C. R. Real-time bioluminescence imaging of glycans on live cells. *J Am Chem Soc* **132**, 8563-8565, doi:10.1021/ja101766r (2010).

13 Myers, E. L. & Raines, R. T. A phosphine-mediated conversion of azides into diazo compounds. *Angew Chem Int Ed Engl* **48**, 2359-2363, doi:10.1002/anie.200804689 (2009).

14 Haymore, B. L., Hughes, M., Mason, J. & Richards, R. L. The N-15 Nuclear Magnetic-Resonance Criterion of Bond Angle in Diazenido-Complexes. *J Chem Soc Dalton*, 2935-2940, doi:DOI 10.1039/dt9880002935 (1988).

15 Pomerantz, M. *et al.* N-15 and P-31 Nmr-Spectroscopy of N-Aryl-P,P,P-Triphenylphospha-Lambda-5-Azenes - Applicability to P-Pi-D-Pi Bonding. *Journal of Organic Chemistry* **50**, 1757-1759, doi:DOI 10.1021/jo00210a039 (1985).

16 Lin, F. L., Hoyt, H. M., van Halbeek, H., Bergman, R. G. & Bertozzi, C. R. Mechanistic investigation of the Staudinger ligation. *Abstr Pap Am Chem S* **229**, U534-U534 (2005).

Supplementary Note 3. X-ray structure reports

1.1 Report for TPP-CL1

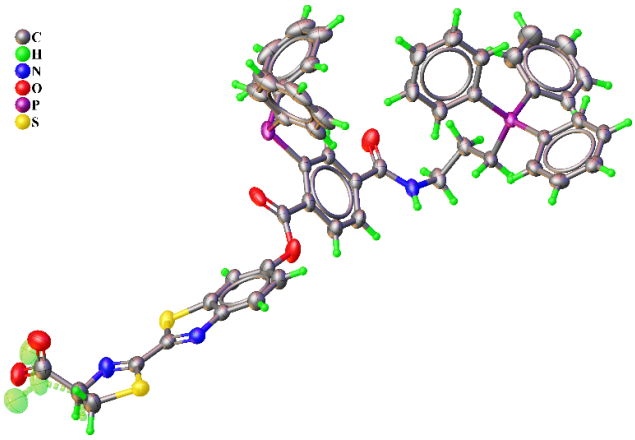

Experimental. Single yellow prism-shaped crystals of **TPP-CL1** (**1**, AB-196) were obtained by recrystallisation from methanol at -20C. A suitable crystal of 0.40×0.20×0.16 mm^3 was selected and mounted on a suitable support on a SuperNova, Dual, Cu at zero, Atlas diffractometer. The crystal was kept at a steady T = 100.00(10) K during data collection. The structure was solved with the **ShelXT** [1, 2] structure solution program using the dual solution method and by using **Olex2**[3] as the graphical interface. The model was refined with version 2018/3 of ShelXL [1, 2] using full matrix least squares on $|F|^2$ minimisation.

Crystal Data. $C_{52}H_{41}N_3O_5P_2S_2$, M_r = 913.94, monoclinic, $I2/a$ (No. 15), a = 27.7068(5) Å, b = 16.7035(2) Å, c = 26.8015(6) Å, β = 102.3414(19)°, α = γ = 90°, V = 12117.1(4) $Å^3$, T = 100.00(10) K, Z = 8, Z' = 1, μ(CuKα) = 1.614, 42956 reflections measured, 12322 unique (R_{int} = 0.0339) which were used in all calculations. The final wR_2 was 0.1277 (all data) and R_1 was 0.0427 (I > 2(I)).

Compound	**TPP-CL1**
Formula	$C_{52}H_{41}N_3O_5P_2S_2$
$D_{calc.}$/ g cm^{-3}	1.002
μ/mm^{-1}	1.614
Formula Weight	913.94
Colour	yellow
Shape	prism
Size/mm^3	0.40×0.20×0.16
T/K	100.00(10)
Crystal System	monoclinic
Space Group	$I2/a$
a/Å	27.7068(5)
b/Å	16.7035(2)
c/Å	26.8015(6)
α/°	90
β/°	102.3414(19)
γ/°	90
V/$Å^3$	12117.1(4)
Z	8
Z'	1
Wavelength/Å	1.54178
Radiation type	CuKα
Θ_{min}/°	3.376
Θ_{max}/°	86.100
Measured Refl.	42956
Independent Refl.	12322
Reflections with I > 2(I)	10053
R_{int}	0.0339
Parameters	605
Restraints	80
Largest Peak/e $Å^{-3}$	0.484
Deepest Hole/e $Å^{-3}$	-0.470
GooF	1.064
wR_2 (all data)	0.1277
wR_2	0.1235
R_1 (all data)	0.0514
R_1	0.0427

A yellow prism-shaped crystal with dimensions of 0.40×0.20×0.16 mm^3 was mounted on a suitable support. Data were collected using a SuperNova, Dual, Cu at zero, Atlas diffractometer operating at T = 100.00(10) K.

Data were measured using ω scans using CuKα radiation. The total number of runs and images was based on the strategy calculation from the program **CrysAlisPro** (Rigaku, V1.171.38.43, 2015) The maximum resolution achieved was Θ = 86.100° (0.83 Å).

The diffraction pattern was indexed. The total number of runs and images was based on the strategy calculation from the program **CrysAlisPro** (Rigaku, V1.171.38.43, 2015) and the unit cell was refined using **CrysAlisPro** (Rigaku, V1.171.38.43, 2015) on 18743 reflections, 44% of the observed reflections.

Data reduction, scaling and absorption corrections were performed using **CrysAlisPro** (Rigaku, V1.171.38.43, 2015). The final completeness is 99.40 % out to 86.100° in Θ. A Gaussian absorption correction was performed using CrysAlisPro 1.171.38.43 (Rigaku Oxford Diffraction, 2015) Numerical absorption correction based on Gaussian integration over a multifaceted crystal model/Empirical absorption correction using spherical harmonics as implemented in SCALE3 ABSPACK scaling algorithm. The absorption coefficient μ of this material is 1.614 mm^{-1} at this wavelength (λ = 1.542Å) and the minimum and maximum transmissions are 0.463 and 1.000.

The structure was solved and the space group $I2/a$ (# 15) determined by the **ShelXT** [1, 2] structure solution program using dual and refined by full matrix least squares on $|F|^2$ using version 2018/3 of ShelXL [1, 2]. All non-hydrogen atoms were refined anisotropically. Hydrogen atom positions were calculated geometrically and refined using the riding model. Hydrogen atom positions were calculated geometrically and refined using the riding model.

There is a single molecule in the asymmetric unit, which is represented by the reported sum formula. In other words: Z is 8 and Z' is 1.

Fractional Atomic Coordinates (×10^4) and Equivalent Isotropic Displacement Parameters (Å^2×10^3) for **TPP-CL1**. U_{eq} is defined as 1/3 of the trace of the orthogonalised U_{ij}.

Atom	x	y	z	U_{eq}
S1	7517.8(2)	9014.6(3)	7011.3(2)	44.63(11)
S2	6377.1(2)	7347.5(3)	7370.9(2)	39.57(10)
P1	4450.2(2)	3889.1(3)	6200.3(2)	39.37(11)
P2	5264.7(2)	-1270.7(2)	6256.8(2)	30.20(9)
O1A	6366.4(14)	10528(2)	6981.3(19)	72.2(11)
O1B	6348(3)	10617(5)	7257(4)	76(2)
O2A	6390.1(14)	10724.8(19)	7775.5(13)	65.4(11)
O2B	6665(4)	10915(5)	8020(4)	115(3)
O3	6134.9(6)	4396.1(8)	6769.7(7)	54.8(4)
O4	5358.1(6)	4778.8(7)	6359.0(4)	45.7(3)
O5	4508.8(6)	1114.1(8)	7191.0(6)	52.3(4)
N1	6788.9(7)	9047.7(10)	7514.9(7)	49.7(4)
N2	7042.9(5)	7369.3(9)	6807.1(5)	35.7(3)
N3	5326.6(6)	686.6(8)	7385.1(5)	34.2(3)
C1A	6576.6(19)	10433(3)	7437.5(19)	56.6(11)
C1B	6649(4)	10491(6)	7663(4)	68(2)
C2	7023.7(9)	9840.3(14)	7603.8(11)	60.9(6)
C3	7412.0(9)	9974.7(13)	7276.9(10)	57.8(5)
C4	7006.9(7)	8623.3(11)	7240.7(7)	40.1(4)
C5	6848.7(6)	7796.8(11)	7112.6(6)	35.9(3)
C6	6441.1(6)	6496.8(11)	7036.3(6)	36.0(3)
C7	6812.6(6)	6619.6(10)	6754.3(6)	34.4(3)

Atom	x	y	z	U_{eq}
C8	6929.9(7)	6004.8(12)	6455.9(7)	41.9(4)
C9	6687.5(8)	5277.2(12)	6452.4(8)	45.2(4)
C10	6331.0(7)	5171.5(11)	6744.8(8)	43.9(4)
C11	6194.5(7)	5761.9(11)	7036.5(7)	42.4(4)
C12	5627.1(7)	4284.3(10)	6597.5(6)	37.3(4)
C13	5455.2(7)	3496.6(10)	6748.6(6)	35.9(4)
C14	4943.3(7)	3248.7(9)	6583.2(5)	32.5(3)
C15	4806.7(6)	2512.9(9)	6760.6(5)	31.3(3)
C16	5157.5(7)	2034.3(10)	7076.7(6)	33.6(3)
C17	5659.4(7)	2290.1(11)	7238.9(7)	42.0(4)
C18	5805.2(7)	3019.4(11)	7074.7(8)	43.1(4)
C19	4967.6(7)	1239.4(10)	7225.8(6)	36.0(4)
C20	5199.3(8)	-99.9(10)	7548.8(6)	40.1(4)
C21	5035.5(7)	-683.4(10)	7120.9(6)	36.4(4)
C22	5478.5(7)	-857.8(10)	6865.8(6)	34.6(3)
C23	5808.9(6)	-1554.1(10)	6017.5(5)	32.2(3)
C24	6217.1(7)	-1018.7(11)	6068.4(6)	39.6(4)
C25	6632.3(7)	-1203.5(13)	5863.2(7)	45.4(4)
C26	6645.3(7)	-1919.8(12)	5615.6(6)	43.4(4)
C27	6241.8(8)	-2452.2(11)	5562.1(6)	41.9(4)
C28	5820.7(7)	-2269.4(10)	5759.0(6)	36.5(3)
C29	4864.9(7)	-2119.1(10)	6295.0(6)	36.4(3)
C30	4338.4(9)	-2038.8(14)	6194.6(9)	55.4(5)
C31	4042.4(10)	-2694.3(17)	6265.6(12)	72.0(7)
C32	4269.8(11)	-3418.0(14)	6427.8(10)	65.9(7)
C33	4786.8(10)	-3489.9(11)	6529.8(7)	51.2(5)
C34	5091.0(8)	-2843.0(10)	6473.4(6)	40.6(4)
C35	4914.3(7)	-523.1(10)	5861.7(6)	34.4(3)
C36	4614.8(8)	-744.3(12)	5401.1(7)	43.4(4)
C37	4352.2(8)	-160.2(13)	5090.7(7)	50.5(5)
C38	4393.9(9)	637.6(13)	5231.8(7)	52.9(5)
C39	4697.2(9)	860.5(12)	5680.4(7)	51.5(5)
C40	4958.8(8)	282.3(11)	5998.1(6)	42.8(4)
C41	4616.3(8)	3892.4(11)	5593.8(6)	43.0(4)
C42	4316.2(10)	4392.0(13)	5239.9(7)	56.1(6)
C43	4414.3(13)	4456.0(15)	4770.2(8)	71.1(8)
C44	4816.4(13)	4048.8(15)	4657.2(7)	73.3(9)
C45	5112.4(12)	3557.7(16)	4994.6(8)	67.6(8)
C46	5010.5(9)	3471.5(13)	5469.5(7)	51.8(5)
C47	3906.6(7)	3200.8(12)	6090.3(6)	41.2(4)
C48	3553.1(9)	3274.7(16)	6394.0(8)	60.6(6)
C49	3149.9(9)	2739(2)	6355.1(10)	75.4(9)
C50	3092.0(8)	2125(2)	6012.3(9)	71.0(8)
C51	3433.0(8)	2050.8(16)	5702.1(8)	56.5(6)
C52	3835.3(7)	2582.2(12)	5740.3(6)	40.9(4)

Anisotropic Displacement Parameters ($\times 10^4$) **TPP-CL1**. The anisotropic displacement factor exponent takes the form: $-2\pi^2[h^2a^{*2} \times U_{11} + ... + 2hka^* \times b^* \times U_{12}]$

Atom	U_{11}	U_{22}	U_{33}	U_{23}	U_{13}	U_{12}
S1	36.0(2)	45.2(3)	51.1(2)	-2.70(19)	5.65(18)	-2.63(18)
S2	46.2(2)	37.4(2)	38.3(2)	6.62(16)	16.03(17)	8.23(17)
P1	65.2(3)	30.8(2)	21.78(17)	3.17(14)	8.46(17)	13.65(19)
P2	41.7(2)	23.25(19)	24.41(16)	1.86(13)	4.37(14)	2.44(15)
O1A	76(2)	62.0(18)	71(2)	-0.3(17)	-1.5(17)	-10.6(14)
O1B	80(4)	71(4)	82(5)	22(4)	30(4)	16(3)
O2A	72(2)	60.2(17)	64.9(19)	-7.3(13)	17.0(16)	23.7(15)
O2B	103(6)	120(6)	111(5)	-57(5)	2(5)	23(4)
O3	51.4(8)	29.7(7)	89.5(11)	15.3(7)	29.4(8)	4.9(6)
O4	80.0(9)	26.2(6)	26.6(5)	1.7(4)	2.1(6)	-3.7(6)
O5	51.7(8)	40.9(7)	70.5(9)	20.8(7)	27.1(7)	5.3(6)
N1	55.1(10)	37.2(9)	58.5(10)	-2.1(7)	15.5(8)	3.4(7)

Atom	U_{11}	U_{22}	U_{33}	U_{23}	U_{13}	U_{12}
N2	37.2(7)	36.2(7)	33.4(6)	4.4(5)	7.3(5)	-0.5(6)
N3	53.0(8)	25.2(7)	25.7(5)	3.9(5)	11.0(5)	4.7(6)
C1A	65(3)	43(2)	66(3)	-1(2)	22(3)	1.7(19)
C1B	83(5)	54(4)	79(5)	-10(4)	44(5)	5(4)
C2	55.3(12)	45.7(12)	83.2(16)	-11.9(11)	18.5(11)	-0.2(10)
C3	52.9(12)	42.5(11)	78.5(15)	-5.1(10)	15.0(11)	-2.7(9)
C4	38.4(9)	39.4(9)	39.8(8)	3.5(7)	2.3(7)	4.6(7)
C5	35.6(8)	39.0(9)	31.6(7)	6.0(6)	3.7(6)	4.6(7)
C6	38.3(9)	36.9(9)	34.3(7)	11.2(6)	11.0(6)	7.8(7)
C7	35.3(8)	35.6(9)	32.2(7)	8.0(6)	7.2(6)	2.0(6)
C8	43.4(9)	42.9(10)	43.5(9)	2.2(7)	18.4(7)	-1.4(8)
C9	49.9(10)	37.0(10)	52.7(10)	1.3(8)	20.2(8)	3.1(8)
C10	46.6(10)	29.5(9)	59.2(10)	12.5(8)	19.3(8)	4.5(7)
C11	44.3(10)	36.3(9)	51.5(10)	14.4(8)	21.0(8)	6.6(7)
C12	59.4(11)	26.1(8)	31.3(7)	-1.6(6)	20.8(7)	3.1(7)
C13	54.2(10)	24.5(8)	32.8(7)	1.6(6)	17.6(7)	4.9(7)
C14	52.1(9)	25.6(7)	22.3(6)	1.0(5)	13.5(6)	7.4(7)
C15	43.6(9)	28.2(8)	24.2(6)	1.0(5)	11.8(6)	5.6(6)
C16	45.7(9)	27.7(8)	30.4(7)	5.4(6)	14.9(6)	5.6(7)
C17	46.9(10)	32.3(9)	46.5(9)	10.8(7)	9.5(8)	8.0(7)
C18	44.7(10)	32.9(9)	53.2(10)	7.6(8)	13.7(8)	3.6(7)
C19	50.4(10)	30.4(8)	30.5(7)	6.9(6)	16.1(7)	7.3(7)
C20	71.3(12)	25.9(8)	25.6(7)	7.0(6)	15.7(7)	4.7(8)
C21	55.2(10)	26.8(8)	29.1(7)	4.4(6)	13.2(7)	1.5(7)
C22	47.8(9)	27.6(8)	27.0(6)	0.2(6)	4.6(6)	5.8(7)
C23	43.3(9)	29.3(8)	22.0(6)	1.6(5)	2.7(6)	4.2(6)
C24	49.1(10)	37.4(9)	31.4(7)	-3.6(6)	6.6(7)	-2.5(7)
C25	43.7(10)	58.0(12)	33.0(8)	-2.4(8)	4.8(7)	-5.2(8)
C26	44.3(10)	56.8(12)	28.2(7)	1.4(7)	5.5(7)	11.7(8)
C27	57.1(11)	39.9(10)	28.2(7)	-0.9(6)	7.8(7)	11.6(8)
C28	50.6(10)	31.3(8)	26.1(6)	0.0(6)	5.1(6)	1.7(7)
C29	52.7(10)	27.2(8)	29.8(7)	1.5(6)	9.9(7)	-1.2(7)
C30	54.2(12)	42.8(11)	68.8(13)	13.2(10)	12.1(10)	-2.0(9)
C31	60.1(14)	63.3(16)	93.7(19)	15.2(14)	19.2(13)	-16.4(12)
C32	96(2)	44.4(12)	63.3(13)	3.7(10)	30.1(13)	-23.4(12)
C33	95.5(17)	28.3(9)	37.5(8)	3.8(7)	31.3(10)	-1.1(9)
C34	66.5(12)	30.7(8)	26.9(7)	3.5(6)	15.0(7)	4.0(8)
C35	44.1(9)	31.7(8)	27.1(6)	4.9(6)	7.0(6)	4.5(7)
C36	53.1(11)	40.1(10)	33.3(8)	2.3(7)	1.1(7)	4.5(8)
C37	58.8(12)	55.9(12)	33.4(8)	9.0(8)	2.0(8)	9.7(9)
C38	71.5(14)	48.5(11)	38.8(9)	17.6(8)	12.4(9)	22.0(10)
C39	84.9(15)	32.3(9)	37.7(9)	9.0(7)	14.0(9)	16.4(9)
C40	64.4(12)	31.6(9)	32.1(7)	5.2(6)	9.6(7)	6.6(8)
C41	74.6(13)	32.3(9)	21.9(6)	-1.3(6)	9.7(7)	-15.6(8)
C42	89.3(16)	43.2(11)	28.9(8)	7.6(7)	-2.9(9)	-20.1(10)
C43	124(2)	53.6(13)	28.7(8)	7.1(9)	1.0(11)	-35.3(15)
C44	140(3)	54.7(14)	27.3(8)	-6.5(9)	22.3(12)	-51.0(16)
C45	105(2)	61.9(14)	45.5(11)	-22.8(10)	37.6(12)	-38.1(14)
C46	80.0(15)	45.8(11)	33.6(8)	-9.7(8)	21.2(9)	-17.7(10)
C47	46.7(10)	49.7(10)	29.3(7)	14.3(7)	12.5(7)	18.9(8)
C48	64.4(14)	85.1(17)	37.6(9)	20.9(10)	22.9(9)	37.8(12)
C49	47.2(12)	129(3)	57.4(13)	43.9(16)	27.5(11)	33.2(14)
C50	38.2(11)	122(2)	51.6(12)	37.6(15)	5.6(9)	-4.5(12)
C51	46.0(11)	81.0(16)	40.0(9)	18.0(10)	3.2(8)	-12.7(10)
C52	39.7(9)	52.7(11)	30.2(7)	9.2(7)	7.2(6)	1.9(8)

Bond Lengths in Å for **TPP-CL1**.

Atom	Atom	Length/Å
S1	C3	1.804(2)
S1	C4	1.784(2)
S2	C5	1.7709(18)
S2	C6	1.7096(18)
P1	C14	1.8615(17)
P1	C41	1.7815(17)

Atom	Atom	Length/Å
P1	C47	1.867(2)
P2	C22	1.7543(16)
P2	C23	1.8229(17)
P2	C29	1.8149(18)
P2	C35	1.7843(16)
O1A	C1A	1.247(5)
O1B	C1B	1.239(7)
O2A	C1A	1.235(4)
O2B	C1B	1.183(6)
O3	C10	1.412(2)
O3	C12	1.396(3)
O4	C12	1.201(2)
O5	C19	1.272(2)
N1	C2	1.472(3)
N1	C4	1.264(3)
N2	C5	1.288(2)
N2	C7	1.399(2)
N3	C19	1.357(2)
N3	C20	1.452(2)
C1A	C2	1.574(5)
C1B	C2	1.535(7)
C2	C3	1.542(3)
C4	C5	1.467(3)
C6	C7	1.416(2)
C6	C11	1.405(3)
C7	C8	1.382(3)
C8	C9	1.388(3)
C9	C10	1.397(3)
C10	C11	1.361(3)
C12	C13	1.485(2)
C13	C14	1.453(3)
C13	C18	1.406(3)
C14	C15	1.399(2)
C15	C16	1.396(2)
C16	C17	1.431(3)

Atom	Atom	Length/Å
C16	C19	1.513(2)
C17	C18	1.385(3)
C20	C21	1.499(2)
C21	C22	1.555(2)
C23	C24	1.425(3)
C23	C28	1.385(2)
C24	C25	1.411(3)
C25	C26	1.372(3)
C26	C27	1.412(3)
C27	C28	1.413(3)
C29	C30	1.432(3)
C29	C34	1.398(2)
C30	C31	1.405(3)
C31	C32	1.389(4)
C32	C33	1.405(4)
C33	C34	1.398(3)
C35	C36	1.383(2)
C35	C40	1.393(2)
C36	C37	1.384(3)
C37	C38	1.383(3)
C38	C39	1.363(3)
C39	C40	1.385(3)
C41	C42	1.396(3)
C41	C46	1.398(3)
C42	C43	1.348(3)
C43	C44	1.393(5)
C44	C45	1.359(4)
C45	C46	1.369(3)
C47	C48	1.406(3)
C47	C52	1.381(3)
C48	C49	1.418(4)
C49	C50	1.362(5)
C50	C51	1.391(3)
C51	C52	1.411(3)

Bond Angles in ° for **TPP-CL1**.

Atom	Atom	Atom	Angle/°
C4	S1	C3	88.96(10)
C6	S2	C5	88.81(8)
C14	P1	C47	101.85(8)
C41	P1	C14	101.68(9)
C41	P1	C47	102.40(8)
C22	P2	C23	106.80(8)
C22	P2	C29	110.08(8)
C22	P2	C35	108.04(8)
C29	P2	C23	112.20(8)
C35	P2	C23	111.04(7)
C35	P2	C29	108.59(8)
C12	O3	C10	118.55(14)
C4	N1	C2	110.44(18)
C5	N2	C7	108.50(14)
C19	N3	C20	120.10(16)
O1A	C1A	C2	122.1(3)
O2A	C1A	O1A	119.3(4)
O2A	C1A	C2	117.9(4)
O1B	C1B	C2	111.9(6)
O2B	C1B	O1B	120.7(8)
O2B	C1B	C2	126.7(8)
N1	C2	C1A	103.1(3)

Atom	Atom	Atom	Angle/°
N1	C2	C1B	111.6(5)
N1	C2	C3	112.13(19)
C1B	C2	C3	121.7(5)
C3	C2	C1A	110.5(3)
C2	C3	S1	106.66(15)
N1	C4	S1	120.53(16)
N1	C4	C5	120.53(18)
C5	C4	S1	118.93(14)
N2	C5	S2	117.20(14)
N2	C5	C4	121.74(16)
C4	C5	S2	121.06(13)
C7	C6	S2	109.18(13)
C11	C6	S2	128.38(13)
C11	C6	C7	122.40(16)
N2	C7	C6	116.32(15)
C8	C7	N2	124.42(15)
C8	C7	C6	119.26(16)
C7	C8	C9	118.78(16)
C8	C9	C10	120.40(18)
C9	C10	O3	117.89(17)
C11	C10	O3	118.72(17)
C11	C10	C9	123.17(18)

Atom	Atom	Atom	Angle/°
C10	C11	C6	115.97(16)
O3	C12	C13	112.81(15)
O4	C12	O3	123.41(16)
O4	C12	C13	123.77(18)
C14	C13	C12	121.23(15)
C18	C13	C12	116.93(17)
C18	C13	C14	121.78(16)
C13	C14	P1	123.92(12)
C15	C14	P1	118.18(13)
C15	C14	C13	117.65(14)
C16	C15	C14	120.37(16)
C15	C16	C17	121.24(15)
C15	C16	C19	115.25(16)
C17	C16	C19	123.51(15)
C18	C17	C16	119.80(16)
C17	C18	C13	119.14(18)
O5	C19	N3	124.38(16)
O5	C19	C16	121.58(15)
N3	C19	C16	114.03(16)
N3	C20	C21	114.23(12)
C20	C21	C22	108.64(15)
C21	C22	P2	109.96(12)
C24	C23	P2	120.17(12)
C28	C23	P2	120.64(14)
C28	C23	C24	119.09(16)
C25	C24	C23	121.44(17)
C26	C25	C24	119.15(18)
C25	C26	C27	119.75(17)
C26	C27	C28	121.68(17)
C23	C28	C27	118.87(17)
C30	C29	P2	121.72(14)

Atom	Atom	Atom	Angle/°
C34	C29	P2	117.40(15)
C34	C29	C30	120.62(17)
C31	C30	C29	120.2(2)
C32	C31	C30	118.8(3)
C31	C32	C33	120.7(2)
C34	C33	C32	121.74(19)
C29	C34	C33	118.0(2)
C36	C35	P2	119.31(14)
C36	C35	C40	119.68(16)
C40	C35	P2	120.92(13)
C35	C36	C37	119.11(18)
C38	C37	C36	120.82(19)
C39	C38	C37	120.27(17)
C38	C39	C40	119.64(19)
C39	C40	C35	120.45(18)
C42	C41	P1	112.91(17)
C42	C41	C46	121.38(18)
C46	C41	P1	125.68(15)
C43	C42	C41	118.2(3)
C42	C43	C44	119.7(3)
C45	C44	C43	123.2(2)
C44	C45	C46	117.9(3)
C45	C46	C41	119.7(2)
C48	C47	P1	119.50(18)
C52	C47	P1	124.15(13)
C52	C47	C48	116.3(2)
C47	C48	C49	122.5(2)
C50	C49	C48	120.1(2)
C49	C50	C51	118.2(2)
C50	C51	C52	121.8(2)
C47	C52	C51	121.06(18)

Torsion Angles in ° for **TPP-CL1**.

Atom	Atom	Atom	Atom	Angle/°
S1	C4	C5	S2	174.85(9)
S1	C4	C5	N2	-5.6(2)
S2	C6	C7	N2	0.52(18)
S2	C6	C7	C8	179.59(14)
S2	C6	C11	C10	-177.78(15)
P1	C14	C15	C16	-175.86(11)
P1	C41	C42	C43	178.57(17)
P1	C41	C46	C45	-176.81(16)
P1	C47	C48	C49	-175.60(16)
P1	C47	C52	C51	175.58(15)
P2	C23	C24	C25	-176.62(13)
P2	C23	C28	C27	177.53(12)
P2	C29	C30	C31	-175.1(2)
P2	C29	C34	C33	176.75(12)
P2	C35	C36	C37	-178.58(16)
P2	C35	C40	C39	177.89(16)
O1A	C1A	C2	N1	-71.4(5)
O1A	C1A	C2	C3	48.6(6)
O1B	C1B	C2	N1	-68.4(10)

Atom	Atom	Atom	Atom	Angle/°
O1B	C1B	C2	C3	67.7(11)
O2A	C1A	C2	N1	98.5(5)
O2A	C1A	C2	C3	-141.5(4)
O2B	C1B	C2	N1	121.4(12)
O2B	C1B	C2	C3	-102.4(13)
O3	C10	C11	C6	173.53(17)
O3	C12	C13	C14	-176.70(14)
O3	C12	C13	C18	5.8(2)
O4	C12	C13	C14	4.3(2)
O4	C12	C13	C18	-173.17(16)
N1	C2	C3	S1	-12.0(3)
N1	C4	C5	S2	-4.2(2)
N1	C4	C5	N2	175.38(17)
N2	C7	C8	C9	177.38(17)
N3	C20	C21	C22	65.4(2)
C1A	C2	C3	S1	-126.3(3)
C1B	C2	C3	S1	-147.9(5)
C2	N1	C4	S1	-0.9(2)
C2	N1	C4	C5	178.14(18)
C3	S1	C4	N1	-5.54(18)
C3	S1	C4	C5	175.40(16)
C4	S1	C3	C2	9.24(18)
C4	N1	C2	C1A	127.4(2)
C4	N1	C2	C1B	149.1(4)
C4	N1	C2	C3	8.6(3)
C5	S2	C6	C7	-0.19(12)
C5	S2	C6	C11	177.36(17)
C5	N2	C7	C6	-0.6(2)
C5	N2	C7	C8	-179.66(16)
C6	S2	C5	N2	-0.17(14)
C6	S2	C5	C4	179.43(14)
C6	C7	C8	C9	-1.6(3)
C7	N2	C5	S2	0.47(18)
C7	N2	C5	C4	-179.13(15)
C7	C6	C11	C10	-0.5(3)
C7	C8	C9	C10	0.1(3)
C8	C9	C10	O3	-173.35(19)
C8	C9	C10	C11	1.3(3)
C9	C10	C11	C6	-1.0(3)
C10	O3	C12	O4	11.7(3)
C10	O3	C12	C13	-167.28(15)
C11	C6	C7	N2	-177.21(16)
C11	C6	C7	C8	1.9(3)
C12	O3	C10	C9	-120.3(2)
C12	O3	C10	C11	64.9(3)
C12	C13	C14	P1	-3.0(2)
C12	C13	C14	C15	-177.25(13)
C12	C13	C18	C17	178.08(16)
C13	C14	C15	C16	-1.3(2)
C14	P1	C41	C42	-175.55(14)
C14	P1	C41	C46	2.54(19)
C14	P1	C47	C48	100.16(15)
C14	P1	C47	C52	-76.50(15)
C14	C13	C18	C17	0.6(3)

Atom	Atom	Atom	Atom	Angle/°
C14	C15	C16	C17	1.8(2)
C14	C15	C16	C19	-177.74(13)
C15	C16	C17	C18	-1.0(3)
C15	C16	C19	O5	-19.0(2)
C15	C16	C19	N3	159.72(14)
C16	C17	C18	C13	-0.2(3)
C17	C16	C19	O5	161.50(18)
C17	C16	C19	N3	-19.8(2)
C18	C13	C14	P1	174.34(13)
C18	C13	C14	C15	0.1(2)
C19	N3	C20	C21	83.8(2)
C19	C16	C17	C18	178.45(16)
C20	N3	C19	O5	-2.4(2)
C20	N3	C19	C16	178.93(13)
C20	C21	C22	P2	-161.54(11)
C22	P2	C23	C24	-45.09(14)
C22	P2	C23	C28	138.61(13)
C22	P2	C29	C30	96.13(17)
C22	P2	C29	C34	-77.97(14)
C22	P2	C35	C36	-165.64(15)
C22	P2	C35	C40	17.81(17)
C23	P2	C22	C21	-173.97(11)
C23	P2	C29	C30	-145.08(15)
C23	P2	C29	C34	40.82(14)
C23	P2	C35	C36	77.55(17)
C23	P2	C35	C40	-99.00(16)
C23	C24	C25	C26	-0.9(3)
C24	C23	C28	C27	1.2(2)
C24	C25	C26	C27	1.1(3)
C25	C26	C27	C28	-0.2(3)
C26	C27	C28	C23	-1.0(2)
C28	C23	C24	C25	-0.3(2)
C29	P2	C22	C21	-51.92(13)
C29	P2	C23	C24	-165.80(12)
C29	P2	C23	C28	17.90(15)
C29	P2	C35	C36	-46.26(17)
C29	P2	C35	C40	137.19(15)
C29	C30	C31	C32	-0.8(4)
C30	C29	C34	C33	2.6(3)
C30	C31	C32	C33	1.3(4)
C31	C32	C33	C34	0.1(3)
C32	C33	C34	C29	-2.0(3)
C34	C29	C30	C31	-1.2(3)
C35	P2	C22	C21	66.50(13)
C35	P2	C23	C24	72.48(14)
C35	P2	C23	C28	-103.82(14)
C35	P2	C29	C30	-21.96(18)
C35	P2	C29	C34	163.94(12)
C35	C36	C37	C38	1.2(3)
C36	C35	C40	C39	1.4(3)
C36	C37	C38	C39	0.2(3)
C37	C38	C39	C40	-0.8(3)
C38	C39	C40	C35	0.1(3)
C40	C35	C36	C37	-2.0(3)
C41	P1	C14	C13	71.25(14)
C41	P1	C14	C15	-

Atom	Atom	Atom	Atom	Angle/°
				114.55(12)
C41	P1	C47	C48	-154.89(15)
C41	P1	C47	C52	28.45(17)
C41	C42	C43	C44	-2.1(3)
C42	C41	C46	C45	1.1(3)
C42	C43	C44	C45	2.4(4)
C43	C44	C45	C46	-0.8(3)
C44	C45	C46	C41	-0.9(3)
C46	C41	C42	C43	0.4(3)
C47	P1	C14	C13	176.77(12)
C47	P1	C14	C15	-9.04(13)
C47	P1	C41	C42	79.37(15)
C47	P1	C41	C46	-102.55(18)
C47	C48	C49	C50	-0.3(3)
C48	C47	C52	C51	-1.2(3)
C48	C49	C50	C51	-0.8(3)
C49	C50	C51	C52	0.9(3)
C50	C51	C52	C47	0.1(3)
C52	C47	C48	C49	1.3(3)

Hydrogen Fractional Atomic Coordinates ($\times 10^4$) and Equivalent Isotropic Displacement Parameters ($Å^2 \times 10^3$) for **TPP-CL1**. U_{eq} is defined as 1/3 of the trace of the orthogonalised U_{ij}.

Atom	x	y	z	U_{eq}
H3	5636.85	805.07	7389.14	41
H2A	7176.85	9911.8	7974.27	73
H2B	7230.23	9790.96	7957.29	73
H3A	7722.54	10184.47	7490.48	69
H3B	7288.36	10364.09	7000.63	69
H8	7171.91	6079.08	6256.93	50
H9	6764.45	4848.34	6249.97	54
H11	5947.43	5681.82	7228.7	51
H15	4473.45	2337.89	6665.53	38
H17	5891.9	1960.57	7458.57	50
H18	6137.45	3195.14	7180.89	52
H20A	4931.48	-39.95	7738.35	48
H20B	5490.46	-323.9	7787.75	48
H21A	4756.94	-456.07	6866.48	44
H21B	4922.47	-1186.08	7254.96	44
H22A	5709.13	-1235.95	7080.09	42
H22B	5659.65	-354.9	6836.81	42
H24	6209.46	-526.59	6244.31	47
H25	6899.33	-836.85	5896.1	54
H26	6924.8	-2056.74	5480.69	52
H27	6253.67	-2946.09	5389.35	50
H28	5550.18	-2630.95	5714.76	44
H30	4188.98	-1541.19	6079.85	67
H31	3693.1	-2643.51	6203.75	86
H32	4073.62	-3869.06	6470.23	79
H33	4933.56	-3991.25	6639.92	61
H34	5440.62	-2893.72	6553.87	49
H36	4589.57	-1290.09	5299.05	52
H37	4140.58	-308.96	4776.71	61
H38	4210.51	1031.69	5015.17	63
H39	4728.87	1409.35	5774.73	62
H40	5170.03	436.28	6311.13	51
H42	4050.15	4678.76	5327.81	67
H43	4210.27	4777.27	4517.5	85

Atom	x	y	z	U_{eq}
H44	4887.23	4117.78	4328.3	88
H45	5381.32	3282.93	4903.91	81
H46	5206.89	3127.12	5713.52	62
H48	3585.6	3699.94	6634.29	73
H49	2919.81	2807.07	6568.43	90
H50	2825.75	1758.54	5985.83	85
H51	3394.02	1630.6	5457.92	68
H52	4060.57	2513.39	5521.73	49

Atomic Occupancies for all atoms that are not fully occupied in **TPP-CL1**.

Atom	Occupancy
O1A	0.657(8)
O1B	0.343(8)
O2A	0.657(8)
O2B	0.343(8)
C1A	0.657(8)
C1B	0.343(8)
H2A	0.657(8)
H2B	0.343(8)

1.2 Report for azido-TPP1

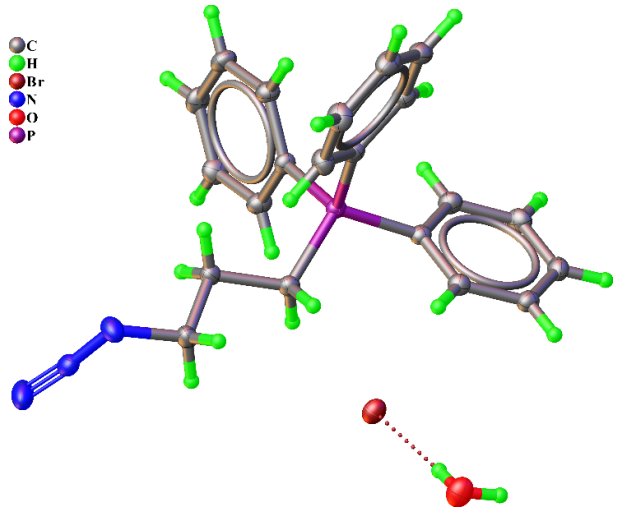

Experimental. Single colorless prism-shaped crystals of **azido-TPP1** (**2**, AB-184) were obtained by recrystallisation from water at 25C. A suitable crystal of 0.47×0.30×0.23 mm^3 was selected and mounted on a suitable support on a SuperNova, Dual, Cu at zero, Atlas diffractometer. The crystal was kept at a steady T = 100.01(10) K during data collection. The structure was solved with the **ShelXT** [1, 2] structure solution program using the dual solution method and by using **Olex2** [3] as the graphical interface. The model was refined with version 2018/3 of ShelXL [1, 2] using full matrix least squares on $|F|^2$ minimisation.

Crystal Data. $C_{21}H_{23}BrN_3OP$, M_r = 444.30, triclinic, $P\bar{1}$ (No. 2), a = 9.4450(3) Å, b = 10.0767(3) Å, c = 11.7449(4) Å, α = 91.245(3)°, β = 109.554(3)°, γ = 100.928(3)°, V = 1029.85(7) Å^3, T = 100.01(10) K, Z = 2, Z' = 1, μ(CuKα) = 3.574, 7019 reflections measured, 4119 unique (R_{int} = 0.0189) which were used in all calculations. The final wR_2 was 0.0617 (all data) and R_1 was 0.0231 (I > 2(I)).

Compound	**Azido-TPP1**
Formula	$C_{21}H_{23}BrN_3OP$
$D_{calc.}$/ g cm^{-3}	1.433
μ/mm^{-1}	3.574
Formula Weight	444.30
Colour	colourless
Shape	prism
Size/mm^3	0.47×0.30×0.23
T/K	100.01(10)
Crystal System	triclinic
Space Group	$P\bar{1}$
a/Å	9.4450(3)
b/Å	10.0767(3)
c/Å	11.7449(4)
α/°	91.245(3)
β/°	109.554(3)
γ/°	100.928(3)
V/Å^3	1029.85(7)
Z	2
Z'	1
Wavelength/Å	1.54184
Radiation type	CuKα
Θ_{min}/°	4.011
Θ_{max}/°	75.497
Measured Refl.	7019
Independent Refl.	4119
Reflections with I > 2(I)	3933
R_{int}	0.0189
Parameters	253
Restraints	1
Largest Peak/e Å^{-3}	0.403
Deepest Hole/e Å^{-3}	-0.342
GooF	1.045
wR_2 (all data)	0.0617
wR_2	0.0609
R_1 (all data)	0.0244
R_1	0.0231

A colourless prism-shaped crystal with dimensions of 0.47×0.30×0.23 mm^3 was mounted on a suitable support. Data were collected using a SuperNova, Dual, Cu at zero, Atlas diffractometer operating at T = 100.01(10) K.

Data were measured using ω scans using CuKα radiation. The total number of runs and images was based on the strategy calculation from the program **CrysAlisPro** (Rigaku, V1.171.38.43, 2015). The maximum resolution achieved was Θ = 75.497° (0.83 Å).

The diffraction pattern was indexed. The total number of runs and images was based on the strategy calculation from the program **CrysAlisPro** (Rigaku, V1.171.38.43, 2015) and the unit cell was refined using **CrysAlisPro** (Rigaku, V1.171.38.43, 2015) on 5810 reflections, 83% of the observed reflections.

Data reduction, scaling and absorption corrections were performed using **CrysAlisPro** (Rigaku, V1.171.38.43, 2015). The final completeness is 99.70 % out to 75.497° in Θ. A Gaussian absorption correction was performed using CrysAlisPro 1.171.38.43 (Rigaku Oxford Diffraction, 2015) Numerical absorption correction based on Gaussian integration over a multifaceted crystal model/Empirical absorption correction using spherical harmonics as implemented in SCALE3 ABSPACK scaling algorithm. The absorption coefficient μ of this material is 3.574 mm^{-1} at this wavelength (λ = 1.542Å) and the minimum and maximum transmissions are 0.379 and 0.572.

The structure was solved and the space group $P\bar{1}$ (# 2) determined by the **ShelXT** [1, 2] structure solution program using dual and refined by full matrix least squares on $|F|^2$ using version 2018/3 of ShelXL-2018/3 [1, 2]. All non-hydrogen atoms were refined anisotropically. Most hydrogen atom positions were calculated geometrically and refined using the riding model, but the hydrogen atoms of water solvent molecule were refined freely.

There is a single molecule in the asymmetric unit, which is represented by the reported sum formula. In other words: Z is 2 and Z' is 1.

Fractional Atomic Coordinates (×10^4) and Equivalent Isotropic Displacement Parameters (Å^2×10^3) for **azido-TPP1**. U_{eq} is defined as 1/3 of the trace of the orthogonalised U_{ij}.

Atom	x	y	z	U_{eq}
Br1	2780.0(2)	4202.9(2)	953.5(2)	22.01(7)
P1	600.6(4)	7045.8(4)	2976.2(3)	15.22(9)
N1	-1304.6(17)	1748.2(14)	2708.1(13)	26.0(3)
N2	-2584.4(16)	1109.3(13)	2061.8(12)	21.4(3)
N3	-3730.4(19)	423.2(17)	1568.6(14)	35.2(4)
C1	67.4(18)	5400.2(15)	2164.9(14)	18.5(3)
C2	-758.3(18)	4264.6(15)	2714.2(14)	19.2(3)
C3	-626.6(19)	2921.1(15)	2184.9(15)	22.7(3)
C4	-1018.8(17)	7399.7(15)	3307.0(14)	17.2(3)
C5	-2426.3(18)	7202.6(16)	2351.2(14)	21.6(3)
C6	-3730.1(19)	7377.0(17)	2589.2(16)	24.3(3)
C7	-3628.4(19)	7750.6(17)	3763.8(16)	23.8(3)
C8	-2233(2)	7955.7(17)	4703.4(15)	23.7(3)
C9	-912.5(18)	7784.7(16)	4485.0(14)	20.2(3)
C10	1207.3(17)	8267.3(15)	2064.1(13)	16.8(3)
C11	823.2(18)	9542.2(16)	2000.1(14)	20.8(3)
C12	1454.4(19)	10497.7(16)	1369.6(15)	23.4(3)
C13	2465.4(18)	10192.4(16)	826.2(14)	22.1(3)
C14	2833.3(18)	8916.8(16)	881.8(14)	20.0(3)
C15	2202.9(17)	7949.3(15)	1496.0(14)	18.9(3)
C16	2230.4(17)	7140.6(15)	4346.3(13)	17.7(3)
C17	2770.2(18)	5987.2(16)	4787.0(15)	23.0(3)

Atom	x	y	z	U_{eq}
C18	4049(2)	6118.8(18)	5834.4(16)	26.6(3)
C19	4804.5(18)	7388.7(18)	6436.4(15)	24.6(3)
C20	4289.6(19)	8540.4(17)	5986.0(15)	23.1(3)
C21	3004.0(18)	8419.3(16)	4949.2(14)	20.5(3)
O1	5871.1(15)	3317.2(13)	515.9(12)	28.7(3)

Anisotropic Displacement Parameters (×10⁴) **azido-TPP1**. The anisotropic displacement factor exponent takes the form: $-2\pi^2[h^2a^{*2} \times U_{11} + ... + 2hka^* \times b^* \times U_{12}]$

Atom	U_{11}	U_{22}	U_{33}	U_{23}	U_{13}	U_{12}
Br1	22.64(11)	23.60(10)	24.66(11)	5.60(6)	11.90(7)	9.13(7)
P1	14.18(18)	16.67(18)	16.09(18)	1.26(13)	5.97(14)	4.93(13)
N1	25.6(7)	22.8(7)	23.4(7)	1.9(5)	3.8(6)	-1.3(6)
N2	26.4(7)	20.1(6)	19.6(6)	3.2(5)	10.7(6)	3.7(6)
N3	31.7(8)	38.5(9)	28.0(8)	3.9(6)	10.0(7)	-9.9(7)
C1	18.5(7)	18.3(7)	19.9(7)	-0.6(6)	8.1(6)	4.0(6)
C2	18.1(7)	19.3(7)	20.6(7)	-0.5(6)	8.0(6)	2.5(6)
C3	23.6(8)	18.6(7)	26.9(8)	-1.7(6)	12.3(7)	0.3(6)
C4	16.3(7)	17.4(7)	20.4(7)	2.4(5)	8.4(6)	6.0(5)
C5	21.5(8)	25.2(8)	19.5(7)	0.9(6)	7.6(6)	7.7(6)
C6	17.5(8)	27.8(8)	27.1(8)	1.5(6)	5.5(6)	7.5(6)
C7	21.5(8)	24.7(8)	32.0(9)	4.6(6)	15.4(7)	9.3(6)
C8	27.6(8)	26.2(8)	22.6(8)	1.1(6)	13.7(7)	9.1(6)
C9	20.1(8)	22.4(7)	18.7(7)	1.4(6)	6.3(6)	6.5(6)
C10	15.9(7)	18.9(7)	15.0(7)	1.2(5)	4.4(6)	3.9(5)
C11	22.0(8)	20.9(7)	21.5(7)	1.5(6)	8.5(6)	7.7(6)
C12	27.7(8)	18.3(7)	25.2(8)	3.4(6)	8.9(7)	7.9(6)
C13	22.7(8)	21.3(7)	21.0(8)	3.2(6)	7.4(6)	1.7(6)
C14	18.3(7)	22.9(7)	19.1(7)	0.6(6)	7.3(6)	4.0(6)
C15	19.2(7)	18.3(7)	19.7(7)	1.8(6)	6.2(6)	6.1(6)
C16	15.0(7)	22.4(7)	17.3(7)	3.6(6)	6.6(6)	5.5(6)
C17	20.9(8)	20.2(7)	26.9(8)	4.2(6)	7.0(6)	4.3(6)
C18	23.9(8)	27.0(8)	28.4(9)	9.9(7)	5.8(7)	9.3(7)
C19	17.6(8)	35.1(9)	19.6(8)	4.9(6)	4.2(6)	5.5(6)
C20	21.1(8)	26.6(8)	20.4(8)	-1.3(6)	6.9(6)	2.8(6)
C21	21.1(8)	21.3(7)	20.7(7)	1.8(6)	7.8(6)	6.9(6)
O1	28.8(7)	29.3(6)	34.9(7)	8.9(5)	15.8(6)	12.9(5)

Bond Lengths in Å for **azido-TPP1**.

Atom	Atom	Length/Å
P1	C1	1.7902(15)
P1	C4	1.7934(15)
P1	C10	1.7866(15)
P1	C16	1.8020(15)
N1	N2	1.233(2)
N1	C3	1.481(2)
N2	N3	1.124(2)
C1	C2	1.538(2)
C2	C3	1.521(2)
C4	C5	1.399(2)
C4	C9	1.394(2)
C5	C6	1.391(2)
C6	C7	1.389(2)
C7	C8	1.382(2)

Atom	Atom	Length/Å
C8	C9	1.395(2)
C10	C11	1.397(2)
C10	C15	1.399(2)
C11	C12	1.393(2)
C12	C13	1.387(2)
C13	C14	1.391(2)
C14	C15	1.387(2)
C16	C17	1.397(2)
C16	C21	1.397(2)
C17	C18	1.389(2)
C18	C19	1.387(2)
C19	C20	1.390(2)
C20	C21	1.386(2)

Bond Angles in ° for **azido-TPP1**.

Atom	Atom	Atom	Angle/°
C1	P1	C4	108.88(7)
C1	P1	C16	110.92(7)
C4	P1	C16	111.06(7)
C10	P1	C1	108.64(7)
C10	P1	C4	111.24(7)
C10	P1	C16	106.07(7)
N2	N1	C3	115.79(14)
N3	N2	N1	172.13(16)
C2	C1	P1	115.40(10)
C3	C2	C1	107.21(12)
N1	C3	C2	112.03(13)
C5	C4	P1	117.72(11)
C9	C4	P1	121.58(12)
C9	C4	C5	120.61(14)
C6	C5	C4	119.32(15)
C7	C6	C5	120.14(15)
C8	C7	C6	120.34(15)
C7	C8	C9	120.45(15)

Atom	Atom	Atom	Angle/°
C4	C9	C8	119.14(15)
C11	C10	P1	121.81(11)
C11	C10	C15	120.55(14)
C15	C10	P1	117.40(11)
C12	C11	C10	119.06(14)
C13	C12	C11	120.43(14)
C12	C13	C14	120.33(15)
C15	C14	C13	119.94(14)
C14	C15	C10	119.67(14)
C17	C16	P1	122.01(12)
C21	C16	P1	118.28(12)
C21	C16	C17	119.65(14)
C18	C17	C16	119.74(15)
C19	C18	C17	120.40(15)
C18	C19	C20	119.99(15)
C21	C20	C19	120.08(15)
C20	C21	C16	120.12(15)

Torsion Angles in ° for **azido-TPP1**.

Atom	Atom	Atom	Atom	Angle/°
P1	C1	C2	C3	-161.12(11)
P1	C4	C5	C6	175.63(12)
P1	C4	C9	C8	-175.57(12)
P1	C10	C11	C12	173.75(12)
P1	C10	C15	C14	-173.37(12)
P1	C16	C17	C18	178.74(13)
P1	C16	C21	C20	-178.12(12)
N2	N1	C3	C2	102.58(17)
C1	P1	C4	C5	-49.92(14)
C1	P1	C4	C9	126.53(13)
C1	P1	C10	C11	140.38(13)
C1	P1	C10	C15	-45.24(14)
C1	P1	C16	C17	-11.08(15)
C1	P1	C16	C21	166.26(12)
C1	C2	C3	N1	176.56(13)
C4	P1	C1	C2	-48.06(13)
C4	P1	C10	C11	20.55(15)
C4	P1	C10	C15	-165.07(11)
C4	P1	C16	C17	110.15(13)
C4	P1	C16	C21	-72.51(13)
C4	C5	C6	C7	0.4(2)
C5	C4	C9	C8	0.8(2)
C5	C6	C7	C8	0.2(3)
C6	C7	C8	C9	-0.3(2)
C7	C8	C9	C4	-0.2(2)
C9	C4	C5	C6	-0.9(2)
C10	P1	C1	C2	-169.34(11)
C10	P1	C4	C5	69.77(14)
C10	P1	C4	C9	-113.78(13)
C10	P1	C16	C17	-128.87(13)
C10	P1	C16	C21	48.48(14)

Atom	Atom	Atom	Atom	Angle/°
C10	C11	C12	C13	-0.8(2)
C11	C10	C15	C14	1.1(2)
C11	C12	C13	C14	1.5(2)
C12	C13	C14	C15	-0.8(2)
C13	C14	C15	C10	-0.4(2)
C15	C10	C11	C12	-0.5(2)
C16	P1	C1	C2	74.45(12)
C16	P1	C4	C5	-172.34(12)
C16	P1	C4	C9	4.11(15)
C16	P1	C10	C11	-100.33(13)
C16	P1	C10	C15	74.06(13)
C16	C17	C18	C19	-0.8(3)
C17	C16	C21	C20	-0.7(2)
C17	C18	C19	C20	-0.6(3)
C18	C19	C20	C21	1.3(2)
C19	C20	C21	C16	-0.6(2)
C21	C16	C17	C18	1.4(2)

Hydrogen Fractional Atomic Coordinates (×10^4) and Equivalent Isotropic Displacement Parameters (Å^2×10^3) for **azido-TPP1**. U_{eq} is defined as 1/3 of the trace of the orthogonalised U_{ij}.

Atom	x	y	z	U_{eq}
H1A	-610.09	5460.93	1325.66	22
H1B	1007.04	5141.37	2116.06	22
H2A	-272.49	4356.28	3608.88	23
H2B	-1851.85	4313.84	2506.82	23
H3A	-1156.19	2828.51	1294.66	27
H3B	470.58	2918.67	2344.08	27
H5	-2490.93	6952.32	1548.01	26
H6	-4691.87	7240.38	1946.92	29
H7	-4522.44	7865.67	3922.29	29
H8	-2173.23	8214.94	5503.45	28
H9	46.91	7928.66	5130.53	24
H11	141.04	9754.64	2381.28	25
H12	1190.92	11364.2	1311.31	28
H13	2908.73	10857.79	414.11	26
H14	3515.84	8708.48	499.23	24
H15	2445.98	7074.97	1530.87	23
H17	2264.07	5116.6	4371.63	28
H18	4409.62	5334.22	6140.5	32
H19	5673.55	7471.39	7156.67	30
H20	4819.72	9411.62	6389.52	28
H21	2647.85	9207.13	4647.57	25
H1C	5150(20)	3540(30)	660(20)	45(7)
H1D	6170(20)	4000(20)	210(20)	34(6)

Hydrogen Bond information for **azido-TPP1**.

D	H	A	d(D-H)/Å	d(H-A)/Å	d(D-A)/Å	D-H-A/deg
C1	H1A	Br1[1]	0.99	2.85	3.8321(16)	172.8
C1	H1B	Br1	0.99	2.76	3.6853(15)	155.1
C2	H2B	O1[2]	0.99	2.61	3.309(2)	127.6
C5	H5	Br1[1]	0.95	3.04	3.9870(16)	173.1
C9	H9	N1[3]	0.95	2.40	3.227(2)	145.3
C15	H15	Br1	0.95	3.06	3.9828(15)	165.5
O1	H1C	Br1	0.822(18)	2.579(19)	3.3996(12)	176(2)
O1	H1D	Br1[4]	0.834(18)	2.538(18)	3.3612(13)	170(2)

––––

[1]-x,1-y,-z; [2]-1+x,+y,+z; [3]-x,1-y,1-z; [4]1-x,1-y,-z

1.3 Report for compound 14

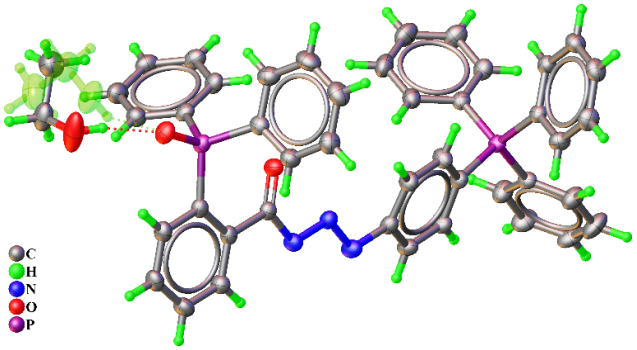

Experimental. Single clear intense orange prism-shaped crystals of **14** (AB-153) were obtained by recrystallisation from mixture EtOH:EtOEt at +4C. A suitable crystal of 0.41×0.23×0.01 mm³ was selected and mounted on a suitable support on a SuperNova, Dual, Cu at zero, AtlasS2 diffractometer. The crystal was kept at a steady T = 140.00(10) K during data collection. The structure was solved with the **ShelXT** [1, 2] structure solution program using the dual solution method and by using **Olex2** [3] as the graphical interface. The model was refined with version 2018/3 of ShelXL [1, 2] using full matrix least squares on $|F|^2$ minimisation.

Crystal Data. $C_{45}H_{39}N_3O_3P_2$, M_r = 731.73, monoclinic, $P2_1/n$ (No. 14), a = 12.1755(2) Å, b = 9.8681(2) Å, c = 31.6381(5) Å, β = 99.658(2)°, α = γ = 90°, V = 3747.41(12) Å³, T = 140.00(10) K, Z = 4, Z' = 1, μ(CuKα) = 1.416, 25938 reflections measured, 7668 unique (R_{int} = 0.0264) which were used in all calculations. The final wR_2 was 0.0971 (all data) and R_1 was 0.0371 (I > 2(I)).

Compound	**14**
Formula	$C_{45}H_{39}N_3O_3P_2$
$D_{calc.}$/ g cm^{-3}	1.297
μ/mm^{-1}	1.416
Formula Weight	731.73
Colour	clear intense orange
Shape	prism
Size/mm³	0.41×0.23×0.01
T/K	140.00(10)
Crystal System	monoclinic
Space Group	$P2_1/n$
a/Å	12.1755(2)
b/Å	9.8681(2)
c/Å	31.6381(5)
α/°	90
β/°	99.658(2)
γ/°	90
V/Å³	3747.41(12)
Z	4
Z'	1
Wavelength/Å	1.54178
Radiation type	CuKα
Θ_{min}/°	3.717
Θ_{max}/°	75.314
Measured Refl.	25938
Independent Refl.	7668
Reflections with I > 2(I)	7017
R_{int}	0.0264
Parameters	508
Restraints	61
Largest Peak/e Å^{-3}	0.346
Deepest Hole/e Å^{-3}	-0.415
GooF	1.026
wR_2 (all data)	0.0971
wR_2	0.0945
R_1 (all data)	0.0408
R_1	0.0371

A clear intense orange prism-shaped crystal with dimensions of 0.41×0.23×0.01 mm³ was mounted on a suitable support. Data were collected using a SuperNova, Dual, Cu at zero, AtlasS2 diffractometer operating at T = 140.00(10) K.

Data were measured using ω scans using CuKα radiation. The total number of runs and images was based on the strategy calculation from the program **CrysAlisPro** (Rigaku, V1.171.38.43, 2015) The maximum resolution achieved was Θ = 75.314° (0.83 Å).

The diffraction pattern was indexed. The total number of runs and images was based on the strategy calculation from the program **CrysAlisPro** (Rigaku, V1.171.38.43, 2015) and the unit cell was refined using **CrysAlisPro** (Rigaku, V1.171.38.43, 2015) on 13395 reflections, 52% of the observed reflections.

Data reduction, scaling and absorption corrections were performed using **CrysAlisPro** (Rigaku, V1.171.38.43, 2015). The final completeness is 100.00 % out to 75.314° in Θ. A multi-scan absorption correction was performed using CrysAlisPro 1.171.38.43 (Rigaku Oxford Diffraction, 2015) Empirical

absorption correction using spherical harmonics, as implemented in SCALE3 ABSPACK scaling algorithm. The absorption coefficient μ of this material is 1.416 mm^{-1} at this wavelength (λ = 1.542Å) and the minimum and maximum transmissions are 0.634 and 1.000.

The structure was solved and the space group $P2_1/n$ (# 14) determined by the **ShelXT** [1, 2] structure solution program using dual and refined by full matrix least squares on $|F|^2$ using version 2018/3 of ShelXL [1, 2]. All non-hydrogen atoms were refined anisotropically. Hydrogen atom positions were calculated geometrically and refined using the riding model.

There is a single molecule in the asymmetric unit, which is represented by the reported sum formula. In other words: Z is 4 and Z' is 1.

Atomic coordinates (x 10^4) and equivalent isotropic displacement parameters (Å^{2}x 10^3) for **14**. U(eq) is defined as one third of the trace of the orthogonalized U^{ij} tensor.

	x	y	z	U(eq)
P(1)	9489(1)	9472(1)	3213(1)	26(1)
P(2)	4227(1)	8131(1)	5738(1)	24(1)
O(1)	10055(1)	9925(1)	2851(1)	34(1)
O(2)	8377(1)	8514(1)	3865(1)	30(1)
N(1)	8605(1)	6465(1)	4248(1)	28(1)
N(2)	7785(1)	6877(1)	4447(1)	26(1)
N(3)	7596(1)	6017(1)	4734(1)	32(1)
C(1)	9886(1)	10635(1)	3652(1)	28(1)
C(2)	11024(1)	10926(2)	3739(1)	35(1)
C(3)	11441(2)	11842(2)	4057(1)	40(1)
C(4)	10731(2)	12492(2)	4290(1)	36(1)
C(5)	9606(2)	12212(2)	4205(1)	36(1)
C(6)	9179(1)	11289(2)	3888(1)	32(1)
C(7)	8013(1)	9450(2)	3015(1)	29(1)
C(8)	7454(2)	10678(2)	2925(1)	37(1)
C(9)	6376(2)	10694(2)	2699(1)	44(1)
C(10)	5850(2)	9501(2)	2557(1)	43(1)
C(11)	6394(1)	8274(2)	2648(1)	40(1)
C(12)	7468(1)	8249(2)	2879(1)	33(1)
C(13)	10026(1)	7795(2)	3383(1)	26(1)
C(14)	10877(1)	7358(2)	3168(1)	31(1)
C(15)	11407(1)	6124(2)	3263(1)	34(1)
C(16)	11088(1)	5299(2)	3575(1)	35(1)
C(17)	10247(1)	5716(2)	3794(1)	31(1)
C(18)	9714(1)	6955(2)	3705(1)	25(1)
C(19)	8818(1)	7402(1)	3950(1)	24(1)
C(20)	6724(1)	6456(1)	4944(1)	27(1)

C(21)	5940(1)	7429(2)	4778(1)	31(1)
C(22)	5168(1)	7877(2)	5018(1)	33(1)
C(23)	5144(1)	7342(2)	5428(1)	27(1)
C(24)	5873(1)	6305(2)	5583(1)	28(1)
C(25)	6653(1)	5859(2)	5341(1)	30(1)
C(26)	4863(1)	9677(2)	5966(1)	27(1)
C(27)	5896(1)	10092(2)	5877(1)	32(1)
C(28)	6383(1)	11272(2)	6060(1)	41(1)
C(29)	5841(2)	12047(2)	6326(1)	44(1)
C(30)	4804(2)	11647(2)	6411(1)	40(1)
C(31)	4318(1)	10462(2)	6236(1)	32(1)
C(32)	2962(1)	8483(1)	5375(1)	25(1)
C(33)	2522(1)	7452(2)	5092(1)	32(1)
C(34)	1597(1)	7707(2)	4785(1)	37(1)
C(35)	1114(1)	8982(2)	4756(1)	36(1)
C(36)	1535(1)	9990(2)	5043(1)	34(1)
C(37)	2458(1)	9748(2)	5355(1)	28(1)
C(38)	4012(1)	7065(1)	6175(1)	26(1)
C(39)	4801(2)	7095(2)	6547(1)	38(1)
C(40)	4673(2)	6267(2)	6891(1)	43(1)
C(41)	3750(2)	5449(2)	6867(1)	43(1)
C(42)	2966(2)	5418(2)	6500(1)	49(1)
C(43)	3101(2)	6208(2)	6148(1)	39(1)
O(3A)	11891(3)	10523(4)	2501(1)	85(1)
C(44A)	12607(3)	11293(4)	2794(1)	50(1)
C(45A)	12128(4)	12676(4)	2851(2)	69(1)
O(3B)	11208(6)	11268(7)	2303(2)	68(2)
C(44B)	11664(6)	12373(9)	2541(3)	65(2)
C(45B)	12673(8)	12070(15)	2851(3)	73(3)

Bond lengths [Å] and angles [°] for **14**.

P(1)-O(1)	1.5015(10)
P(1)-C(7)	1.8008(16)
P(1)-C(1)	1.8024(15)
P(1)-C(13)	1.8264(15)
P(2)-C(23)	1.7846(14)
P(2)-C(38)	1.7917(13)
P(2)-C(32)	1.7945(14)
P(2)-C(26)	1.8037(15)
O(2)-C(19)	1.2308(18)
N(1)-N(2)	1.3303(17)

N(1)-C(19)	1.3768(18)
N(2)-N(3)	1.2909(17)
N(3)-C(20)	1.4112(18)
C(1)-C(6)	1.391(2)
C(1)-C(2)	1.396(2)
C(2)-C(3)	1.384(2)
C(2)-H(2)	0.9500
C(3)-C(4)	1.384(2)
C(3)-H(3)	0.9500
C(4)-C(5)	1.379(2)
C(4)-H(4)	0.9500
C(5)-C(6)	1.389(2)
C(5)-H(5)	0.9500
C(6)-H(6)	0.9500
C(7)-C(12)	1.391(2)
C(7)-C(8)	1.396(2)
C(8)-C(9)	1.385(3)
C(8)-H(8)	0.9500
C(9)-C(10)	1.379(3)
C(9)-H(9)	0.9500
C(10)-C(11)	1.387(3)
C(10)-H(10)	0.9500
C(11)-C(12)	1.387(2)
C(11)-H(11)	0.9500
C(12)-H(12)	0.9500
C(13)-C(14)	1.4002(19)
C(13)-C(18)	1.4139(19)
C(14)-C(15)	1.387(2)
C(14)-H(14)	0.9500
C(15)-C(16)	1.386(2)
C(15)-H(15)	0.9500
C(16)-C(17)	1.391(2)
C(16)-H(16)	0.9500
C(17)-C(18)	1.391(2)
C(17)-H(17)	0.9500
C(18)-C(19)	1.5069(18)
C(20)-C(21)	1.393(2)
C(20)-C(25)	1.4046(19)
C(21)-C(22)	1.376(2)
C(21)-H(21)	0.9500
C(22)-C(23)	1.4058(19)
C(22)-H(22)	0.9500

C(23)-C(24)	1.390(2)
C(24)-C(25)	1.388(2)
C(24)-H(24)	0.9500
C(25)-H(25)	0.9500
C(26)-C(27)	1.396(2)
C(26)-C(31)	1.401(2)
C(27)-C(28)	1.389(2)
C(27)-H(27)	0.9500
C(28)-C(29)	1.384(3)
C(28)-H(28)	0.9500
C(29)-C(30)	1.391(3)
C(29)-H(29)	0.9500
C(30)-C(31)	1.383(2)
C(30)-H(30)	0.9500
C(31)-H(31)	0.9500
C(32)-C(37)	1.388(2)
C(32)-C(33)	1.402(2)
C(33)-C(34)	1.381(2)
C(33)-H(33)	0.9500
C(34)-C(35)	1.386(2)
C(34)-H(34)	0.9500
C(35)-C(36)	1.387(2)
C(35)-H(35)	0.9500
C(36)-C(37)	1.386(2)
C(36)-H(36)	0.9500
C(37)-H(37)	0.9500
C(38)-C(43)	1.385(2)
C(38)-C(39)	1.388(2)
C(39)-C(40)	1.390(2)
C(39)-H(39)	0.9500
C(40)-C(41)	1.376(3)
C(40)-H(40)	0.9500
C(41)-C(42)	1.373(3)
C(41)-H(41)	0.9500
C(42)-C(43)	1.393(2)
C(42)-H(42)	0.9500
C(43)-H(43)	0.9500
O(3A)-C(44A)	1.388(4)
O(3A)-H(3A)	0.8400
C(44A)-C(45A)	1.506(5)
C(44A)-H(44A)	0.9900
C(44A)-H(44B)	0.9900

C(45A)-H(45A)	0.9800
C(45A)-H(45B)	0.9800
C(45A)-H(45C)	0.9800
O(3B)-C(44B)	1.388(10)
O(3B)-H(3B)	0.8400
C(44B)-C(45B)	1.469(8)
C(44B)-H(44C)	0.9900
C(44B)-H(44D)	0.9900
C(45B)-H(45D)	0.9800
C(45B)-H(45E)	0.9800
C(45B)-H(45F)	0.9800

O(1)-P(1)-C(7)	107.29(6)
O(1)-P(1)-C(1)	107.43(6)
C(7)-P(1)-C(1)	113.50(7)
O(1)-P(1)-C(13)	107.81(6)
C(7)-P(1)-C(13)	112.21(7)
C(1)-P(1)-C(13)	108.34(6)
C(23)-P(2)-C(38)	110.74(7)
C(23)-P(2)-C(32)	106.27(7)
C(38)-P(2)-C(32)	112.79(7)
C(23)-P(2)-C(26)	108.82(7)
C(38)-P(2)-C(26)	107.32(6)
C(32)-P(2)-C(26)	110.88(7)
N(2)-N(1)-C(19)	111.17(12)
N(3)-N(2)-N(1)	111.56(12)
N(2)-N(3)-C(20)	111.43(12)
C(6)-C(1)-C(2)	118.75(14)
C(6)-C(1)-P(1)	126.78(12)
C(2)-C(1)-P(1)	114.41(11)
C(3)-C(2)-C(1)	120.67(15)
C(3)-C(2)-H(2)	119.7
C(1)-C(2)-H(2)	119.7
C(2)-C(3)-C(4)	120.17(16)
C(2)-C(3)-H(3)	119.9
C(4)-C(3)-H(3)	119.9
C(5)-C(4)-C(3)	119.55(15)
C(5)-C(4)-H(4)	120.2
C(3)-C(4)-H(4)	120.2
C(4)-C(5)-C(6)	120.76(15)
C(4)-C(5)-H(5)	119.6
C(6)-C(5)-H(5)	119.6

C(5)-C(6)-C(1)	120.10(15)
C(5)-C(6)-H(6)	119.9
C(1)-C(6)-H(6)	119.9
C(12)-C(7)-C(8)	119.01(15)
C(12)-C(7)-P(1)	120.97(12)
C(8)-C(7)-P(1)	118.99(12)
C(9)-C(8)-C(7)	120.18(16)
C(9)-C(8)-H(8)	119.9
C(7)-C(8)-H(8)	119.9
C(10)-C(9)-C(8)	120.48(16)
C(10)-C(9)-H(9)	119.8
C(8)-C(9)-H(9)	119.8
C(9)-C(10)-C(11)	119.83(16)
C(9)-C(10)-H(10)	120.1
C(11)-C(10)-H(10)	120.1
C(10)-C(11)-C(12)	120.03(17)
C(10)-C(11)-H(11)	120.0
C(12)-C(11)-H(11)	120.0
C(11)-C(12)-C(7)	120.45(15)
C(11)-C(12)-H(12)	119.8
C(7)-C(12)-H(12)	119.8
C(14)-C(13)-C(18)	118.64(14)
C(14)-C(13)-P(1)	113.26(11)
C(18)-C(13)-P(1)	128.05(11)
C(15)-C(14)-C(13)	121.41(14)
C(15)-C(14)-H(14)	119.3
C(13)-C(14)-H(14)	119.3
C(16)-C(15)-C(14)	119.61(13)
C(16)-C(15)-H(15)	120.2
C(14)-C(15)-H(15)	120.2
C(15)-C(16)-C(17)	119.94(15)
C(15)-C(16)-H(16)	120.0
C(17)-C(16)-H(16)	120.0
C(18)-C(17)-C(16)	121.11(14)
C(18)-C(17)-H(17)	119.4
C(16)-C(17)-H(17)	119.4
C(17)-C(18)-C(13)	119.28(13)
C(17)-C(18)-C(19)	120.41(13)
C(13)-C(18)-C(19)	120.32(13)
O(2)-C(19)-N(1)	128.56(13)
O(2)-C(19)-C(18)	118.34(12)
N(1)-C(19)-C(18)	113.10(12)

C(21)-C(20)-C(25)	118.99(13)
C(21)-C(20)-N(3)	123.87(12)
C(25)-C(20)-N(3)	117.15(13)
C(22)-C(21)-C(20)	120.19(13)
C(22)-C(21)-H(21)	119.9
C(20)-C(21)-H(21)	119.9
C(21)-C(22)-C(23)	120.66(14)
C(21)-C(22)-H(22)	119.7
C(23)-C(22)-H(22)	119.7
C(24)-C(23)-C(22)	119.47(13)
C(24)-C(23)-P(2)	123.26(10)
C(22)-C(23)-P(2)	117.11(11)
C(25)-C(24)-C(23)	119.62(13)
C(25)-C(24)-H(24)	120.2
C(23)-C(24)-H(24)	120.2
C(24)-C(25)-C(20)	120.78(14)
C(24)-C(25)-H(25)	119.6
C(20)-C(25)-H(25)	119.6
C(27)-C(26)-C(31)	119.69(14)
C(27)-C(26)-P(2)	120.59(11)
C(31)-C(26)-P(2)	119.72(11)
C(28)-C(27)-C(26)	119.92(15)
C(28)-C(27)-H(27)	120.0
C(26)-C(27)-H(27)	120.0
C(29)-C(28)-C(27)	120.18(16)
C(29)-C(28)-H(28)	119.9
C(27)-C(28)-H(28)	119.9
C(28)-C(29)-C(30)	120.13(16)
C(28)-C(29)-H(29)	119.9
C(30)-C(29)-H(29)	119.9
C(31)-C(30)-C(29)	120.26(16)
C(31)-C(30)-H(30)	119.9
C(29)-C(30)-H(30)	119.9
C(30)-C(31)-C(26)	119.81(15)
C(30)-C(31)-H(31)	120.1
C(26)-C(31)-H(31)	120.1
C(37)-C(32)-C(33)	120.33(13)
C(37)-C(32)-P(2)	121.91(11)
C(33)-C(32)-P(2)	117.68(11)
C(34)-C(33)-C(32)	119.76(15)
C(34)-C(33)-H(33)	120.1
C(32)-C(33)-H(33)	120.1

C(33)-C(34)-C(35)	119.99(15)
C(33)-C(34)-H(34)	120.0
C(35)-C(34)-H(34)	120.0
C(34)-C(35)-C(36)	120.08(15)
C(34)-C(35)-H(35)	120.0
C(36)-C(35)-H(35)	120.0
C(37)-C(36)-C(35)	120.65(15)
C(37)-C(36)-H(36)	119.7
C(35)-C(36)-H(36)	119.7
C(36)-C(37)-C(32)	119.13(14)
C(36)-C(37)-H(37)	120.4
C(32)-C(37)-H(37)	120.4
C(43)-C(38)-C(39)	119.95(13)
C(43)-C(38)-P(2)	121.93(11)
C(39)-C(38)-P(2)	118.10(12)
C(38)-C(39)-C(40)	119.88(16)
C(38)-C(39)-H(39)	120.1
C(40)-C(39)-H(39)	120.1
C(41)-C(40)-C(39)	119.95(16)
C(41)-C(40)-H(40)	120.0
C(39)-C(40)-H(40)	120.0
C(42)-C(41)-C(40)	120.35(15)
C(42)-C(41)-H(41)	119.8
C(40)-C(41)-H(41)	119.8
C(41)-C(42)-C(43)	120.34(17)
C(41)-C(42)-H(42)	119.8
C(43)-C(42)-H(42)	119.8
C(38)-C(43)-C(42)	119.47(15)
C(38)-C(43)-H(43)	120.3
C(42)-C(43)-H(43)	120.3
C(44A)-O(3A)-H(3A)	109.5
O(3A)-C(44A)-C(45A)	111.3(3)
O(3A)-C(44A)-H(44A)	109.4
C(45A)-C(44A)-H(44A)	109.4
O(3A)-C(44A)-H(44B)	109.4
C(45A)-C(44A)-H(44B)	109.4
H(44A)-C(44A)-H(44B)	108.0
C(44A)-C(45A)-H(45A)	109.5
C(44A)-C(45A)-H(45B)	109.5
H(45A)-C(45A)-H(45B)	109.5
C(44A)-C(45A)-H(45C)	109.5
H(45A)-C(45A)-H(45C)	109.5

H(45B)-C(45A)-H(45C)	109.5
C(44B)-O(3B)-H(3B)	109.5
O(3B)-C(44B)-C(45B)	114.6(9)
O(3B)-C(44B)-H(44C)	108.6
C(45B)-C(44B)-H(44C)	108.6
O(3B)-C(44B)-H(44D)	108.6
C(45B)-C(44B)-H(44D)	108.6
H(44C)-C(44B)-H(44D)	107.6
C(44B)-C(45B)-H(45D)	109.5
C(44B)-C(45B)-H(45E)	109.5
H(45D)-C(45B)-H(45E)	109.5
C(44B)-C(45B)-H(45F)	109.5
H(45D)-C(45B)-H(45F)	109.5
H(45E)-C(45B)-H(45F)	109.5

Symmetry transformations used to generate equivalent atoms:

Anisotropic displacement parameters ($Å^2 x\ 10^3$) for **14**. The anisotropic displacement factor exponent takes the form: $-2\pi^2[\ h^2 a^{*2} U^{11} + ... + 2\ h\ k\ a^*\ b^*\ U^{12}\ ]$

	U^{11}	U^{22}	U^{33}	U^{23}	U^{13}	U^{12}
P(1)	32(1)	28(1)	20(1)	0(1)	11(1)	-2(1)
P(2)	28(1)	27(1)	17(1)	3(1)	8(1)	1(1)
O(1)	42(1)	40(1)	24(1)	1(1)	15(1)	-6(1)
O(2)	36(1)	29(1)	28(1)	3(1)	14(1)	3(1)
N(1)	34(1)	30(1)	24(1)	2(1)	13(1)	4(1)
N(2)	32(1)	27(1)	20(1)	-1(1)	9(1)	-2(1)
N(3)	43(1)	30(1)	27(1)	4(1)	17(1)	4(1)
C(1)	37(1)	26(1)	22(1)	2(1)	10(1)	-3(1)
C(2)	36(1)	34(1)	35(1)	-1(1)	10(1)	2(1)
C(3)	37(1)	37(1)	43(1)	-3(1)	1(1)	-2(1)
C(4)	48(1)	30(1)	30(1)	-2(1)	3(1)	-3(1)
C(5)	48(1)	33(1)	30(1)	-4(1)	16(1)	-3(1)
C(6)	37(1)	34(1)	29(1)	-2(1)	14(1)	-5(1)
C(7)	35(1)	34(1)	20(1)	3(1)	10(1)	2(1)
C(8)	48(1)	34(1)	32(1)	5(1)	11(1)	5(1)
C(9)	48(1)	46(1)	40(1)	12(1)	11(1)	16(1)
C(10)	37(1)	59(1)	34(1)	8(1)	4(1)	8(1)
C(11)	38(1)	46(1)	35(1)	1(1)	5(1)	-2(1)
C(12)	36(1)	34(1)	30(1)	2(1)	6(1)	3(1)
C(13)	28(1)	30(1)	22(1)	-4(1)	7(1)	-2(1)
C(14)	31(1)	37(1)	26(1)	-4(1)	12(1)	-3(1)
C(15)	30(1)	41(1)	33(1)	-6(1)	12(1)	3(1)
C(16)	35(1)	36(1)	35(1)	-1(1)	11(1)	8(1)
C(17)	34(1)	33(1)	27(1)	1(1)	9(1)	2(1)
C(18)	26(1)	31(1)	20(1)	-4(1)	5(1)	-2(1)
C(19)	27(1)	28(1)	19(1)	-3(1)	6(1)	-2(1)
C(20)	35(1)	27(1)	22(1)	-2(1)	12(1)	-3(1)
C(21)	35(1)	38(1)	21(1)	6(1)	10(1)	1(1)
C(22)	34(1)	41(1)	25(1)	9(1)	12(1)	6(1)
C(23)	31(1)	31(1)	20(1)	3(1)	10(1)	1(1)
C(24)	39(1)	28(1)	20(1)	3(1)	11(1)	1(1)
C(25)	41(1)	26(1)	26(1)	3(1)	12(1)	5(1)
C(26)	30(1)	30(1)	20(1)	5(1)	5(1)	0(1)
C(27)	30(1)	37(1)	30(1)	6(1)	7(1)	1(1)
C(28)	34(1)	45(1)	42(1)	8(1)	4(1)	-9(1)
C(29)	53(1)	40(1)	36(1)	-2(1)	2(1)	-14(1)
C(30)	55(1)	39(1)	28(1)	-5(1)	12(1)	-6(1)

C(31)	38(1)	38(1)	22(1)	0(1)	11(1)	-4(1)
C(32)	29(1)	29(1)	19(1)	3(1)	7(1)	-1(1)
C(33)	41(1)	30(1)	26(1)	-2(1)	7(1)	1(1)
C(34)	41(1)	43(1)	24(1)	-6(1)	4(1)	-5(1)
C(35)	32(1)	50(1)	26(1)	3(1)	2(1)	1(1)
C(36)	34(1)	38(1)	32(1)	5(1)	7(1)	5(1)
C(37)	32(1)	29(1)	24(1)	1(1)	9(1)	-1(1)
C(38)	34(1)	27(1)	18(1)	3(1)	10(1)	3(1)
C(39)	43(1)	44(1)	28(1)	9(1)	5(1)	-7(1)
C(40)	60(1)	44(1)	24(1)	10(1)	2(1)	-4(1)
C(41)	73(1)	33(1)	25(1)	6(1)	13(1)	-9(1)
C(42)	68(1)	43(1)	35(1)	6(1)	9(1)	-25(1)
C(43)	50(1)	39(1)	27(1)	3(1)	5(1)	-11(1)
O(3A)	68(2)	106(2)	95(2)	-59(2)	56(2)	-44(2)
C(44A)	45(2)	61(2)	49(2)	-14(2)	24(1)	-15(2)
C(45A)	55(2)	62(2)	89(3)	0(2)	15(2)	0(2)
O(3B)	72(4)	77(4)	59(3)	6(3)	25(3)	-27(3)
C(44B)	55(4)	69(4)	69(4)	-6(3)	4(3)	-18(3)
C(45B)	59(5)	110(8)	51(4)	17(5)	10(4)	-14(6)

Hydrogen coordinates (x 10^4) and isotropic displacement parameters (Å^{2}x 10^3) for **14**.

	x	y	z	U(eq)
H(2)	11516	10491	3579	42
H(3)	12218	12026	4116	48
H(4)	11016	13126	4507	44
H(5)	9117	12657	4364	43
H(6)	8402	11103	3834	39
H(8)	7813	11505	3019	45
H(9)	5997	11532	2641	53
H(10)	5116	9519	2397	52
H(11)	6030	7450	2553	48
H(12)	7834	7406	2944	40
H(14)	11096	7917	2952	37
H(15)	11987	5847	3115	40
H(16)	11443	4449	3640	42
H(17)	10033	5145	4008	37
H(21)	5938	7784	4499	37
H(22)	4646	8555	4905	39
H(24)	5838	5903	5853	34
H(25)	7146	5142	5446	36
H(27)	6265	9568	5691	38
H(28)	7091	11548	6002	49
H(29)	6177	12853	6451	52
H(30)	4429	12190	6589	48
H(31)	3617	10182	6299	39
H(33)	2857	6580	5111	39
H(34)	1293	7009	4594	44
H(35)	493	9166	4539	43
H(36)	1187	10854	5027	41
H(37)	2741	10439	5553	33
H(39)	5426	7681	6566	46
H(40)	5223	6265	7142	52
H(41)	3653	4903	7105	52
H(42)	2329	4853	6487	59
H(43)	2573	6161	5891	46
H(3A)	11276	10443	2585	127
H(44A)	13330	11393	2693	60
H(44B)	12745	10819	3073	60

H(45A)	12648	13193	3061	103
H(45B)	11416	12579	2954	103
H(45C)	12009	13155	2576	103
H(3B)	11038	10666	2468	102
H(44C)	11095	12750	2698	78
H(44D)	11843	13081	2342	78
H(45D)	12929	12893	3011	110
H(45E)	13258	11743	2698	110
H(45F)	12506	11370	3051	110

Torsion angles [°] for **14**.

C(19)-N(1)-N(2)-N(3)	-178.64(12)
N(1)-N(2)-N(3)-C(20)	-179.91(12)
O(1)-P(1)-C(1)-C(6)	130.77(13)
C(7)-P(1)-C(1)-C(6)	12.33(15)
C(13)-P(1)-C(1)-C(6)	-113.00(14)
O(1)-P(1)-C(1)-C(2)	-46.29(13)
C(7)-P(1)-C(1)-C(2)	-164.73(11)
C(13)-P(1)-C(1)-C(2)	69.94(12)
C(6)-C(1)-C(2)-C(3)	0.3(2)
P(1)-C(1)-C(2)-C(3)	177.60(13)
C(1)-C(2)-C(3)-C(4)	-0.6(3)
C(2)-C(3)-C(4)-C(5)	0.5(3)
C(3)-C(4)-C(5)-C(6)	-0.1(2)
C(4)-C(5)-C(6)-C(1)	-0.2(2)
C(2)-C(1)-C(6)-C(5)	0.1(2)
P(1)-C(1)-C(6)-C(5)	-176.84(12)
O(1)-P(1)-C(7)-C(12)	98.41(12)
C(1)-P(1)-C(7)-C(12)	-143.07(11)
C(13)-P(1)-C(7)-C(12)	-19.83(14)
O(1)-P(1)-C(7)-C(8)	-69.83(13)
C(1)-P(1)-C(7)-C(8)	48.69(13)
C(13)-P(1)-C(7)-C(8)	171.93(11)
C(12)-C(7)-C(8)-C(9)	-0.7(2)
P(1)-C(7)-C(8)-C(9)	167.80(12)
C(7)-C(8)-C(9)-C(10)	-0.7(3)
C(8)-C(9)-C(10)-C(11)	1.3(3)
C(9)-C(10)-C(11)-C(12)	-0.5(3)
C(10)-C(11)-C(12)-C(7)	-0.8(2)
C(8)-C(7)-C(12)-C(11)	1.4(2)
P(1)-C(7)-C(12)-C(11)	-166.83(12)
O(1)-P(1)-C(13)-C(14)	4.41(13)
C(7)-P(1)-C(13)-C(14)	122.34(11)
C(1)-P(1)-C(13)-C(14)	-111.57(11)
O(1)-P(1)-C(13)-C(18)	-178.11(12)
C(7)-P(1)-C(13)-C(18)	-60.19(14)
C(1)-P(1)-C(13)-C(18)	65.91(14)
C(18)-C(13)-C(14)-C(15)	0.4(2)
P(1)-C(13)-C(14)-C(15)	178.16(12)
C(13)-C(14)-C(15)-C(16)	0.4(2)
C(14)-C(15)-C(16)-C(17)	-0.6(2)

C(15)-C(16)-C(17)-C(18)	0.1(2)
C(16)-C(17)-C(18)-C(13)	0.7(2)
C(16)-C(17)-C(18)-C(19)	-178.93(14)
C(14)-C(13)-C(18)-C(17)	-1.0(2)
P(1)-C(13)-C(18)-C(17)	-178.32(11)
C(14)-C(13)-C(18)-C(19)	178.70(13)
P(1)-C(13)-C(18)-C(19)	1.3(2)
N(2)-N(1)-C(19)-O(2)	2.1(2)
N(2)-N(1)-C(19)-C(18)	-177.83(11)
C(17)-C(18)-C(19)-O(2)	179.08(13)
C(13)-C(18)-C(19)-O(2)	-0.6(2)
C(17)-C(18)-C(19)-N(1)	-1.00(19)
C(13)-C(18)-C(19)-N(1)	179.35(12)
N(2)-N(3)-C(20)-C(21)	19.3(2)
N(2)-N(3)-C(20)-C(25)	-160.99(13)
C(25)-C(20)-C(21)-C(22)	5.4(2)
N(3)-C(20)-C(21)-C(22)	-174.94(15)
C(20)-C(21)-C(22)-C(23)	-1.3(2)
C(21)-C(22)-C(23)-C(24)	-3.1(2)
C(21)-C(22)-C(23)-P(2)	172.58(13)
C(38)-P(2)-C(23)-C(24)	-20.56(15)
C(32)-P(2)-C(23)-C(24)	-143.38(13)
C(26)-P(2)-C(23)-C(24)	97.18(14)
C(38)-P(2)-C(23)-C(22)	163.97(12)
C(32)-P(2)-C(23)-C(22)	41.15(14)
C(26)-P(2)-C(23)-C(22)	-78.30(13)
C(22)-C(23)-C(24)-C(25)	3.3(2)
P(2)-C(23)-C(24)-C(25)	-172.08(12)
C(23)-C(24)-C(25)-C(20)	0.8(2)
C(21)-C(20)-C(25)-C(24)	-5.2(2)
N(3)-C(20)-C(25)-C(24)	175.14(14)
C(23)-P(2)-C(26)-C(27)	1.67(14)
C(38)-P(2)-C(26)-C(27)	121.55(12)
C(32)-P(2)-C(26)-C(27)	-114.87(12)
C(23)-P(2)-C(26)-C(31)	-177.89(11)
C(38)-P(2)-C(26)-C(31)	-58.00(13)
C(32)-P(2)-C(26)-C(31)	65.58(13)
C(31)-C(26)-C(27)-C(28)	0.7(2)
P(2)-C(26)-C(27)-C(28)	-178.89(12)
C(26)-C(27)-C(28)-C(29)	-0.8(2)
C(27)-C(28)-C(29)-C(30)	0.0(3)
C(28)-C(29)-C(30)-C(31)	1.1(3)

C(29)-C(30)-C(31)-C(26)	-1.3(2)
C(27)-C(26)-C(31)-C(30)	0.4(2)
P(2)-C(26)-C(31)-C(30)	179.95(12)
C(23)-P(2)-C(32)-C(37)	-130.82(11)
C(38)-P(2)-C(32)-C(37)	107.66(12)
C(26)-P(2)-C(32)-C(37)	-12.73(13)
C(23)-P(2)-C(32)-C(33)	45.96(13)
C(38)-P(2)-C(32)-C(33)	-75.56(12)
C(26)-P(2)-C(32)-C(33)	164.05(11)
C(37)-C(32)-C(33)-C(34)	1.7(2)
P(2)-C(32)-C(33)-C(34)	-175.18(12)
C(32)-C(33)-C(34)-C(35)	0.4(2)
C(33)-C(34)-C(35)-C(36)	-2.1(2)
C(34)-C(35)-C(36)-C(37)	1.7(2)
C(35)-C(36)-C(37)-C(32)	0.4(2)
C(33)-C(32)-C(37)-C(36)	-2.0(2)
P(2)-C(32)-C(37)-C(36)	174.66(11)
C(23)-P(2)-C(38)-C(43)	-95.74(14)
C(32)-P(2)-C(38)-C(43)	23.21(15)
C(26)-P(2)-C(38)-C(43)	145.61(13)
C(23)-P(2)-C(38)-C(39)	83.14(14)
C(32)-P(2)-C(38)-C(39)	-157.91(12)
C(26)-P(2)-C(38)-C(39)	-35.51(14)
C(43)-C(38)-C(39)-C(40)	-0.1(3)
P(2)-C(38)-C(39)-C(40)	-178.98(14)
C(38)-C(39)-C(40)-C(41)	-1.9(3)
C(39)-C(40)-C(41)-C(42)	1.8(3)
C(40)-C(41)-C(42)-C(43)	0.3(3)
C(39)-C(38)-C(43)-C(42)	2.2(3)
P(2)-C(38)-C(43)-C(42)	-178.97(15)
C(41)-C(42)-C(43)-C(38)	-2.3(3)

1.4 Report for compound 17

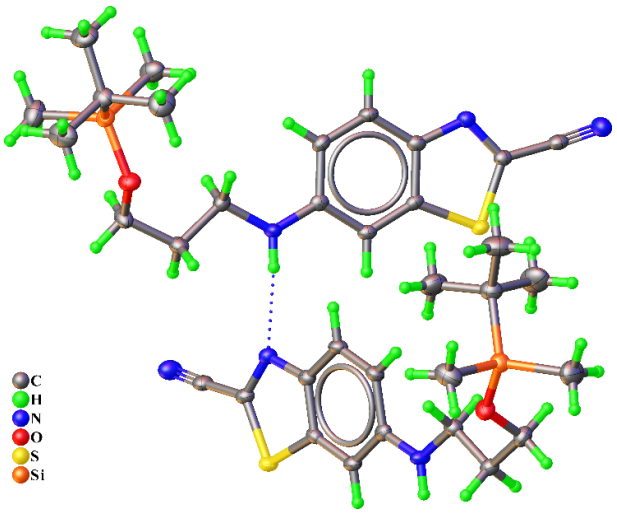

Experimental. Single yellow prism-shaped crystals of **17** (AB-161) were obtained by recrystallisation from methanol at 25C. A suitable crystal of 0.46×0.24×0.13 mm^3 was selected and mounted on a suitable support on a Bruker P4 diffractometer. The crystal was kept at a steady T = 120(2) K during data collection. The structure was solved with the **ShelXT** [1, 2] structure solution program using the dual solution method and by using **Olex2** [3] as the graphical interface. The model was refined with version 2018/3 of **ShelXL** [1, 2] using full matrix least squares on $|F|^2$ minimisation.

Crystal Data. $C_{17}H_{25}N_3OSSi$, M_r = 347.55, monoclinic, $P2_1/c$ (No. 14), a = 12.0200(10) Å, b = 6.7762(14) Å, c = 46.566(7) Å, β = 96.539(9)°, $\alpha = \gamma$ = 90°, V = 3768.1(10) $Å^3$, T = 120(2) K, Z = 8, Z' = 2, μ(MoKα) = 0.243, 28983 reflections measured, 5943 unique (R_{int} = 0.0431) which were used in all calculations. The final wR_2 was 0.1122 (all data) and R_1 was 0.0498 (I > 2(I)).

Compound	**17**
Formula	$C_{17}H_{25}N_3OSSi$
$D_{calc.}$/ g cm^{-3}	1.225
μ/mm^{-1}	0.243
Formula Weight	347.55
Colour	yellow
Shape	prism
Size/mm^3	0.46×0.24×0.13
T/K	120(2)
Crystal System	monoclinic
Space Group	$P2_1/c$
a/Å	12.0200(10)
b/Å	6.7762(14)
c/Å	46.566(7)
α/°	90
β/°	96.539(9)
γ/°	90
V/$Å^3$	3768.1(10)
Z	8
Z'	2
Wavelength/Å	0.71073
Radiation type	MoKα
Θ_{min}/°	1.705
Θ_{max}/°	24.406
Measured Refl.	28983
Independent Refl.	5943
Reflections with I > 2(I)	5142
R_{int}	0.0431
Parameters	425
Restraints	0
Largest Peak/e $Å^{-3}$	0.347
Deepest Hole/e $Å^{-3}$	-0.310
GooF	1.188
wR_2 (all data)	0.1122
wR_2	0.1075
R_1 (all data)	0.0594
R_1	0.0498

A yellow prism-shaped crystal with dimensions of 0.46×0.24×0.13 mm^3 was mounted on a suitable support. Data were collected using a Bruker P4 diffractometer operating at T = 120(2) K.

Data were measured using ω scans using MoKα radiation. The total number of runs and images was based on the strategy calculation from the program **XS** [4]. The maximum resolution achieved was Θ = 24.406° (0.86 Å).

The diffraction pattern was indexed. The total number of runs and images was based on the strategy calculation from the program **XS** [4] and the unit cell was refined using EvalCCD [5] on 126 reflections, 0% of the observed reflections.

Data reduction, scaling and absorption corrections were performed using EvalCCD [5]. The final completeness is 96.20 % out to 24.406° in Θ. A multi-scan absorption correction was performed using **SADABS**-2008/1 (Bruker, 2008) was used for absorption correction[6]. wR_2(int) was 0.0936 before and 0.0604 after correction. The Ratio of minimum to maximum transmission is 0.8425. The $\lambda/2$ correction factor is 0.0015. The absorption coefficient μ of this material is 0.243 mm^{-1} at this wavelength (λ = 0.711Å) and the minimum and maximum transmissions are 0.628 and 0.745.

The structure was solved and the space group $P2_1/c$ (# 14) determined by the **ShelXT** [1, 2] structure solution program using dual and refined by full matrix least squares on $|F|^2$ using version 2018/3 of **ShelXL** [1, 2]. All non-hydrogen atoms were refined anisotropically. Hydrogen atom positions were calculated geometrically and refined using the riding model.

The value of Z' is 2. This means that there are two independent molecules in the asymmetric unit.

Fractional Atomic Coordinates (×10^4) and Equivalent Isotropic Displacement Parameters (Å^2×10^3) for **17**. U_{eq} is defined as 1/3 of the trace of the orthogonalised U_{ij}.

Atom	x	y	z	U_{eq}
S1	6607.9(5)	3715.8(10)	2761.2(2)	19.83(18)
Si1	7548.7(7)	15096.4(12)	4209.0(2)	23.5(2)
O1	6329.2(16)	14333(3)	4046.9(4)	25.6(5)
N1	8827(2)	-269(4)	2651.5(5)	30.0(6)
N2	8646.2(18)	4024(3)	3024.8(4)	20.3(5)
N3	6019.0(18)	10292(3)	3318.3(5)	21.4(5)
C1	8426(2)	1121(4)	2736.6(6)	22.4(6)
C2	7991(2)	2899(4)	2849.4(5)	19.6(6)
C3	6931(2)	5785(4)	2978.7(5)	17.8(6)
C4	8063(2)	5650(4)	3103.3(5)	19.3(6)
C5	8501(2)	7136(4)	3292.6(5)	20.9(6)
C6	7832(2)	8673(4)	3358.6(5)	20.4(6)
C7	6688(2)	8801(4)	3238.0(5)	18.6(6)
C8	6243(2)	7337(4)	3041.6(5)	19.0(6)
C9	6426(2)	11874(4)	3515.1(6)	21.3(6)
C10	5471(2)	13235(4)	3574.8(6)	23.4(6)
C11	5871(3)	14983(4)	3763.1(6)	27.8(7)
C12	8699(3)	13789(5)	4047.0(6)	36.1(8)
C13	7716(3)	17805(5)	4156.7(7)	42.2(9)
C14	7532(2)	14476(4)	4604.6(6)	26.9(7)
C15	6600(3)	15640(6)	4729.2(6)	42.7(9)
C16	7333(3)	12257(5)	4638.6(7)	42.4(9)
C17	8674(3)	15032(6)	4771.8(6)	41.9(8)
S2	1641.2(5)	10901.4(10)	2742.5(2)	20.33(18)
Si2	1884.7(7)	-297.5(12)	4329.4(2)	24.3(2)
O2	1212.1(16)	668(3)	4032.7(4)	27.2(5)
N4	3833(2)	14948(4)	2646.7(5)	31.5(6)
N5	3645.7(18)	10683(3)	3026.3(4)	20.1(5)

Atom	x	y	z	U_{eq}
N6	1052.8(18)	4309(3)	3295.2(5)	22.4(5)
C18	3440(2)	13554(4)	2730.1(5)	22.0(6)
C19	3003(2)	11760(4)	2842.2(5)	19.9(6)
C20	1956(2)	8858(4)	2967.2(5)	18.4(6)
C21	3065(2)	9039(4)	3103.8(5)	18.6(6)
C22	3486(2)	7611(4)	3304.4(5)	21.6(6)
C23	2816(2)	6062(4)	3365.6(5)	20.2(6)
C24	1700(2)	5858(4)	3226.5(5)	20.4(6)
C25	1276(2)	7284(4)	3023.2(5)	19.8(6)
C26	1454(2)	2782(4)	3501.1(5)	21.6(6)
C27	536(2)	1280(4)	3535.8(5)	21.3(6)
C28	922(2)	-275(4)	3760.7(6)	25.6(6)
C29	1294(3)	1000(5)	4631.7(6)	39.6(8)
C30	1598(3)	-2998(5)	4342.5(7)	41.8(8)
C31	3438(2)	200(5)	4338.9(6)	29.5(7)
C32	4060(3)	-467(6)	4630.7(7)	47.4(9)
C33	3644(3)	2415(5)	4301.1(7)	42.1(8)
C34	3918(3)	-923(6)	4093.3(8)	49.2(10)

Anisotropic Displacement Parameters ($\times 10^4$) **17**. The anisotropic displacement factor exponent takes the form: $-2\pi^2[h^2a^{*2} \times U_{11} + \ldots + 2hka^* \times b^* \times U_{12}]$

Atom	U_{11}	U_{22}	U_{33}	U_{23}	U_{13}	U_{12}
S1	16.4(4)	21.9(4)	20.5(3)	-2.7(3)	-1.0(3)	-0.9(3)
Si1	25.9(4)	24.3(4)	19.8(4)	-3.5(3)	0.2(3)	0.6(3)
O1	25.5(11)	32.9(12)	17.6(9)	-0.6(8)	-1.1(8)	0.6(9)
N1	26.0(14)	30.8(15)	32.4(13)	-5.2(12)	-0.7(11)	4.4(12)
N2	17.5(12)	22.7(13)	20.5(11)	0.2(10)	0.9(9)	0.6(10)
N3	14.1(12)	23.2(13)	26.1(11)	-4.8(10)	-1.6(9)	2.0(10)
C1	17.4(15)	27.1(17)	21.6(13)	1.7(12)	-2.9(11)	-2.0(13)
C2	17.6(14)	21.3(15)	19.1(13)	2.4(11)	-0.4(11)	-0.9(12)
C3	16.3(14)	21.1(14)	15.8(12)	1.6(11)	0.6(10)	-5.2(11)
C4	16.4(14)	22.7(15)	19.0(13)	2.3(11)	1.9(11)	-0.8(12)
C5	15.4(14)	26.0(15)	20.7(13)	0.7(11)	-1.1(11)	-2.0(12)
C6	19.5(15)	22.8(15)	18.4(13)	-1.8(11)	0.7(11)	-4.1(12)
C7	17.8(14)	20.9(15)	17.2(12)	3.7(11)	2.8(10)	-2.5(12)
C8	15.5(14)	23.4(15)	17.7(13)	1.9(11)	-0.1(11)	-1.3(12)
C9	21.2(15)	20.3(15)	21.7(13)	-0.1(11)	-0.3(11)	-2.0(12)
C10	20.9(15)	27.9(16)	20.2(13)	-0.4(12)	-2.6(11)	4.7(12)
C11	32.6(17)	26.2(16)	22.6(14)	-3.0(12)	-5.4(12)	9.0(14)
C12	28.3(17)	47(2)	33.3(16)	-8.9(15)	5.4(13)	-1.6(15)
C13	60(2)	31.2(19)	33.5(17)	-2.2(14)	-2.0(16)	-5.3(17)
C14	28.6(16)	31.3(17)	20.0(13)	-2.6(12)	-0.5(12)	2.3(13)
C15	41(2)	61(2)	27.3(16)	-7.6(16)	8.1(14)	9.6(18)
C16	53(2)	44(2)	29.1(16)	7.7(15)	-0.6(15)	-1.3(17)
C17	40(2)	54(2)	28.4(16)	-7.1(16)	-7.9(14)	0.9(17)
S2	16.4(4)	23.1(4)	20.6(3)	1.5(3)	-1.4(3)	0.2(3)
Si2	25.4(4)	25.4(4)	21.5(4)	1.2(3)	0.9(3)	1.9(3)
O2	32.1(12)	26.8(11)	21.5(10)	-2.3(8)	-2.4(8)	1.9(9)
N4	26.1(14)	33.5(16)	34.0(13)	5.8(12)	-0.7(11)	-1.4(12)
N5	17.0(12)	22.6(13)	20.5(11)	-0.7(10)	0.9(9)	-0.9(10)
N6	15.4(12)	24.9(13)	25.4(12)	3.5(10)	-3.6(9)	-1.3(10)
C18	17.6(15)	27.7(17)	19.5(13)	0.6(12)	-3.1(11)	0.1(13)
C19	16.3(14)	24.9(15)	18.2(13)	-2.0(11)	0.4(11)	-0.6(12)
C20	17.3(14)	20.9(15)	16.6(12)	-1.8(11)	0.5(10)	4.9(12)
C21	17.0(14)	22.1(15)	16.4(12)	-2.8(11)	1.4(10)	0.9(12)
C22	15.5(14)	25.8(16)	22.6(13)	-1.4(12)	-2.5(11)	1.5(12)
C23	17.1(14)	22.4(15)	20.5(13)	1.3(11)	-0.5(11)	3.6(12)
C24	18.6(14)	21.9(15)	21.0(13)	-5.6(11)	3.5(11)	0.5(12)
C25	15.7(14)	24.5(15)	18.6(13)	-3.5(11)	-0.4(11)	0.9(12)
C26	20.1(15)	24.3(15)	19.9(13)	-0.9(11)	-0.2(11)	1.7(12)
C27	18.9(15)	24.4(15)	20.5(13)	-2.0(11)	1.6(11)	-1.4(12)

Atom	U_{11}	U_{22}	U_{33}	U_{23}	U_{13}	U_{12}
C28	28.9(16)	23.0(16)	24.1(14)	-2.6(12)	-0.1(12)	-4.0(13)
C29	37.8(19)	52(2)	29.2(16)	0.8(15)	4.6(14)	11.8(17)
C30	44(2)	32.6(19)	48(2)	8.2(16)	1.2(16)	-3.1(16)
C31	26.2(16)	34.5(18)	27.4(15)	-0.3(13)	1.2(12)	1.4(14)
C32	30.7(19)	66(3)	43.5(19)	9.9(18)	-5.8(15)	1.1(18)
C33	31.0(19)	45(2)	49(2)	4.5(17)	-1.9(15)	-9.0(16)
C34	33(2)	65(3)	52(2)	-14.6(19)	17.5(16)	0.1(18)

Bond Lengths in Å for **17**.

Atom	Atom	Length/Å
S1	C2	1.756(3)
S1	C3	1.747(3)
Si1	O1	1.654(2)
Si1	C12	1.872(3)
Si1	C13	1.865(3)
Si1	C14	1.892(3)
O1	C11	1.441(3)
N1	C1	1.149(4)
N2	C2	1.312(3)
N2	C4	1.378(3)
N3	C7	1.370(3)
N3	C9	1.458(3)
C1	C2	1.436(4)
C3	C4	1.420(4)
C3	C8	1.390(4)
C4	C5	1.401(4)
C5	C6	1.372(4)
C6	C7	1.427(4)
C7	C8	1.412(4)
C9	C10	1.522(4)
C10	C11	1.519(4)
C14	C15	1.537(4)
C14	C16	1.534(4)
C14	C17	1.545(4)

Atom	Atom	Length/Å
S2	C19	1.750(3)
S2	C20	1.751(3)
Si2	O2	1.6543(19)
Si2	C29	1.867(3)
Si2	C30	1.864(3)
Si2	C31	1.893(3)
O2	C28	1.426(3)
N4	C18	1.144(4)
N5	C19	1.309(3)
N5	C21	1.384(3)
N6	C24	1.366(4)
N6	C26	1.455(3)
C18	C19	1.445(4)
C20	C21	1.415(4)
C20	C25	1.387(4)
C21	C22	1.399(4)
C22	C23	1.372(4)
C23	C24	1.428(4)
C24	C25	1.407(4)
C26	C27	1.522(4)
C27	C28	1.520(4)
C31	C32	1.542(4)
C31	C33	1.535(5)
C31	C34	1.539(4)

Bond Angles in ° for **17**.

Atom	Atom	Atom	Angle/°
C3	S1	C2	88.58(13)
O1	Si1	C12	108.97(12)
O1	Si1	C13	110.56(14)
O1	Si1	C14	105.55(12)
C12	Si1	C14	112.17(14)
C13	Si1	C12	108.52(17)
C13	Si1	C14	111.03(14)
C11	O1	Si1	123.30(18)
C2	N2	C4	110.0(2)
C7	N3	C9	123.3(2)
N1	C1	C2	176.5(3)
N2	C2	S1	116.6(2)
N2	C2	C1	119.8(2)
C1	C2	S1	123.6(2)
C4	C3	S1	108.96(19)
C8	C3	S1	129.1(2)
C8	C3	C4	121.9(2)
N2	C4	C3	115.8(2)
N2	C4	C5	125.2(2)
C5	C4	C3	119.0(2)

Atom	Atom	Atom	Angle/°
C6	C5	C4	119.9(2)
C5	C6	C7	121.4(2)
N3	C7	C6	120.4(2)
N3	C7	C8	120.2(2)
C8	C7	C6	119.3(2)
C3	C8	C7	118.5(2)
N3	C9	C10	110.8(2)
C11	C10	C9	112.5(2)
O1	C11	C10	110.7(2)
C15	C14	Si1	110.0(2)
C15	C14	C17	109.2(3)
C16	C14	Si1	109.7(2)
C16	C14	C15	109.6(3)
C16	C14	C17	109.1(3)
C17	C14	Si1	109.2(2)
C19	S2	C20	88.40(13)
O2	Si2	C29	104.58(13)
O2	Si2	C30	109.93(13)
O2	Si2	C31	109.64(12)
C29	Si2	C31	110.94(15)

Atom	Atom	Atom	Angle/°
C30	Si2	C29	110.48(17)
C30	Si2	C31	111.08(15)
C28	O2	Si2	127.71(18)
C19	N5	C21	110.0(2)
C24	N6	C26	123.1(2)
N4	C18	C19	176.9(3)
N5	C19	S2	116.9(2)
N5	C19	C18	119.6(2)
C18	C19	S2	123.4(2)
C21	C20	S2	109.2(2)
C25	C20	S2	129.0(2)
C25	C20	C21	121.8(2)
N5	C21	C20	115.4(2)
N5	C21	C22	125.2(2)
C22	C21	C20	119.4(2)
C23	C22	C21	119.5(2)
C22	C23	C24	121.5(2)
N6	C24	C23	119.9(2)
N6	C24	C25	120.8(2)
C25	C24	C23	119.3(2)
C20	C25	C24	118.6(2)
N6	C26	C27	110.8(2)
C28	C27	C26	111.6(2)
O2	C28	C27	109.0(2)
C32	C31	Si2	110.3(2)
C33	C31	Si2	110.1(2)
C33	C31	C32	108.6(3)
C33	C31	C34	108.6(3)
C34	C31	Si2	110.3(2)
C34	C31	C32	109.0(3)

Torsion Angles in ° for **17**.

Atom	Atom	Atom	Atom	Angle/°
S1	C3	C4	N2	1.5(3)
S1	C3	C4	C5	-178.5(2)
S1	C3	C8	C7	176.6(2)
Si1	O1	C11	C10	131.6(2)
O1	Si1	C14	C15	-63.4(2)
O1	Si1	C14	C16	57.2(2)
O1	Si1	C14	C17	176.8(2)
N2	C4	C5	C6	-178.9(2)
N3	C7	C8	C3	-176.2(2)
N3	C9	C10	C11	-176.2(2)
C2	S1	C3	C4	-1.00(19)
C2	S1	C3	C8	-178.6(2)
C2	N2	C4	C3	-1.2(3)
C2	N2	C4	C5	178.8(2)
C3	S1	C2	N2	0.4(2)
C3	S1	C2	C1	-178.5(2)
C3	C4	C5	C6	1.1(4)
C4	N2	C2	S1	0.4(3)
C4	N2	C2	C1	179.3(2)
C4	C3	C8	C7	-0.7(4)
C4	C5	C6	C7	-0.1(4)
C5	C6	C7	N3	176.6(2)
C5	C6	C7	C8	-1.4(4)
C6	C7	C8	C3	1.7(4)
C7	N3	C9	C10	-176.9(2)
C8	C3	C4	N2	179.3(2)
C8	C3	C4	C5	-0.7(4)
C9	N3	C7	C6	3.4(4)
C9	N3	C7	C8	-178.7(2)
C9	C10	C11	O1	-64.7(3)
C12	Si1	O1	C11	-76.8(2)
C12	Si1	C14	C15	178.1(2)
C12	Si1	C14	C16	-61.3(3)
C12	Si1	C14	C17	58.2(3)
C13	Si1	O1	C11	42.4(2)
C13	Si1	C14	C15	56.5(3)
C13	Si1	C14	C16	177.1(2)
C13	Si1	C14	C17	-63.4(3)
C14	Si1	O1	C11	162.6(2)
S2	C20	C21	N5	-2.0(3)
S2	C20	C21	C22	177.2(2)

Atom	Atom	Atom	Atom	Angle/°
S2	C20	C25	C24	-176.4(2)
Si2	O2	C28	C27	-168.08(18)
O2	Si2	C31	C32	173.2(2)
O2	Si2	C31	C33	53.3(2)
O2	Si2	C31	C34	-66.5(3)
N5	C21	C22	C23	179.0(2)
N6	C24	C25	C20	178.2(2)
N6	C26	C27	C28	-177.3(2)
C19	S2	C20	C21	1.43(19)
C19	S2	C20	C25	179.4(3)
C19	N5	C21	C20	1.5(3)
C19	N5	C21	C22	-177.6(3)
C20	S2	C19	N5	-0.7(2)
C20	S2	C19	C18	178.7(2)
C20	C21	C22	C23	-0.1(4)
C21	N5	C19	S2	-0.3(3)
C21	N5	C19	C18	-179.7(2)
C21	C20	C25	C24	1.4(4)
C21	C22	C23	C24	0.7(4)
C22	C23	C24	N6	-179.2(2)
C22	C23	C24	C25	-0.3(4)
C23	C24	C25	C20	-0.7(4)
C24	N6	C26	C27	179.0(2)
C25	C20	C21	N5	179.8(2)
C25	C20	C21	C22	-1.0(4)
C26	N6	C24	C23	-1.9(4)
C26	N6	C24	C25	179.2(2)
C26	C27	C28	O2	60.6(3)
C29	Si2	O2	C28	-148.2(2)
C29	Si2	C31	C32	58.2(3)
C29	Si2	C31	C33	-61.7(2)
C29	Si2	C31	C34	178.5(2)
C30	Si2	O2	C28	-29.6(3)
C30	Si2	C31	C32	-65.1(3)
C30	Si2	C31	C33	175.0(2)
C30	Si2	C31	C34	55.2(3)
C31	Si2	O2	C28	92.8(2)

Hydrogen Fractional Atomic Coordinates ($\times 10^4$) and Equivalent Isotropic Displacement Parameters ($Å^2 \times 10^3$) for **17**. U_{eq} is defined as 1/3 of the trace of the orthogonalised U_{ij}.

Atom	x	y	z	U_{eq}
H3	5308.1	10294.41	3247.7	26
H5	9260.21	7079.95	3375.17	25
H6	8135.77	9673.19	3487.41	24
H8	5490.41	7412.05	2954.53	23
H9A	7004.28	12643.78	3428.95	26
H9B	6774.37	11299.85	3699.16	26
H10A	5090.27	13726.76	3388.84	28
H10B	4918.18	12474.97	3671.82	28
H11A	6450.91	15714.09	3671.54	33
H11B	5236.46	15889.8	3780.02	33
H12A	8604	12359.84	4065.68	54
H12B	9423.69	14184.3	4148.39	54
H12C	8670.74	14137.51	3842.04	54
H13A	7734.49	18085.27	3950.8	63
H13B	8416.75	18248.72	4265.69	63
H13C	7084.47	18503.65	4225.99	63
H15A	6593.62	15301.5	4933.64	64

Atom	x	y	z	U_{eq}
H15B	5875.09	15303.13	4622.42	64
H15C	6737.33	17057.91	4711.09	64
H16A	7966.61	11520.62	4577.03	64
H16B	6643.66	11873.14	4518.79	64
H16C	7261.99	11958.71	4841.61	64
H17A	9271.16	14297.26	4692.52	63
H17B	8671.04	14699.44	4976.53	63
H17C	8802.5	16451.18	4752.38	63
H6A	360.77	4231.46	3210.89	27
H22	4228.75	7713.15	3397.49	26
H23	3101.18	5102.89	3503.61	24
H25	539.54	7170.39	2926.42	24
H26A	1701.73	3393.6	3690.71	26
H26B	2105.3	2105.28	3433.21	26
H27A	-128.3	1970.3	3594.22	26
H27B	313.61	628.52	3347.8	26
H28A	314.79	-1242.81	3776.13	31
H28B	1579.01	-988.09	3702.43	31
H29A	499.25	665.54	4628.47	59
H29B	1372.83	2429.12	4608.76	59
H29C	1699.03	586.67	4816.41	59
H30A	1817.11	-3629.39	4168.18	63
H30B	796.74	-3211.98	4352.54	63
H30C	2028.41	-3571.56	4513.65	63
H32A	3775.09	271.31	4787.97	71
H32B	4863.39	-213.8	4632.25	71
H32C	3936.6	-1881.12	4657.48	71
H33A	4443.76	2646.44	4291.25	63
H33B	3405.02	3138.05	4465.73	63
H33C	3215.06	2876.44	4122.08	63
H34A	4719.7	-641.14	4099.11	74
H34B	3530.96	-499.15	3906.86	74
H34C	3807.89	-2343.77	4117.51	74

References

1. Sheldrick, G.M. SHELXT - Integrated space-group and crystal-structure determination. *Acta Crystallogr A* **71**, 3-8 (2015).
2. Sheldrick, G.M. Crystal structure refinement with SHELXL. *Acta Crystallogr C* **71**, 3-8 (2015).
3. Dolomanov, O.V., Bourhis, L.J., Gildea, R.J., Howard, J.A.K. & Puschmann, H. OLEX2: a complete structure solution, refinement and analysis program. *J Appl Crystallogr* **42**, 339-341 (2009).
4. Sheldrick, G.M. A short history of SHELX. *Acta Crystallographica Section A* **64**, 112-122 (2008).
5. Duisenberg, A.J.M., Kroon-Batenburg, L.M.J. & Schreurs, A.M.M. An intensity evaluation method: EVAL-14. *J Appl Crystallogr* **36**, 220-229 (2003).
6. Blessing, R.H. An Empirical Correction for Absorption Anisotropy. *Acta Crystallographica Section A* **51**, 33-38 (1995).